INTERNATIONAL CENTER FOR AGGREGATES RESEARCH

ICAR

CHARACTERIZATION OF UNBOUND GRANULAR LAYERS IN FLEXIBLE PAVEMENTS

RESEARCH REPORT ICAR - 502-3

Sponsored by the
Aggregates Foundation
for Technology, Research and Education

Technical Report Documentation Page

1. Report No.ICAR/502-3	2. Government Accession No.	3. Recipient's Catalog No.
4. Title and Subtitle CHARACTERIZATION OF UNBOUND GRANULAR LAYERS IN FLEXIBLE PAVEMENTS		5. Report Date: December 2000 6. Performing Organization Code
7. Author(s): Alex Adu-Osei		8. Performing Organization Report No. Report No. 502-3
9. Performing Organization Name and Address Texas Transportation Institute The Texas A&M University System College Station, Texas 77843-3135		10. Work Unit No. (TRAIS) 11. Contract or Grant No. Project No. 404001
12. Sponsoring Agency Name and Address Aggregates Foundation for Technology, Research, and Education 2101 Wison Blvd, Suite 100 Arlington, VA 22201-3062		13. Type of Report and Period Covered Final: December 2000 14. Sponsoring Agency Code

15. Supplementary Notes
Research performed in cooperation with International Center for Aggregates Research and Aggregates Foundation for Technology, Research, and Education.

Research Project Title: Evaluation of Superpave Aggregate Specifications

16. Abstract

The mathematical characterization of unbound granular materials should ideally be based on the behavior of the individual constituent elements and their interaction. Until particulate mechanics are developed to a level where it can easily be applied to characterize unbound granular materials, a nonlinear and cross-anisotropic model must be used to characterize the behavior of granular materials in pavements.

Existing pavement design and analysis methods have generally taken a very conservative view of the relative strength properties of granular materials used as base and subbase layers in conventional flexible pavements.

The mechanical properties of unbound granular layers in flexible pavements are important to the overall structural integrity of the pavement structure. Linear elastic analysis can be used with reasonable confidence for pavements with full depth asphalt layers, but it is inappropriate for unsurfaced or thinly surfaced flexible pavements unless the nonlinear behavior of unbound granular materials are properly taken into account.

Work done by several researchers suggest that incorporating a cross-anisotropic elastic model significantly improves isotropic models and drastically reduces the tensile stresses computed within granular layers. This is due to the fact that the behavior of granular materials depends on particle arrangement. The laboratory determination of cross-anisotropic properties of granular materials has been a difficult task for researchers. In this study, a new laboratory testing protocol has been developed based on the theories of elasticity to determine cross-anisotropic properties of granular materials. The testing protocol is efficient and precise. The test is also an excellent tool for comparative analysis of compacted materials.

The behavior of four unbound granular materials was studied. The resilient responses of the materials obey the Uzan type nonlinear model. It was observed that under low stress levels accumulation of permanent strain could stabilize in granular layers. However, at high stress levels, permanent strain will continuously accumulate.

A finite element program was modified to incorporate the cross-anisotropic material model. Pavement sections were analyzed with the finite element program. It was observed that cross-anisotropic modeling eliminates the presence of tension zones predicted by isotropic resilient models.

Deflection bowls predicted by nonlinear resilient models agree with field deflection bowls.

17. Key Words: fine aggregate angularity, CAR test, Hough Transformation, Unified image analysis, VDG-40,	18. Distribution Statement No restrictions. This document is available to the public through NTIS: National Technical Information Service 5285 Port Royal Road, Springfield, Virginia 22161

19. Security Classif.(of this report) Unclassified	20. Security Classif.(of this page) Unclassified	21. No. of Pages 260	22. Price

Form DOT F 1700.7 (8-72) **Reproduction of completed page authorized**

CHARACTERIZATION OF UNBOUND GRANULAR LAYERS IN FLEXIBLE PAVEMENTS

by

Alex Adu-Osei
Graduate Research Assistant
Texas A&M University

Report No 502-3

Project No. 404001
Research Report Title: Structural Characteristics of Unbound Aggregate Bases to Meet AASHTO Design Requirements

Sponsored by
Aggregates Foundation for Technology, Research and Education

December 2001

Texas A&M University
TEXAS TRANSPORTATION INSTITUTE
College Station, Texas 77840
MS 3135

DISCLAIMER

The contents of this report reflect the views of the authors, who are responsible for the facts and the accuracy of the data presented herein. The contents do not necessarily reflect the official views or policies of the International Center for Aggregate Research (ICAR), Texas Transportation Institute (TTI), or Texas A&M University. The report does not constitute a standard, specification, or regulation, nor is it intended for construction, bidding, or permit purposes.

TABLE OF CONTENTS

Chapter Page

TABLE OF CONTENTS (Cont'd)

Chapter Page

TABLE OF CONTENTS (Cont'd)

CHAPTER Page

CHAPTER I

INTRODUCTION

Pavements are civil engineering structures used for the purpose of carrying vehicular traffic safely and economically. Since the first hot mixed asphalt was placed on Pennsylvania Avenue in Washington, D.C., in 1876, flexible pavements have increased to 94% of the 12.9 million lane kilometers (8 million lane miles) paved roads in the U.S. (FHWA, 1990).

A conventional flexible pavement consists of a prepared subgrade or foundation and layers of subbase, base and surface courses (AASHTO 1993). The layers are selected to spread traffic loads to a level that can be withstood by the subgrade without failure. The surface course consists of a mixture of mineral aggregates cemented by a bituminous material. The base and subbase course usually consists of unbound granular materials. In flexible pavements, and especially for thinly surfaced pavements, the unbound granular layers serve as major structural components of the pavement system.

1.1 Problem Statement

Existing and past pavement design procedures have generally taken a very conservative view of the relative strength properties of unbound granular materials. There has been a recent move towards the use of mechanistic-empirical approaches to design and analyze pavement structures.

The format of this dissertation follows that of the *Journal of Transportation Engineering* of the American Society of Civil Engineers.

Conventional flexible pavements have been analyzed as layered elastic systems resting on a homogeneous semi-infinite half-space. The development of the layered elastic system solution started when Boussinesq (1885) solved for the stress, strain and displacement in a semi-infinite linear elastic homogeneous half-space due to a point load acting on the surface. Burmister (1943) developed a true layered elastic theory for a two-layer system and extended it to a three-layer system (Burmister, 1945). With the advent of computers, the theory has been applied to multilayer system with any number of layers with specified moduli and Poisson's ratios.

The mechanical properties of unbound granular layers in flexible pavements are important to the overall structural integrity of the pavement structure. The resilient (elastic) properties of unbound granular materials are non-linear and stress dependent (Hicks and Monismith, 1971; Uzan, 1985).

Linear elastic analysis can be used with reasonable confidence for pavements with full depth asphalt layers, but it is inappropriate for unsurfaced or thinly surfaced flexible pavements unless the nonlinear behavior of unbound granular materials are properly taken into account (Brown, 1996). To account for the nonlinear behavior of unbound granular materials, the layers are usually subdivided into sub-layers to accommodate variation in resilient modulus caused by the change in stress which occur with depth as a result of both traffic and overburden loads. There are different sub-layering methods available for assigning moduli to granular materials. The sub-layering methods depend on the design method or pavement structure and are totally different from each other (Wardle et. al., 1998). This multiple layered elastic process can account for variation in vertical stress but cannot effectively account for variation in lateral or horizontal stresses. Due to the non-linear behavior of unbound granular materials, and the variation of vertical and horizontal stresses within a pavement profile, the finite element method has recently been preferred to analyze pavements over the layered elastic method (Brown, 1996).

Due to the large amount of computer time and storage required of most finite element method programs, they have been used primarily for research analysis instead of routine design. With the advent of faster and larger memory computers, it has become possible to use finite element method programs to analyze pavements on personal computers.

One of the problems encountered by researchers developing finite element method programs for pavement systems with compacted unbound granular materials concerns the tendency for horizontal stresses to be computed in the granular layers. Since unbound granular materials have negligible tensile strength aside from that induced by suction and particle interlock, adjustments are usually applied to avoid predicting false failure conditions in the granular layers (Brown, 1996).

Recent developments in pavement materials research suggest that directional or anisotropic elastic modeling can reduce and even reverse horizontal tensile stresses predicted in unbound granular layers with isotropic elastic properties (Tutumluer, 1995). However, the determination of cross-anisotropic elastic properties using a conventional triaxial setup is difficult.

1.2 Objectives

The main objectives of this study are to:

- identify and assess the most accurate models used to characterize unbound granular layers which can be effectively incorporated into a layered (non-linear) elastic or finite element model
- develop improved characterization protocols and models to provide a more accurate assessment of the contribution of unbound granular layers to the overall structural integrity of flexible pavements
- evaluate the revised characterization model to aggregate variables through a laboratory study and assess the impact of these variables on performance.

1.3 Outline of Dissertation

This dissertation consists of eight chapters. An extensive literature survey on the characterization of unbound granular materials is included in Chapter II. The literature review summarizes existing laboratory, analysis, resilient modeling and permanent deformation modeling used to characterize the behavior of unbound granular materials in flexible pavements. Based on the findings of the literature review, nonlinear cross-anisotropic resilient modeling was identified to be the best available model to characterize granular materials.

The development of a new laboratory testing protocol to determine the nonlinear cross-anisotropic resilient response of unbound granular materials is presented in Chapter III. The testing protocol involves applying dynamic stress regimes within static stress levels and measuring material response (strains). The measured strains are used as input into a system identification method to determine five stress dependent cross-anisotropic properties of unbound granular materials.

A comprehensive laboratory test matrix was developed to study the resilient and permanent deformation behavior of four granular materials. Chapter IV includes description of the laboratory characterization phase of this study. The laboratory test results are presented and discussed in Chapter V. The effect of moisture, gradation, and material type on the deformational response of granular materials are also discussed.

A finite element program was modified to include cross-anisotropic material modeling in pavement layers. Chapter VI contains the development and modifications made to the finite element program. The finite element program was used to analyze resilient pavement response for 27 different pavement sections. Pavement response in the form of stress distributions was obtained for different material models. Chapter VI also discusses the pavement sections analyzed and evaluates the effect of different material models on the distribution of stresses within the pavement sections.

Chapter VII presents field validation of the resilient response. The pavement sections and data collection methods are detailed in this chapter. Falling Weight Deflectometer and Multi-Depth Deflectometer data were used to backcalculate material properties of two pavement sections. Comparisons were made between field deflection bowls and deflection bowls predicted by different material models using the finite element program.

The major findings of this research are outlined in Chapter VIII. Recommendations are also made in this chapter for future research.

CHAPTER II

LITERATURE REVIEW

Unbound granular materials are multi-phase materials comprised of aggregate particles, air voids and water. The mathematical characterization of unbound granular materials should ideally be based on the behavior of the individual constituent elements and their interaction. This calls for the use of particulate mechanics techniques to characterize the behavior of unbound granular materials. However, such an approach can be rather complex and would not be particularly suitable in pavement engineering applications. As faster computers become available, particulate mechanics becomes a more suitable means to characterize the behavior of unbound granular materials. Also, since the scale of practical interest is in the range of tens to hundreds of feet, the microscopic effects of unbound granular materials can be averaged and treated as a continuum (Chen and Mizuno, 1990).

The mechanical behavior of unbound granular materials, like soils, is influenced by factors such as density, stress history, void ratio, temperature, time, and pore water pressure. It is difficult to adequately incorporate these factors in a simple mathematical model and then to implement the model realistically into a computer-based numerical analysis, within the framework of continuum mechanics.

Existing pavement design and analysis methods rely on empirical procedures developed through long-term experience with specific types of pavement structure and a limited number of types of pavement construction material under limited conditions. These empirical methods have generally taken a very conservative view of the relative strength properties of granular materials used as base and subbase layers in conventional flexible pavements.

Use of empirical models should be limited to the conditions on which they are based and cannot usually account for changes in loading and environmental conditions. There has been a recent emphasis on the use of mechanistic-empirical approaches to design and analyze pavement structures. In mechanistic-empirical procedures, models based on physics and engineering principles are used to predict pavement response. This is adjusted, or calibrated, to fit observed performance, or empirical data. Understanding the behavior of pavement materials and their accurate characterization are important to the successful implementation of any mechanistic-empirical procedure.

2.1 Characterization of Unbound Granular Materials

The purpose of laboratory methods is to subject a representative pavement material sample to an environment (consisting of simulated traffic loading and environmental conditioning) that closely simulates field conditions. The general stress regime experienced by an element of material within a pavement structure as a result of a moving wheel load on the surface consists of pulses of vertical and horizontal stresses accompanied by a double pulse of shear stress. Also, the principal stresses in an element of pavement material rotate with the approach and departure of a wheel load (Lekarp et al., 2000).

Laboratory testing equipment must be capable of applying a load which accurately simulates the effects of traffic. For pavements, this could demand complex facilities. However, laboratory testing methods must also be simple and repeatable enough so that highway agencies can perform them routinely and quickly acquire necessary material parameters.

It has been reported that a close match to field conditions can be obtained by the use of a Hollow Cylinder Apparatus (Alavi, 1992, Chan et al 1994), with which the rotation of principal stresses can be accommodated. The use of a Hollow Cylinder Apparatus (HCA) is complex and has only been used for research. However, simpler testing protocols exist which involve the use of stress invariants and which express stress regimes in terms of octahedral shear and normal stresses (Brown, 1996). The invariant approach has been applied in conjunction with repeated load triaxial testing to characterize the response of granular materials in recent years. The deformation of unbound granular materials under repeated traffic loading is defined by a resilient response which is important for the load carrying ability of the pavement and a permanent strain response, which characterizes rutting and long-term pavement deformation (Lekarp et. al., 2000).

Granular material base and subbase layers are generally partially saturated in pavements. Varying the moisture regime in laboratory triaxial test specimens is straightforward, and the effects of moisture changes on material response parameters can be easily measured. Appropriate models can be constructed from the results. Pappin et. al. (1992) showed that the resilient response modeled for dry granular material is equally applicable to saturated and partially saturated conditions, provided the principle of effective stress is observed. In practice, although laboratory modeling of moisture effects is readily accomplished, estimation of the effective stress state in a pavement granular layer in the field may not be straightforward (Brown, 1996).

2.2 Repeated Load Triaxial Testing

The study of the mechanical properties of unbound granular materials calls for a test in which principal stresses and strains that span the range of expected conditions can be evaluated so that extrapolations used by structural models are kept to a minimum. The most convenient standard test, which allows for the direct measurement of principal stresses and strains, is the cylindrical triaxial test (Figure 2.1). The shape of the sample required is simple and practical for both field representation and easy laboratory preparation. The minor principal stress, σ_3, and intermediate principal stress, σ_2, are equal to the confining stress applied to the sample. The triaxial test has been used with notable success in the field of geotechnical engineering and its principles have been extended to the field of pavement engineering.

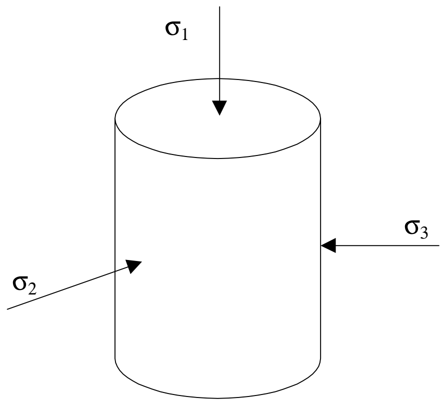

Figure 2.1 Cylindrical Triaxial Test.

In geotechnical engineering the triaxial test is used to determine the shear strength parameters of soils. The problem being analyzed usually dictates the rate of shear and drainage conditions applied to the cylindrical sample.

Some modifications have been made to the traditional triaxial test for pavement engineering applications. In pavement engineering, the repeated load triaxial test is preferred to the triaxial shear test. The measurement of principal stresses and strains are maintained, but unlike the traditional triaxial shear test, transient loads, which are well below material failure stresses, are applied to a cylindrical sample of pavement material. Also, strict drainage conditions and sample consolidation are not enforced. Triaxial testing data have been used to provide input for the material properties in pavement structural models to determine the stresses and strains that lead to performance predictions.

In the repeated load triaxial test, a constant confining stress is usually applied to the cylindrical samples and a deviatoric stress is axially cycled for a predetermined number of times. Allen (1973) used variable confining stresses and reported higher values of Poisson’s ratio compared to the constant confining stress.

The transient loads are chosen so that they best represent typical stress conditions within a pavement. Charts are available that can be used to select the cycle of a transient load (Barksdale, 1971). A typical transient load consists of a 1.0-second cycle sinusoidal load consisting of 0.1-second load duration and a 0.9-second rest. This load cycle was established to simulate the application of traffic loads on the pavement (Barksdale, 1971).

The repeated load triaxial test has been used extensively to study the behavior of unbound granular materials, despite its inability to simulate the rotation of principal stresses associated with shear stress reversal under a rolling wheel load. Allen (1973) conducted triaxial tests in which the chamber confining pressure was varied simultaneously with the deviator stress. While the technique did not account for the rotation of principal planes, it attempted to better simulate conditions under a moving wheel load. Stress pulse duration was 0.15 seconds for the primary test series. Results of the variable confining pressure tests yielded slightly lower values of the resilient modulus than did the constant confining pressure tests. However, the difference was not constant and did not appear to be significant. Using a Hollow Cylinder Apparatus (HCA), Chan (1990) demonstrated that resilient strains were unaffected by the rotation of principal stress phenomenon. He also showed that the principal planes of strain remained coincident with those of stress. These findings support the use of an invariant approach for pavement analysis and the use of relatively simple resilient strain models derived from triaxial tests rather than a more complex apparatus such as the HCA.

There has been extensive work in the development of the repeated load triaxial test in both Europe and North America. The test has been used in the U.S. since the 1950's (Seed *et al.*, 1955). The American Association of State Highway and Transportation Officials (AASHTO) have adopted three procedures for measuring the resilient modulus of granular materials in the past. The recent AASHTO standard procedure (AASHTO T294-94; “Resilient Modulus of Unbound Granular Base/Subbase Materials and

Subgrade Soils" - SHRP Protocol P46) includes method for measuring axial deformations on the specimen using externally mounted Linear Variable Differential Transducers (LVDTs). The procedure does not provide methods for measuring the lateral/radial strains. Also, confining stresses are not cycled and only deviator stresses are cycled.

Other researchers (Nazarian, 1996 and Tutumluer, 1998) have recommended changes to AASHTO T-294-94 to include measurement of lateral strains and specimen conditioning. In Europe, a triaxial apparatus was developed at Nottingham University (Boyce 1976) which has a system for cycling both deviator and confining stresses. Pore water pressure is also measured during the test. Details of the Nottingham apparatus are outlined in Boyce (1976), Pappin (1979), Boyce et. al. (1976), and Brown et. al. (1989). It can be seen that a single testing protocol has not been universally adopted.

For pavement applications the strains measured in a repeated load triaxial test are separated into elastic or resilient part, for resilient modulus, and a plastic part, for permanent deformation (Lekarp et. al., 2000).

2.3 Behavior of Unbound Granular Layers in Pavements

Consolidation, distortion and attrition occur when a granular material deforms under load (Lekarp, et. al. 2000). The response of an element of granular material in a pavement depends on its stress history, the current stress level, and the degree of saturation. Granular materials are not elastic but experience some non-recoverable deformation after each load application. In the case of transient loads, and after the first few load applications, the increment of non-recoverable deformation is much smaller compared to the increment of resilient/recoverable deformation. This resilient behavior of granular layers is the main justification for using elastic theory to analyze their response to traffic loads (Brown, 1996). The engineering parameter generally used to characterize this behavior is resilient modulus (M_R). The resilient modulus is obtained from repeated load triaxial tests, and it is calculated based on the axial recoverable strain under repeated axial loads.

The nonlinear stress-strain relationship of unbound aggregates at strain levels existing in pavements has been represented through the application of stress-dependent models of the resilient modulus and Poisson’s ratio. The factors affecting the resilient modulus and Poisson’s ratio have been studied by many researchers including Hicks (1970), Hicks and Monismith (1971), Allen (1973), Uzan (1985), Barksdale and Itani (1989) and Sweere (1990). Factors identified to influence the resilient modulus and Poisson’s ratio of unbound granular materials include stress levels, density, gradation, moisture, stress history, aggregate type and particle shape. Lekarp et. al (2000) provided an extensive literature review on resilient modeling and factors affecting the resilient properties of unbound granular materials. Although researchers seem to agree on the influence of stress and moisture on modulus, there are conflicting reports on the other factors.

Moduli variations due to moisture changes can be quantified in the laboratory. Anticipated seasonal variations in moisture content of granular layers must be included in the design process, so that appropriate laboratory derived model can be used properly.

The term “resilient” has a precise meaning. It refers to that portion of the energy that is put into a material while it is being loaded that is completely recovered when it is unloaded. As noted in the SHRP A-005 project (Report A357), the Poisson’s ratio of a resilient material is also stress dependent and is tied to the same material constants as the resilient modulus. The importance of this fact is that immediately beneath a tire load, an unbound aggregate generates its own lateral confining pressure and becomes very stiff, almost as if it were forming a moving vertical column that travels along immediately beneath the load (Lytton, 1998). How large the confining pressure and how stiff the aggregate base becomes depend strongly upon how large the Poisson’s ratio becomes. Contrary to linear elastic materials in which the Poisson’s ratio cannot rise above 0.5, in unbound aggregate bases, the Poisson’s ratio has been measured in the laboratory and the field to be above 0.5 (Allen, 1973). This is possible because both the resilient modulus and the Poisson’s ratio depend upon the stress level instead of being independent of it as in a linearly elastic material.

A Poisson’s ratio of 0.5 means that when a load is applied to a material it may change in shape but not in volume. A Poisson’s ratio less than 0.5 mean that when a material is loaded in compression, it may change in shape but it also decreases in volume (consolidation). A Poisson’s ratio larger than 0.5 means that the material may change in shape, but it will also increase in volume (dilate). It is this tendency to increase in volume under load, dilatancy, which makes unbound granular base layers so useful in a pavement structure (Lytton, 1998). When a collection of particles (aggregate) is loaded, the individual particles will try to wedge or rotate past the other particles. If the particles have been well compacted, this wedging and rotating action will force the particle apart, causing the overall volume to change.

This volume change will occur even if all of the particles are spheres, that is , perfectly round (Lytton, 1998). A different amount of volume change will occur if the particles are oblong or flat or plate shaped. Naturally, if the volume change depends upon the shape of the particles, then the Poisson’s ratio depends on their shape. Similarly, the range and distribution of the individual particle sizes also affect what the Poisson’s ratio will be under different states of stress (Lytton, 1998). The impact of particle shape and gradation on the Poisson’s ratio and the effect of the Poisson’s ratio on the performance of unbound aggregates in a pavement under load should be accommodated by granular material constitutive models in mechanistic pavement design.

Unbound granular materials like most geologic materials exhibit anisotropic behavior. During compaction, some anisotropy is induced in the granular layers before traffic loads impose further anisotropy. After incorporating anisotropic elastic modeling in the GT-PAVE finite element code, Tutumluer (1995) reported that cross-anisotropic elastic modeling can predict the behavior of unbound granular layers better than isotropic elastic model. The significance of this directional-dependent nature of the modulus and Poisson’s ratio will be discussed in detail later.

2.4 Resilient Behavior Modeling of Unbound Granular Materials

Resilient response of unbound granular materials is usually characterized by resilient modulus and Poisson's ratio or by shear and bulk modulus. For repeated load triaxial tests with constant confining stress, the resilient modulus and Poisson's ratio are defined as (Lekarp et. al., 2000):

$$M_R = \frac{\Delta(\sigma_1 - \sigma_3)}{\varepsilon_1} \tag{2.1}$$

$$\nu = -\frac{\varepsilon_3}{\varepsilon_1} \tag{2.2}$$

where;

M_R = Resilient modulus,

ν = Resilient Poisson's ratio,

σ_1 = Major principal or axial stress,

σ_3 = Minor principal or confining stress,

ε_1 = Major principal or axial resilient strain, and

ε_3 = Minor principal or radial resilient strain.

For repeated load triaxial test with variable confining stress, resilient modulus and Poisson's ratio are defined as (Lekarp et. al., 2000):

$$M_R = \frac{\Delta(\sigma_1 - \sigma_3)\,\Delta(\sigma_1 + 2\sigma_3)}{\varepsilon_1\,\Delta(\sigma_1 + \sigma_3) - 2\varepsilon_3\,\Delta\sigma_3} \tag{2.3}$$

$$\nu = \frac{\Delta\sigma_1\varepsilon_3 - \Delta\sigma_1\varepsilon_1}{2\Delta\sigma_3\varepsilon_3 - \varepsilon_1\Delta(\sigma_1 + \sigma_3)} \tag{2.4}$$

Many researchers have used laboratory data to model the nonlinear stress-dependence of resilient modulus and Poisson's ratio. The following discussion of selected models is intended to highlight the importance of stress levels to describe the resilient behavior of unbound granular materials.

2.4.1 Confining Pressure Model

Seed et al., (1967) subjected sand and gravel, both saturated and dry, to repeated load triaxial testing and expressed the results in the form:

$$M_R = k_1 \sigma_3^{k_2} \tag{2.5}$$

where k_1 and k_2 are regression constants. They used Equation 2.5 with success to predict the deflections in prototype pavements.

2.4.2 k-θ Model

A practical nonlinear description of the resilient modulus of unbound granular materials was reported by Hicks and Monismith (1971) and implemented in the AASHTO Guide for the Design of Pavement Structures. The resilient modulus was described as depending upon the sum of the principal stresses (Equation 2.6).

$$M_R = k_1 \theta^{k_2} \tag{2.6}$$

where θ = sum of principal stresses or first stress invariant ($\sigma_1 + 2\sigma_3$).

Equation 2.6 has become the most common representation of the resilient modulus, relating effects of the state of stress to layer stiffness for use in pavement design. Allen (1973) compared the results from constant confining pressure triaxial tests with those from variable confining pressure tests. Similar results were obtained from each test type, although constant confining pressure conditions yielded higher values for Poisson’s ratio. The data showed that Equation 2.6 fit the data better than Equation 2.5.

Uzan (1988) discusses a shortcoming of the k-θ resilient model (Equation 2.6). He points out that the model fails to account for the effects of shear stress on the resilient modulus and is therefore applicable over a small range of stress paths. This discrepancy is illustrated by Figure 2.2 from Uzan (1988), where the value of the resilient modulus predicted by equation 2.6 is plotted against axial strain and the relation is compared with test data. The predicted values of the modulus increase with increasing axial strain, in contrast to the test data, which shows the modulus to be decreasing. Other models have been proposed which yield more accurate predictions of the effects of shear stress and strain.

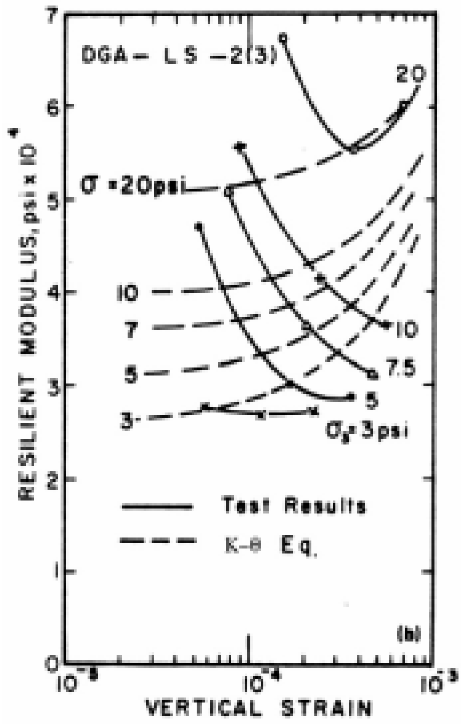

Figure 2.2 Test Results versus Modulus/Strain Relation from Equation 2.6 [after Uzan (1988)].

2.4.3 Uzan Model

Uzan (1985) proposed a modification to the model k-2 model, which accounts for shear behavior by the addition of a deviator stress term. The model is defined by:

$$M_R = k_1 \theta^{k_2} \sigma_d{}^{k_3} \qquad (2.7)$$

where σ_d = Deviator Stress (σ_1 -σ_3) and k_1, k_2, and k_3 are regression constants. Figure 2.3, from Uzan (1988), compares measured values for the modulus with predictions from Equation 2.7. The Uzan model appears to adequately account for shear and dilation effects and to fit the test data better than does the k-2 model (Equation 2.6).

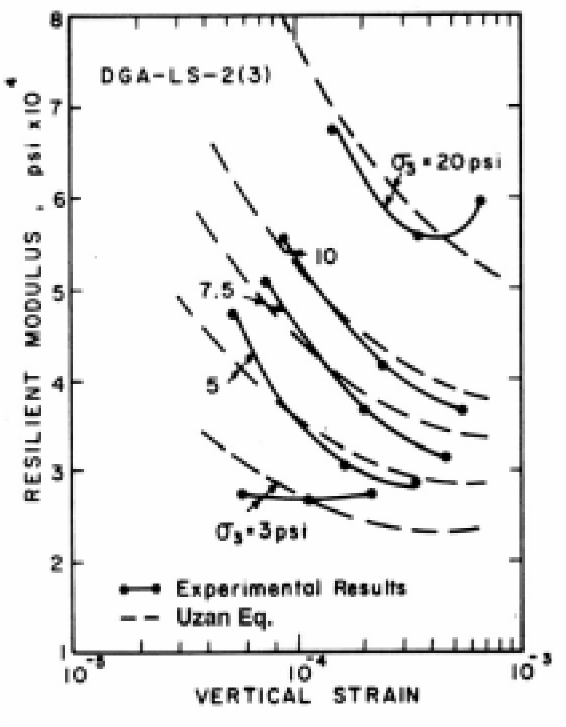

Figure 2.3 Experimental Results Compared to Uzan Model. [After Uzan (1988)].

Witczak and Uzan (1988) modified Equation 2.7 by replacing the deviator stress term with octahedral shear stress and non-dimensionalized the model (Equation 2.8) to facilitate easy conversion between different units. The Uzan model has been accepted as a universal material model for pavement materials and has become popular in routine pavement analysis.

$$M_R = k_1 P_a \left(\frac{I_1}{P_a} \right)^{k_3} \left(\frac{\tau_{oct}}{P_a} \right)^{k_3} \qquad (2.8)$$

where;

I_1= First stress invariant (sum of principal stresses),

τ_{oct} = Octahedral shear stress, and

P_a = Atmospheric pressure.

2.4.4 Lytton Model

Lytton (1995) argues that unbound granular materials in pavements are normally unsaturated and applied the principles of unsaturated soil mechanics to the Uzan model. To determine the effective resilient properties of unsaturated granular materials Lytton (1995) added a suction term to the Uzan model and expressed the resilient modulus as:

$$M_R = k_1 P_a \left(\frac{I_1 - 3\theta f h_m}{P_a} \right)^{k_2} \left(\frac{\tau_{oct}}{P_a} \right)^{k_3} \quad or \quad M_R = k_1 P_a \left(\frac{I_1 - 3k_4}{P_a} \right)^{k_2} \left(\frac{\tau_{oct}}{P_a} \right)^{k_3} \tag{2.9}$$

where

θ = Volumetric water content,
h_m = matric suction,
f = function of the volumetric water content, and
$k_4 = \theta f h_m$.

2.4.5 Contour Model

The nonlinear stress-strain behavior of unbound granular materials have also been modeled by decomposing both stresses and strains into volumetric and shear components (Boyce, 1976). Brown and Papin (1981) modified the contour model originally developed by Boyce (1976) to account for stress path effects. The model uses bulk and shear moduli to describe material properties. Equations 2.10, 2.11, and 2.12 are used to calculate volumetric and shear strains.

$$\varepsilon_v = \frac{1}{K_i} \left(\frac{I_1}{P_o} \right)^{k_1 - 1} \left[1 - \beta \left(\frac{\sigma_d}{P_o} \right)^2 \right] I_1 \tag{2.10}$$

$$\varepsilon_q = \frac{1}{3G_i} \left(\frac{I_1}{P_o} \right)^{k_2 - 1} \sigma_d \tag{2.11}$$

$$\Delta\varepsilon_q = \frac{1}{3G_i} \left[\left(\frac{I_{12}}{P_o} \right)^{k_2} \frac{\sigma_{d2}}{I_{12}} - \left(\frac{I_{11}}{P_o} \right)^{k_2} \frac{\sigma_{d1}}{I_{11}} \right] l^{k_3} \tag{2.12}$$

where

K_i and G_i are initial bulk and shear moduli,

$I_1 = \sigma_1 + \sigma_2 + \sigma_3$,

$\sigma_d = \sigma_1 - \sigma_3$,

p_o = reference pressure,

I_{11}, σ_{d1} and I_{12}, σ_{d2} are I_1 and σ_d at stress states 1 and 2 respectively,

$1 = (\Delta I_1^2 + \Delta\sigma_d^{\,2})^{½}$, and

β, k_1, k_2 , and k_3 are statistical material constants. This model yields accurate values for the resilient modulus over a wide range of stress paths. However, since the model requires determination of four material constants, laboratory and analytical procedures may be too complicated for routine design use (Tutumluer, 1995). Other models based on the contour models have also been proposed (Jouve et al., 1987; Thom, 1988; Sweere, 1990).

A review of the literature reveals that while the Uzan type of model is highly favored in the U.S., the bulk and shear moduli models are popular in Europe.

The resilient Poisson's ratio has also been modeled to depend on stress levels by a few researchers. Hicks and Monismith (1971) observed that the resilient Poisson's ratio increases with decreasing confining pressure and used a third-order polynomial to describe resilient Poisson ratio (Equation 2.13).

$$\nu = A + B\left(\frac{\sigma_1}{\sigma_3}\right) + C\left(\frac{\sigma_1}{\sigma_3}\right)^2 + D\left(\frac{\sigma_1}{\sigma_3}\right)^3 \qquad (2.13)$$

where A, B, C and D are regression coefficients.

Lytton et al. (1993) derived a partial differential equation based on thermodynamic principles to relate the resilient Poisson's ratio with stress (Equation 2.14).

$$\frac{2}{3}\frac{\partial \nu}{\partial J_2^{/}} + \frac{1}{I_1}\frac{\partial \nu}{\partial I_1} = \nu\left[\frac{1}{3}\frac{k_3}{J_2^{/}} + \frac{k_2}{I_1^2}\right] + \left[-\frac{1}{6}\frac{k_3}{J_2^{/}} + \frac{k_2}{I_1^2}\right] \qquad (2.14)$$

where

$J_2^{/}$ is second stress invariant of the deviatoric stress tensor, and

K_i are the regression coefficients from the Uzan model.

The solution to this partial differential equation led to two more regression coefficients including the three coefficients from the Uzan model. This model was termed the k_1-k_5 model. There are infinite number of solutions to this partial differential equation. Lytton et al. observed from laboratory data that for pavement materials, the particular solution can be expressed as:

$$v = k_4(-u_1)^{k_5} x^{k_2} y^{k_3^{/}} + \frac{x^{k_2} y^{k_3} 3^{k_3^{/}}}{2(x^2 - 3y)^{\frac{k_2}{2}+k_3^{/}}} \left[-k_2 B_v\left(\frac{k_2}{2} + k_3^{/}, -k_3^{/} + 1\right) + k_3^{/} B_v\left(\frac{k_2}{2} + k_3^{/}, -k_3^{/}\right)\right] \tag{2.15}$$

where

$x = I_1$,

$y = J_2^{/}$,

$u_1 = 3y - x^2$,

$B_v(c,d)$ is the incomplete Beta function,

$K_3^{/} = k_3 / 2$,

k_1, k_2, k_3 are regression coefficients determined from the Uzan model, and

k_4, k_5 are new regression coefficients.

2.5 Permanent Deformation Models

Resilience characteristics of paving materials are most important in fatigue cracking analyses. However, predictive procedures for rutting in flexible pavements require the assessment of the permanent deformation potential of granular layers.

Energy is put into a material when it is loaded. The resilient energy is that part of the applied energy that can be recovered when the material is unloaded. The rest of the energy that is not recovered is capable of doing work on the material. In unbound aggregates, most of the work goes into permanent strain that accumulates with repeated loading and unloading. It is this accumulating permanent strain in an aggregate base course that creates rutting. Rutting is made up of two parts, permanent volumetric compression and permanent lateral shearing movements. An unbound aggregate base course contributes to both of these (Lytton, 1998).

The criterion of mechanistic design methods for flexible pavements are usually to control the resilient tensile strain at the bottom of the asphalt layer in order to limit fatigue damage and resilient vertical compressive strain at the top of the subgrade for overall pavement rutting. Rutting (permanent deformation) in granular base and subbase layers is generally assumed to be negligible. This assumption is not always true because serious rutting can occur within the granular base and subbase layers if they are not properly designed, constructed or characterized (Park, 2000). Repeated load triaxial tests are capable of characterizing both the resilient and permanent deformation behaviors of unbound granular materials. The measurement of permanent deformation characteristics of unbound aggregates has received relatively less experimental attention than resilient modulus, although some notable contributions have been made. This is partly because the experiments are inherently destructive and require many specimens to be tested compared to the lower stress level, essentially non-destructive, resilient strain tests (Lekarp et. al., 2000). Aggregate characteristics including shape, angularity, surface texture, and roundness have an important influence on the resilient and permanent deformation response of an unbound aggregate (Barksdale, 1991). The permanent deformation accumulation in an unbound aggregate also depends on the stress level as well as the stress history. Moisture content, principal stress rotation and density also affect the accumulation of plastic strains in unbound granular materials (Lekarp, et. al., 2000). Like resilient behavior, the importance of applied stress is strongly emphasized in the literature. Permanent strain is related directly to deviator stress and inversely to confining stress. Many researchers have demonstrated that insignificant permanent deformation develops at low stress levels. Limiting the repeated stresses to about 60% of the triaxial shear strength of a granular material limits permanent deformation to acceptable levels. Thompson (1998) states that permanent deformation is primarily related to ultimate shear strength and not resilient modulus. Lekarp and

Dawson (1996) argue that failure in granular materials under repeated loading is a gradual process and not a sudden collapse as in static failure tests.

Barksdale (1972) observed after studying the behavior of granular materials that a 5% decrease in density was accompanied by an average of 185% increase in plastic strain. Allen (1973) reported a reduction in total plastic strain of 80% in crushed limestone and 22% in gravel as the specimen density was increased from Proctor to modified Proctor density.

The flow theory of plasticity has been used with much success in the geotechnical engineering field to predict plastic strains in soils. Several researchers (Mroz et al., 1978; Dafalias et al, 1982; Desai et al., 1986) have worked in the development of isotropic and anisotropic hardening models to predict the behavior of soils under cyclic and monotonic loading.

In pavement engineering, several researchers have studied the permanent deformation characteristics of unbound granular materials and proposed simpler models to characterize them. Plastic strains are usually related to the number of load applications or stress condition. The following discussion examines models for characterizing the permanent deformation behavior of unbound aggregates.

2.5.1 Hyperbolic Model

The hyperbolic plastic stress-strain model developed by Duncan and Chang is suitable for predicting plastic deformation properties over a very wide range of stress states under static loading only. The hyperbolic model relates confining stress, cohesion, angle of internal friction, and ratio of measured strength to ultimate hyperbolic strength. The model is expressed as:

$$\varepsilon_p = \frac{\sigma_d}{k_1 \sigma_3^{k_2}} \Bigg/ \left[\left(1 - \frac{\sigma_d R_f}{2(C\cos\phi + \sigma_3 \sin\phi)} \right) \frac{1}{(1-\sin\phi)} \right] \qquad (2.16)$$

where,

ε_p = Axial plastic strain,

$k_1 \sigma_3^{\ k2}$ = Relationship defining the initial tangent modulus as a function of

Confining pressure with k_1 and k_2 as constants,

C = Cohesion,

ϕ = Angle of internal friction, and

R_f = Ratio of measured strength to ultimate hyperbolic strength.

Barksdale (1972) used the hyperbolic model to fit experimental data for different material types and number of load repetitions.

2.5.2 VESYS Model

The VESYS computer program (FHWA, 1978) incorporated a method for predicting the rut depth in a pavement. This method is based on the assumption that the permanent strain is proportional to the resilient strain by:

$$\varepsilon_p(N) = \varepsilon \mu N^{-\alpha} \tag{2.17}$$

where

$\varepsilon_p(N)$ = permanent or plastic strain due to single load or Nth application,

ε = the elastic/resilient strain at the 200th repetition,

N = the number of load application,

μ = Parameter representing the constant of proportionality between permanent and elastic strain, and

α = Parameter indicating the rate of decrease in permanent strain with number of load applications.

2.5.3 Exponential/ Log N Model

The most commonly used model for characterizing permanent deformation behavior of granular material was developed by Lentz and Baladi (1981). They indicated that the change in permanent strain is large during the first few cycles and then gradually decreases as load repetitions continue. The accumulation of permanent deformation in an unbound aggregate can be expressed as:

$$\varepsilon_p = AN^b \quad or \quad \log \varepsilon_p = a + b \log N \tag{2.18}$$

where:

N = number of repeated load application,

ε_p = permanent strain,

a and *b* = experimentally determined factors, and

A = Antilog of *a*.

2.5.4 Ohio State University (OSU) Model

Researchers from Ohio State University (OSU) proposed a permanent deformation prediction model for the Ohio Department of Transportation (Majidzadeh, 1991). The OSU model is:

$$\frac{\varepsilon_p}{N} = AN^m \qquad (2.19)$$

where

ε_p and N are as defined above

A = experimental constant dependent on material and state of stress conditions; and

m = experimental constant depending on material type.

If the b term from the exponential/log N model is known, m is equal to b-1.

Various data indicate that for reasonable stress states (considerably below material failure strength), the *b* term for soils and unbound granular materials is generally within the range of 0.12 to 0.2. The lower values are for soils. The *A* term is variable and depends on material type, repeated stress state, and factors influencing material shear strength.

2.5.5 Texas A&M Model

Tseng and Lytton (1986) characterized permanent deformation in pavement materials with a three-parameter model as:

$$\varepsilon_p = \varepsilon_o \exp-\left(\frac{\rho}{N}\right)^{\beta} \qquad (2.20)$$

where

ε_p = Permanent axial strain, and

ε_0, β, and ρ = material parameters.

The material parameters are different for each material and also depend upon test conditions such as confining and deviator stresses and density.

2.5.6 Rutting Rate (RR) Model

Thompson and Naumann (1993) introduced the rate of rutting (RR) model and validated it by analyzing the AASHO road test data. The rate of rutting is given by:

$$RR = \frac{RD}{N} = \frac{A}{N^{B}} \qquad (2.21)$$

where:

RR = Rutting Rate,

RD = Rut depth, inches, and

A, B = terms developed from field calibration testing data and information.

Thompson (1993) indicated that stable pavement rutting trends were related to estimated pavement structure responses, particularly the Subgrade Stress Ratio (SSR). He summarized that since stress ratio is a valid indicator of rutting potential, the factors influencing the stress state and strength of the in-situ granular materials are important for characterizing permanent deformation of granular materials. Garg and Thompson (1997) used equation (2.21) to determine rutting potential in MnRoad bases and subbases. They reported the parameter, A, to be a function of the material shear strength and recommended determining shear strength from results of the rapid shear test performed with a confining pressure of 15 psi. Thompson (1998) states that the University of Illinois testing protocol for evaluating granular base/subbase materials includes this type of shear testing for categorizing rutting potential. Prior to rapid shear testing, this specimen is conditioned by application of 1000 repetitions of 310-kPa (45-psi) deviator stress at 103-kPa (15-psi) confining pressure. Conditioning at lower stress ratios appeared to be insufficient for establishing rutting potential. The University of Illinois procedure adequately differentiated among aggregates with excellent to inadequate rutting resistance (Thompson (1998)).

2.5.7 Yield Surface Model

Bonaquist and Witczak (1998) developed a method for incorporating permanent deformation of unbound granular base and subbase layers in the design of conventional flexible pavements. This method employs the use of yield surfaces from a flow theory model as design criteria for limiting permanent deformations in granular layers. The model is based on a hierarchical approach for constitutive modeling of geologic materials (Desai 1986). The model consists of a series of yield surfaces that expand with increasing plastic strains.

The yield surfaces define the magnitude of permanent deformation occurring on the first cycle of loading. Bonaquist and Witczak used the exponential type model to fit a set of repeated load triaxial test data and observed that the permanent strain at a load cycle is related to the permanent strain induced on the first cycle and the number of load cycles:

$$\xi_N = \frac{1}{N^{1.06}} \xi_i \tag{2.22}$$

where:

ξ_N = Permanent strain for load cycle N;

N = number of load cycles; and

ξ_i = permanent strain for the first load cycle.

The accumulated permanent strain is then the sum of the permanent strain on each cycle as given by:

$$\varepsilon_p = \sum \xi = \sum \left(\frac{1}{N^{1.06}} \right) \xi_i \tag{2.23}$$

where $\Sigma\xi$ is the accumulated permanent strain.

Thus, minimizing the first-cycle permanent deformation strain provides a reasonable criterion for minimizing the permanent deformation throughout the life of the pavement. The concept used in developing this model is consistent with the flow theory of plasticity. Bonaquist and Witzak (1997) used the isotropic hardening model in the development of Equation 2.23. However, for repetitive action of loads when hysteric phenomena are of essential importance, the anisotropic hardening model would be more appropriate.

2.5.8 Shakedown Model

At low levels of stress the accumulation of permanent deformation with load application eventually reaches a stable asymptotic value. At high stresses, however, permanent deformation is likely to accumulate continuously with load repetition, resulting in eventual failure (Lekarp, et. al., 2000). This has raised the possibility of the existence of critical stress level separating the stable and failure conditions in a pavement.

Some researchers (Sharp and Booker, 1984; Raad et al., 1989) have developed computational procedures for pavement analysis based on the so-called shakedown theory. The shakedown theory states that, a pavement will develop a progressive accumulation of permanent deformation under repeated loading if the magnitude of the applied loads exceeds a limiting value, called the shakedown load. On the other hand, if the applied loads are lower than the shakedown limit, a stable accumulation of permanent deformation will be developed and the response of the pavement will be resilient under additional load applications.

The shakedown theory is usually applied to the whole pavement structure. Using repeated load triaxial tests on different granular materials, Lekarp and Dawson (1998) according to Lekarp et al., (2000), applied the principles of shakedown theory and derived an expression for permanent strain (Equation 2.24).

$$\frac{\varepsilon_p(N)}{L/P_o} = a\left(\frac{\sigma_d}{I_1}\right)_{\max}^{b} \tag{2.24}$$

where;

L = stress path, and

a, b are material properties.

2.6 Analysis of Pavements with Unbound Granular Materials

Conventional flexible pavements are usually analyzed as elastic layered systems resting on a homogeneous semi-infinite half-space. The wheel load applied on the surface of the pavement is considered as a uniform load distributed over a circular area where the contact pressure is taken as the tire pressure (Huang, 1993).

Several computer programs based on the Burmister's (1845) layered elastic theory have been developed over the years for analyzing pavement systems. One of the earliest and best known is the CHEVRON program develop by the Chevron Research Company (Warren and Dieckmann, 1963). The program was modified by the Asphalt Institute in the DAMA program to account for non-linear elastic behavior of granular materials (Hwang and Witczak, 1979). Another well-publicized program is BISAR developed by Shell, which considers not only vertical loads but also horizontal loads (De Jong et al., 1973). The University of California, Berkeley (Kopperman et al., 1986) also developed a program called ELSYM5. This program has become very popular in the U.S. and is used by many highway agencies for routine flexible pavement design. A recent addition to the layered elastic computer programs is CIRCLY (Wardle et al., 1998). The latest version, CIRCLY4 was programmed in windows environment and it can automatically divide layers into sub-layers for material non-linearity. It is the only layered elastic computer program that incorporates granular material anisotropy.

The limitation of the layered elastic is that elastic moduli must be constant within each horizontal layer and thus, the method cannot effectively deal with material non-linearity exhibited by unbound granular materials. The layered elastic process can account for variation in vertical stress through the iteration approach but cannot effectively account for variation in lateral stresses. Since the variation of lateral stresses within a pavement profile is as important as the variation of vertical stresses, the finite element method (FEM) has recently been preferred to analyze pavements.

A number of computer programs have been developed based on the finite element method that accommodates nonlinear stress-strain models. Due to the large amount of computer time and storage required of most finite element method programs, they have not been used for routine design purposes. With the advent of faster and larger memory computers, it has become possible to use finite element method programs to analyze pavements on personal computers.

Work done by some researchers (Jouve and Elhannani; 1993, Tutumluer and Barksdale; 1995, Tutumuluer and Thompson; 1996) have suggested that incorporating anisotropic behavior of granular materials significantly improves models and drastically reduces the tensile stresses computed within granular layers. Some finite element programs have incorporated anisotropic modeling to characterize the behavior of unbound granular materials. However, the laboratory determination of anisotropic properties of unbound granular materials has been a difficult task for researchers. One of the research objectives of this study is the development of a reliable laboratory protocol to determine the anisotropic properties of granular materials.

CHAPTER III

DEVELOPMENT OF ANISOTROPIC RESILIENT MODEL AND LABORATORY TESTING

3.1 Background

One of the problems encountered in the analysis of flexible pavement systems with compacted unbound granular layers is the tendency for horizontal stresses to be computed in the granular layers. If the models were precise, this situation (false failure) would not occur, because granular materials have negligible tensile strength. Work done by several researchers (Jouve and Elhannani, 1993; Tutumluer, 1995; Tutumuluer and Thompson, 1997; Hornych et al., 1998) has suggested that incorporating cross-anisotropic behavior of granular materials significantly improves isotropic models and drastically reduces the tensile stresses computed within granular layers.

An unbound granular layer in a flexible pavement provides load distribution through aggregate interlock. The load transfer is achieved through compression and shear forces among the particles. Because tensile forces can not be transferred from particle to particle, when such forces act in the horizontal direction, the behavior of the granular layer is significantly affected by a directional dependency of material stiffness which can be accommodated by using anisotropic approach (Tutumluer, 1995).

The word anisotropy is a synthesis of the Greek word *anisos*, which means unequal, and *tropos*, which means manner. As the derivation of the word indicates, it means in general a different (unequal) manner of response. The mechanical properties of an anisotropic elastic material depend on direction.

The behavior of granular layers, like most geologic materials, depends on particle arrangement which is usually determined by aggregate characteristics, construction methods, and loading conditions. An apparent anisotropy is induced in an unbound granular layer during construction, becoming stiffer in the vertical direction than in the horizontal direction even before traffic loads impose further anisotropy. Tutumuluer and

Thompson (1997) indicated that the non-linear anisotropic approach can effectively account for the dilative behavior of unbound granular layers observed under wheel loads and the effects of compaction induced residual stresses. The main advantage of using anistropic modeling in unbound granular layers is the drastic reduction or elimination of significant tensile stresses generally predicted by using an isotropic approach.

Barksdale, Brown and Chan (1989) observed from instrumented test sections that a linear cross-anisotropic modeling of unbound granular base is equal to or better than more complicated nonlinear isotropic models for predicting general pavement response. A cross-anisotropic representation has different material properties in the vertical and horizontal directions. The conventional isotropic models have the same material properties in all directions.

Tutumluer (1995) developed a finite element computer program (GT-PAVE) to predict the resilient response of flexible pavements. The program accounts for:

- Material non-linearity,
- Horizontal residual stresses due to initial compaction, and
- Correction of tensile stresses at the bottom of unbound granular layers obtained in isotropic elastic analysis.

Finite element predictions of response variables such as stress, strain, and deformation at different locations in the pavement were compared to the results obtained from experiments with full-scale test sections. The comparison shows very good agreement when a non-linear elastic analysis is performed with cross-anisotropic material behavior in the unbound granular layers (Tutumluer, 1995).

A cross-anisotropic representation of the unbound granular layers was shown to reduce the predicted tensile stresses from isotropic elastic analysis in these layers by up to 75%. Tutumluer (1995) observed that using 15% of the vertical resilient modulus as the horizontal resilient modulus was necessary to correctly predict the horizontal and vertical measured strain in the unbound granular base. A constant Poisson's ratio was assumed for the analysis.

Porter et. al.(1999) characterized granular layers as cross-anisotropic in the CIRCLY computer program and observed that measured deflection bowls were narrower than those estimated from elastic layer analysis with isotropic characterization. After performing a finite element method (FEM) analysis, Porter obtained similar response when granular materials were modeled as non-linear (stress-dependent) isotropic and linear anisotropic. Upon recommendations from Porter et. al. (1999) The National Association of Australian State Road Authorities (NAASRA) adopted a modular ratio (E_x/E_y) of 0.5 for unbound granular layers in their Guide to the Structural Design of Road Pavements. NAASRA also assumes that vertical and horizontal Poisson's ratios are the same.

Five material properties are needed to define anisotropy under conditions of axial symmetry. Tutumluer and Thompson (1997) defined cross-anisotropic response from triaxial test data with measured vertical and radial strains as follows:

$$E_y = \frac{\sigma_d}{\varepsilon_{axial}} \quad \text{(Standard definition)} \tag{3.1}$$

$$E_x = \frac{\sigma_3}{\varepsilon_{radial}} \quad \text{(New definition)} \tag{3.2}$$

$$G_{xy} = \frac{\sigma_d}{2(\varepsilon_{axial} - \varepsilon_{radial})} \quad \text{(New definition)} \tag{3.3}$$

where

E_y = Vertical resilient modulus,

E_x = Horizontal resilient modulus,

G_{xy} = Resilient shear modulus,

ε_{axial} = resilient axial strain, and

ε_{radial} = resilient radial strain.

Tutumluer and Thompson (1997) then used the Uzan type model to relate each modulus to the bulk and deviator stress as:

$$E_y = k_1 P_a \left(\frac{I_1}{P_a}\right)^{k_2} \left(\frac{\sigma_d}{P_a}\right)^{k_3} \tag{3.4}$$

$$E_x = k_4 P_a \left(\frac{I_1}{P_a} \right)^{k_5} \left(\frac{\sigma_d}{P_a} \right)^{k_6} \tag{3.5}$$

$$G_{xy} = k_7 P_a \left(\frac{I_1}{P_a} \right)^{k_8} \left(\frac{\sigma_d}{P_a} \right)^{k_9} \tag{3.6}$$

where:

I_1 = first stress invariant (bulk stress),

J'_2 = second stress invariant of the deviatoric stress tensor, and

k_i = material parameters.

Tutumluer and Thompson (1997) used triaxial test data, and the fit was good for all the above definitions. They selected constant vertical and horizontal Poisson's ratios to satisfy the requirements of positive strain energy. The parameters were then used as input into GT-PAVE to analyze the anisotropic model in different types of unbound granular layers in conventional flexible pavements. The horizontal resilient modulus generally varied from 3% to 21% of the vertical resilient modulus, and the resilient shear modulus varied from 18% to 35% of the vertical. Computed tensile stresses in the granular layers were drastically reduced.

Hornych et al., (1998) studied the resilient behavior of granular materials and observed that the non-linear isotropic model developed by Boyce (1976) did not adequately characterize the behavior of granular materials. Hornych et al., (1998) introduced a coefficient of anisotropy into the Boyce model and obtained a good fit for laboratory data.

Sweere (1990) noted that, if resilient properties are defined in terms of stress dependent moduli; then a corresponding value of Poisson's ratio is required which should itself be stress dependent. Lytton (1998) proposed that a full description of the anisotropic behavior of unbound granular materials should include stress-dependent Poisson's ratio models.

Perhaps the most significant example of material behavior that can not be modeled by standard layered elastic programs is the dilation observed under shearing in particulate media in a dense state of packing. Because of the assumption of an isotropic, homogeneous material, traditional layered elastic programs can only accommodate materials with Poisson's ratio below 0.5. For most granular materials, a fixed Poisson's ratio is normally used. A typical value of Poisson's ratio lies within the range 0.30 to 0.40. However, when a material dilates, Poisson's ratios can be as high as 1.20 or higher (Crockford et al., 1990; Uzan et al, 1992; Allen, 1973). This tendency to dilate is caused by the motion of particles that tend to roll over one another when a shearing stress is applied. Most researchers agree that dense graded granular materials start to dilate when the principal stress ratio exceeds a certain value. Allen (1973) expressed the relationship between Poisson's ratio and stress state. Chen and Saleeb (1982), Lade and Nelson (1987) derived relationships between the Poisson's ratio and the resilient modulus based on thermodynamic constraints.

Although there is strong evidence in the literature that nonlinear cross-anisotropic elastic models are superior to isotropic models in characterizing granular materials, it has been extremely difficult to determine the cross-anisotropic material properties of unbound granular materials using the conventional triaxial setup. To obtain the cross-anisotropic parameters of granular materials, a truly triaxial setup with multi-axial devices must be used instead of the conventional cylindrical triaxial setup. The truly triaxial device permits application of three independent principal stresses on six faces of a cubical specimen of a material.

Graham et al., (1983) proposed a mathematical technique using elasticity theory to determine anisotropic material parameters from triaxial test data. The technique proposed by Graham et al., (1983) is not suitable for unbound granular materials because the material is assumed to be linearly elastic.

Tutumluer et al., (2000) modified the standard AASHTO 294-94 to determine cross-anisotropic parameters of several granular materials. In the modified test, Tutumluer et al., (2000) used both triaxial compression and extension tests. The stress states recommended in AASHTO 294-94 is maintained but the principal stresses are interchanged after each triaxial compression, to induce a triaxial extension. This way, there is enough data to determine the vertical and horizontal moduli. However, the resilient shear modulus cannot be determined from the modified AASHTO 294-94 test.

One the objective of this study is to develop an improved testing protocol based on traditional elasticity theories. The developments of anisotropic resilient model and testing method for unbound granular materials are discussed in the following sections.

3.2 Constitutive Model

For a linear, elastic, homogeneous and continuous material, the general constitutive relation relating stress and strain tensors can be written as:

$$\sigma_{ij} = C_{ijkl}\varepsilon_{kl} \tag{3.7}$$

where:

σ_{ij} = stress tensor;

C_{ijkl} = tensor of elastic constants; and

ε_{ij} = strain tensor.

Repeated indices imply summation. Indices *i*, *j*, *k* take the values 1, 2, 3. In the most general three-dimensional case, the tensor of elastic constants C_{ijkl} has 81 independent components. However, due to the symmetry of both the strain and stress tensors, there are at most 36 distinct elastic constants. This number is reduced to 21 if a strain energy function is applied. Equation 3.7 can be rewritten as:

$$\varepsilon_{ij} = A_{ijkl}\sigma_{kl} \tag{3.8}$$

where:

A_{ijkl} = a tensor of compliance with 21 distinct components, and

A_{ijkl} and C_{ijkl} are symmetric and are inverse to each other in the sense that;

$$C_{ijkl}A_{klrs} = \frac{1}{2}(\delta_{ir}\delta_{js} + \delta_{is}\delta_{jr}) \tag{3.9}$$

where δ_{ij} is the Kronecker Delta.

If we consider the matrix representation of the tensor ε_{ij}, σ_{kl}, and A_{ijkl} in an arbitrary x, y, z coordinate system, Equation 3.8 is equivalent to (Amadei, 1983):

$$\varepsilon_{xyz} = [A]\{\sigma\}_{xyz} \tag{3.10}$$

or

$$\begin{bmatrix} & & \\ & \begin{matrix} a_{ij} \\ i = 1, 6 \\ j = 1, 6 \end{matrix} & \\ & & \end{bmatrix} \begin{Bmatrix} \sigma_x \\ \sigma_y \\ \sigma_z \\ \tau_{yz} \\ \tau_{xz} \\ \tau_{xy} \end{Bmatrix} = \begin{Bmatrix} \varepsilon_x \\ \varepsilon_y \\ \varepsilon_z \\ \gamma_{yz} \\ \gamma_{xz} \\ \gamma_{xy} \end{Bmatrix} \tag{3.11}$$

The coefficient a_{ij} play different roles and have different physical meanings. If the material possesses symmetry of any kind, then symmetry can be observed in its elastic properties and the number of independent components of the tensor of compliance or elastic constants is less than 21.

3.2.1 Orthogonal Planes of Elastic Symmetry

A plane of elastic symmetry exists at a point if the elastic constants or compliance have the same values for every pair of coordinate systems that are the reflected image of one another with respect to the plane (Amadei, 1983). Assuming that the Cartesian *x*O*z* plane (Figure 3.1) is a plane of elastic symmetry and assuming that three orthogonal planes of elastic symmetry pass through each point of the material, and each one is perpendicular to x, y, or z, then Equation 3.11 reduces to:

$$\begin{bmatrix} \frac{1}{E_x} & -\frac{\nu_{xy}}{E_y} & -\frac{\nu_{xz}}{E_z} & 0 & 0 & 0 \\ & \frac{1}{E_y} & -\frac{\nu_{zy}}{E_z} & 0 & 0 & 0 \\ & & \frac{1}{E_z} & 0 & 0 & 0 \\ & & & \frac{1}{G_{zy}} & 0 & 0 \\ & & & & \frac{1}{G_{xz}} & 0 \\ & & & & & \frac{1}{G_{xy}} \end{bmatrix} \begin{Bmatrix} \sigma_x \\ \sigma_y \\ \sigma_z \\ \tau_{zy} \\ \tau_{xz} \\ \tau_{xy} \end{Bmatrix} = \begin{Bmatrix} \varepsilon_x \\ \varepsilon_y \\ \varepsilon_z \\ \gamma_{zy} \\ \gamma_{xz} \\ \gamma_{xy} \end{Bmatrix} \tag{3.12}$$

The number of independent elastic constants or compliance is reduced to 9. There are three Young's moduli E_x, E_y, E_z, three shear moduli G_{yz}, G_{xz}, G_{xy}, and three Poisson's ratios ν_{yx}, ν_{zx}, and ν_{zy}. A material that possesses this type elastic symmetry is called orthotropic (Amadei, 1983).

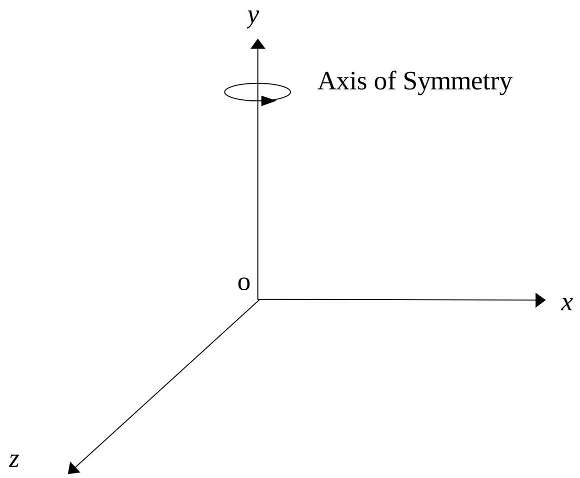

Figure 3.1 Three-Dimensional Cartesian Coordinate System.

An axis of elastic symmetry *g* of order *n* exists at a point when there are sets of equivalent elastic directions that can be superimposed by a rotation through an angle of $2\pi/n$. An axis of the second order is equivalent to a plane of elastic symmetry. For an axis of the third or fourth order, the number of independent elastic constants or compliances is reduced to 7. For an axis of order larger than or equal to 6, all directions in the planes normal to it are equivalent with respect to the elastic properties. If the y-axis coincides with the axis of elastic symmetry *g*, the material is isotropic within the *x*O*z* plane. The y-axis is defined as axis of radial elastic symmetry of axis of elastic symmetry of rotation. A material with this type of elastic symmetry is called transversely isotropic (Amadei, 1983). Geotechnical engineers popularly refer to a transversely isotropic material as cross-anisotropic. In this report anisotropic and cross-anisotropic material have been used interchangeably to describe a transversely isotropic material. Unbound granular materials in pavements can be assumed to possess this type of elastic symmetry. The *x*O*z* plane and each plane perpendicular to it are planes of elastic symmetry. Thus, the number of elastic constants is reduced to 5 as follows (Pickering, 1970):

$$\begin{bmatrix} \frac{1}{E_x} & -\frac{\nu_{xy}}{E_x} & -\frac{\nu_{xx}}{E_x} & 0 \\ & \frac{1}{E_y} & -\frac{\nu_{xy}}{E_x} & 0 \\ & & \frac{1}{E_x} & 0 \\ & & & \frac{1}{G_{xy}} \end{bmatrix} \begin{Bmatrix} \sigma_x \\ \sigma_y \\ \sigma_x \\ \tau_{xy} \end{Bmatrix} = \begin{Bmatrix} \varepsilon_x \\ \varepsilon_y \\ \varepsilon_x \\ \gamma_{xy} \end{Bmatrix} \tag{3.13}$$

where:

E_y = vertical elastic modulus,

E_x = horizontal elastic modulus,

G_{xy} = shear modulus,

ν_{xy} = vertical Poisson’s ratio, and

ν_{xx} = horizontal Poisson’s ratio.

The elastic constants have ranges of possible variation that are limited since thermodynamic considerations require that the strain energy be positive. The strain energy is given by (Pickering, 1970):

$$\Omega = \frac{1}{2}\{\sigma\}^T{}_{xyz}\,[A]\{\sigma\}_{xyz} \tag{3.14}$$

If this quadratic form is positive definite, the strain energy will be positive as required by thermodynamics. The necessary and sufficient conditions that the quadratic form should be positive definite are that all the principal minors of [*A*] should be positive (Pickering, 1970). The following conditions must then be satisfied:

$$E_y > 0 \quad ; \quad E_x > 0 \quad ; \quad G_{xy} > 0 \quad ; \quad -1 \le \nu_{xx} \le 1 \tag{3.15}$$

The constitutive relations defined by Equations 3.7 or 3.8 together with the elastic symmetries can be used to model the response of unbound granular layers in pavements. The unbound granular layers which are assumed to be homogeneous, continuous and transversely isotropic, thus need 5 elastic independent parameters to fully describe their behavior in pavements. Two parameters, Poisson's ratio and a modulus are needed if the material is assumed to be isotropic.

3.2.2 Anisotropic Work Potential

The elastic work per unit volume (*dW*) can be expressed as (Lytton, 1998):

$$\oint dW = \oint (\sigma)^T (d\varepsilon) \tag{3.16}$$

The law of energy conservation requires that the total work be path independent and Equation 3.16 can also be written as (Lytton, 1998):

$$\oint dW = \oint \frac{I_1 dI_1}{9E_y}\left[1 + 2\frac{E_y}{E_x} - 4\nu_{xy}\frac{E_y}{E_x} - 2\nu_{xx}\frac{E_y}{E_x}\right] + \frac{dJ_2^{/}}{2G_{xy}} = 0 \tag{3.17}$$

According to Green's theorem this can be written as (Lytton, 1998):

$$\oint \left(Pdx + Qdy\right) = \iint_A \left(\frac{dQ}{dx} - \frac{dP}{dy}\right) dA \tag{3.18}$$

where:

$P = dW/dx$, and

$Q = dW/dy$.

The work potential can thus be written as:

$$dW = \frac{dW}{dI_1} dI_1 + \frac{dW}{dJ_2^{/}} dJ_2^{/} = 0 \tag{3.19}$$

where:

$$\frac{dW}{dI_1} = \frac{I_1}{9E_y}\left[1 + 2\frac{E_y}{E_x} - 4\nu_{xy}\frac{E_y}{E_x} - 2\nu_{xx}\frac{E_y}{E_x}\right] \tag{3.20}$$

and,

$$\frac{dW}{dJ_2^{/}} = \frac{1}{2G_{xy}} \tag{3.21}$$

But,

$$\frac{d^2W}{dI_1 dJ_2^{/}} = \frac{d^2W}{dJ_2^{/} dI_1} \tag{3.22}$$

Based on the requirements that total work be path independent, Equations 3.22, 3.4, 3.5 and 3.6 can be combined to generate a partial differential equation for the vertical and horizontal Poisson's ratios as (Lytton, 1998):

$$2\frac{\partial \nu_{xy}}{\partial J_2^{/}} - \frac{k_6}{I_1 J_2^{/}}\nu_{xy} = -\frac{\phi_1(I_1, J_2^{/})}{2I_1} \tag{3.23}$$

$$2\frac{\partial \nu_{xx}}{\partial J_2^{/}} - \frac{k_6}{I_1 J_2^{/}}\nu_{xx} = -\frac{\phi_2(I_1, J_2^{/})}{2I_1} \tag{3.24}$$

where:

$\phi_i(I_1, J_2^{/})$ = functions of I_1, $J_2^{/}$.

This set of equations will be needed to obtain the five parameters which fully describe the anisotropic behavior of unbound granular materials. The five elastic properties are assumed to be stress dependent.

3.3 Testing Protocol

A truly triaxial device that permits the application of three independent principal stresses on six faces of a cubical specimen of a material is desirable for use in the laboratory. The setup of a truly triaxial device is complex, and preparation of the cubical specimen is extremely difficult. Laboratory testing devices must be simple enough so that highway agencies can use them routinely and quickly to acquire necessary material parameters. The most convenient standard test which allows for the direct measurement of principal stresses and strains is the cylindrical triaxial test.

The triaxial testing protocol permits the application of both confining and deviatoric stresses on a compacted cylindrical sample. These stresses can be manipulated to obtain a variety of stress combinations. The direction of the principal stresses (σ_1, σ_2, and σ_3) and strains (ε_1, ε_2, and ε_3) are forced to coincide, and this allows for simple analysis. The particular order of the principal stresses as major, intermediate, and minor stresses depends on the type of triaxial test performed.

The stress tensor, *T* in a triaxial test is given by:

$$T = \begin{bmatrix} \sigma_2 & 0 & 0 \\ 0 & \sigma_1 & 0 \\ 0 & 0 & \sigma_3 \end{bmatrix} \tag{3.25}$$

where:

σ_1, σ_2 , and σ_3 are the principal stresses.

Let directions 1, 2, and 3 be equal to y, x, z in the Cartesian coordinates system, respectively, then the stress tensor can be expressed as:

$$T = \begin{bmatrix} \sigma_x & 0 & 0 \\ 0 & \sigma_y & 0 \\ 0 & 0 & \sigma_z \end{bmatrix} \tag{3.26}$$

In a conventional triaxial test on compacted cylindrical samples, the intermediate and minor principal stresses (σ_2, and σ_3) are the same and the stress tensor becomes:

$$T = \begin{bmatrix} \sigma_x & 0 & 0 \\ 0 & \sigma_y & 0 \\ 0 & 0 & \sigma_x \end{bmatrix} \tag{3.27}$$

This simplification unfortunately reduces the number of equations in Equation 3.13 from 4 to 3. Also, since the shear stress and strain (τ_{xy}, and γ_{xy}) can not be measured in a cylindrical triaxial set up, only 2 equations are available to solve for 4 of the 5 material properties of a cross-anisotropic elastic material (Equation 3.28).

$$\begin{bmatrix} \dfrac{1}{E_x} & -\dfrac{\nu_{xy}}{E_x} & -\dfrac{\nu_{xx}}{E_x} \\ -\dfrac{\nu_{xy}}{E_x} & \dfrac{1}{E_y} & -\dfrac{\nu_{xy}}{E_x} \end{bmatrix} \begin{Bmatrix} \sigma_x \\ \sigma_y \\ \sigma_x \end{Bmatrix} = \begin{Bmatrix} \varepsilon_x \\ \varepsilon_y \end{Bmatrix} \tag{3.28}$$

Equation 3.28 can be written in stress-strain incremental form as:

$$\begin{bmatrix} \dfrac{1}{E_x} & -\dfrac{\nu_{xy}}{E_x} & -\dfrac{\nu_{xx}}{E_x} \\ -\dfrac{\nu_{xy}}{E_x} & \dfrac{1}{E_y} & -\dfrac{\nu_{xy}}{E_x} \end{bmatrix} \begin{Bmatrix} \Delta\sigma_x \\ \Delta\sigma_y \\ \Delta\sigma_x \end{Bmatrix} = \begin{Bmatrix} \Delta\varepsilon_x \\ \\ \Delta\varepsilon_y \end{Bmatrix} \tag{3.29}$$

To numerically solve for the five anisotropic elastic properties, a new testing protocol was developed. A programmed loading sequence involving ten stress states that represent typical stresses within unbound granular layers in pavements is used in the testing protocol. Three different triaxial regimes were established and implemented within each stress state in the development of the new testing protocol. The following assumptions were made in developing the testing protocol:

- The elastic moduli obey the Uzan (1988) model,
- The non-linear tangential moduli are smooth functions of the isotropic stress invariants (Equations 3.4, 3.5, 3.6),
- Variations of these tangential moduli are negligible within infinitesimal changes in stress at a particular stress state,
- The material is assumed to behave linearly elastic within a small excursion of stresses.

The three triaxial regimes implemented within each stress state are discussed in the following sections.

3.3.1 Triaxial Compression Regime

In this test regime, a sample is loaded statically to a target stress state (axial stress σ_y, and radial stress, σ_x). Then radial stress is kept constant while the axial stress is dynamically cycled in stress increments of $\Delta\sigma_y$. Equation 3.29 can then be expressed as:

$$\begin{bmatrix} \dfrac{1}{E_x} & -\dfrac{\nu_{xy}}{E_x} & -\dfrac{\nu_{xx}}{E_x} \\ -\dfrac{\nu_{xy}}{E_x} & \dfrac{1}{E_y} & -\dfrac{\nu_{xy}}{E_x} \end{bmatrix} \begin{Bmatrix} \Delta\sigma_x^c \\ \Delta\sigma_y^c \\ \Delta\sigma_x^c \end{Bmatrix} = \begin{Bmatrix} \Delta\varepsilon_x^c \\ \\ \Delta\varepsilon_y^c \end{Bmatrix} \tag{3.30}$$

where:

$\Delta\varepsilon_x{}^c$ is a change in radial strain due to an infinitesimal change in axial stress $\Delta\sigma_y{}^c$ in triaxial compression,

$\Delta\varepsilon_y{}^c$ is a change in axial strain due to an infinitesimal change in axial stress $\Delta\sigma_y{}^c$ in triaxial compression, and

$\Delta\sigma_x{}^c = 0$

3.3.2 Triaxial Shear Regime

After a sample is loaded to a static stress state (axial stress σ_y, and radial stress σ_x), a small dynamic axial stress increment of $\Delta\sigma_y{}^S$ is applied to the sample while the radial stress is reduced by a small change in dynamic stress of $\Delta\sigma_x{}^S$ such that:

$$\Delta\sigma_x^s = -\frac{1}{2}\Delta\sigma_y^s \tag{3.31}$$

and,

$$\begin{bmatrix} \dfrac{1}{E_x} & -\dfrac{\nu_{xy}}{E_x} & -\dfrac{\nu_{xx}}{E_x} \\ -\dfrac{\nu_{xy}}{E_x} & \dfrac{1}{E_y} & -\dfrac{\nu_{xy}}{E_x} \end{bmatrix} \begin{Bmatrix} \Delta\sigma_x^s \\ \Delta\sigma_y^s \\ \Delta\sigma_x^s \end{Bmatrix} = \begin{Bmatrix} \Delta\varepsilon_x^s \\ \\ \Delta\varepsilon_y^s \end{Bmatrix} \tag{3.32}$$

The change in first stress invariant, ΔI_1 is zero:

$$\Delta I_1 = \Delta\sigma_y^s + 2\Delta\sigma_x^s = \Delta\sigma_y^s - 2\frac{1}{2}\Delta\sigma_y^s = 0 \tag{3.33}$$

The change in second invariant of the deviatoric stress tensor, $\Delta J^{/}_2$ is given by:

$$\Delta J_2^{/s} = \frac{1}{3}(\Delta\sigma_y^s - \Delta\sigma_x^s) \tag{3.34}$$

Substituting Equation 3.31 into 3.34,

$$\Delta J_2^{/s} = \frac{3}{4}(\Delta\sigma_y^s)^2 \tag{3.35}$$

The change in strain energy, ΔE^S is given by:

$$\Delta E^{s} = \frac{1}{2}(\Delta\sigma_x^s \, \Delta\varepsilon_x^s + \Delta\sigma_y^s \, \Delta\varepsilon_y^s + \Delta\sigma_x^s \, \Delta\varepsilon_x^s) \tag{3.36}$$

Substituting Equation 3.31 into 3.36 yields,

$$\Delta E^{s} = \frac{1}{2}\Delta\sigma_y^s(\Delta\varepsilon_y^s + \Delta\varepsilon_x^s) \tag{3.37}$$

But from Equation 3.17 and since the change in first stress invariant, ΔI_1, is zero, the change in strain energy can be written as:

$$\Delta E^{s} = \frac{\Delta J_2^{/}}{2G_{xy}} \tag{3.38}$$

Substituting Equations 3.35 and 3.37 into 3.38 yields,

$$G_{xy} = \frac{3}{4}\frac{\Delta\sigma_y^s}{(\Delta\varepsilon_y^s - \Delta\varepsilon_x^s)} \tag{3.39}$$

Thus the triaxial shear regime can be used to determine the shear modulus, G_{xy} at any stress state by Equation 3.39.

3.3.3 Triaxial Extension Regime

In this triaxial regime, the static axial stress, σ_y is reduced by a small change in dynamic stress, $\Delta\sigma_y^e$ while the radial stress, $\Delta\sigma_x$ is increased by a small dynamic stress of $\Delta\sigma_x^e$. Thus, the net change in stress state is in an extension mode but the principal stresses are not reversed. Here, Equation 3.29 is expressed as:

$$\begin{bmatrix} \frac{1}{E_x} & -\frac{\nu_{xy}}{E_x} & -\frac{\nu_{xx}}{E_x} \\ -\frac{\nu_{xy}}{E_x} & \frac{1}{E_y} & -\frac{\nu_{xy}}{E_x} \end{bmatrix} \begin{Bmatrix} \Delta\sigma_x^e \\ \Delta\sigma_y^e \\ \Delta\sigma_x^e \end{Bmatrix} = \begin{Bmatrix} \Delta\varepsilon_x^e \\ \\ \Delta\varepsilon_y^e \end{Bmatrix} \tag{3.40}$$

where:

$\Delta\varepsilon_x^e$ is a change in radial strain due to an infinitesimal change in axial stress $\Delta\sigma_y^c$ and radial stress $\Delta\sigma_x^e$, and

$\Delta\varepsilon_y^c$ is a change in axial strain due to an infinitesimal change in axial stress $\Delta\sigma_y^c$ and radial stress $\Delta\sigma_x^e$.

The stresses applied and the strains obtained from the three stress regimes described are used in a system identification scheme to determine the five cross-anisotropic parameters.

3.4 System Identification Method

The objective of the system identification (SID) process is to estimate the system characteristics using only input and output data from the system to be identified (Wang and Lytton, 1993). The simplest method for representing the behavior of a physical process is to model it with a mathematical representation, for example Equation 3.29. The model is said to be ‘identified’ when the error between the model and the real process is minimized to some level. Otherwise the model must be modified until the desired level of agreement is achieved.

Figure 3.2 is a schematic diagram of the SID procedure. The model response, Y_k, is compared to the actual response of the system, Y, and the error, e, between the two is used to adjust the parameters of the model by means of an algorithm, which optimizes some prescribed criterion.

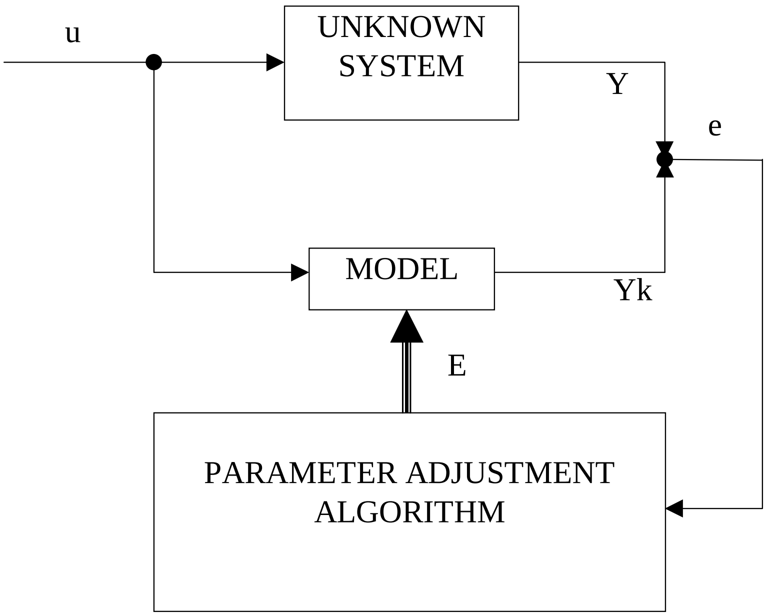

Figure 3.2 System Identification Scheme.

The SID method requires accurately measured output data of the unknown system, a suitable model to represent the behavior of the system, and an efficient parameter adjustment algorithm that converges accurately and rapidly.

An algorithm can be developed for adjusting model parameters on the basis of Taylor's series expansion. Let the mathematical model of some process be defined by *n* parameters:

$$f = f(p_1, p_2, \cdots, p_n; x, t) \tag{3.41}$$

where x and t are independent spatial and temporal variables.

Then any function $f_k(p_1, p_2, \ldots, p_n; x_k, t_k)$ may be expanded in a Taylor's series as:

$$f_k(p + \Delta p) = f_k(p) + \nabla f_k \cdot \Delta p + \delta^2 \tag{3.42}$$

where the parameters have all been collected into a vector

$$p = [p_1, p_2, \ldots, p_n]^T$$

If we assume $f_k(p+)p)$ to be the actual output of the system and $f_k(p)$ the output of the model for the most recent set of parameters, the error between the two outputs becomes:

$$\left.\begin{aligned} e_k &= f_k(p+\mathit{\Delta} p)-f_k(p) \\ &= \nabla f_k \cdot \mathit{\Delta} p \\ &= \frac{\partial f_k}{\partial p_1}\mathit{\Delta} p_1+\frac{\partial f_k}{\partial p_2}\mathit{\Delta} p_2+\cdots+\frac{\partial f_k}{\partial p_n}\mathit{\Delta} p_n \end{aligned}\right\} \tag{3.43}$$

It should be noted that e_k represents the difference between the actual system output and the model output for each observed point k. If the error is evaluated at m values ($m \geq n$) of the independent variables, m equations will be generated as:

$$\left.\begin{aligned} e_1 &= \frac{\partial f_1}{\partial p_1}\mathit{\Delta} p_1+\frac{\partial f_1}{\partial p_2}\mathit{\Delta} p_2+\cdots+\frac{\partial f_1}{\partial p_n}\mathit{\Delta} p_n \\ e_2 &= \frac{\partial f_2}{\partial p_1}\mathit{\Delta} p_1+\frac{\partial f_2}{\partial p_2}\mathit{\Delta} p_2+\cdots+\frac{\partial f_2}{\partial p_n}\mathit{\Delta} p_n \\ &\vdots \\ e_m &= \frac{\partial f_m}{\partial p_1}\mathit{\Delta} p_1+\frac{\partial f_m}{\partial p_2}\mathit{\Delta} p_2+\cdots+\frac{\partial f_m}{\partial p_n}\mathit{\Delta} p_n \end{aligned}\right\} \tag{3.44}$$

Equation 3.44 can be conveniently non-dimensionalized by dividing both sides by f_k to give:

$$\frac{e_k}{f_k} = \sum_{\substack{i=1\\k=1}}^{\substack{i=n\\k=m}} \frac{\partial f_k}{\partial p_i}\frac{p_i}{f_k}\frac{\mathit{\Delta} p_i}{p_i} \tag{3.45}$$

Matrix values r, F, and α are defined as:

$$r = [r_1\, r_2 \ldots r_m]^T$$

$$r_k = \frac{e_k}{f_k}$$

$$F = [F_{ki}]$$

$$F_{ki} = \frac{\partial f_k}{\partial p_i}\cdot\frac{p_i}{f_k}$$

$$\alpha = [\alpha_1\, \alpha_2 \ldots \alpha_n]^T$$

$$\alpha_i = \frac{\Delta p}{p_i}$$

Then, Equation 3.45 can be written as:

$$r = F\alpha \qquad (3.46)$$

The vector r is completely determined from the outputs of the model and the real system. The matrix F is usually called the sensitivity matrix, because its elements F_{ki} reflect the sensitivity of the output f_k to the parameter p_i (Wang and Lytton, 1993). It is generated by the differentials of the output f_k with respect to the parameter p_i.

The unknown vector α reflects the relative changes of the parameters. It can be obtained by using a generalized inverse procedure to solve equation 3.46. However, there might be column degeneracy in the sensitivity matrix F (Wang and Lytton, 1993). This condition may occur when two or more parameters have similar effects, or any parameter has a negligible effect on the behavior of the model. In these cases Equation 3.46 may be ill conditioned and more powerful numerical techniques such as the singular value decomposition (Lytton, 1998) and Han’s method (Han, 1976) must be used to give meaningful solutions.

Once the vector α is obtained, a new set of parameters is determined as:

$$p_i^{r+1} = p_i^r (1+\alpha) \qquad (3.47)$$

where r is the iteration number.

The iteration process is continued until the desired convergence is reached. In order to avoid convergence problems, the new set of parameters are not changed by more than 60% of the adjustment vector α. The value 0.6 acts as a relaxation factor for smooth convergence.

Applying the procedure described above to the triaxial model expressed in Equation 3.29, there are 4 parameters (E_y , E_x , ν_{xy} , ν_{xx}) and 2 outputs ($\Delta\varepsilon_x$, $\Delta\varepsilon_y$). The actual system outputs are the measured axial and radial strains. The model strains (model output) can be determined from the values of the parameters, which can be guessed initially from the system output. The difference between the measured strains and the model strains (model output) represents the error, which can be improved through the parameter adjustment routine until a desired criterion is achieved.

The matrices in Equation 3.46 may be defined as:

$$F = \begin{bmatrix} \frac{\partial(\Delta\varepsilon_x)}{\partial E_x}\cdot\frac{E_x}{\Delta\varepsilon_x^{\wedge}} & \frac{\partial(\Delta\varepsilon_x)}{\partial \nu_{xy}}\cdot\frac{\nu_{xy}}{\Delta\varepsilon_x^{\wedge}} & \frac{\partial(\Delta\varepsilon_x)}{\partial \nu_{xx}}\cdot\frac{\nu_{xx}}{\Delta\varepsilon_x^{\wedge}} & \frac{\partial(\Delta\varepsilon_x)}{\partial E_y}\cdot\frac{E_y}{\Delta\varepsilon_x^{\wedge}} \\ \frac{\partial(\Delta\varepsilon_y)}{\partial E_x}\cdot\frac{E_x}{\Delta\varepsilon_y^{\wedge}} & \frac{\partial(\Delta\varepsilon_y)}{\partial \nu_{xy}}\cdot\frac{\nu_{xy}}{\Delta\varepsilon_y^{\wedge}} & \frac{\partial(\Delta\varepsilon_y)}{\partial \nu_{xx}}\cdot\frac{\nu_{xx}}{\Delta\varepsilon_y^{\wedge}} & \frac{\partial(\Delta\varepsilon_y)}{\partial E_y}\cdot\frac{E_y}{\Delta\varepsilon_y^{\wedge}} \end{bmatrix} \tag{3.48}$$

$$\alpha = \begin{bmatrix} \frac{E_x^{r+1}}{E_x^r} & \frac{\nu_{xy}^{r+1}}{\nu_{xy}^r} & \frac{\nu_{xx}^{r+1}}{\nu_{xx}^r} & \frac{E_y^{r+1}}{E_y^r} \end{bmatrix}^T \tag{3.49}$$

$$r = \begin{Bmatrix} \frac{\Delta\varepsilon_x^m - \Delta\varepsilon_x^{\wedge}}{\Delta\varepsilon_x^{\wedge}} \\ \frac{\Delta\varepsilon_y^m - \Delta\varepsilon_y^{\wedge}}{\Delta\varepsilon_y^{\wedge}} \end{Bmatrix} \tag{3.50}$$

where:

$$\frac{\partial\Delta\varepsilon_x}{\partial E_x} = -\frac{1}{E_x^2}\left[(1-\nu_{xx})\Delta\sigma_x - \nu_{xy}\Delta\sigma_y\right],$$

$$\frac{\partial\Delta\varepsilon_x}{\partial \nu_{xy}} = -\frac{1}{E_x}\Delta\sigma_y,$$

$$\frac{\partial\Delta\varepsilon_x}{\partial \nu_{xx}} = -\frac{1}{E_x}\Delta\sigma_x,$$

$$\frac{\partial\Delta\varepsilon_x}{\partial E_y} = 0,$$

$$\frac{\partial\Delta\varepsilon_y}{\partial E_x} = \frac{2\nu_{xy}}{E_x^2}\Delta\sigma_x,$$

$$\frac{\partial\Delta\varepsilon_y}{\partial E_x} = -\frac{2}{E_x}\Delta\sigma_x,$$

$$\frac{\partial \Delta\varepsilon_y}{\partial \nu_{xx}} = 0\,,$$

$$\frac{\partial \Delta\varepsilon_y}{\partial E_y} = -\frac{1}{E_y^2}\Delta\sigma_y\,,$$

$\Delta\varepsilon_x^m$ = measured (actual system) radial strain,

$\Delta\varepsilon_y^m$ = measured (actual system) axial strain,

$\Delta\varepsilon_x^\wedge$ = calculated (model) radial strain, and

$\Delta\varepsilon_y^\wedge$ = calculated (model) axial strain.

In order to generate enough elements in the sensitivity matrix (F) and to control row degeneracy, the three stress regimes (triaxial-compression, -shear, and -extension) were combined to give one F-matrix and one r-matrix at each stress state. Thus, at each stress state, Equation 3.46 can be rewritten as:

$$\underset{6X4}{\begin{bmatrix} F^{TC} \\ F^{TS} \\ F^{TE} \end{bmatrix}} \underset{4X1}{\begin{Bmatrix} \alpha \end{Bmatrix}} = \underset{6X1}{\begin{Bmatrix} r^{TC} \\ r^{TS} \\ r^{TE} \end{Bmatrix}} \qquad (3.51)$$

where:

F^{TC} = the sensitivity matrix for triaxial compression regime,

F^{TS} = the sensitivity matrix for triaxial shear regime,

F^{TE} = the sensitivity matrix for triaxial extension regime,

r^{TC} = the r-vector for triaxial compression regime,

r^{TS} = the r-vector for triaxial shear regime, and

r^{TE} = the r-vector for triaxial extension regime.

At a particular stress state, Equation 3.51 is needed by the parameter adjustment algorithm to determine vertical and horizontal moduli, as well as the vertical and horizontal Poisson’s ratios. The shear modulus can be determined from Equation 3.39.

CHAPTER IV

LABORATORY TESTING

4.1 Equipment

The triaxial test cell was used for testing samples in this study. Triaxial testing data have been traditionally used to provide input for the material properties in pavement structural models. The triaxial test has been used with notable success in the field of geotechnical engineering for applications such as earthquake and tunnel modeling as well as pavements.

Tests are performed on materials to establish their engineering properties and these properties are then used in a structural model to determine the stresses and strains that lead to performance predictions. By setting boundary conditions in the structural model, it is not necessary for a material property test to exactly mimic the field condition. However, the testing should, if practical, span a range of expected conditions so that extrapolations used by the structural model are kept to a minimum.

In the past, the traditional fluid-filled geotechnical type triaxial cell, that enables confining pressure to be applied to a specimen while a range of vertical loads are applied, has been the major apparatus used in this type of testing. However, the amount of time and attention to detail necessary to set up and carry out tests with this equipment make it unsuitable for production use in the field for Quality-Control/Quality-Assurance purposes (QC/QA). One other problem associated with the traditional triaxial cell is that the membrane around the sample is secured to top and bottom platens with rubber bands (O-rings). This assembly system induces high shear stresses at the top and bottom of samples tested. To eliminate this problem, it is highly encouraged that sample sizes be maintained at a 2.0 height to diameter ratio.

In this study, the Rapid Triaxial Testing (RaTT) cell system developed by Industrial Process Controls (IPC) Melbourne, Australia, was used for testing. The RaTT cell system is based on a concept that was conceived in Texas Transportation Institute

(TTI) and has been in use with the Texas Department of Transportation (TxDOT). Unlike the traditional triaxial cell, the RaTT cell uses a larger diameter confining cylinder around the specimen, which is fitted with an internal rubber membrane that can be inflated to apply confining pressure to the specimen. The rubber membrane is not rigidly fastened to the top and bottom platens and thus there is a relatively uniform distribution of stresses within the height of samples during testing.

The IPC system provides automated control of cell movement to simplify specimen handling, and computer control of both confining and axial stress, together with Linear Variable Differential Transducers (LVDTs) for vertical and horizontal strains. Figures 4.1 and 4.2 are pictures with the cell lowered and raised, respectively of the RaTT cell.

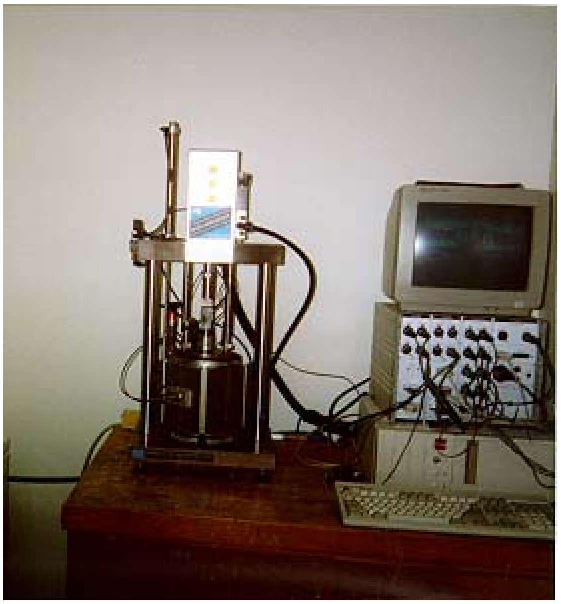

Figure 4.1 Lowered RaTT Cell.

Figure 4.2 Raised RaTT Cell.

Automated control of the physical movement of the cell turns the extremely tedious job of getting a specimen in and out of a standard geotechnical cell and positioning all the instrumentation in the standard cell into a quick and easy operation taking less than a minute. Servo-control of the cell pressure enables a vacuum to be applied to the cell, which draws the pressure membrane and the horizontal LVDT away from the sides of the specimen. Once the vacuum has been applied, a pneumatic actuator lifts the entire cell up out of the way so that the previously tested specimen may be removed and the next specimen may be placed in position. The cell may then be lowered over a new specimen on the command of the operator using a single keystroke command to the software.

The apparatus can perform tests at multiple frequencies as well as multiple stress states. This capability enables the machine to quantify not only time-dependent responses, but also stress-dependent responses of the material, two features that are required for flexible pavement materials characterization.

The IPC RaTT cell is supported by software that provides researchers and engineers with a tool capable of conducting a range of uniaxial or multiaxial loading tests on both bound and unbound construction materials. The software can be specifically customized to provide the operator with a unique testing sequence and output. Other researchers have customized the RaTT cell to fit their specific needs and purposes. Examples are the University of Illinois Fast Cell (UIFC) and the TUDelft (The Netherlands) cell.

4.2 Materials

Four base material types, California granite, Texas crushed limestone, Texas gravel and Minnesota gravel were tested in the laboratory to determine their cross-anisotropic elastic properties.

These materials were selected based on material variability, usage, and on-going research. The California granite and the Texas limestone are rough textured, angular crushed rock, the Texas gravel is rounded pit gravel, and the Minnesota gravel is rounded glacial sandy gravel. A comprehensive laboratory study was performed to determine the cross-anisotropic elastic properties of the four materials. Three different gradations, well-graded, fine-graded and coarse-graded, were prepared for all aggregate types and the samples were tested at optimum, wet of optimum, and dry of optimum moisture contents. Table 4.1 and Figure 4.3 show the three gradations batched. Three sample replicates were prepared at each moisture and gradation condition. Table 4.2 is a laboratory test matrix that was generally followed to complete the testing phase of this study.

Thus, in the original test matrix, a total of 108 samples (4 materials by 3 gradations by 3 moisture levels by 3 replicates) were to be prepared. A few samples were abandoned because they were both difficult to compact at the levels of moisture and gradation or were too soft and unstable to test.

Table 4.1 Gradation

Sieve Size (mm)	Percent Passing (%)		
	Fine Graded	Well Graded	Coarse Graded
25.00	100	100	100
19.00	85	85	85
12.50	74	74	72
9.50	70	66	62
4.75	67	54	40
2.36	62	41	25
1.18	52	30	18
0.60	42	23	14
0.30	34	18	10
0.15	28	14	8
0.075	20	10	7

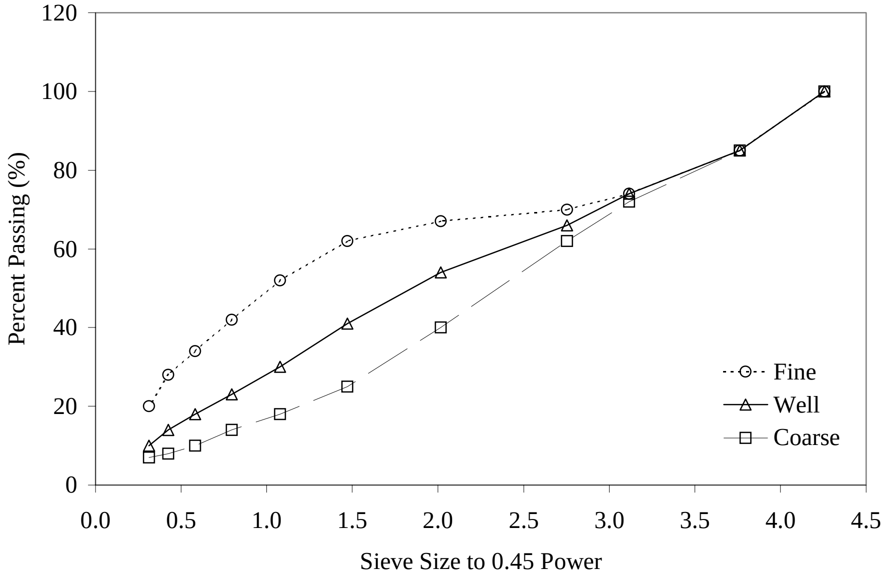

Figure 4.3 Gradation on a 0.45 power Sheet.

Table 4.2 Test Matrix.

Moisture Conditions	Aggregate Source											
	Texas Limestone			Texas Gravel			Minnesota Gravel			California Granite		
	Gradation											
	C	W	F	C	W	F	C	W	F	C	W	F
Wet	3	3	3	3	3	3	3	3	3	3	3	3
Optimum	3	3	3	3	3	3	3	3	3	3	3	3
Dry	3	3	3	3	3	3	3	3	3	3	3	3

Key:

C- Coarse-graded

W- Well-graded

F- Fine-graded.

4.3 Sample Size

The implication of preparing samples with height to diameter ratio of 1:1 instead of the traditional 2:1 ratio used in triaxial testing was investigated. In geotechnical engineering the triaxial test is used to determine the shear strength parameters of soils. The problem being analyzed usually dictates the rate of shear and drainage conditions applied to the cylindrical sample.

Some modifications have been made to the traditional triaxial test for pavement engineering applications. In pavement engineering, the repeated load triaxial test is preferred to the triaxial shear test.

In the repeated load triaxial test, a static confining stress is usually applied to the cylindrical sample and a deviatoric stress is axially cycled for a predetermined number of times. The transient loads are chosen so that they best represent typical stress conditions within a pavement. Charts are available that can be used to select the cycle of a transient load (Barksdale, 1971). A typical transient load consists of a 1.0-second cycle sinusoidal load consisting of 0.1-second load duration and a 0.9-second rest. This load cycle simulates the application of traffic loads on the pavement.

The main disadvantage of the cylindrical triaxial test is the non-uniform distribution of stresses and deformations within specimens. This non-uniformity is mainly caused by the presence of friction at the soil-platen interface (Figure 4.4). The friction is a result of soil-platen interaction and it is compounded by rubber bands (O-rings) used to rigidly secure the membrane around the sample to the top and bottom platens. This problem has been addressed in past by using lubricated platens for triaxial test.

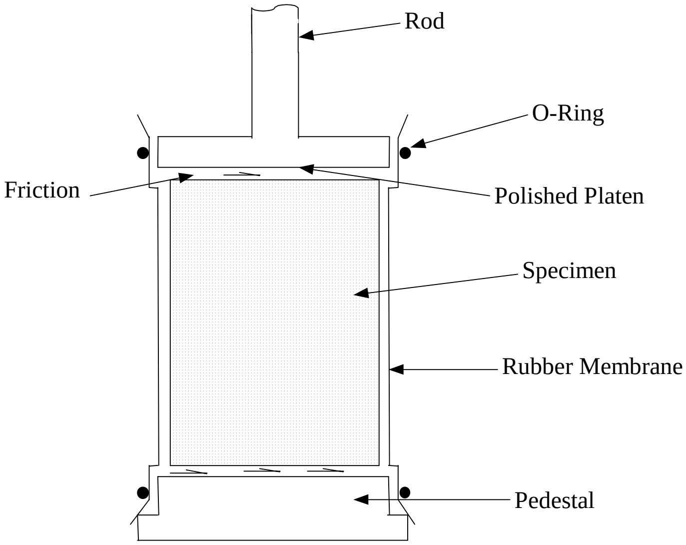

Figure 4.4 Triaxial Tests Set-up.

Experimental work done by Taylor (1941) indicates that reliable results could be obtained with soil specimens having regular ends provided the slenderness (height to diameter ratio, *l*/*d*) is in the range of 1.5 to 3.0. According to Lee (1978) this study established the standard that the slenderness (*l*/*d*) of triaxial specimens for soil be limited to 2.0-2.5 for tests with regular ends. Since then, many researchers (Rowe *et al*., 1964; Bishop *et al*., 1965; Duncan *et al*., 1968; Lee, 1978) have studied end restraint effects on the shear strength of soils and concluded that sample slenderness can be reduced to 1.0 if frictionless platens are used. Rowe and Barden (1964) concluded that if the friction angle between the soil and the end platen can be kept below 1°, end restraint effects can be considered negligible and the end platens can be considered to be ‘‘frictionless’’.

The drained shear strength of soils using regular ends and *l*/*d* = 2.0 are reduced by up to 10% when frictionless ends are used. For an undrained test, the shear strength is reduced by about up to 5% when frictionless ends are used. Consider a failed cylindrical soil sample with ϕ-value of 40°, where the failure plane makes an angle θ with the horizontal (Figure 4.5), then fundamentals of geometry suggests that the height to diameter ratio of the sample must be tan (45+ϕ/2) = 2.1.

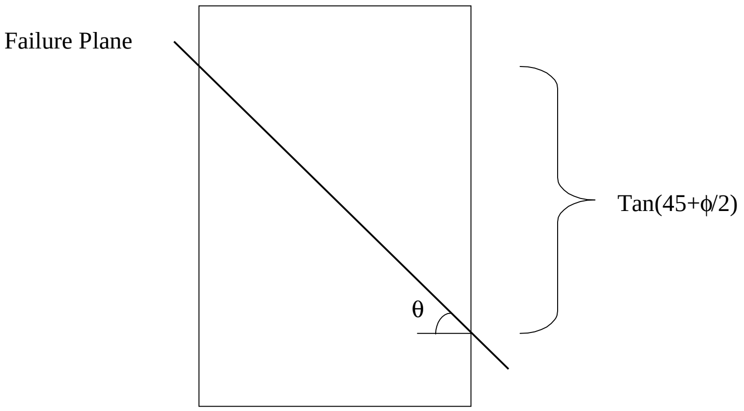

Figure 4.5 Failed Cylindrical Sample.

Frictionless ends allow the use of shorter sample sizes (*l*/*d* = 1) in a triaxial test. Laboratory samples with a height to diameter ratio of 1:1 appear to be more stable and practical for unbound granular layers in pavements. Unbound granular layers in pavements are usually compacted in lifts of 150-mm (6-in) to reduce the existence of density gradients. However, the conventional 2:1 sample height to diameter ratio in traditional triaxial shear test has been maintained in the development of repeated load triaxial test for pavement application. It is important to know whether maintaining a 2:1 sample size is better than the more stable and practical 1:1 sample size.

Unlike the traditional triaxial cell, the RaTT cell shown in Figure 4.6 uses a larger diameter confining cylinder around the specimen, which is fitted with an internal rubber membrane that can be inflated to apply confining pressure to the specimen. A smooth plastic coated paper is placed between the soil-platen interfaces to facilitate easy lateral displacement of the sample during testing. The rubber membrane is not rigidly fastened to the top and bottom platens by O-rings, and this produces a relative reduction in friction at the soil-platen interface.

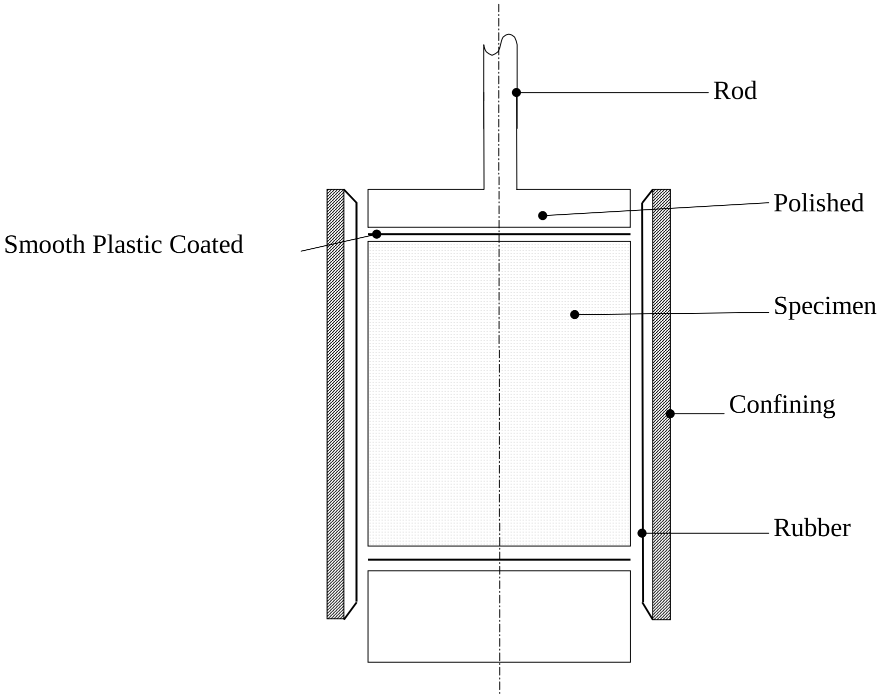

Figure 4.6 Rapid Triaxial Tester.

4.3.1 Stress Distribution in a Cylindrical Sample

Balla (1960) analytically solved for stresses and strains in a cylindrical specimen with any height to diameter ratio and subjected to axial and radial loads. Balla also studied the influence of end restraint at different degrees of roughness. The modern computer and finite element method have now made it easier to numerically study the distribution of stresses within a triaxial specimen with different sizes.

A finite element method was used to numerically determine the distribution of stresses in a cylindrical sample subjected to unconfined compression, which is illustrated in Figure 4.7. The material property was assumed to be linear isotropic. The distribution of stresses was determined for both fixed and frictionless platens.

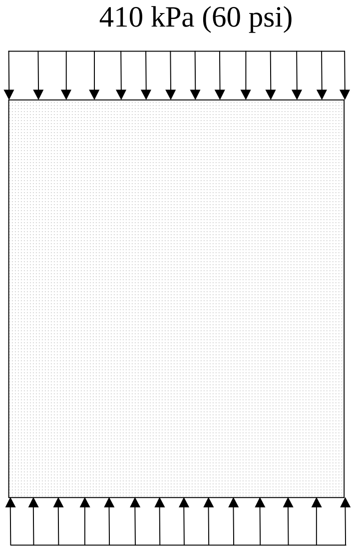

Figure 4.7 Unconfined Compression.

Figures 4.8 and 4.9 are axisymmetric finite element meshes for a frictionless platen and a fully fixed platen, respectively. The frictionless mesh represents a sample with fully lubricated end platens, and the fixed mesh represents a sample with maximum friction. The platen conditions of a traditional triaxial sample with regular end caps are assumed to be very similar to the fixed mesh, and the RaTT cell is assumed to be more similar to the frictionless mesh.

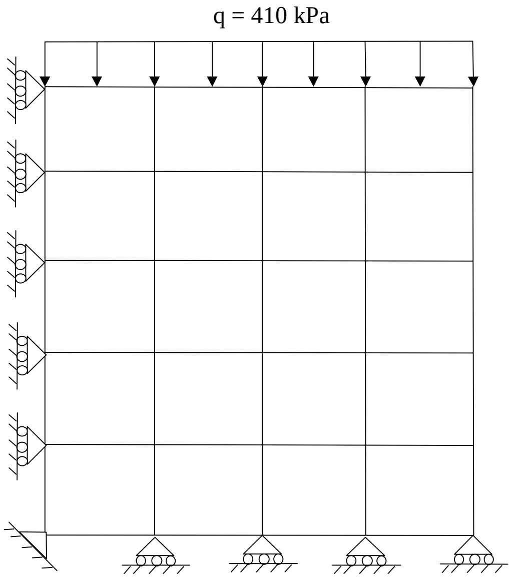

Figure 4.8 Axisymmetric Mesh for a Frictionless Platen.

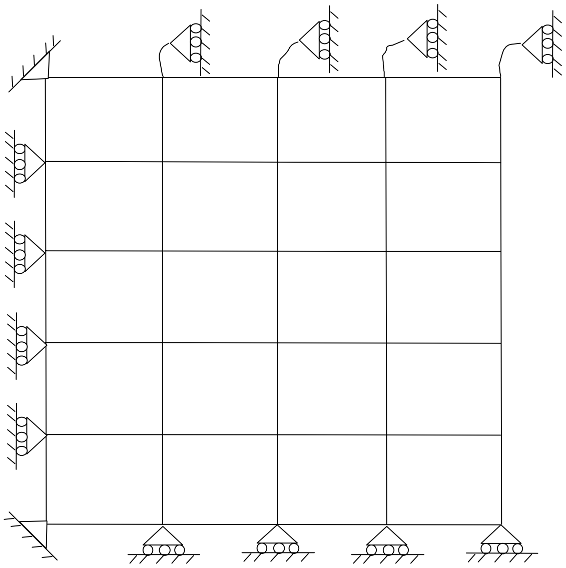

Figure 4.9 Axisymmetric Mesh for a Fixed Platen.

Figures 4.10 and 4.11 show the distribution of vertical and shear stresses, respectively, obtained from the finite element analysis of samples with a 1:1 height to diameter ratio. Figures 4.12 and 4.13 are plots of vertical and shear stresses, respectively, obtained for samples with a 2:1 height to diameter ratio. No shear stresses develop in samples with frictionless platens, and the distributions of vertical stresses are uniform within the sample. The frictionless platen allows the sample setup to fulfill the main purpose of producing principal stresses and measuring strains in a sample. High shear stresses develop at the ends and diminish at the mid-height of a sample with regular end platens. The developments of high shear stresses at the ends of a regular platen induce a non-uniform distribution of vertical stresses within the sample. The vertical stresses at the ends increase and converge to a uniform value in the middle of the specimen. For a frictionless platen, the distribution of shear and vertical stresses remain the same when the sample dimension is increased from 1:1 to 2:1 height to diameter ratio. When the sample size is changed from 1:1 to 2:1, the portion in the sample where shear stresses diminish for a uniform distribution of vertical stresses increases, as shown in Figures 4.10 to 4.13.

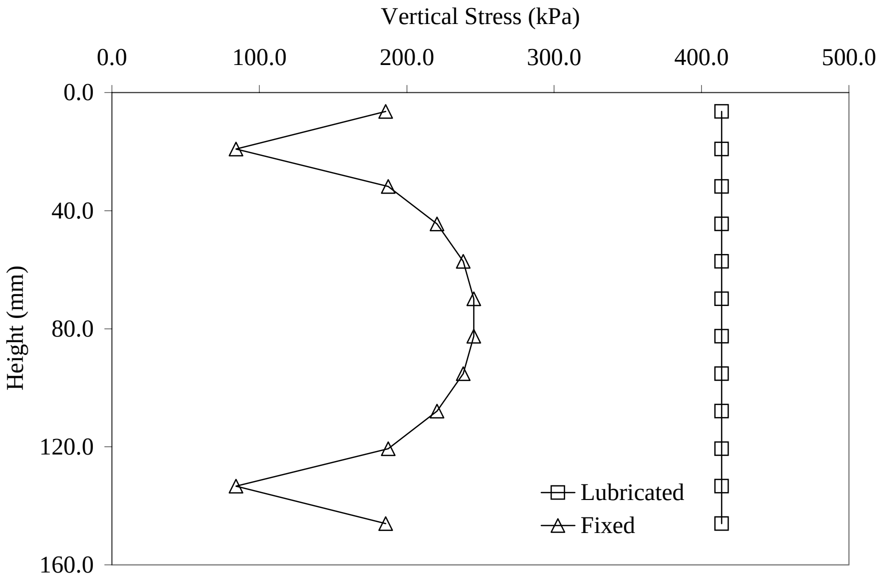

Figure 4.10 Distribution of Vertical Stresses in 1:1 Sample Size.

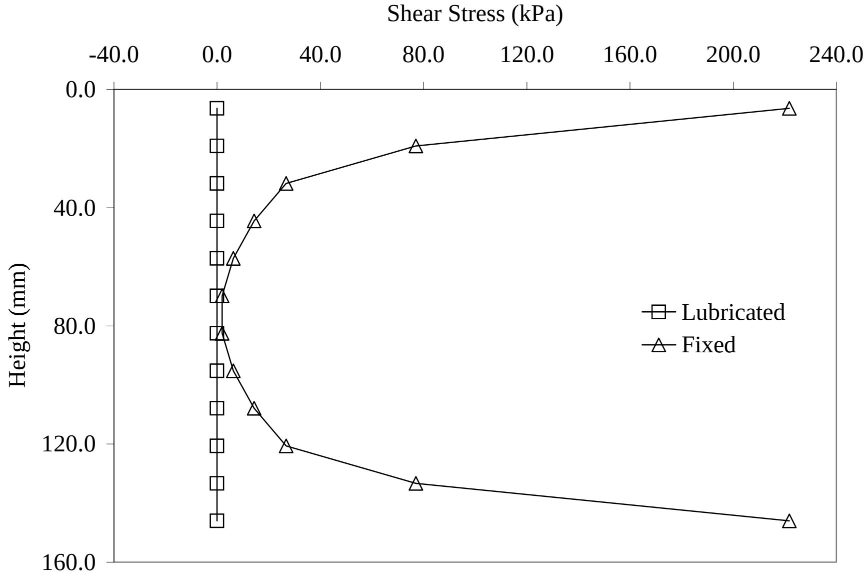

Figure 4.11 Distribution of Shear Stresses in a 1:1 Sample Size.

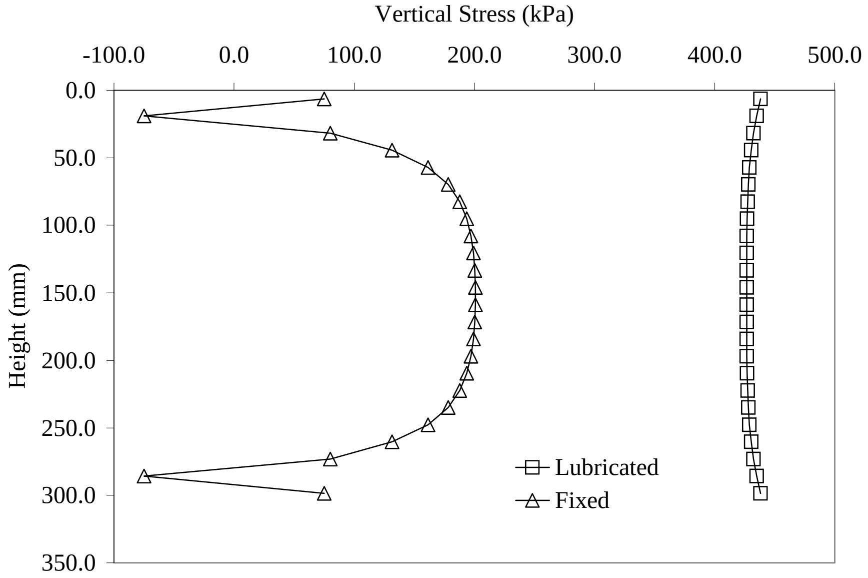

Figure 4.12 Distribution of Vertical Stresses in a 2:1 Sample Size.

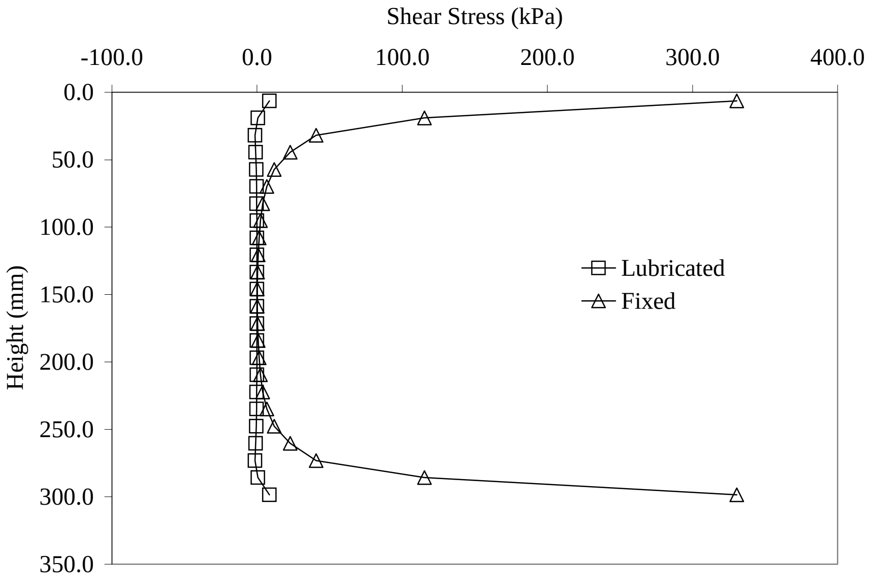

Figure 4.13 Distribution of Shear Stresses in a 2:1 Sample Size.

Figures 4.10 through 4.13 suggest that the presence of friction at the end platens of a triaxial specimen induce non-uniform stresses within the sample. However, if a uniform stress distribution can be induced in the middle portion of the sample, the end restraint effect can be acceptable. Increasing the height to diameter ratio does not eliminate the non-uniform stress distribution but rather increase the portion where shear stresses are acceptably diminished. Lubricating the end platens eliminates non-uniform stress distributions and development of shear stresses.

4.3.2 Preliminary Testing

The effect of reducing the sample height to diameter ratio from 2.0 to 1.0 in the repeated load triaxial test was investigated through laboratory testing. Since stresses and strains induced in a sample are well below the failure stress, it is expected that reducing the sample size would not have significant effects on the resilient modulus.

A base material was tested in general accordance with AASHTO T-294. Two sample sizes were prepared at the same moisture content in accordance with AASHTO

T-180. The sample sizes were 300-mm high by 150-mm diameter (2:1) and 150-mm high by 150-mm diameter (1:1). The samples were tested using the standard triaxial cell with regular end platens. Testing was performed at the University of Wisconsin and the University of Illinois.

Figure 4.14 shows plots of resilient modulus versus bulk stress for both sample sizes. A dummy variable analysis was performed on the resilient modulus values plotted in Figure 4.14 to determine whether the use of 1:1 sample size significantly affects the resilient modulus values. A summary of the statistic obtained is given as (Milton and Arnold, 1995):

$$y = \beta_0 + \beta_1 x_1 + \beta_2 x_2 \tag{4.1}$$

where

y = resilient modulus,

x_1 = bulk modulus,

x_2 = 1 if 1:2 sample size is used, and 0 if 1:1 sample size is used.

$\beta_0 = 165.1$, $\beta_1 = 0.361$, and $\beta_2 = 1.284$

and,

Sum of squares error, SSE = 25122.74

Variance, $\sigma = 30.5$

$T_{27} = 0.115$

Based on this statistic, we do not reject the hypothesis that H_0: $\beta_2 = 0$ at the 99.9% level of confidence. It can be concluded that the sample size used is not an important factor in predicting the resilient modulus of the samples tested. This suggests that even in a standard triaxial cell with regular end platens where friction is assumed to exist, resilient modulus values were not affected by the sample size. This observation may be due to the fact that the stresses applied in the resilient triaxial test are well below the failure stress.

As a result, the maximum particle size of a base material must be the limiting factor in choosing sample size in a repeated load triaxial test. Instead of the traditional 2:1 sample height to diameter ratio, the more stable and practical size of 1:1 can be used in repeated load triaxial test. Throughout this study, 1:1 height to diameter ratio samples was prepared for testing. The selection of 1:1 height to diameter ratio samples is further justified by the fact that the level of end friction in RaTT is relatively lower than the traditional triaxial cell with regular platens.

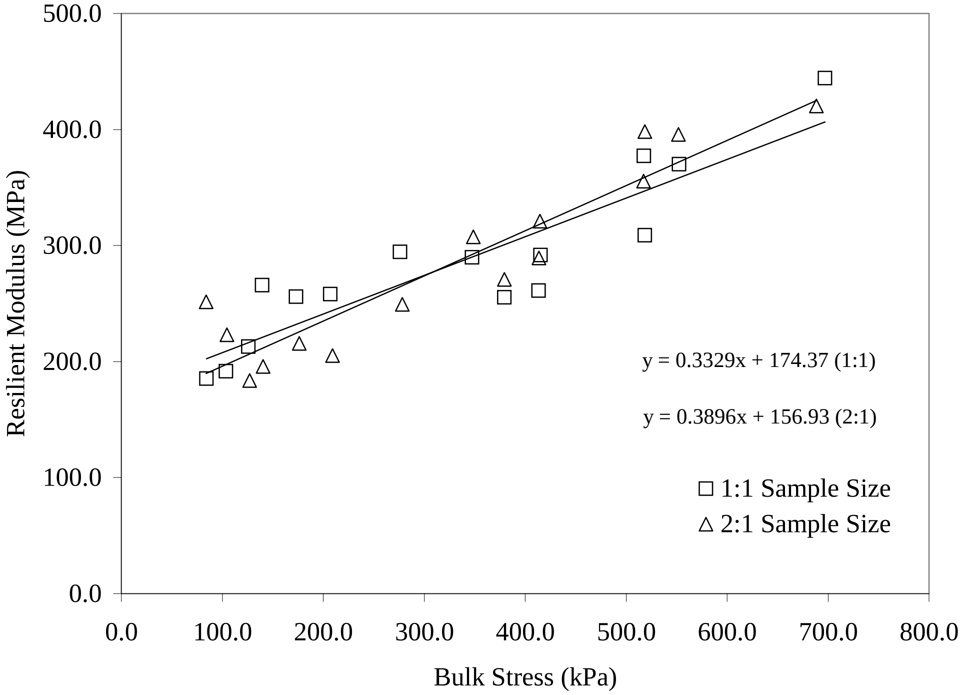

Figure 4.14 Resilient Modulus versus Bulk Stress.

4.4 Preparation of Samples

The mechanical properties of unbound granular layers are improved through compaction. Compaction forces the individual particles of unbound granular materials together and enhances increased particle-to-particle contact. Increasing densities through compaction increases the load carrying capacity of unbound granular layers. Allen (1973) and Marek et al. (1974) demonstrated that the decrease in permanent deformation for small increases in density through compaction is very significant.

The laboratory compaction characteristics of unbound granular materials are important to the behavior and performance of a flexible pavement. Three different compaction methods; impact, vibratory and gyratory shear were investigated in this study to determine their effects on the anisotropic properties of unbound granular materials. For each compaction method, two different compactive efforts were investigated.

4.4.1 Compaction Methods

There are five major compaction methods that are commonly used to fabricate unbound aggregate specimens for laboratory testing. These methods are briefly described below (Milberger et. al., 1966).

4.4.1.1 Impact Compaction

The first scientific approach to determine laboratory compaction characteristics of soils is credited to R.R Proctor (1933). His procedure was slightly revised and adopted as a standard by the American Association of State Highway Officials in 1939 (AASHTO Designation: T-99). It was later modified to allow higher compaction effort (AASHTO Designation: T-180). In these methods, the sample is compacted in a rigid mold by dropping a hammer of known weight from a specified height. One of the main disadvantages of the impact compaction method is that aggregate orientation and distribution are dissimilar to that achieved in field compaction. As a result, it is difficult to achieve reproducible results, and there are some disparities in the stress-strain distributions predicted in the pavement structure based on the laboratory-derived resilient moduli. The primary variables that can be controlled in impact compaction are the weight of the hammer, the height of hammer drop, and the number of blows per layers. If any of these are increased to achieve high densities at low moisture contents, much of the additional compactive energy is spent in degrading the material rather than in compacting it.

4.4.1.2 Static Compaction

As the name suggests, samples are compacted in a rigid mold by applying static compressive stresses to plungers on one or both ends of a specimen. There is no standard method for applying this method to unbound granular materials. The compaction characteristics and particle orientation achieved by this method do not reproduce field compaction. Also, friction between the particles and the mold walls tend to produce significant density gradients within the sample (Milberger et. al., 1966).

4.4.1.3 Kneading Compaction

Conventional field compaction equipment such as the sheepsfoot and rubber-tired rollers apply loads with little or no impact, but they produce some kneading action. According to Milberger et. al. (1966) the California Highway Department developed a mechanical kneading laboratory compactor in 1937. A revised design of this compactor was adopted in a standard procedure (AASHO T-173). This method of compaction is not widely used by highway agencies. Although particle distribution and orientation closely matches field compaction, some hand finishing is required to prepare samples for testing in the laboratory (Milberger et. al., 1966).

4.4.1.4 Vibratory Compaction

In this method, the material is confined in a rigid mold, and a surcharge weight is placed on the surface of the material. Either the wall of the mold is tapped or the entire mold is placed on a vibrating mechanism. Vibratory compaction has been successfully applied to the compaction of dry cohesionless soils, primarily sands. The advent of hand held vibratory equipment has increased the use of vibratory compaction methods for preparing unbound granular material specimens. Here, layers of material, usually 50-mm (2-in layers), are compacted to predetermined densities using hand held vibrators in a rigid mold. Material degradation is reduced using vibratory compaction (Milberger et. al., 1966).

4.4.1.5 Shear Gyratory Compaction

In the early 1940's the Texas Highway Department began compacting specimens by gyratory shear action (Milberger et. al., 1966). In this method a known stress is applied to a sample in a rigid mold after the mold has been inclined at an angle. The mold is rotated at an angle with a stress applied to the sample until the desired density is achieved. Application of gyratory compaction to asphalt concrete mixtures was one of the major contributions of the Strategic Highway Research Program (SHRP). This method is also widely used in Texas to compact unbound granular materials and bituminous-stabilized bases. The Texas Department of Transportation (TxDOT) has a standard procedure (Test Method Tex-126-E) for compacting unbound granular and bituminous base materials with a gyratory compactor. The applied stress and time or number of gyrations can be varied to achieve a desired density at specific moisture contents. Researchers at Texas Transportation Institute (Moore and Milberger 1968) investigated the issue of density gradient, and it was concluded that if the sample height to diameter ratio is kept below about 1.4, a uniformly compacted specimen is generally achieved.

Figure 4.15 shows a picture of the gyratory compactor. The development and validation of the gyratory compactor for use in molding unbound granular materials can be found in Milberger and Dunlop (1966) and Moore and Milberger (1968). According to Milberger and Dunlop (1966) the particle distribution and orientation in samples compacted with the gyratory compaction method closely matches field compaction.

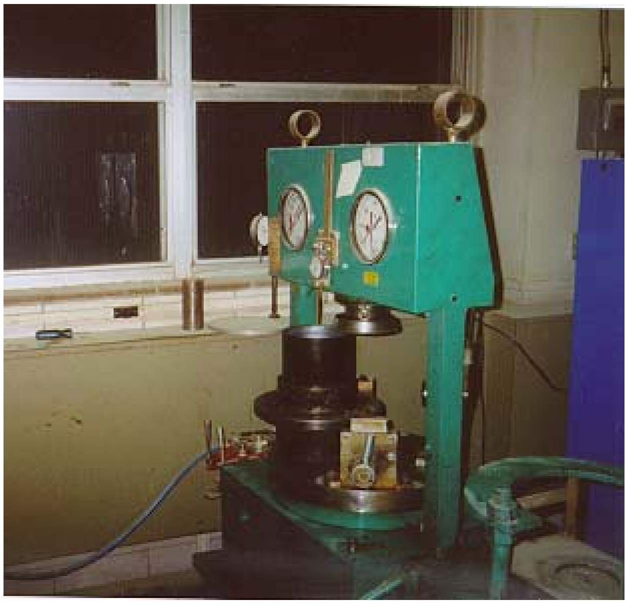

Figure 4.15 Texas Gyratory Compactor.

In this study, 150-mm (6-in) diameter and 150-mm (6-in) height samples were molded with the Texas Gyratory Compactor for testing. Some samples were prepared using the gyratory, vibratory and impact compaction methods. The specimens in the text matrix (Table 4.2) were prepared using the gyratory compactor. Only a few samples were compacted using the impact and vibratory compactors. The purpose of using the impact and vibratory compactors is to evaluate the effect of compaction type and effort on the cross-anisotropic properties of unbound granular materials. It is assumed that the level of cross-anisotropy in a sample is related to particle orientation and thus different compaction methods and efforts would result in different levels of anisotropy. The static and kneading compactors were not used on preparing any of the samples tested because these compactors were not available in the laboratory at the time of this study.

Two materials, well-graded Texas limestone and well-graded Texas gravel, were used to study the effect of compaction on cross-anisotropic properties. The other materials, Minnesota gravel and California granite, were yet to be acquired during the compaction study phase. For each compaction method studied, a low and a high compaction effort were used.

Samples prepared with the impact compaction method were compacted in general accordance with AASHTO T-180, using a 4.54-kg hammer and a 457-mm drop. The samples with high compaction effort were prepared by applying either 50 blows per 50-mm thick layers, and the samples with low compaction effort were compacted using 25 blows per 50-mm thick layers.

For the vibratory compaction method, the higher compaction effort samples were prepared in three lifts (50-mm thick per lift). A hand vibrator was used to compact each lift until AASHTO T-180 density was achieved. The lower compaction effort samples were prepared in two lifts (75-mm thick) until 90% of the AASHTO T-180 density was achieved.

Samples prepared with a high compaction effort using the gyratory compaction method were fabricated by applying 275-kPa pressure on samples inclined at 3° and gyrated for 60 seconds. Lower compaction effort samples were prepared by applying 137-kPa pressure on samples inclined at 3° and gyrated for 45 seconds. The gyratory compactor was set to a constant speed of 30 gyrations per minute. Three lifts of the specimen were compacted statically and then the entire specimens were compacted dynamically. After compaction, the top of the samples was leveled with the same pressure applied during gyrations.

The specimens prepared with the impact and gyratory compaction methods were tested with the Rapid Triaxial Tester (RaTT) using the testing protocol developed in this project in which the anisotropic properties of an unbound granular material are backcalculated using system identification. Details of the testing protocol are discussed in Section 4.5. The specimens prepared with the vibratory compaction method were tested with the University of Illinois FastCell (UIFC). The differences between these two triaxial cells are the mode of application of confining pressure and the range of linear variable differential transformers (LVDTs). The RaTT uses air for confinement and the UIFC uses oil. Also, the LVDTs on the UIFC have a wider deflection range and need to be adjusted for small and large deflections.

4.5 Resilient Testing Protocol

The stresses used in the triaxial testing were chosen to represent the stress conditions induced in a typical base layer of a flexible pavement by traffic loads. The testing protocol itself involves a programmed loading sequence employing ten static stress states. At each static stress state, small dynamic changes in stresses are applied to obtain three triaxial stress regimes such that the net stress changes represent triaxial compression, triaxial shear, and triaxial extension. The resilient axial and radial strains are determined for each stress regime and implemented in the system identification scheme to backcalculate the five anisotropic elastic properties at that particular stress state.

Before each test is started, the specimen is mounted in the RaTT cell as described in the operator's test procedure manuals (IPC, 1998). The loading sequence is outlined in the following steps:

1. A mounted sample is loaded to a static stress state (axial stress σ_y, and confining stress σ_x, shown as static stress in Table 4.3). The confining stress is then kept constant while the axial stress is given a small dynamic stress increment of $\Delta\sigma_y$, shown as triaxial compression in Table 4.3. The incremental loading is applied for 25 repetitions until a stable resilient strain is achieved. A cycle of loading consists of 1.5 seconds loading followed by 1.5 seconds rest period. Since the RaTT cell uses air for confinement, the loading cycle was selected to allow for easy application of variable confinement.
2. At the same static stress state (σ_x, σ_y) as in step 1, the axial stress is changed by a small dynamic stress increment of $\Delta\sigma_y$ for 25 repetitions as before, while the radial stress is reduced by $\Delta\sigma_x$ such that the change in the first stress invariant (ΔI_1) is zero in each load cycle. This is shown as triaxial shear in Table 4.3.
3. At the same controlled static stress state (σ_x, σ_y) as in step 1, the axial stress is reduced by a small amount, $\Delta\sigma_y$, while the radial stress is increased by $\Delta\sigma_x$. Thus, the net change in stress state is in an extension mode but the principal stresses are

not reversed. The dynamic stresses are applied for 25 repetitions as before until stable resilient strains are achieved. This is shown as triaxial extension in Table 4.3.

4. These steps are repeated for the ten different stress states shown in Table 4.3. At each stress state, the resilient axial and radial strains are measured for use as input into the SID scheme.

At the frequencies tested (1.5 seconds loading and 1.5 seconds rest), it takes about one and a half hours to complete testing on one sample at all ten stress states. The measured axial and radial strains at each stress state are used as input to the parameter adjustment routine, Equation 3.51, of the system identification scheme. A computer program was developed that systematically backcalculates the five anisotropic elastic material properties based on the SID method.

After each resilient test, part of the sample is tested for soil potential (suction) in general accordance with ASTM designation D-5298-94. The moisture content of each sample was determined before and after the resilient test in accordance with ASTM D 2216-92.

Table 4.3 Static and Dynamic Stresses.

Stress State	Static Stress (kPa)		Dynamic Stress (kPa)					
			Triaxial Compression		Triaxial Shear		Triaxial Extension	
	σ_y	σ_x	$\Delta\sigma_y^c$	$\Delta\sigma_x^c$	$\Delta\sigma_y^s$	$\Delta\sigma_x^s$	$\Delta\sigma_y^e$	$\Delta\sigma_x^e$
1	40	25	5	0	10	-5	-5	5
2	50	25	10	0	10	-5	-10	5
3	70	40	10	0	10	-5	-10	10
4	130	60	20	0	20	-10	-10	10
5	150	70	20	0	20	-10	-10	10
6	170	100	20	0	20	-10	-20	20
7	220	120	30	0	30	-15	-20	20
8	250	140	30	0	30	-15	-20	20
9	250	120	30	0	30	-15	-20	20
10	250	105	30	0	30	-15	-20	20

4.6 Permanent Deformation Testing

The repeated load triaxial test was also used to study the permanent deformation characteristics of the four aggregate types. The permanent deformation study was performed on only well graded samples compacted at optimum moisture.

Samples of 150-mm height by 150-mm diameter were compacted using the Texas Gyratory Compactor at high compaction effort. The permanent deformation behavior of the materials was studied at four stress levels shown in Table 4.4. At each stress level, static confining stresses were applied to the samples and deviatoric stresses were axially cycled for 10,000 times. The confining and deviatoric stress values are tabulated in Table 4.4. Strains measured are separated into resilient and plastic strains. Plastic strains are then used to characterize the permanent deformation behavior of the material. The deviatoric stress consists of a haversine pulse-load applied for 0.1 seconds with a 0.9 seconds rest at a frequency of 1 cycle per second. This load cycle was used for the permanent deformation test because the confining pressure was not cycled.

Table 4.4 Confining and Deviatoric Stresses for Permanent Deformation.

	Stress Levels			
Stress	1	2	3	4
Confining, σ_3, kPa	70	35	105	70
Deviatoric, $(\sigma_1-\sigma_3)$, kPa	70	105	145	180

CHAPTER V

LABORATORY TEST RESULTS AND ANALYSIS

5.1 General

The liquid limits and plasticity indices (ASTM D 4318-95) of the material tested are tabulated in Table 5.1. The original materials were separated by size down to the #200 sieve, and the individual particle sizes were recombined to obtain well-graded, fine-graded, and coarse-graded samples. The screen sizes used for separation were the same as those given in Table 4.1. It was difficult to compact coarse graded samples of materials with low plasticity indexes (California granite and Minnesota gravel), so coarse graded samples were not molded for these materials.

Table 5.1 Atterberg's Limits.

Specimen	Liquid Limit (%)	Plasticity Index (%)
Texas Gravel	20.2	11.8
Texas Limestone	14.9	4.4
Minnesota Gravel	18.4	2.0
California Granite	11.6	NP

A three-parameter equation (Fredlund and Xing, 1994) was used to fit the three gradations. This equation allows for a continuous fit and proper definition of the extremes of the gradation curve and is given by:

$$P_p = \frac{100}{\ln\left[\exp(1)+\left(\frac{g_a}{d}\right)^{g_n}\right]^{g_m}}\left[1-\left[\frac{\ln\left(1+\frac{d_r}{d}\right)}{\ln\left(1+\frac{d_r}{d_m}\right)}\right]^{7}\right] \qquad (5.1)$$

where:

P_p = percent passing a particular grain-size, d,

g_a = fitting parameter corresponding to the initial break in the grain-size curve,

g_n = fitting parameter corresponding to the maximum slope of the grain-size curve,

g_m = fitting parameter corresponding to the curvature of the grain-size curve,

d = particle diameter (mm),

d_r = residual particle diameter (mm), and

d_m = minimum particle diameter (mm).

Non-linear regression analysis was used to obtain the three parameters of Equation 5.1 that fit the three gradations considered. The values of the parameters are tabulated in Table 5.2.

Table 5.2 Gradation Parameters.

Parameter	Coarse Graded	Well Graded	Fine Graded
g_a	13.272	11.997	4.726
g_n	0.988	0.976	1.361
g_m	2.414	1.544	0.685

At each gradation, three moisture levels were used in molding the samples. The samples were compacted dry of optimum, at optimum and wet of optimum. Three replicate samples were compacted at each moisture and gradation combination. Some samples were abandoned because they were both difficult to compact at the levels of moisture and gradation or were too soft and unstable to test.

The samples were compacted with the Texas Gyratory Compactor (TGC). A few of the samples were compacted with the impact hammer and the vibratory compactor. The purpose of using the impact and vibratory compaction methods was to investigate the effect of compaction method and level on the mechanical properties of the materials.

The average values and standard deviation (in brackets) of dry densities, molding moisture contents and matric suction are tabulated in Table 5.3 through Table 5.6.

Table 5.3 Moisture Content and Dry Densities for Texas Limestone.

	Coarse	Well			Fine		
	Optimum	Dry	Optimum	Wet	Dry	Optimum	Wet
Moisture Content (%)	2.8	3.5	4.1	4.9	4.7	5.4	5.9
	(0.2)	(0.1)	(0.04)	(0.1)	(0.1)	(0.3)	(0.2)
Matric Suction (kPa)	19.3	49.0	17.9	12.7	55.7	20.5	16.2
Dry Density (kg/m^3)	2144	2260	2350	2315	2251	2302	2334
	(3.5)	(11.7)	(7.9)	(2.6)	(18.7)	(16.7)	(8.3)

Table 5.4 Moisture Content and Dry Densities for Texas Gravel.

	Coarse	Well			Fine	
	Optimum	Dry	Optimum	Wet	Dry	Optimum
Moisture Content (%)	5.5	5.5	7.7	9.3	5.4	7.5
	(0.7)	(0.1)	(0.2)	(0.1)	(0.2)	(0.1)
Matric Suction (kPa)	14.8	29.6	15.4	8.9	94.7	51.2
Dry Density (kg/m^3)	2020	2062	2240	2079	2075	2210
	(78.9)	(60.2)	(54.5)	(13.4)	(14.5)	(9.2)

Table 5.5 Moisture Content and Dry Densities for Minnesota Gravel.

	Well			Fine	
	Dry	Optimum	Wet	Dry	Optimum
Moisture Content (%)	4.5 (0.2)	6.2 (0.1)	7.7 (0.2)	4.7 (0.2)	7.6 (0.1)
Matric Suction (kPa)	1179.8	21.8	8.9	3705.3	50.6
Dry Density (kg/m^3)	2139 (37.9)	2167 (11.3)	2240 (7.2)	2159 (14.7)	2296 (8.1)

Table 5.6 Moisture Content and Dry Densities for California Granite.

	Well			Fine		
	Dry	Optimum	Wet	Dry	Optimum	Wet
Moisture Content (%)	3.5 (0.2)	4.0 (0.1)	4.6 (0.2)	4.1 (0.3)	4.6 (0.1)	5.9 (0.1)
Matric Suction (kPa)	116.2	28.0	21.5	268.4	26.7	10.3
Dry Density (kg/m^3)	2179 (31.4)	2218 (7.5)	2192 (5.1)	2177 (11.4)	2215 (4.8)	2278 (6.7)

5.2 Resilient

Samples, 150-mm diameter by 150-mm height, were compacted and tested in the IPC RaTT cell. Each sample was tested at the ten static stress states described in the previous Section 4.5. At each stress state, small stress changes were applied to the sample so that the net changes in stresses are a triaxial compression, triaxial shear and triaxial extension. The static stresses applied are typical stresses induced in an unbound granular base layer due to traffic loads. These static stresses are well below the failure envelope of unbound granular materials. Figures 5.1 and 5.2 are plots of static stresses and small stress changes applied to a single sample at the ten stress-states in a σ_1-σ_3 and $\sqrt{J_2^{/}}$-I_1 stress space, respectively.

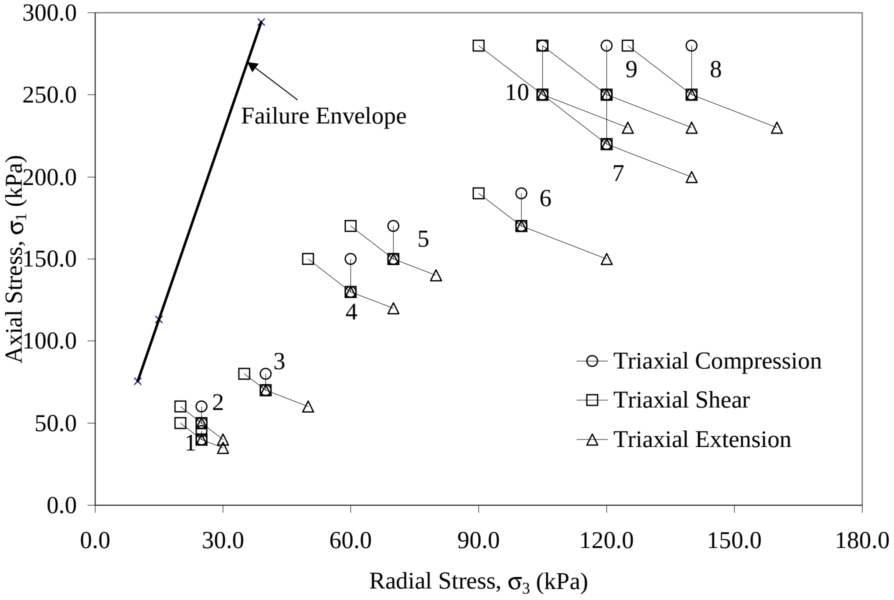

Figure 5.1 Applied Stresses in a σ_1-σ_3 Stress Space.

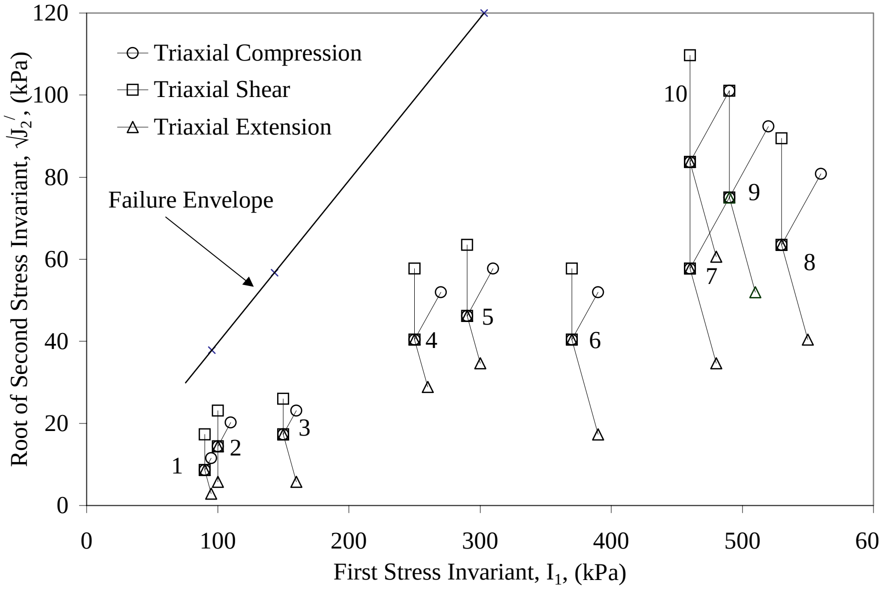

Figure 5.2 Applied Stesses in a $\sqrt{J_2^{/}}$-I_1 Stress Space.

The resilient axial and radial strains due to small stress changes were measured at each stress state and used as input into the system idenfication scheme to compute the resilient moduli and Poisson's ratios. The values of static stresses and average resilient strains (axial and radial) due to small stress changes are tabulated in Table 5.7 for a well graded Texas limestone compacted at optimum moisture. The corresponding standard deviation are tabulated Table 5.8. Similar results were obtained for the other combination of gradations and moisture levels in the test matrix and are tabulated in Appendix A.

Table 5.7 Average Resilient Strains for Texas Limestone at Optimum Moisture.

Stress State		Triaxial Compression		Triaxial Shear		Triaxial Extension	
Stress (kPa)		Strain (με)		Strain (με)		Strain (με)	
Axial	Radial	Axial	Radial	Axial	Radial	Axial	Radial
40.0	25.0	28.6	-12.4	98.0	-78.1	-72.4	51.1
50.0	25.0	51.0	-24.6	78.7	-72.3	-100.3	74.9
70.0	40.0	38.7	-16.7	54.1	-41.5	-97.1	75.4
130.0	60.0	50.5	-22.2	74.4	-67.0	-49.2	46.3
150.0	70.0	44.2	-19.2	64.5	-55.3	-42.7	39.3
170.0	100.0	41.6	-16.2	57.1	-39.3	-89.3	68.1
220.0	120.0	53.7	-19.0	73.4	-53.3	-67.9	53.0
250.0	140.0	47.7	-15.9	64.0	-43.1	-57.6	42.1
250.0	120.0	49.0	-17.4	66.6	-52.9	-60.2	51.5
250.0	105.0	48.3	-19.7	68.8	-63.1	-54.6	49.0

Table 5. 8 Standard Deviation of Resilient Strains for Texas Limestone at Optimum Moisture Content.

Stress State		Triaxial Compression		Triaxial Shear		Triaxial Extension	
Stress (kPa)		Standard Deviation		Standard Deviation		Standard Deviation	
Axial	Radial	Axial	Radial	Axial	Radial	Axial	Radial
40.0	25.0	0.6	0.4	1.0	0.3	1.2	0.4
50.0	25.0	3.0	1.8	6.2	11.1	7.7	9.7
70.0	40.0	1.7	1.3	3.7	4.6	5.5	5.5
130.0	60.0	1.8	1.6	4.7	6.8	4.2	4.2
150.0	70.0	0.7	0.8	4.4	6.3	1.4	3.0
170.0	100.0	2.8	0.6	4.0	2.8	4.7	3.3
220.0	120.0	2.0	2.1	4.7	6.4	6.5	3.8
250.0	140.0	1.9	1.3	3.9	4.6	4.4	3.9
250.0	120.0	1.9	1.0	2.2	4.2	2.5	3.4
250.0	105.0	2.9	2.4	5.4	11.0	3.7	7.2

The measured axial and radial resilient strains are the actual system outputs of the system identification method. The measured resilient strains act as a nerve center of the parameter adjustment algorithm of the SID scheme. Therefore, it is very important to obtain accurate measurements of the resilient strains. In this study, the resilient strains were measured with externally mounted Linear Variable Differential Transducers (LVDTs). The LVDTs used are very sensitive to changes in deflection and were suitable for this study. Two LVDTs each were used to measure axial and radial resilient strains, respectively and the results are reported as the mean value of these measurements.

A computer program was developed to determine the anisotropic resilient properties of each sample in the test matrix at the ten stress states using the system identification method. Figure 5.3 is a schematic of the program structure for the system identification method. The input parameters include the static and dynamic stresses and the axial and radial resilient strains. Initial values of the five anisotropic resilient properties are then computed from the dynamic stresses and measured strains. The computed initial properties are then used to calculate the model output (calculated strains) from Equations 3.30, 3.32 and 3.40.

The sensitivity matrices *F* and the *r*-vectors can then be obtained from Equations 3.48 and 3.50, respectively, for the three triaxial regimes. The three *F* matrices and three *r*-vectors are then combined to obtain one *F* matrix and one *r*-vector (Equation 3.51). The α-vector is then determined from Equation 3.46 and used to compute a new set of model properties. If the initial values of the five anisotropic properties are precise they will be equivalent to the new set of model properties and the measured strains, and calculated strains will also be equivalent to each other. When this occurs, the system is termed ‘identified’. The criterion for identification is based on the components of the α-vector. In this study, the criterion is 1%, and this means that the system and model properties are equivalent whenever the difference between the measured and calculated strains is less than 1% of the calculated strain. If the 1% criterion is not satisfied, a new set of model output is calculated and the iteration process is continued until the desired criterion is reached.

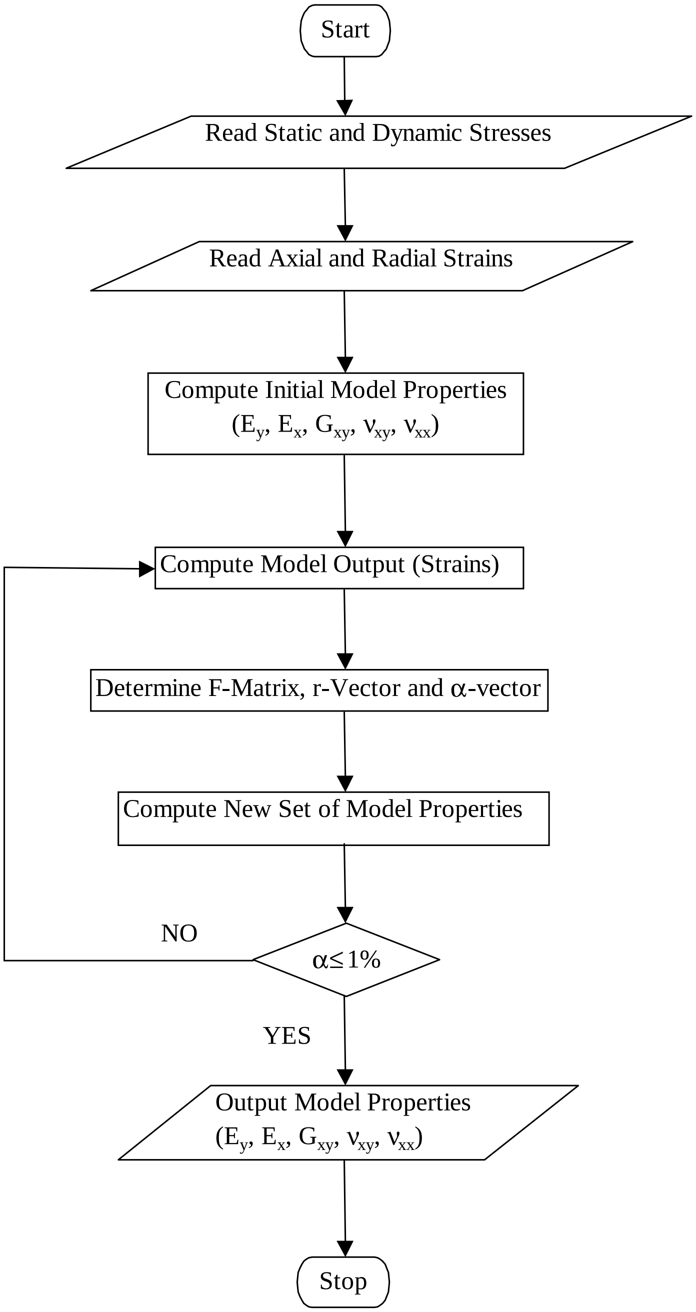

Figure 5.3 Program Structure for the System Identification Method.

As an example, consider the strains obtained at the first stress state for a well-graded Texas crushed limestone at optimum moisture content (Table 5.7).

Step 1 Input Data

Static Axial Stress, σ_y = 40.0 kPa

Static Radial Stress, σ_x = 25.0 kPa

Dynamic Change in Axial Stress for Triaxial Compression, $\Delta\sigma_y^c$, = 5 kPa

Dynamic Change in Radial Stress for Triaxial Compression, $\Delta\sigma_x^c$, = 0 kPa

Dynamic Change in Axial Stress for Triaxial Shear, $\Delta\sigma_y^s$, = 10 kPa

Dynamic Change in Radial Stress for Triaxial Shear, $\Delta\sigma_x^s$, = -5 kPa

Dynamic Change in Axial Stress for Triaxial Extension, $\Delta\sigma_y^e$, = -5 kPa

Dynamic Change in Radial Stress for Triaxial Extension, $\Delta\sigma_x^e$, = 5 kPa

Axial Resilient Strain for Triaxial Compression, $\Delta\varepsilon_y^c$ = 28.6E-06

Radial Resilient Strain for Triaxial Compression, $\Delta\varepsilon_x^c$ = -12.4E-06

Axial Resilient Strain for Triaxial Shear, $\Delta\varepsilon_y^s$ = 98.0E-06

Radial Resilient Strain for Triaxial Shear, $\Delta\varepsilon_x^s$ = -78.1E-06

Axial Resilient Strain for Triaxial Extension, $\Delta\varepsilon_y^e$ = -72.4E-06

Radial Resilient Strain for Triaxial Extension, $\Delta\varepsilon_x^e$ = 51.1E-06

Step 2 Initial Model Parameters:

$$E_y = \frac{\Delta\sigma_y^c}{\Delta\varepsilon_y^c} = \frac{5.0}{28.6E-06} = 174825.17\,kPa$$

$$E_x = \frac{\Delta\sigma_x^s}{\Delta\varepsilon_x^s} = \frac{-5.0}{-78.1E-06} = 64020.49\,kPa$$

$$G_{xy} = \frac{3}{4}\frac{\Delta\sigma_y^s}{(\Delta\varepsilon_y^s - \Delta\varepsilon_x^s)} = \frac{3}{4}\frac{10}{(98.0+78.1)E-06} = 42589.44\,kPa$$

$$\nu_{xy} = \left(\frac{\Delta\sigma_y^s}{E_y} - \Delta\varepsilon_y^s\right)\left(\frac{E_x}{2\Delta\sigma_x^s}\right) = \left(\frac{64020.49}{174825.17} - 98.0E-06\right)\left(\frac{64020.49}{2(-5)}\right) = 0.261$$

$$\nu_{xx} = 1 - \left(\left(\Delta\varepsilon_x^s + \frac{\nu_{xy}\Delta\sigma_y^s}{E_x}\right)\left(\frac{E_x}{\Delta\sigma_x^s}\right)\right)$$

$$= 1 - \left(\left(-78.1E-06 + \frac{(0.261)(10)}{64020.49}\right)\left(\frac{64020.49}{-5}\right)\right) = 0.522$$

<u>Step 3 Model Output (Calculated Strains)</u>:

Calculated Axial Resilient Strain for Triaxial Compression, $\Delta\varepsilon_y^{c\wedge}$

$$\Delta\varepsilon_y^{c\wedge} = -\frac{2\nu_{xy}\Delta\sigma_x^c}{E_x} + \frac{\Delta\sigma_y^c}{E_y} = -\frac{(2)(0.261)(0)}{64020.49} + \frac{5}{174825.17} = 28.60E-06$$

Calculated Radial Resilient Strain for Triaxial Compression, $\Delta\varepsilon_x^{c\wedge}$

$$\Delta\varepsilon_x^{c\wedge} = \frac{\Delta\sigma_x^c(1-\nu_{xx})}{E_x} - \frac{\nu_{xy}\Delta\sigma_y^c}{E_x} = \frac{(0)(1-0.522)}{64020.49} - \frac{(0.261)(5)}{64020.49} = -20.4E-06$$

Calculated Axial Resilient Strain for Triaxial Shear, $\Delta\varepsilon_y^{s\wedge}$

$$\Delta\varepsilon_y^{s\wedge} = -\frac{2\nu_{xy}\Delta\sigma_x^s}{E_x} + \frac{\Delta\sigma_y^s}{E_y} = -\frac{(2)(0.261)(-5)}{64020.49} + \frac{10}{174825.17} = 98.0E-06$$

Calculated Radial Resilient Strain for Triaxial Shear, $\Delta\varepsilon_x^{s\wedge}$

$$\Delta\varepsilon_x^{s\wedge} = \frac{\Delta\sigma_x^s(1-\nu_{xx})}{E_x} - \frac{\nu_{xy}\Delta\sigma_y^s}{E_x} = \frac{(-5)(1-0.522)}{64020.49} - \frac{(0.261)(10)}{64020.49} = -78.1E-06$$

Calculated Axial Resilient Strain for Triaxial Extension, $\Delta\varepsilon_y^{e\wedge}$

$$\Delta\varepsilon_y^{e\wedge} = -\frac{2\nu_{xy}\Delta\sigma_x^e}{E_x} + \frac{\Delta\sigma_y^e}{E_y} = -\frac{(2)(0.261)(5)}{64020.49} + \frac{-5}{174825.17} = 69.40E-06$$

Calculated Radial Resilient Strain for Triaxial Extension, $\Delta\varepsilon_x^{e\wedge}$

$$\Delta\varepsilon_x^{e\wedge} = \frac{\Delta\sigma_x^e(1-\nu_{xx})}{E_x} - \frac{\nu_{xy}\Delta\sigma_y^e}{E_x} = \frac{(5)(1-0.522)}{64020.49} - \frac{(0.261)(-5)}{64020.49} = 57.7E-06$$

Step 4 Determine *F*-matrix, Equations 3.48 and 3.51:

$$F = \begin{bmatrix} F^{TC} \\ F^{TS} \\ F^{TE} \end{bmatrix} = \begin{bmatrix} -1.00 & 1.00 & 0.00 & 0.00 \\ 0.00 & 0.00 & 0.00 & -1.00 \\ -1.00 & 0.52 & -0.52 & 0.00 \\ -0.42 & 0.42 & 0.00 & -0.58 \\ -1.00 & 0.35 & -0.71 & 0.00 \\ -0.59 & 0.59 & 0.00 & -0.41 \end{bmatrix}$$

Step 5 Determine *r*-vector, Equations 3.50 and 3.51:

$$r = \begin{Bmatrix} r^{TC} \\ r^{TS} \\ r^{TE} \end{Bmatrix} = \begin{Bmatrix} -0.39 \\ -6.36E-08 \\ 0.00 \\ 0.00 \\ -0.11 \\ 4.32E-02 \end{Bmatrix}$$

Step 6 Solve for α-vector:

From Equations 3.46 and 3.51,

$$r = F\alpha$$

and,

$$\alpha = \begin{Bmatrix} \dfrac{E_x^{r+1} - E_x^r}{E_x^r} \\ \dfrac{\nu_{xy}^{r+1} - \nu_{xy}^r}{\nu_{xy}^r} \\ \dfrac{\nu_{xx}^{r+1} - \nu_{xx}^r}{\nu_{xx}^r} \\ \dfrac{E_y^{r+1} - E_y^r}{E_y^r} \end{Bmatrix} = \begin{Bmatrix} 7.19E-02 \\ -18.26E-02 \\ -13.33E-02 \\ -9.36E-02 \end{Bmatrix}$$

Step 7 Compute New Set of Model Properties:

The new anisotropic properties, α^{r+1} are thus:

$$E_x^{r+1} = E_x^r\left(1+(0.6)(\alpha(1))\right) = (64020.49)(1+(0.6)(7.19E-02)) = 66782.04\ kPa$$

$$\nu_{xy}^{r+1} = \nu_{xy}^r\left(1+(0.6)(\alpha(2))\right) = (0.261)(1+(0.6)(-18.26E-02)) = 0.233$$

$$\nu_{xx}^{r+1} = \nu_{xx}^r\left(1+(0.6)(\alpha(3))\right) = (0.522)(1+(0.6)(-13.33E-02)) = 0.481$$

$$E_y^{r+1} = E_y^r\left(1+(0.6)(\alpha(4))\right) = (174825.17)(1+(0.6)(-9.36E-02)) = 174825.20\ kPa$$

Since all the components in the α-vector are not less than 1% for this iteration, the new set of parameters are used to compute a new model output (calculated strains) and steps 3 through 7 are repeated until the convergence criteria is reached ($\alpha \leq 1\%$).

For this particular example, convergence is reached after seven iterations. The α-values and adjusted model properties are tabulated in Table 5.9. The shear modulus G_{xy} was not included in the parameter adjustment algorithm because its value, once computed from Equation 3.39 does not need further adjustment. Typical SID converging processes for moduli, and Poisson's ratios at the stress-state in the example are shown in Figures 5.4 and 5.5, respectively. Here, the initial estimates of the moduli and Poisson's ratio were close to the system values and the optimum values were achieved after 7 iterations.

Table 5.9 Model Properties and Parameter Adjustment Values at Stress State 1 for Well Graded Texas Limestone at Optimum Moisture.

Iteration	$\alpha(1)$	$\alpha(2)$	$\alpha(3)$	$\alpha(4)$	E_x (MPa)	ν_{xy}	ν_{xx}	E_y (MPa)
1	0.072	-0.183	-0.133	-0.094	64.0	0.261	0.522	175.0
2	0.039	-0.116	-0.098	-0.054	66.8	0.233	0.481	165.0
3	0.020	-0.068	-0.064	-0.033	68.3	0.216	0.452	160.0
4	0.010	-0.038	-0.039	-0.020	69.1	0.208	0.435	157.0
5	0.005	-0.021	-0.023	-0.012	69.6	0.203	0.425	155.0
6	0.003	-0.011	-0.013	-0.007	69.8	0.200	0.419	154.0
7	0.001	-0.006	-0.007	-0.004	69.9	0.199	0.416	153.0

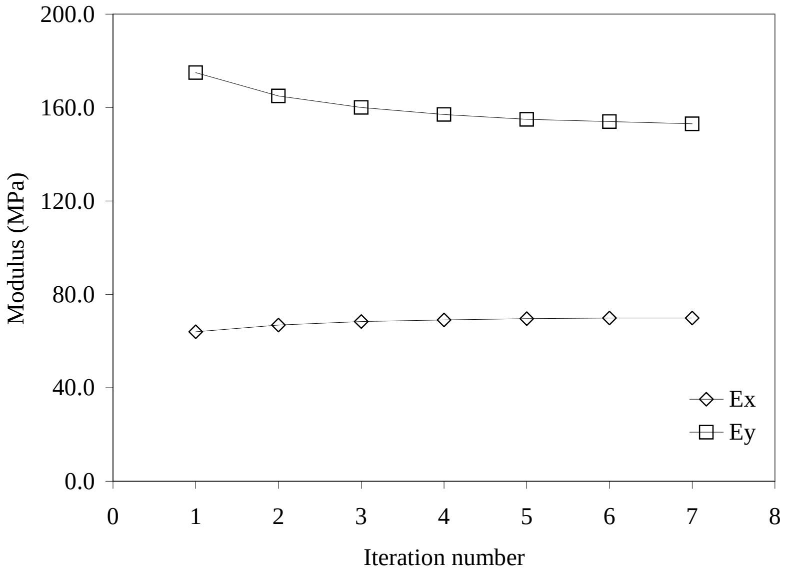

Figure 5.4 Converging Process for Moduli.

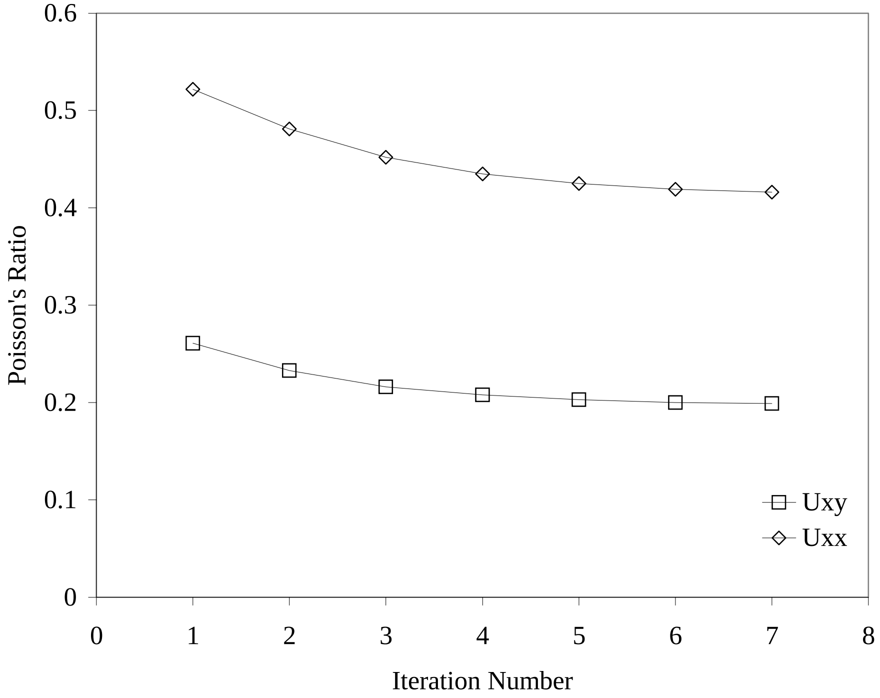

Figure 5.5 Converging Process for Poisson’s Ratios.

The parameter adjustment algorithm described in steps 1 through 7 was performed on the stresses and average strains from all the ten stress states to determine the stress dependent cross-anisotropic resilient properties for all samples. The stresses, moduli and Poisson’s ratios obtained using the SID program for a well-graded Texas crushed limestone at optimum moisture are tabulated in Table 5.10. Similar values were obtained for the other samples and are tabulated in Appendix B. Figures 5.6 through5.9 are plots of moduli and Poisson’s ratio with normalized stress states ($\sqrt{J'_2}$/Pa and I_1/Pa). Moduli values generally increase with increasing stress levels. Although, the moduli values increase with increasing I_1, the moduli tend to peak at high levels of J'_2. This means that resilient moduli values will not increase indefinitely with increasing bulk stresses but will peak at high octahedral shear stresses (Uzan’s model).

Table 5.10 Moduli and Poisson's Ratios for Texas Crushed Limestone at Optimum Moisture Content.

Stress (kPa)		Moduli (MPa)			Poisson's Ratio	
Axial	Radial	Vertical	Horizontal	Shear	Vertical	Horizontal
40.0	25.0	153.0	69.9	42.6	0.199	0.416
50.0	25.0	176.0	69.7	49.7	0.181	0.336
70.0	40.0	241.0	116.0	78.5	0.206	0.385
130.0	60.0	391.0	154.0	106.0	0.176	0.402
150	70.0	448.0	185.0	125.0	0.182	0.406
170	100.0	462.0	249.0	156.0	0.207	0.396
220	120.0	544.0	285.0	178.0	0.187	0.402
250	140.0	616.0	352.0	210.0	0.192	0.417
250	120.0	602.0	288.0	188.0	0.172	0.388
250	105.0	632.0	250.0	171.0	0.166	0.441

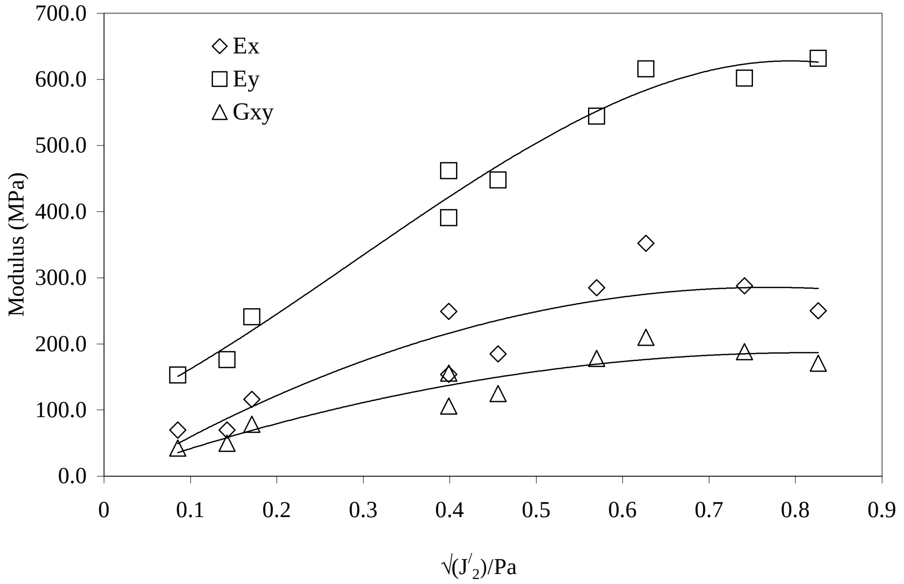

Figure 5.6 Modulus versus $\sqrt{J'_2}/P_a$.

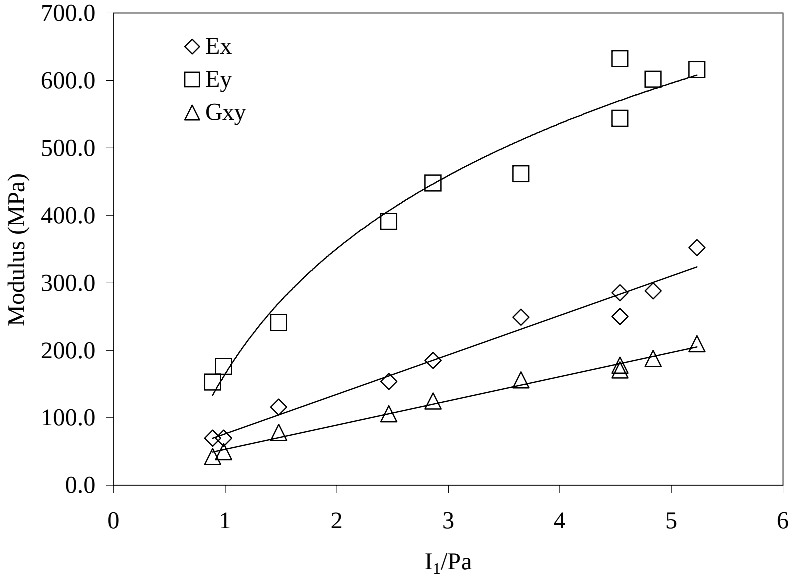

Figure 5.7 Modulus versus I_1/P_a.

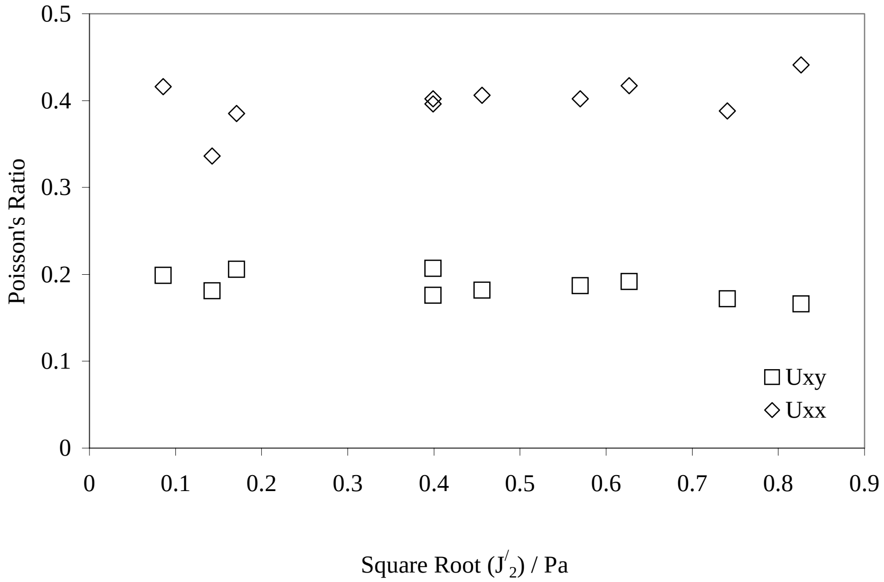

Figure 5.8 Poisson’s Ratio versus Square Root of $(J'_2)/P_a$.

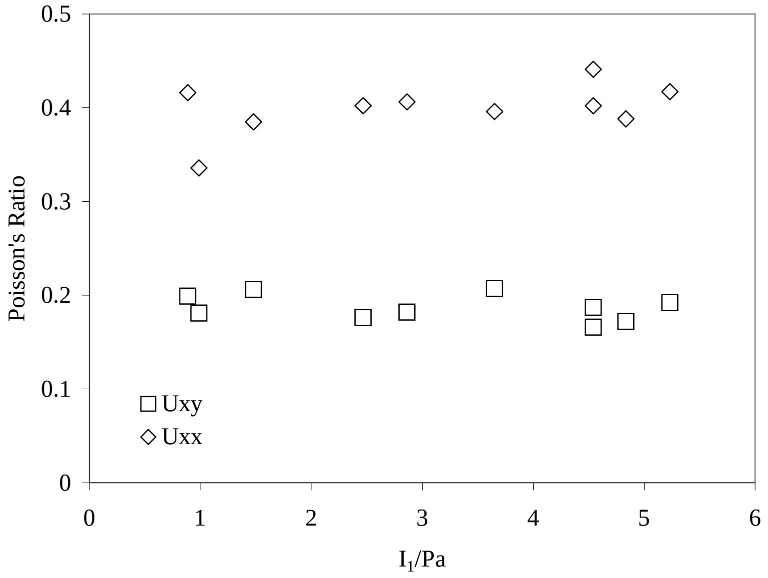

Figure 5.9 Poisson's Ratio versus I_1/P_a.

In general, resilient modulus values were higher in the vertical direction than in the horizontal direction for all samples. The resilient shear modulus values were the lowest among the three resilient moduli. Also, the horizontal Poisson's ratio always remained greater than the vertical Poisson's ratio.

Gradation, moisture level and material type have different effects on the resilient moduli. For both well- and fine-graded materials compacted at optimum moisture content, increased resilient moduli were observed for increasing plasticity index. Figures 5.10 and 5.11 are plots of vertical modulus versus $\sqrt{(J'_2)}/P_a$ for well-graded and fine-graded materials at optimum moisture content, respectively. California gravel (non-plastic) and Minnesota gravel (PI = 2.0%) recorded lower resilient moduli than Texas gravel (PI = 11.8%) and Texas limestone (PI = 4.4%). However, Texas limestone recorded higher moduli than Texas gravel for both well-graded and for fine graded samples. Thus, although moduli values increase with increasing plasticity index, there is an optimum plasticity index above which moduli will decrease, especially for fine gradation at moisture levels wet of optimum.

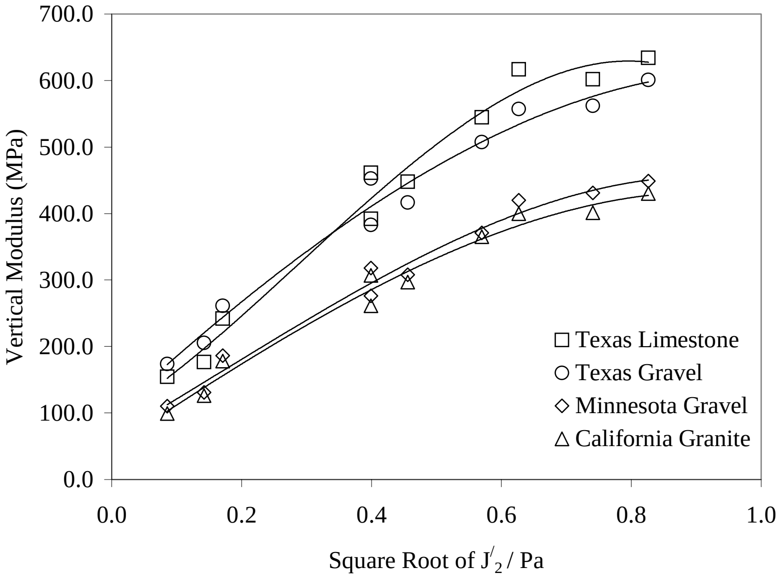

Figure 5.10 Vertical Modulus for Well-Graded Materials Compacted at Optimum Moisture Content.

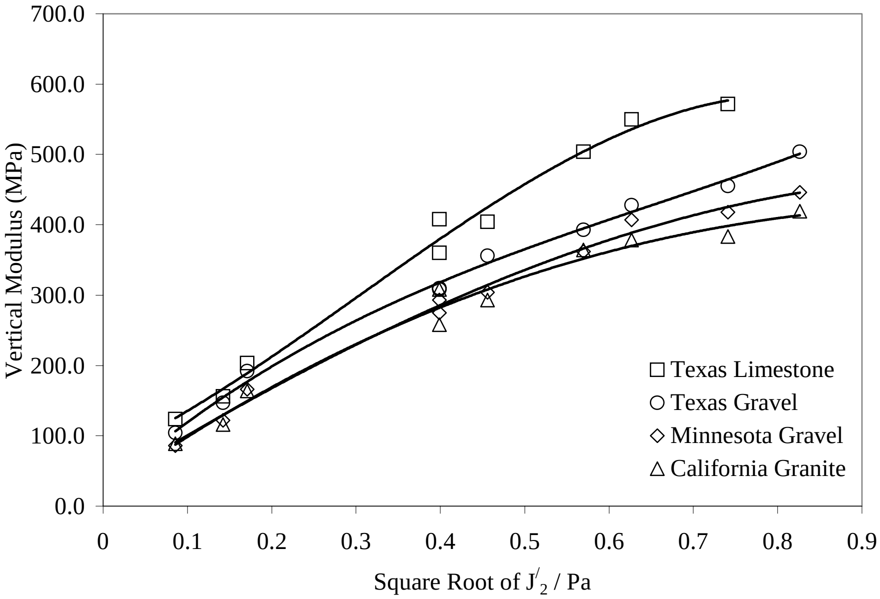

Figure 5.11 Vertical Modulus for Fine-Graded Materials Compacted at Optimum Moisture Content.

Well-graded samples generally have higher resilient moduli values than coarse graded samples followed by fine graded samples (Figures 5.12, 5.13, 5.14 and 5.15). The variation in resilient moduli with gradation is more significant in high plasticity materials. Between well graded and fine graded samples compacted at optimum moisture content, vertical resilient modulus values of fine graded Texas gravel varied between 60% to 85% of the well graded samples at all the stress states. The variation was between 80% to 95% for Texas limestone, 80% to 99.5% for Minnesota gravel and only 90% to 99.7% for California granite. Similar variations were observed with respect to horizontal and shear resilient moduli. For California granite, there were increases in the horizontal and shear moduli values. Coarse graded samples of Minnesota gravel and California granite could not be compacted and tested because of their low plasticity.

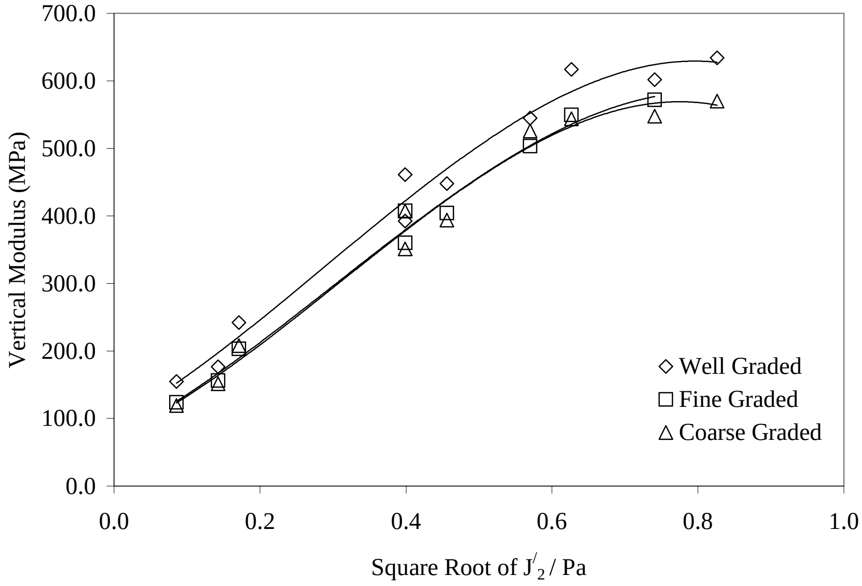

Figure 5.12 Variation of Vertical Modulus with Gradation for Texas Limestone at Optimum Moisture Content.

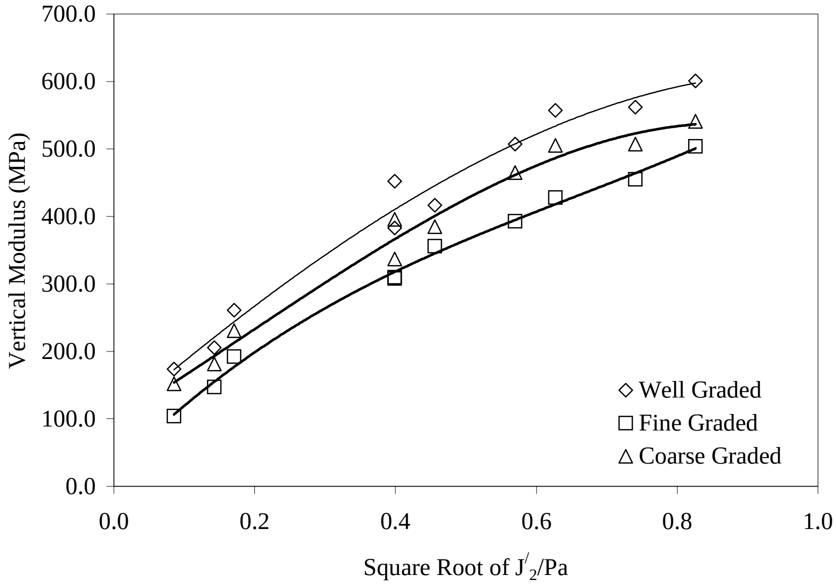

Figure 5.13 Variation of Vertical Modulus with Gradation for Texas Gravel at Optimum Moisture Content.

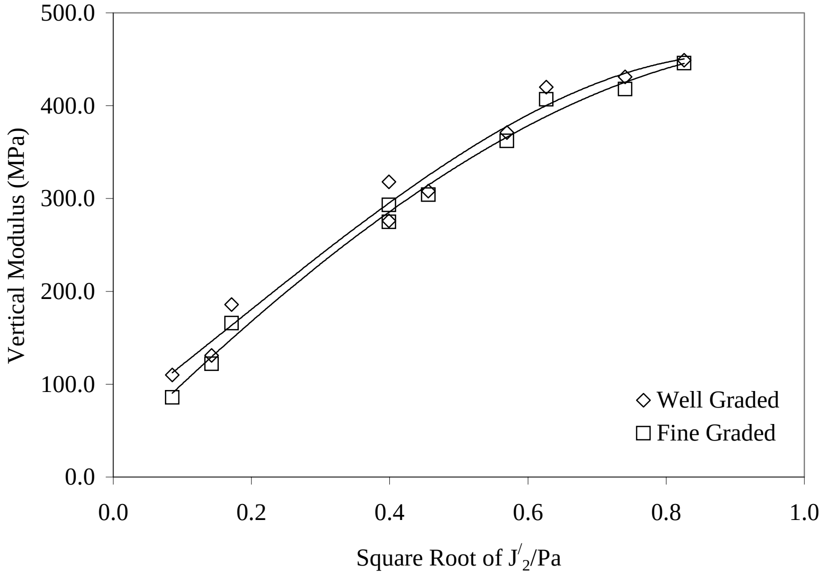

Figure 5.14 Variation of Vertical Modulus with Gradation for Minnesota Gravel at Optimum Moisture Content.

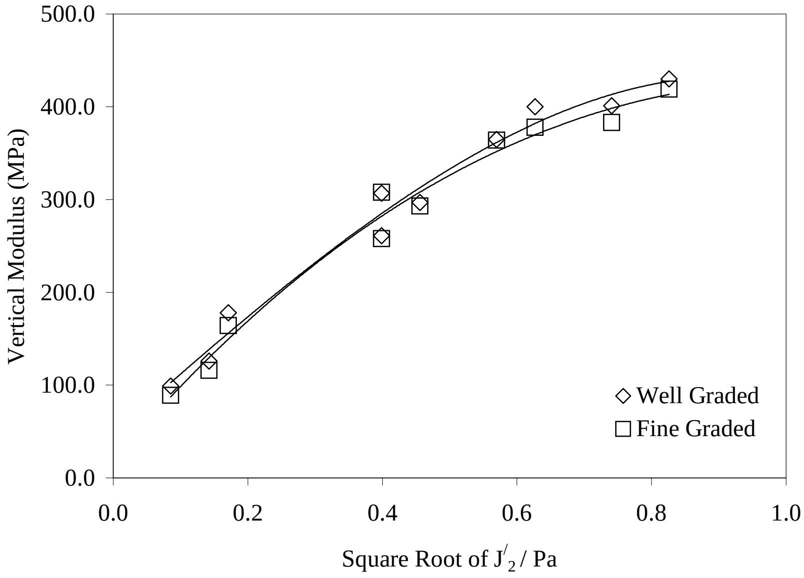

Figure 5.15 Variation of Vertical Modulus with Gradation for California Granite at Optimum Moisture Content.

For a particular gradation, samples compacted at optimum and dry of optimum generally recorded higher resilient moduli than samples compacted at wet of optimum. The effect of moisture on resilient moduli depends on material and gradation. An increase in plasticity and fine content are generally accompanied by a significant variation in moduli due to moisture. Fine graded Texas gravel and Minnesota gravel samples could not be tested because they were too soft and unstable for the stress levels applied. Figures 5.16 through 5.21 illustrate the effect of moisture on resilient moduli. Similar effects were observed for horizontal and shear resilient moduli. The modular ratios, horizontal to vertical modulus, *n*, and shear to vertical modulus ratios, *m*, at all stress states was fairly constant for a particular sample. The average *n*-value for well graded Texas limestone at optimum moisture is about 0.5 and the *m*-value is about 0.3.

The Poisson's ratio values varied with the level of stress applied to the sample. The advantage of using the system identification method is that the parameters obtained satisfy traditional theories of elasticity. As an example, consider Table 5.7 and at stress level 1.

Static Axial Stress, σ_y = 40.0 kPa

Static Radial Stress, σ_x = 25.0 kPa

Dynamic Change in Axial Stress for Triaxial Compression, $\Delta\sigma_y^c$, = 5 kPa

Dynamic Change in Radial Stress for Triaxial Compression, $\Delta\sigma_x^c$, = 0 kPa

Dynamic Change in Axial Stress for Triaxial Shear, $\Delta\sigma_y^s$, = 10 kPa

Dynamic Change in Radial Stress for Triaxial Shear, $\Delta\sigma_x^s$, = -5 kPa

Dynamic Change in Axial Stress for Triaxial Extension, $\Delta\sigma_y^e$, = -5 kPa

Dynamic Change in Radial Stress for Triaxial Extension, $\Delta\sigma_x^e$, = 5 kPa

Axial Resilient Strain for Triaxial Compression, $\Delta\varepsilon_y^c$ = 28.6E-06

Radial Resilient Strain for Triaxial Compression, $\Delta\varepsilon_x^c$ = -12.4E-06

Axial Resilient Strain for Triaxial Shear, $\Delta\varepsilon_y^s$ = 98.0E-06

Radial Resilient Strain for Triaxial Shear, $\Delta\varepsilon_x^s$ = -78.1E-06

Axial Resilient Strain for Triaxial Extension, $\Delta\varepsilon_y^e$ = -72.4E-06

Radial Resilient Strain for Triaxial Extension, $\Delta\varepsilon_x^e$ = 51.1E-06

Then from Equations 2.2,

Poisson’s ratio for the triaxial compression regime = 0.43

Poisson’s ratio for the triaxial shear regime = 0.80

Poisson’s ratio for the triaxial extension regime = 0.71

Thus the material dilated during the triaxial shear and extension regimes. However, after integrating the changes in stresses and strains into the system identification scheme, the vertical and horizontal Poisson’s ratio values were 0.2 and 0.42, respectively. Vertical Poisson’s ratio values determined for all the samples were below 0.5 as required by traditional theories of elasticity. Horizontal Poisson’s ratio values can be higher than 0.5 according to elasticity theories (Equation 3.15).

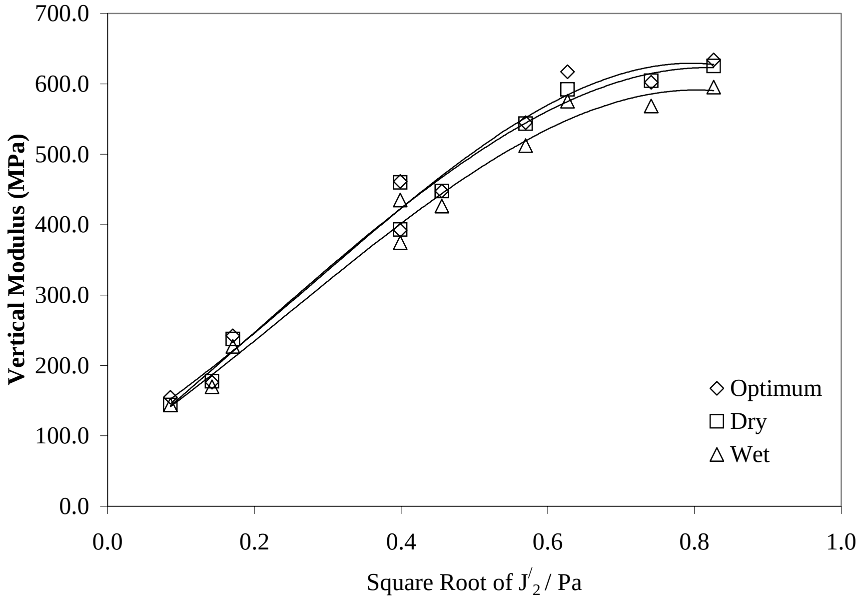

Figure 5.16 Variation of Vertical Modulus with Moisture for Well Graded Texas Limestone.

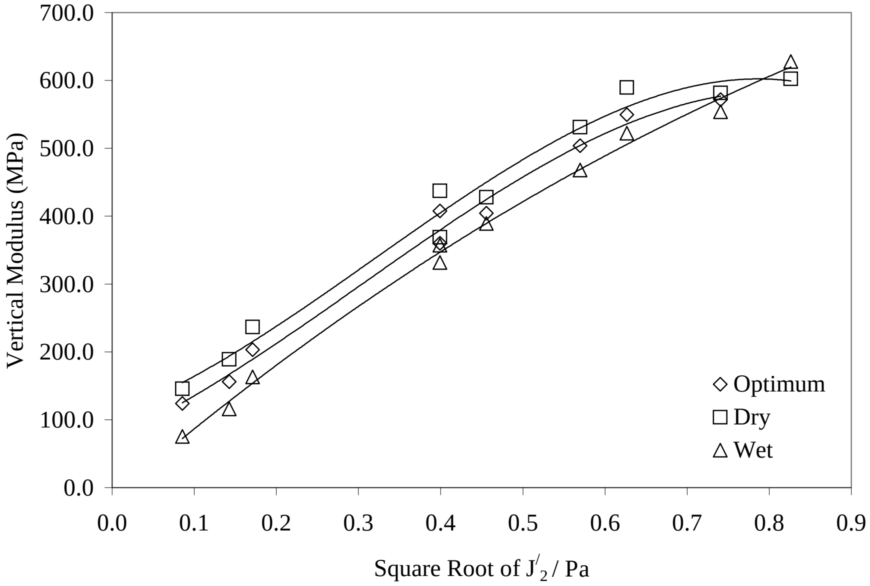

Figure 5.17 Variation of Vertical Modulus with Moisture for Fine Graded Texas Limestone.

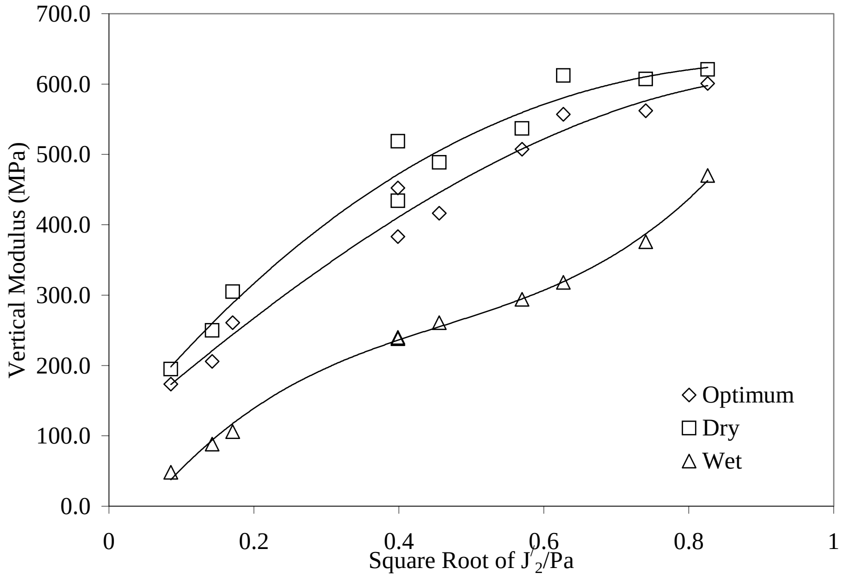

Figure 5.18 Variation of Vertical Modulus with Moisture for Well Graded Texas Gravel.

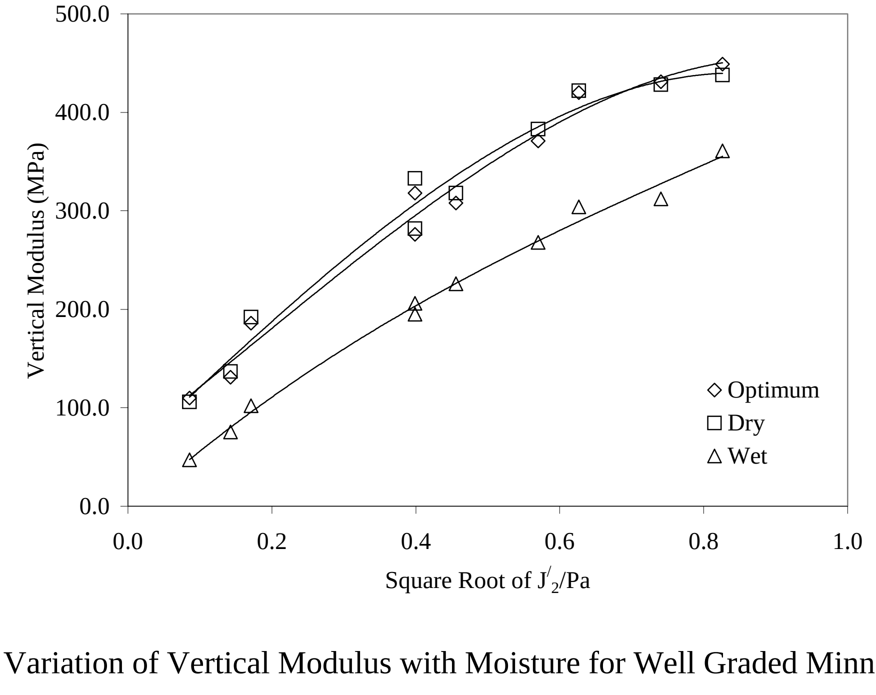

Figure 5.19 Variation of Vertical Modulus with Moisture for Well Graded Minnesota Gravel.

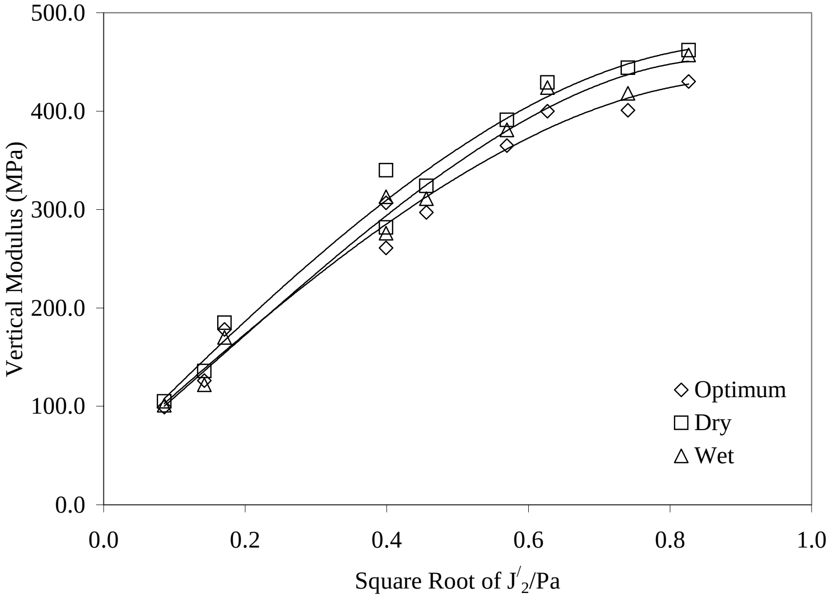

Figure 5.20 Variation of Vertical Modulus with Moisture for Well Graded California Granite.

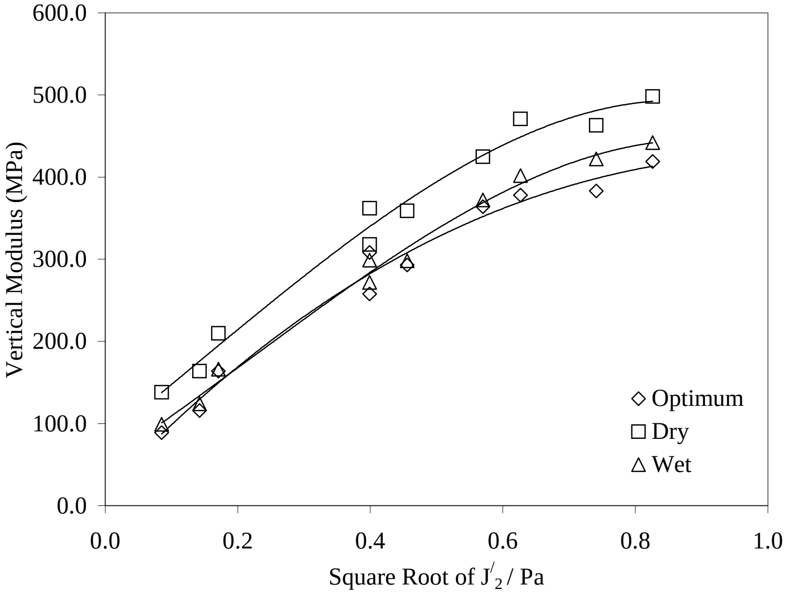

Figure 5.21 Variation of Vertical Modulus with Moisture for Fine Graded California Granite.

5.2.1 Regression Analysis

It is assumed that the resilient moduli obey the Uzan model and thus, the non-linear tangential moduli are smooth functions of the isotropic stress invariants (Equations 3.4, 3.5 and 3.6). It is also assumed that the variations of these tangential moduli are negligible under infinitesimal changes in stresses at a particular stress state. Thus, the elastic strains generated due to small changes in stresses at a particular stress state depend on the elastic properties at that stress state.

Regression analysis was used to determine the k-values for each gradation and moisture condition. The data fitted well with the Uzan-type model (Equations 3.4, 3.5, and 3.6) and the R-square values determined for the elastic parameters at all conditions were above 0.90. Tables 5.11, 5.12, 5.13 and 5.14 are summaries of average k-values for the gradation and moisture conditions tested. The negative values of k_6 and k_9 indicate that the horizontal and shear moduli were more sensitive to high shear stress softening. The k-values, k_1, k_4 and k_7, are indications of how well a material can spread traffic loads. The other k-values are shape parameters and they indicate how stress levels affect the resilient moduli (Lytton, 1998).

The resilient moduli values also fitted well with Lytton’s model (Equation 2.9).

Lytton’s Model

$$M_R = k_1^{/} P_a \left(\frac{I_1 - 3\theta f h_m}{P_a} \right)^{k_2^{/}} \left(\frac{\tau_{oct}}{P_a} \right)^{k_3^{/}} \quad or \quad M_R = k_1^{/} P_a \left(\frac{I_1 - 3k_4^{/}}{P_a} \right)^{k_2^{/}} \left(\frac{\tau_{oct}}{P_a} \right)^{k_3^{/}}$$

The k-values are related to each other. The standard deviation of k_1-values (Uzan model) was about twice the standard deviation of $k^{/}_1$-values (Lytton’s model). The k-values of all the materials could not be explained by gradation parameters (g_a, g_n and g_m), suction and dry density. However, the k-values of the individual materials are related to the gradation parameters.

$$k_1 = 3332 + 3027k_2 + 3688k_3 \qquad R^2 = 0.60$$

$k_4 = 2158 - 1472k_5 + 616k_6$ R^2 = 0.66

$k_4 = \frac{1042}{k_5} - \frac{0.6}{k_6} - 663$ R^2 = 0.87

$k_7 = 1329 - 1071k_8 + 543k_9$ R^2 = 0.70

$k_7 = \frac{698}{k_8} - \frac{0.7}{k_9} - 470$ R^2 = 0.76

$k_4 = (k_1)^{-0.56}(k_7)^{1.76}$ R^2 = 0.90

$k_7 = (k_1)^{0.32}(k_4)^{0.56}$ R^2 = 0.83

Texas Limestone:

$g_a = -0.029k_1 + 114.5k_2 + 243.3k_3$ R^2 = 0.64

$g_m = -0.005k_1 + 19.3k_2 + 43.0k_3$ R^2 = 0.65

$g_n = 0.001k_1 - 2.9k_2 - 10.4k_3$ R^2 = 0.64

Minnesota Gravel:

$g_a = -0.008k_1 + 39.6k_2 + 64.8k_3$ R^2 = 0.91

$g_m = -0.001k_1 + 4.9k_2 + 7.8k_3$ R^2 = 0.92

$g_n = 0.001k_1 + 0.2k_2 - 2.5k_3$ R^2 = 0.69

California Granite:

$g_a = -0.04k_4 - 0.05k_5 - 57.4k_6$ R^2 = 0.96

$g_m = -0.005k_4 + 0.08k_5 - 6.8k_6$ R^2 = 0.96

$g_n = 0.004k_4 + 1.13k_5 + 3.2k_6$ R^2 = 0.86

Table 5.11 Average k-Values for Texas Limestone.

	Coarse Graded	Well Graded			Fine Graded		
	Optimum	Dry	Optimum	Wet	Dry	Optimum	Wet
k_1	3670	4171	3860	3839	3783	5629	5734
k_2	0.398	0.354	0.398	0.369	0.370	0.217	0.186
k_3	0.314	0.362	0.326	0.344	0.334	0.568	0.576
k_4	426	429	316	364	443	210	230
k_5	1.058	1.198	1.281	1.174	1.120	1.328	1.275
k_6	-0.001	-0.254	-0.372	-0.303	-0.197	-0.265	-0.052
k_7	444	452	380	430	467	296	318
k_8	0.878	0.910	0.964	0.867	0.841	0.993	0.943
k_9	-0.068	-0.060	-0.136	-0.068	-0.057	-0.057	0.097

Table 5.12 Average k-Values for Texas Gravel.

	Coarse Graded	Well Graded		Fine Graded	
	Optimum	Dry	Optimum	Dry	Optimum
k_1	3779	4245	4152	3010	6250
k_2	0.301	0.306	0.299	0.330	0.015
k_3	0.332	0.242	0.316	0.190	0.645
k_4	803	2589	824	1151	416
k_5	0.625	0.483	0.694	0.526	0.961
k_6	-0.053	-0.001	-0.140	-0.247	-0.240
k_7	586	1219	627	680	496
k_8	0.601	0.507	0.642	0.524	0.667
k_9	0.009	0.055	-0.024	-0.103	0.042

Table 5.13 Average k-Values for Minnesota Gravel.

	Well Graded			Fine Graded	
	Dry	Optimum	Wet	Dry	Optimum
k_1	3879	2834	3232	3779	3462
k_2	0.217	0.360	0.302	0.301	0.248
k_3	0.513	0.310	0.388	0.332	0.372
k_4	169	273	180	280	803
k_5	1.227	1.188	1.267	1.080	0.625
k_6	-0.204	-0.412	-0.405	-0.376	-0.053
k_7	217	322	232	586	331
k_8	0.945	0.861	0.957	0.601	0.791
k_9	-0.066	-0.145	-0.165	0.009	-0.125

Table 5.14 Average k-Values for California Granite.

	Well Graded			Fine Graded		
	Dry	Optimum	Wet	Dry	Optimum	Wet
k_1	3179	2934	3251	3572	2872	3500
k_2	0.329	0.326	0.313	0.289	0.326	0.262
k_3	0.372	0.366	0.417	0.344	0.376	0.458
k_4	266	266	215	406	366	246
k_5	1.136	1.136	1.229	0.997	0.970	1.123
k_6	-0.404	-0.404	-0.349	-0.356	-0.363	-0.273
k_7	315	277	250	419	379	283
k_8	0.854	0.871	0.951	0.759	0.729	0.866
k_9	-0.146	-0.087	-0.141	-0.132	-0.085	-0.068

5.2.2 Compaction Results

The molding moisture contents and the resulting dry densities for each combination of compaction type and effort are shown in Table 5.15. The k-values are shown in Tables 5.16 and 5.17 for Texas gravel and Texas limestone, respectively. The recorded moduli values at low, medium and high stress states are tabulated in Tables 5.18 and 5.19 for Texas gravel and Texas limestone, respectively.

In this study a low stress state is equivalent to a confining stress of 40 kPa and a deviator stress of 30 kPa. A medium stress state is equivalent to a confining stress of 100 kPa and a deviator stress of 70 kPa. A high stress state is equivalent to a confining stress of 120 kPa and a deviator stress of 130 kPa.

Table 5.15 Molding Moisture Content and Dry Density.

	Texas Limestone					
	Impact		Vibratory		Gyratory	
	Low	High	Low	High	Low	High
Moisture Content, %	6.0	6.0	6.0	6.0	5.0	5.0
Dry Density, kg/m^3	2150	2160	1944	2160	2180	2200
	Texas Gravel					
	Impact		Vibratory		Gyratory	
	Low	High	Low	High	Low	High
Moisture Content, %	5.0	5.0	5.0	5.0	4.0	4.0
Dry Density, kg/m^3	2300	2350	2115	2350	2350	2360

Table 5.16 Model Parameters for Siliceous Gravel.

	Impact		Vibratory		Gyratory	
	Low Effort	High Effort	Low Effort	High Effort	Low Effort	High Effort
k_1	2553	3736	3910	2517	4726	4057
k_2	0.327	0.220	0.058	0.378	0.218	0.269
k_3	0.071	0.103	0.148	0.080	0.139	0.061
k_4	1195	838	465	771	358	992
k_5	0.637	0.797	0.745	0.652	1.242	0.556
k_6	-0.089	-0.083	-0.036	-0.031	-0.057	-0.030
k_7	696	695	621	559	500	754
k_8	0.550	0.593	0.449	0.638	0.799	0.522
k_9	-0.012	-0.004	0.060	0.019	0.019	-0.005
νxy	0.18	0.17	0.06	0.14	0.16	0.17
νxx	0.36	0.35	0.11	0.32	0.31	0.40

Table 5.17 Model Parameters for Crushed Limestone.

	Impact		Vibratory		Gyratory	
	Low Effort	High Effort	Low Effort	High Effort	Low Effort	High Effort
k_1	3112	4663	2315	2109	4533	5085
k_2	0.312	0.344	0.452	0.604	0.257	0.241
k_3	0.124	0.084	0.062	0.057	0.134	0.099
k_4	441	639	271	622	267	781
k_5	1.053	1.068	0.925	0.899	1.254	0.960
k_6	0.019	-0.063	-0.058	-0.028	-0.025	-0.044
k_7	447	635	319	676	366	691
k_8	0.785	0.813	0.793	0.666	0.895	0.736
k_9	0.042	-0.011	-0.007	0.046	0.026	-0.003
νxy	0.15	0.20	0.05	0.12	0.19	0.18
νxx	0.30	0.42	0.09	0.27	0.41	0.40

Table 5.18 Resilient Moduli for Siliceous Gravel.

Stress State	Impact		Vibratory		Gyratory	
	Low Effort	High Effort	Low Effort	High Effort	Low Effort	High Effort
	Vertical Resilient Modulus, MPa					
Low	192.0	208.0	148.0	169.0	232.0	305.0
Medium	305.0	349.0	258.0	321.0	411.0	464.0
High	394.0	449.0	315.0	415.0	531.0	581.0
	Horizontal Resilient Modulus, MPa					
Low	277.0	201.0	91.1	152.0	111.0	152.0
Medium	376.0	306.0	160.0	200.0	232.0	214.0
High	395.0	345.0	142.0	225.0	263.0	258.0
	Resilient Shear Modulus, MPa					
Low	105.0	99.3	55.0	71.8	78.3	101.0
Medium	152.0	157.0	99.8	134.0	145.0	159.0
High	173.0	183.0	101.0	146.0	167.0	178.0

Table 5.19 Resilient Moduli for Crushed Limestone.

Stress State	Impact		Vibratory		Gyratory	
	Low Effort	High Effort	Low Effort	High Effort	Low Effort	High Effort
	Vertical Resilient Modulus, MPa					
Low	161.0	326.0	174.0	174.0	231.0	323.0
Medium	298.0	550.0	349.0	391.0	428.0	503.0
High	411.0	707.0	421.0	514.0	588.0	642.0
	Horizontal Resilient Modulus, MPa					
Low	64.9	165.0	70.9	120.0	104.0	178.0
Medium	156.0	312.0	121.0	247.0	232.0	310.0
High	238.0	391.0	127.0	250.0	271.0	387.0
	Resilient Shear Modulus, MPa					
Low	54.3	111.0	49.6	71.2	71.5	111.0
Medium	112.0	198.0	99.8	147.0	145.0	189.0
High	145.0	234.0	108.0	178.0	180.0	222.0

It is observed from Table 5.15 that compaction method and effort generally affect the dry density of a compacted sample. These increases in density obtained going from a lower compactive effort to a higher one resulted in higher values of resilient moduli. Samples prepared with the vibratory compaction method at low compaction effort recorded the lowest values in moduli. The highest vertical moduli values were recorded from samples prepared with gyratory compaction method at high compaction effort.

The materials were generally stiffer in the vertical direction. However, the horizontal resilient modulus values were slightly higher at each stress state than the vertical resilient modulus for gravel samples compacted with impact compaction method at low effort (25 blows per layer). When the compaction effort was increased to 50 blows per layer the horizontal resilient moduli were lower, but the average value was

80% of the vertical modulus as compared to 46%-60% in the case of the other compaction methods and efforts. The degree of anisotropy is defined as the ratio of horizontal to vertical modulus. It is assumed that the degree of anisotropy is related to particle orientation in the unbound granular material. Thus, the induced anisotropy by the impact compaction method was not significant. Samples compacted with the vibratory compaction method recorded unusually low Poisson's ratios. This may be due to the differences in LVDT range between RaTT and UIFC as mentioned earlier.

The non-linear anisotropic properties (k-values) are useful in determining pavement response with a finite element code. The anisotropic model generally reduces and/or reverses the horizontal tensile stresses predicted in the base course with isotropic elastic properties. Although using impact compaction results in acceptable densities, distribution and orientation of individual particles makes the material to behave like an isotropic material. The orientation of particles in a compacted unbound granular material is important to its load carrying capabilities. Further study needs to be done to establish how the compaction methods considered are related to compaction levels achieved in the field. Field cores of unbound granular materials should be obtained and tested in the laboratory to confirm the observations made on compaction methods.

5.3 Permanent Deformation

The repeated load triaxial test was used to study the permanent deformation characteristics of the four aggregate types. The permanent deformation study was performed only on well graded samples compacted at optimum moisture.

Samples, 150-mm in height by 150-mm diameter, were compacted using the Texas Gyratory Compactor with the high compaction effort. One sample was prepared for each stress level because this test is destructive in nature. The permanent deformation behavior of the materials was studied at four stress levels. At each stress level, static confining stresses were applied to the samples and deviatoric stresses were axially cycled for 10,000 times. A haversine pulse-load was applied for 0.1 seconds with a 0.9 seconds rest at a frequency of 1 cycle per second.

The strain values at first load cycle are tabulated in Table 5.20. The plastic strains measured are plotted against the number of load applications in Figures 5.22 through 5.25.

Table 5.20 Plastic Strain at First Load Cycle

Stress Level	Stress (kPa)	Plastic Strain at First Load Cycle ($\mu\varepsilon$) TX Limestone	TX Gravel	MN Gravel	CA Granite
1	σ_3 = 70 σ_d = 70	365.2	584.4	672.2	389.4
2	σ_3 = 35 σ_d = 105	792.7	3535.4	2664.2	807.2
3	σ_3 = 105 σ_d = 145	655.2	3090.2	1619.0	656.5
4	σ_3 = 70 σ_d = 180	598.2	3036.2	4826.2	1886.3

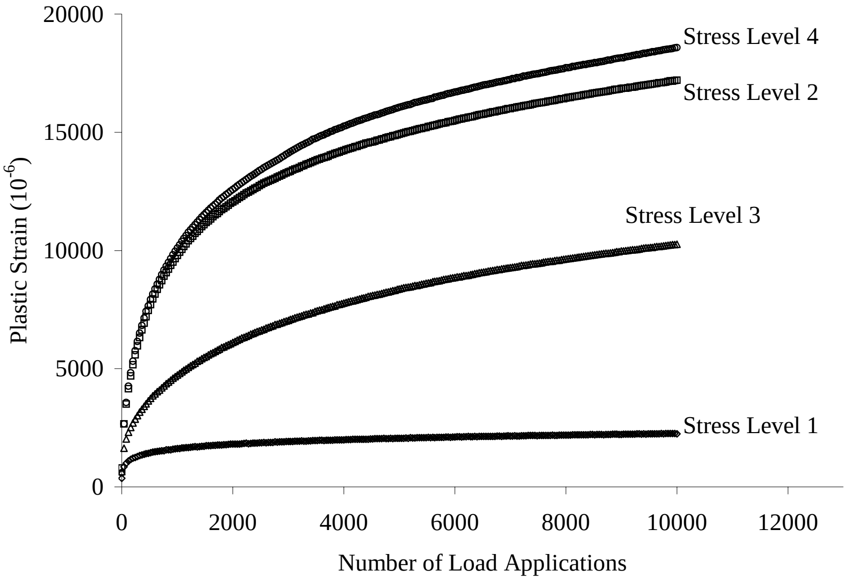

Figure 5.22 Plastic Strain versus Number of Load Applications for Texas Limestone.

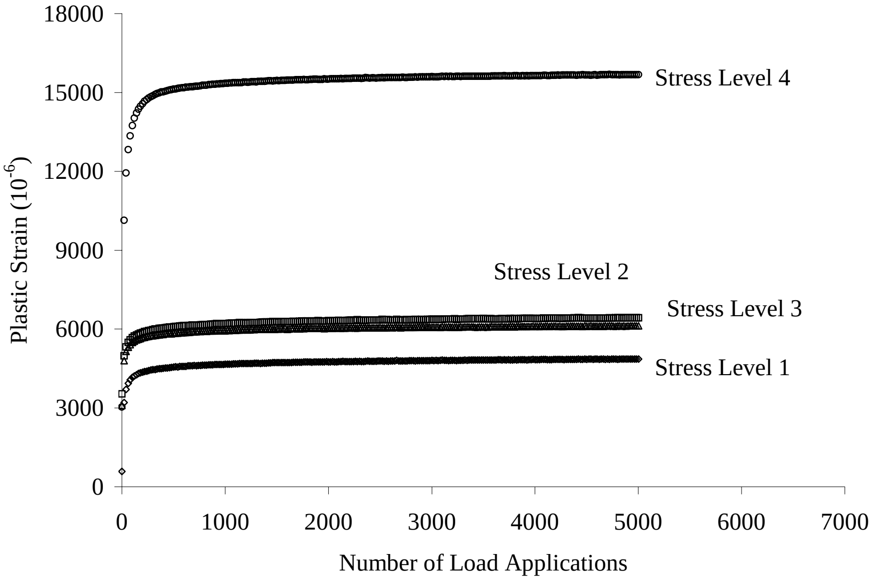

Figure 5.23 Plastic Strain versus Number of Load Applications for Texas Gravel.

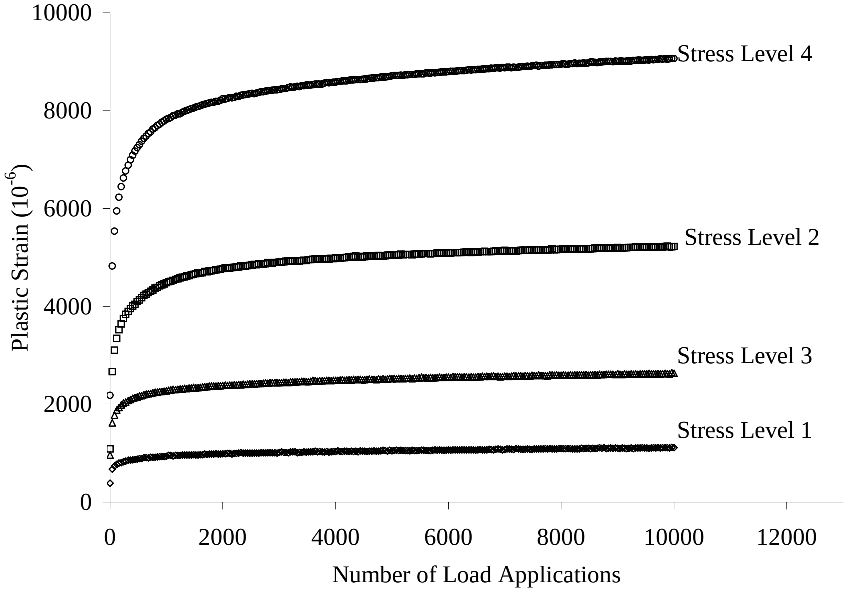

Figure 5.24 Plastic Strain versus Number of Load Applications for Minnesota Gravel.

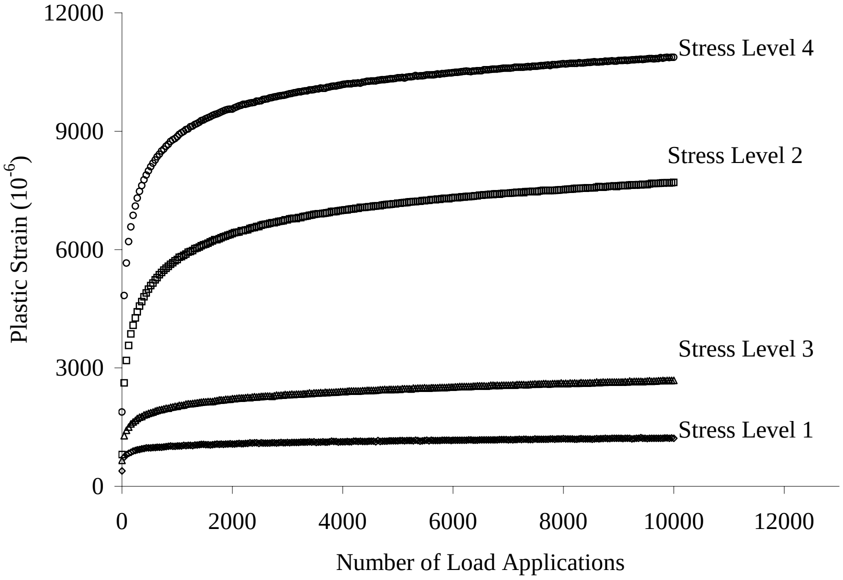

Figure 5.25 Plastic Strain versus Number of Load Applications for California Granite.

Plastic strains generally accumulate with increasing number of load applications. However, the rates at which plastic strains accumulate with load applications are different for the four materials considered.

The highest plastic strains at first load cycle were observed in Texas gravel, but the rates of accumulation of plastic strains after the first few cycles reached an equilibrium state for all stress levels.

The lowest plastic strains at first load cycle were observed in Texas limestone. However, there was a continuous increase in plastic strain accumulation with load cycles for stress levels 2, 3 and 4. The accumulation of plastic strains stabilized after the first few cycles for stress level 1.

Equilibrium state at stress levels 1 and 3 was established in the accumulation of plastic strains after approximately 1,000 load applications for both Minnesota gravel and California granite. However, at stress levels 2 and 4 there was continuous increase in plastic strain accumulation for both Minnesota gravel and California granite.

Figures 5.22 to 5.25 suggest that different materials behave differently under repeated load applications. Stress level is the most important factor that affects the accumulation of plastic strains with load application. An increase in deviatoric stress is generally accompanied by an increase in plastic strain. A decrease in confining stress results in an increase in plastic strain.

Permanent deformation parameters were determined for the materials by fitting the repeated load triaxial data with the Vesys model (Equation 2.17) and the Three-Parameter model (Equation 2.20). The model parameters, μ, α, ε_o, ρ and β are included in Tables 5.21, 5.22, 5.23 and 5.24 for stress levels 1, 2, 3 and 4, respectively.

Vesys Model $$\varepsilon_p(N) = \mu N^{-\alpha}$$

Three-Parameter model $$\varepsilon_p = \varepsilon_o \exp - \left(\frac{\rho}{N}\right)^{\beta}$$

Table 5.21 Permanent Deformation Parameters for Stress Level 1.

Model Parameter	TX Limestone	TX Gravel	MN Gravel	CA Granite
	Vesys Model			
μ	560.7	3051.9	532.3	570.3
α	-0.152	-0.053	-0.080	-0.083
	Three-Parameter Model			
ε_o	8415.9	55018.0	1938.7	2184.5
ρ	160.7 E03	5.6	61.6	87.6
β	0.099	0.448	0.113	0.112

Table 5.22 Permanent Deformation Parameters for Stress Level 2.

Model Parameters	TX Limestone	TX Gravel	MN Gravel	CA Granite
	Vesys Model			
μ	1575.5	4837.3	2399.7	2092.2
α	-0.271	-0.034	-0.087	-0.144
	Three-Parameter Model			
ε_o	65563.6	6858.5	6458.4	11788.1
ρ	32740.7	0.2	18.6	239.8
β	0.180	0.276	0.250	0.230

Table 5.23 Permanent Deformation Parameters for Stress Level 3.

Model Parameters	TX Limestone	TX Gravel	MN Gravel	CA Granite
	Vesys Model			
μ	487.9	4541.2	1356.3	854.2
α	-0.332	-0.034	-0.073	-0.125
	Three-Parameter Model			
ε_o	647885.1	6457.0	3802.0	16414.2
ρ	1.85E12	0.37	10.3	158.28E6
β	0.0745	0.289	0.144	0.062

Table 5.24 Permanent Deformation Parameters for Stress Level 4.

Model Parameters	TX Limestone	TX Gravel	MN Gravel	CA Granite
	Vesys Model			
μ	1695.9	10702.9	4291.1	4144.9
α	-0.254	-0.044	-0.083	-0.107
	Three-Parameter Model			
ε_o	36815.3	16137.6	11457.0	14775.7
ρ	3233.8	3.9	14.6	54.2
β	0.239	0.467	0.222	0.228

A small α-value indicates that the material that has low resistance to permanent deformation (Lytton, 1998). These model parameters can be used to predict the accumulation of permanent deformation within unbound granular layers in flexible pavements. It is easy to determine model parameters to characterize the permanent deformation behavior of unbound granular materials. However, the process is time consuming because a new specimen has to be prepared for each stress level to eliminate the effect of stress history.

Although the laboratory setup for characterizing permanent deformation is simple, the levels of stresses that need to be applied must be determined accurately. This is because stress levels, especially confining stress, have a significant impact on the rate and magnitude of accumulation of plastic strain.

The stresses within a pavement structure can be determined by analytical methods. Layered linear elastic methods are usually used to determine the stresses in a pavement. The limitation of the layered elastic model is that elastic moduli must be constant within each horizontal layer and thus, the method cannot effectively deal with material non-linearity exhibited by unbound granular materials.

The layered elastic process can account for variation in vertical stress but cannot effectively account for variation in lateral (confining) stresses. Since the variation of lateral stresses within a pavement profile is as important as the variation of vertical stresses, the finite element method (FEM) has recently been preferred to analyze pavements. A finite element computer program was developed in this study and the details are discussed in the next chapter.

5.3.1 Accelerated Rutting Parameters

Park (2000) developed a finite element computer program (FERUT) to predict the accumulation of permanent deformation in granular materials. FERUT uses the Vesys and Three Parameter models.

The formulation of the Vesys model implies that the plastic strain is an exponential function of the number of load cycles. The Three-Parameter model states that the plastic strain has a limit, ε_o, and a logarithmic rate of work hardening and also that the plastic strain increases with the number of load applications.

One mechanism that can seriously affect the performance of unbound granular layers is accelerated rutting due to fatigue from load repetitions. The repeated load action of traffic does not allow the build up of pore water pressure on the soil skeleton to dissipate. Accelerated rutting is assumed to occur under repeated load when the effective stress in unbound granular layers become equal to zero (Lytton, 1998).

Unbound granular materials are in an unsaturated state in most of the time. Unbound granular materials like soils have a property called suction, which is a measure of the tendency of the soil to undergo change in moisture content. Soil suction is defined as the affinity of the soil for pure water (Lytton, 1995). The same value of soil suction leads to different values of moisture content in soils of different textures (Lytton, 1995). The more clayey the soil, the higher the value of its moisture content at a given suction.

The α-value in the Vesys model will decrease, as the pore water pressure becomes less and less negative (Lytton, 1998). The α-value has been determined to be (Lytton, 1998):

$$\alpha = 1 - \frac{f\theta^2\left(\frac{\partial h}{\partial \theta}\right)N\,e^{-k\left(\frac{\partial h}{\partial \theta}\right)t_v\left(\frac{D_{10}}{d_m}\right)}}{K(1-n+\theta)} \qquad 5.2$$

where

θ = volumetric water content,

n = porosity,

N = number of load applications after water enters the granular layer,

$\left(\frac{\partial h}{\partial \theta}\right)$ = the slope of the soil-volumetric water content curve,

k = the unsaturated permeability,

t_v = the time between vehicles,

K = bulk modulus of the granular layer,

D_{10} = the particle diameter that is lager than 10% of all the particles,

d_m = the maximum particle size, and

f = a moisture lead factor that is equal to 1.0 when the granular layer is at or drier than optimum and 0.5 when saturated.

Park (2000) determined α-values for accelerated rutting and used them in a comparative analysis to determine accelerated rutting potential of three granular materials, Caliche, Iron Ore (IO) gravel, and limestone. The variations of alpha values with load application based on Equation 5.2 are shown in Figure 5.26 for the three granular materials. The accelerated rutting is assumed to occur when there is ingress of water into the base layer. The analytical technique was able to closely duplicate the field behavior of the materials under accelerated loading device as shown in Figure 5.27 for a Caliche base layer.

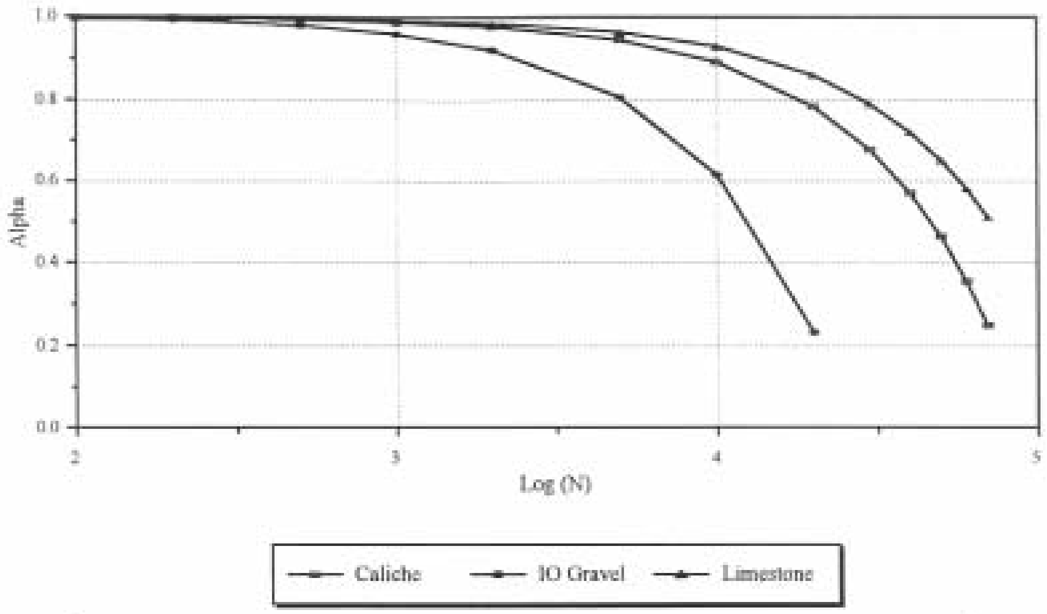

Figure 5.26 Variation of Accelerated Rutting Parameter with Load Application [After Park, (2000)].

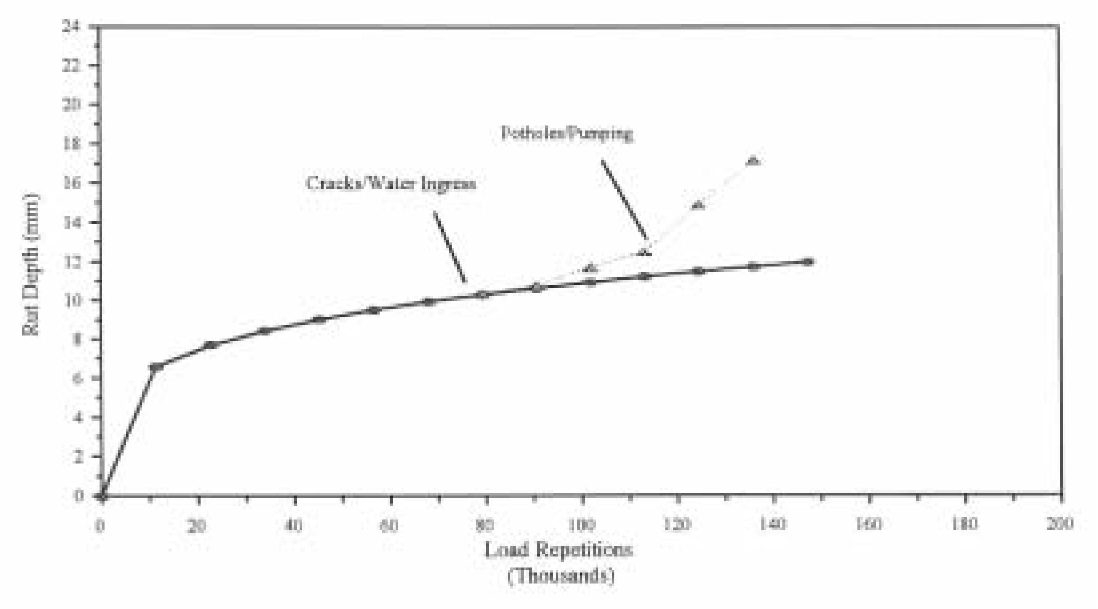

Figure 5.27 Variation of Rut Depth with Ingress of Water in Caliche Base Layer [After Park, (2000)].

CHAPTER VI

DEVELOPMENT OF FINITE ELEMENT PROGRAM

6.1 Background

The finite element method has evolved in the past 40 years from a specialized technique for aircraft frame analysis to a general numerical solution to a broad range of physical problems. The historic paper written by Turner, Clough, and Topp (1956) is credited by many for having established the method. Clough (1960) coined the term ‘finite element method’. The finite element method represents an approximate numerical solution of a boundary-value problem described by a differential equation.

Typically engineering problems in mechanics are addressed by deriving equations relating the variables of interest to basic principles of physics. These principles include equilibrium, potential energy, strain energy, conservation of total energy, virtual work, thermodynamics, conservation of mass, and many more. Finding a solution that satisfies a differential equation throughout a region, and also yields the boundary conditions, is a very difficult and often an impossible task for all but the most elementary problems. The finite element method addresses this difficulty by dividing a region into small sub-regions so that the solution within each sub-region can be represented by a simplified function compared to that required for the entire region. The sub-regions are joined mathematically by enforcing sub-region to sub-region boundary compatibility while satisfying the entire region boundary requirements (Owen and Hinton, 1980).

The finite element method is capable of including material and element non-linearity, as well as different types of loading and interface conditions in the solution. This highly efficient and versatile numerical technique has been applied to pavements since the late 1960’s. However, one problem that has been identified by many researchers (Duncan et al., 1968; Hicks, 1970) is the false prediction of horizontal tensile stresses within unbound granular layers in flexible pavements. Unbound granular materials are known to have negligible tensile strength aside from that induced by suction and particle interlock. Therefore, they cannot accommodate the high tensile stresses predicted. Contrary to the predicted horizontal tensile stresses, conventional flexible pavements with granular layers have been used to carry traffic loads for decades with a remarkable performance history.

Much research has been directed at improving pavement response models to explain the performance of flexible pavements and to reverse the prediction of horizontal tensile stresses in the unbound granular layers. Three primary approaches have been used to correct the predicted horizontal tensile stresses in unbound granular layers in flexible pavements (Tutumluer, 1995). These are:

- A no tension analysis based on stress transfer or failure envelop limitations,
- The presence of overburden and compressive residual stresses, and
- Improved constitutive models.

The stress transfer method to correct tension was proposed by Zienkiewicz et al. (1968). In this procedure, equal compressive stresses are applied to counteract predicted horizontal tensile stresses so that equilibrium is maintained. To improve inherent convergence problems in the original stress transfer method, Doddihal and Pandey (1984) modified the technique for pavements.

The Mohr-Coulomb failure envelope criterion has also been incorporated into finite element method programs (ILLI-PAVE and MICH-PAVE) to reverse the prediction of horizontal tensile stresses in unbound granular layers. Here, predicted stresses are adjusted such that they remain within the Mohr-Coulomb failure envelope in the compressive zone.

Residual compressive stresses have also been incorporated into some finite element programs to correct predicted horizontal tensile stresses. Crockford and Bendana (1990) and Tutumluer (1995) successfully incorporated this technique into the TTI-PAVE and GT-PAVE finite element computer programs, respectively. It is believed that residual stresses exist in compacted unbound granular layers. Many researchers (Stewart et al., 1985; Uzan, 1985; Barksdale et al., 1993; Tutumluer, 1995) have investigated the existence of residual stresses. The residual compressive stresses are believed to be in the range of 13.8-kPa to 27.6-kPa (2 to 4-psi).

Some researchers have also worked on improving constitutive models used to describe the dilation behavior of unbound granular materials. Lytton et al. (1993) derived a differential equation describing the variation of Poisson's ratio with stress state. The solution to this differential equation resulted in what is known as the k_1-k_5 model. This model was incorporated in a finite element program (Liu, 1993) and the results were very impressive. Cross-anisotropy has also been incorporated into finite element programs to improve materials response in unbound granular materials (Zienkiewicz, 1966; Crockford et al., 1990; Tutumluer, 1995). After incorporating cross-anisotropic elastic modeling in the GT-PAVE finite element code, Tutumluer (1995) reported that cross-anisotropic elastic modeling can reduce and even reverse horizontal tensile stresses predicted in unbound granular layers with isotropic elastic model. In his work, Tutumluer (1995) assumed modular ratios and Poisson's ratios to satisfy strain energy conditions.

Although the no tension correction techniques have been used successfully to reverse predicted horizontal tensile stresses in unbound granular layers, if the constitutive models were accurate enough, such corrections would not be necessary. This research focused much of its attention on improving the cross-anisotropic elastic model (Tutumluer, 1995) with stress dependent Poisson's ratios (Lytton et al., 1993; Liu, 1993). Instead of assuming modular ratios, one of the main objectives of this study was the development of a laboratory testing protocol for determining the anisotropic elastic parameters of unbound granular materials. A triaxial laboratory testing protocol to determine the five cross-anisotropic elastic parameters, which has been elusive to many researchers until now, was developed in this study and discussed in Chapters III and IV.

6.2 Finite Element Formulation

A finite element program was developed to model a flexible pavement’s response to traffic loads. The finite element procedures and code are derived from the elasto-plastic formulation, originally developed by Owen and Hinton (1980). The code was developed to analyze an axisymmetric problem with material non-linearity. Liu (1993) was the first to modify the original program to analyze pavements. The modification included mesh generation, the implementation of different constitutive models (hypoelastic, hyperelastic, k_1-k_5, and elasto-plastic models), non-symmetric solutions and the flexible boundary conditions. Park (2000) also made modifications to the code for pavement applications. Both of these modifications included stress dependent Poisson's ratio and non-linear analysis using load increments. The major modification made in this research was to incorporate cross-anisotropic material properties in the code developed by Park (2000).

The principle of virtual work can be used to formulate the finite element method. Consider a solid body, Ω, in which the internal stresses, σ, the distributed loads per unit volume, b, and external applied force, f, form an equilibrium field, to undergo an arbitrary virtual displacement pattern, δd^*, which results in compatible strains, $\delta\varepsilon^*$, and internal displacements, δu^*. The principle of virtual work requires that (Liu, 1993):

$$\int_{\Omega} (\delta\varepsilon^{*T}\ \sigma - \delta u^{*T}\ b) d\Omega - \delta d^{*T}\ f = 0 \tag{6.1}$$

The expressions for the displacements and strains within any discrete finite element are given by (Liu, 1993):

$$\delta u^* = N\delta d^* \qquad\qquad \delta\varepsilon^* = B\delta d^* \tag{6.2}$$

where N is the matrix of shape functions, and B is the elastic strain matrix. Substituting Equation 6.2 into Equation 6.1 yields:

$$\int_{\Omega} \delta d^{*T}\ (B^T\sigma - N^T b) d\Omega - \delta d^{*T}\ f = 0 \tag{6.3}$$

The volume integration over the solid represents the sum of the individual element contributions. Since Equation 6.3 is true for any arbitrary δd^*, then (Liu, 1993);

$$\int_{\Omega} B^T \sigma d\Omega - f - \int_{\Omega} N^T b d\Omega = 0 \tag{6.4}$$

Rewriting Equation 6.4 in incremental form,

$$\int_{\Omega} B^T d\sigma d\Omega - df - \int_{\Omega} N^T dbd\Omega = 0 \tag{6.5}$$

But the incremental stress-strain relationship is given by (Liu, 1993):

$$d\sigma = C\delta\varepsilon = CBdu \tag{6.6}$$

where C is the material constitutive matrix. For an axisymmetric isotropic material model, the matrix C can be written as (Tutumluer, 1995):

$$C = \frac{E}{(1+\nu)(1-2\nu)}\begin{bmatrix} (1-\nu) & \nu & \nu & 0 \\ \nu & (1-\nu) & \nu & 0 \\ \nu & \nu & (1-\nu) & 0 \\ 0 & 0 & 0 & \dfrac{(1-2\nu)}{2} \end{bmatrix} \tag{6.7}$$

where E is the elastic modulus and ν is the Poisson's ratio. For an axisymmetric anisotropic material model, the C matrix is given by:

$$C = A\begin{bmatrix} n(1-n\nu_{xy}{}^2) & n(\nu_{xx}-n\nu_{xy}{}^2) & n\nu_{xy}P & 0 \\ n(\nu_{xx}+n\nu_{xy}{}^2) & n(1-n\nu_{xy}{}^2) & n\nu_{xy}P & 0 \\ n\nu_{xy}P & n\nu_{xy}P & (1-\nu_{xx}{}^2) & 0 \\ 0 & 0 & 0 & mPQ \end{bmatrix} \tag{6.8}$$

where

$$\begin{aligned} P &= (1+\nu_{xx}) \\ Q &= (1-\nu_{xx}-2n\nu_{xy}{}^2) \\ A &= \frac{E_y}{PQ} \\ n &= \frac{E_x}{E_y} \\ m &= \frac{G_{xy}}{E_y} \end{aligned} \tag{6.9}$$

Substituting Equation 6.6 into Equation 6.5 gives:

$$K_T du = df + \int_{\Omega} N^T dbd\Omega \tag{6.10}$$

and,

$$K_T = \int_{\Omega} B^T C B d\Omega \tag{6.11}$$

In Equation 6.10, K_T is the global stiffness matrix, and the displacement vector *du* is the only unknown. The solution to Equation 6.5 can then be solved by conventional matrix inversion methods. The finite element program developed uses an axisymmetric, isoparametric 8-node elements and a 3rd order quadrature with 9 integration points (Park, 2000). The material parameters needed for the finite element analysis are the non-linear vertical resilient modulus k-values (k_1, k_2, k_3), the moduli ratios (*n*, *m*) and the value of the vertical Poisson's ratio as well as the ratio of the horizontal to vertical Poisson's ratios. For the materials tested during this study, the moduli ratios were different for each material but were fairly constant for a particular material at all stress states. Based on this observation, moduli ratios were rather used as input to the finite program instead of k_1 through k_9.

The vertical Poisson's ratio was assumed to be stress-dependent (Lytton et al., 1993; Liu, 1993) as expressed by Equation (2.14):

$$\frac{2}{3}\frac{\partial \nu_{xy}}{\partial J_2^/} + \frac{1}{I_1}\frac{\partial \nu_{xy}}{\partial I_1} = \nu_{xy}\left[\frac{1}{3}\frac{k_3}{J_2^/} + \frac{k_2}{I_1^2}\right] + \left[-\frac{1}{6}\frac{k_3}{J_2^/} + \frac{k_2}{I_1^2}\right]$$

A numerical solution to Equation 2.14 based on the backward difference method was included in the finite element code by Park (2000). Park (2000) described the numerical stepwise solution in detail.

Equation 6.5 will not generally be satisfied at any stage of computation. An iteration algorithm is included in the program to ensure convergence. There are two convergence criteria in the finite element program. The equilibrium criteria are based on residual force values such that (Park, 2000):

$$\frac{\sqrt{\sum_{i=1}^{N}(\psi_i^r)^2}}{\sqrt{\sum_{i=1}^{N}(f_i)^2}}\times 100 \leq TOLLER \qquad (6.12)$$

where,

N = the total number of nodal points,

r = the iteration number,

ψ = the total applied force,

f = the applied nodal force, and

TOLLER = tolerance in convergence (percent).

Park (2000) describes the equilibrium criterion in detail. In order to prevent unreasonable predicted moduli values at low stress levels, cutoff values for both the first stress invariant and octahedral shear stress are specified as input in the program. Also the value of the vertical Poisson's ratio was not allowed to exceed 0.48. Although it is common to observe Poisson's ratios above 0.5 for unbound granular materials in the laboratory, the presence of confinement in field conditions prompted the use of 0.48 as the maximum vertical Poisson's ratio.

The finite element program was used to analyze a set of pavement sections. The unbound granular base layers were modeled as linear isotropic, nonlinear isotropic, linear anisotropic and nonlinear anisotropic.

6.3 Pavement Analysis

The elasto-plastic finite element solutions have been observed to be unstable and divergent when the friction angle of a material is greater than 50º (Liu, 1993). Since the friction angle of unbound granular materials can be greater than 50º, the Uzan's non-linear elastic model (Equation 2.8) was implemented in the finite element program instead of the elasto-plastic model.

Uzan Model: $$E_R = k_1 P_a \left(\frac{I_1}{P_a} \right)^{k_2} \left(\frac{\tau_{oct}}{P_a} \right)^{k_3}$$

The formulation of Equation 2.8 is general. It can easily be downgraded to a linear elastic model when the material parameters, k_2, and k_3 are set to zero. Apart from the non-linear material parameters, the modular ratios (*n*, *m*) and the ratio of horizontal to vertical Poisson's ratio (μ) are needed as input parameters.

where:

$n = \frac{E_x}{E_y}$,

$n = \frac{G_{xy}}{E_y}$, and

$\mu = \frac{\nu_{xx}}{\nu_{xy}}$

A matrix of 27 different pavement sections was analyzed using the finite element program. The pavement sections were selected to investigate the effect of layer thicknesses and subgrade moduli on pavement response using different constitutive models within the unbound granular base course. The pavement matrix is a combination of 50-, 100-, and 150-mm thick hot mix asphalt (HMA) layers on 150-, 300-, and 450-mm thick base courses resting on sub-grades with stiffness of 20.7-, 103.4-, and 206.8-MPa. The pavement structure is shown in Figure 6.1. A standard wheel load of 40 kN was modeled on the surface of each pavement. The loads are assumed to be uniformly distributed over circular areas with radii of 136-mm each.

The pavements were analyzed using linear isotropic, non-linear isotropic, linear anisotropic and non-linear anisotropic constitutive models for the base course. The base material properties used in the analysis are those of a well-graded crushed limestone, compacted at optimum moisture. For all the pavements analyzed in the matrix, the HMA layers and sub-grades were assumed to be non-linear isotropic. Thus, a total of 108 computer runs were performed using the finite element program to predict the pavements' response to a standard wheel load. Table 6.1 is a summary of the material properties used in the analysis.

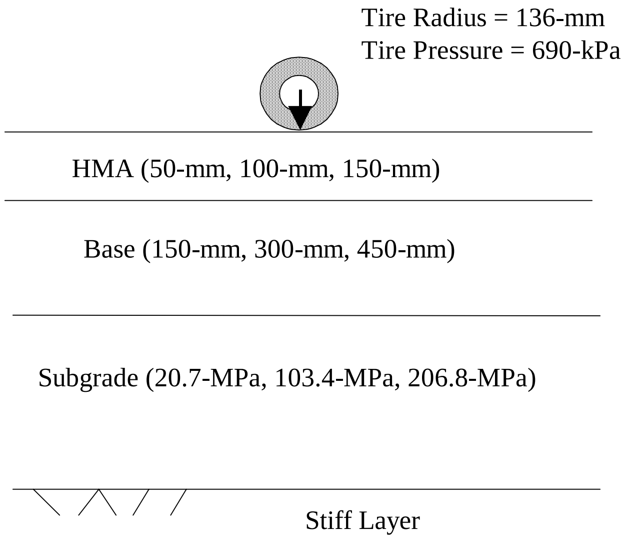

Figure 6.1 Pavement Structure for Finite Element Analysis.

Table 6.1 Pavement Material Properties.

HMA Layer (Linear Isotropic Model)			
k_1 = 28,000 k_2 = 0.100 k_3 = 0.001 n = 1.00 m = 0.38 ν_{xy} = 0.35 μ = 1.00			
Base Course			
Linear Isotropic	Non-Linear Isotropic	Linear Cross-Anisotropic	Non-Linear Cross-Anisotropic
k_1 = 3,500 k_2 =0.0, k_3=0.0 n =1.0, m=0.38 ν_{xy}=0.2, μ = 1.0	k_1=3,500 k_2=0.455, k_3=0.295 n=1.0, m=0.38 ν_{xy}=0.2, μ = 1.0	k_1=3,500 k_2=0.0, k_3=0.0 n=0.5, m=0.38 ν_{xy}=0.2, μ = 1.5	k_1=3,500 k_2=0.455, k_3=0.295 n=0.5, m=0.38 ν_{xy}=0.2, μ = 1.5
Sub-grade (Non-linear Isotropic Model)			
k_1 = 207, 1035, 2070 k_2 = 0.001 k_3 = 0.300 n = 1.00 m = 0.38 ν_{xy} = 0.35 μ = 1.00			

A typical axisymmetric finite element mesh used in the finite element analysis is shown Figure 6.2. The nodal radial strains were assumed to be negligible at approximately 10 times R (radius of loaded area) from the area of applied wheel load. Also, the nodal stresses and displacements were assumed to be negligible at 20 times R below the pavement surface.

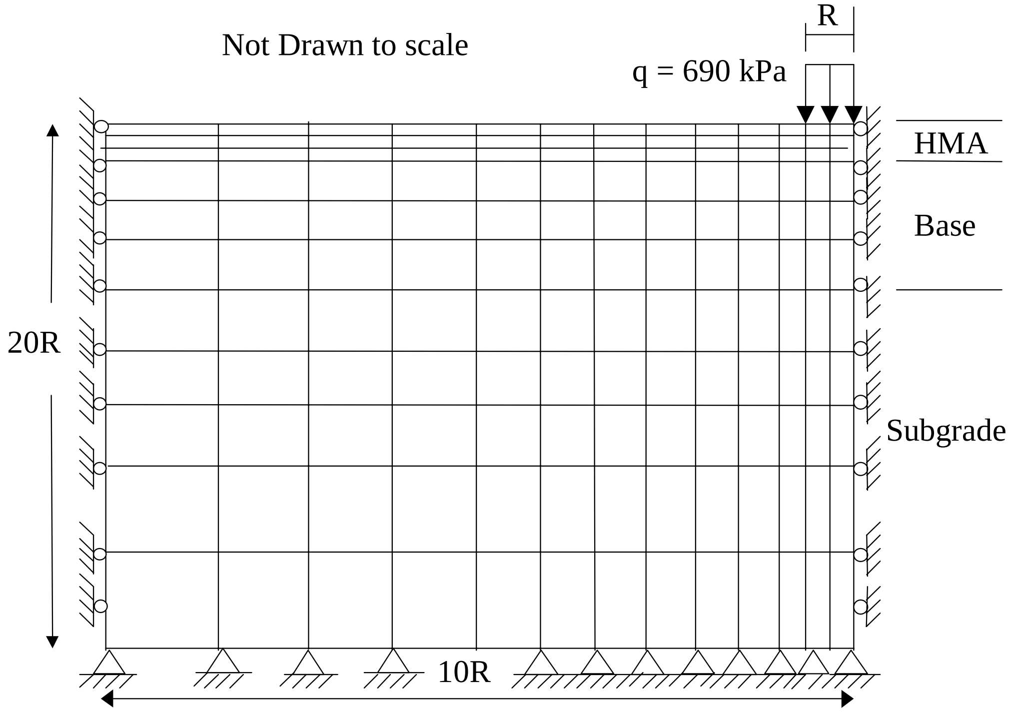

Figure 6.2 Typical Finite Element Mesh for Pavement Analysis.

Typical plots of vertical and horizontal stress distribution within the unbound granular base course at the center of loaded area are plotted in Figures 6.3 through 6.8 for a pavement section with 50-mm HMA layer, 300-mm base layer and 20.7-MPa, 103.4-MPa, and 206.8-MPa moduli sub-grades. Similar trends were obtained on the other pavement sections and the plots are shown in Appendix C. The finite element program adopts a compression-is-negative sign convention. Gravity stresses due to overburden load and residual compaction stresses were not included in the finite element analysis because more emphasis was placed on constitutive modeling.

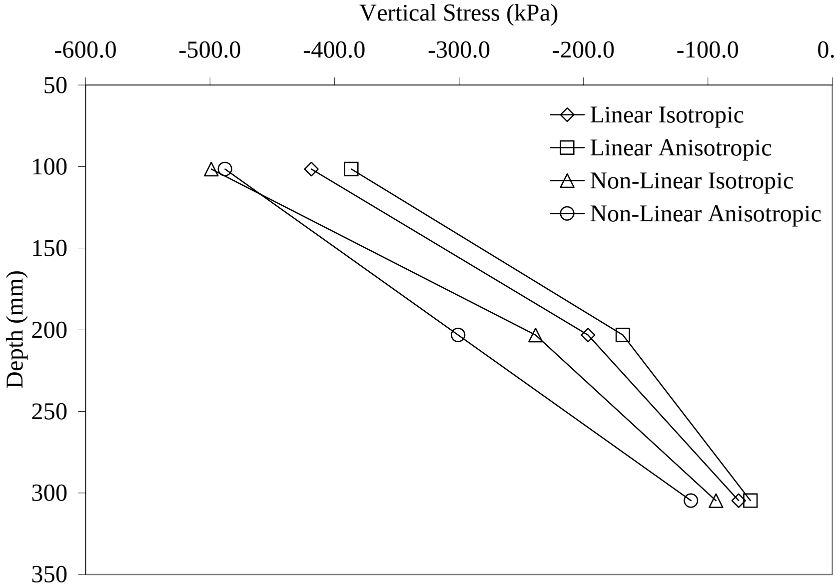

Figure 6.3 Vertical Stress for 50-mm HMA, 300-mm Base and 20.7-MPa Sub-grade.

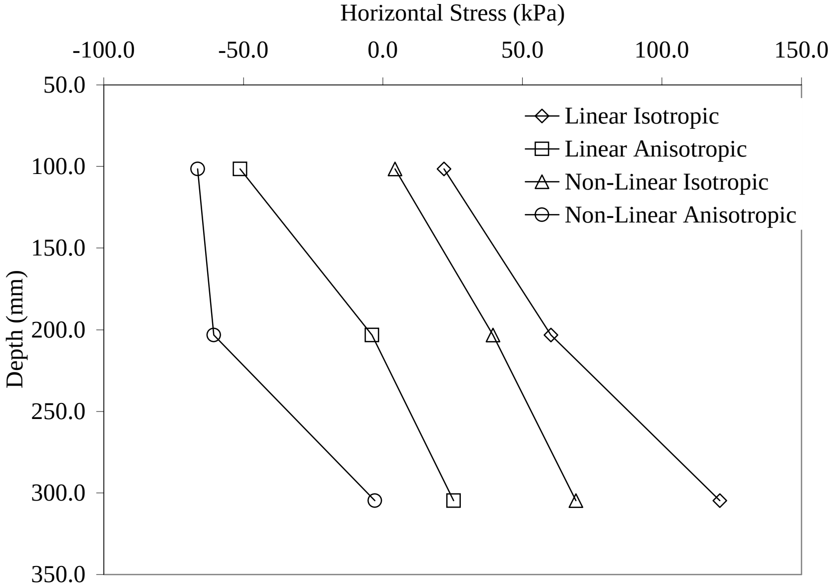

Figure 6.4 Horizontal Stress for 50-mm HMA, 300-mm Base and 20.7-MPa Sub-grade.

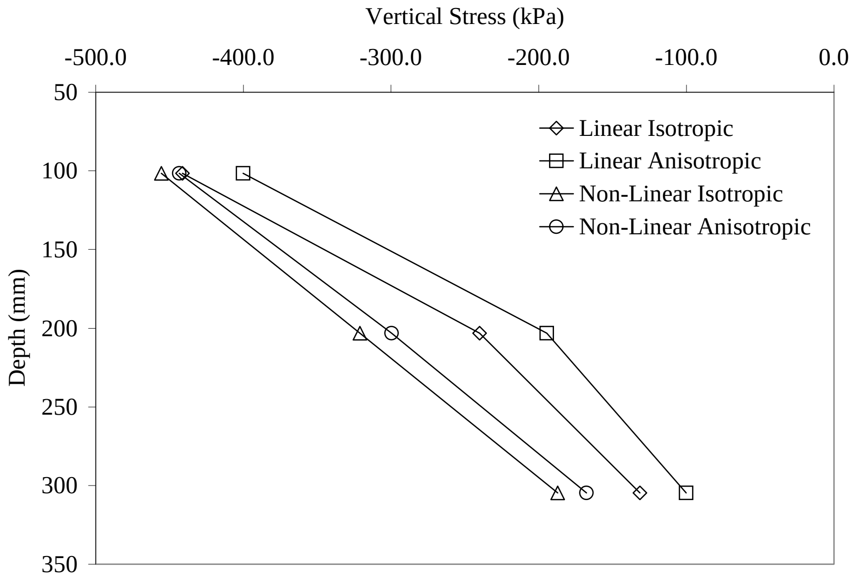

Figure 6.5 Vertical Stress for 50-mm HMA, 300-mm Base and 103.4-MPa Sub-grade.

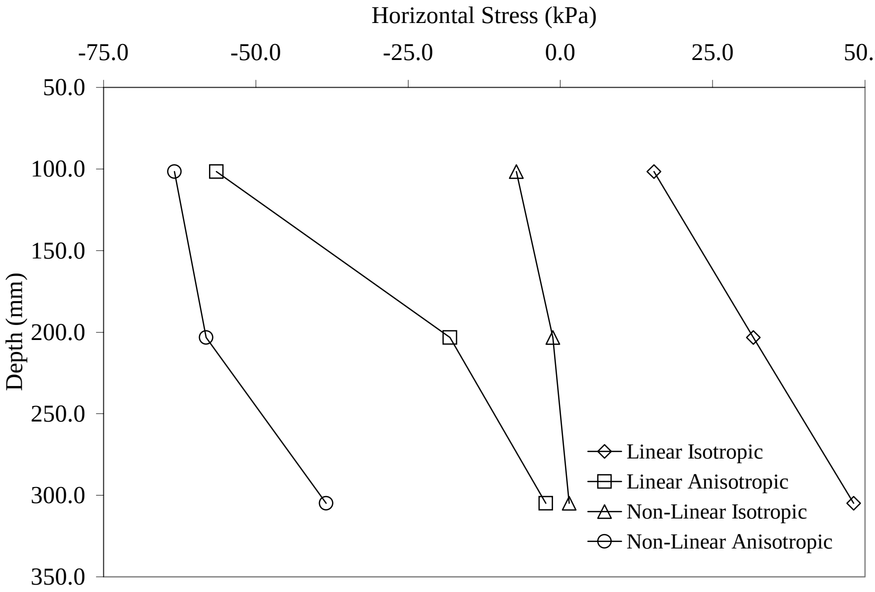

Figure 6.6 Horizontal Stress for 50-mm HMA, 300-mm Base and 103.4-MPa Sub-grade.

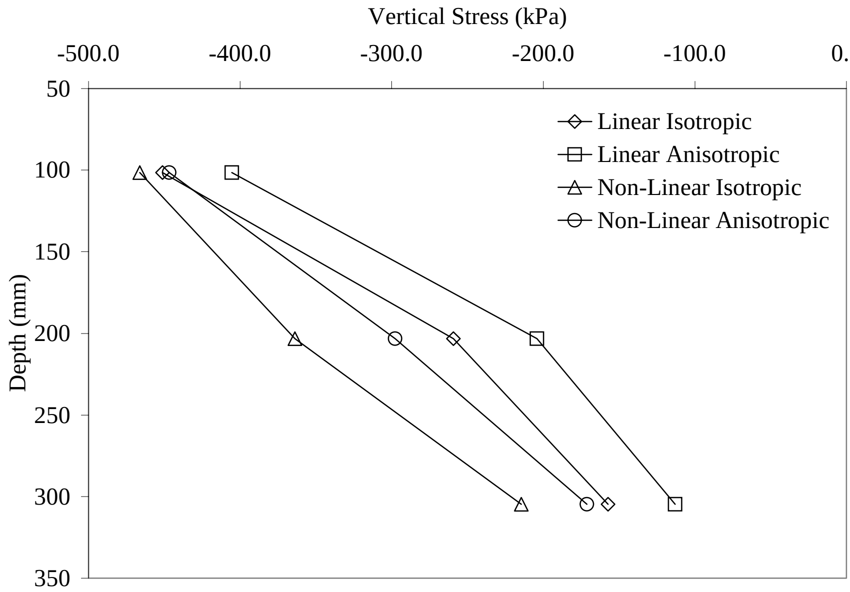

Figure 6.7 Vertical Stress for 50-mm HMA, 300-mm Base and 206.8-MPa Sub-grade.

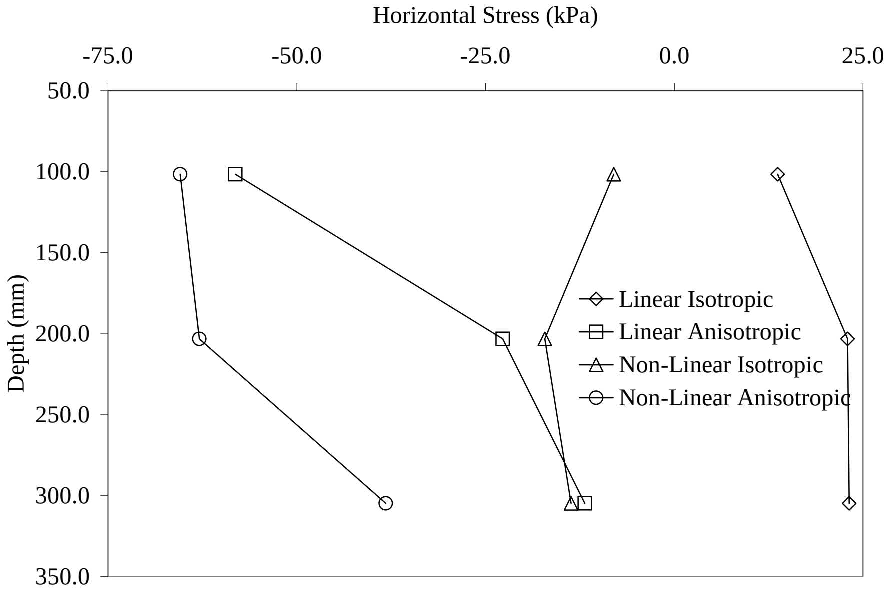

Figure 6.8 Horizontal Stress for 50-mm HMA, 300-mm Base and 206.8-MPa Sub-grade.

Different trends were observed in the distribution of vertical and horizontal stresses within the unbound granular base course. Variation in layer thickness, the constitutive model used to characterize the base layer, and sub-grade moduli have a significant effect on the distribution of stresses. The contributions of these factors to the way stresses are distributed in the base layer are discussed in the following sections.

6.3.1 Constitutive Models

Pavement sections were analyzed using different material constitutive models within the unbound granular base layer. The models considered were:

- Linear isotropic,
- Non-linear isotropic,
- Linear cross-anisotropic, and
- Non-linear cross-anisotropic.

The distributions of vertical compressive stresses within the base layers do not follow an exact trend with respect to the models considered for the pavement sections. In a majority of the pavement sections evaluated, lower vertical stresses were observed with the linear anisotropic model. The layer thickness and sub-grade moduli more significantly affect the distribution of vertical stresses than material constitutive models.

The effect of material constitutive models on pavement response is more pronounced in the distribution of horizontal stresses within the unbound granular base layer. Horizontal stress distribution within the base layer follows a particular trend with respect to material constitutive modeling. The magnitude of the horizontal stress at a point within the base course depends on the layer thickness and subgrade modulus but, whether the stress is compressive or tensile is dictated by the material constitutive model used.

In all the pavement sections analyzed, cross-anisotropic models eliminated the false tension zones predicted by isotropic models. The linear isotropic model always predicted increasing horizontal tensile stresses within the depth of the unbound granular base layer. Although non-linear isotropic modeling significantly reduced the magnitude of the tensile horizontal stresses predicted by linear isotropic modeling, tension zones still existed in the base layer for most of the pavement sections. The only pavement sections where some compressive stresses were observed with the non-linear isotropic model were pavements with very high sub-grade modulus. Increasing the base layer thickness decreased the magnitude of the horizontal tensile stresses but did not remove the presence of tension zones.

Except for a few pavement sections, especially those with weak subgrades, horizontal compressive stresses were predicted with linear cross-anisotropic modeling. Non-linear cross-anisotropic model was observed to always predict compressive horizontal stresses, and the magnitudes of these stresses were higher than those predicted by linear cross-anisotropic model.

Modeling the unbound granular base layer as linear isotropic, non-linear isotropic, linear anisotropic and non-linear anisotropic in that order, gradually shifts the horizontal stresses from a tension zone to a compressive zone. This observation implies that if appropriate models are used to characterize the behavior of unbound granular materials, the base layers are capable of mobilizing enough confinement to withstand wheel loads. This is in agreement with the observation made by Barksdale, Brown and Chan (1989) that linear cross-anisotropy is equal to or better than a more complicated non-linear isotropic model for predicting unbound granular layer response to traffic loads. It is the ability of unbound granular layers to develop confinement that can be used to explain their historic performance in flexible pavements. The confinement can be used to confirm a comment made by Lytton (1998) that immediately beneath a tire load an unbound granular layer generates its own lateral confining pressure and becomes very stiff almost as if it were forming a moving vertical column that travels along with the load. This is illustrated in Figure 6.9. The presence of confinement within the unbound granular base layer means that a tension zone does not exist as predicted by isotropic modeling. Also, there is an increase in bulk stress and modulus to facilitate the spread of wheel loads.

Determining the stress profile within a pavement is important for accurate prediction of permanent deformation. Researchers and Engineers agree on the existence of confinement in unbound granular base layers for spreading wheel loads. Non-linear cross-anisotropic modeling has recently been reported (Adu-Osei *et al*., 2000; Tutumluer, 1995, 1999) as a superior model for predicting the behavior of unbound granular materials. It has been difficult to absolutely establish and quantify the extent of confinement in base layers but the non-linear cross-anisotropic elastic model with stress dependent Poisson's ratio can be used to explain this important phenomenon in unbound granular layers.

The material properties used to characterize unbound granular materials were determined based on established elastic theories. During laboratory testing, dilation was observed in the materials. After incorporating strains measured into the system identification method and resolving material response into five cross-anisotropic properties, vertical Poisson's ratios were generally determined to be below 0.5 as required by theories of elasticity. The dilation observed has been explained by the development of self-confinement in the granular base layers.

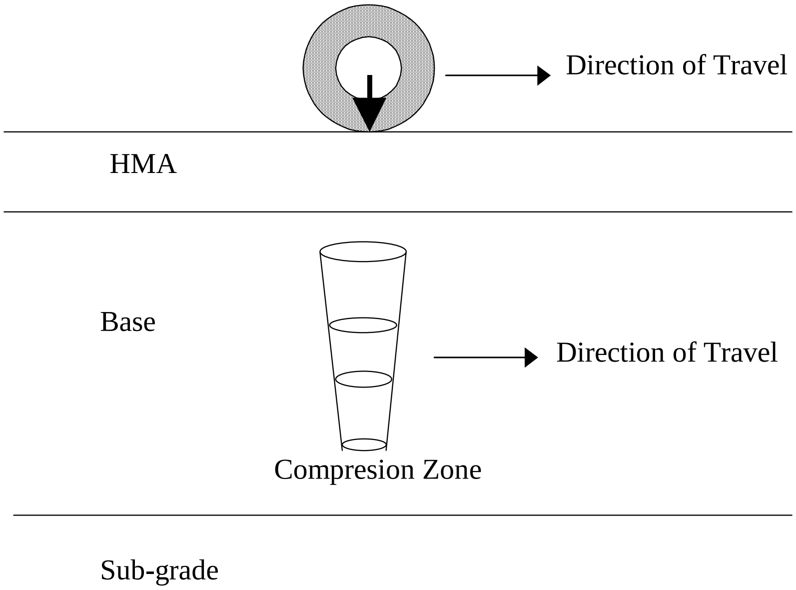

Figure 6.9 Illustration of Compressive Zone in Unbound Granular Layer.

6.3.2 Layer Thickness

For a given base layer thickness and subgrade modulus, increasing the thickness of the HMA layer decreases the magnitude of the vertical and horizontal stresses at any point in the base layer. Similar trends were observed in increasing the base layer thickness for a given HMA layer and sub-grade modulus.

Increasing the HMA or base layer thickness did not explain the existence of tension or compression zone in the unbound granular base layer. Thus the design philosophy in which the thickness of the unbound granular base layer is increased until the tension zone, as predicted by isotropic elastic methods, diminishes is very conservative. This design practice would result in pavement sections that are much thicker than needed.

6.3.3 Subgrade Modulus

The subgrade moduli values of 20.7-, 103.4-, and 206.8-MPa used in this study represent a weak, strong, and chemically stabilized subgrade, respectively. Increasing the subgrade modulus did not significantly change the distribution of vertical stresses within the base layer.

For a given pavement section, an increase in subgrade modulus did not significantly change the horizontal compressive stresses predicted with the non-linear cross-anisotropic model. However, the following were observed for the other material models:

- Increasing the subgrade modulus shifted the few tension zones in the base layer predicted by the linear cross-anisotropic model into compression zones.
- Increasing subgrade modulus shifted most of the tension zones in the base layer predicted by the non-linear isotropic model into compression zones.
- Although the magnitudes of the stresses in the tension zones in the base layer predicted by linear isotropic modeling were significantly reduced, increasing the subgrade modulus did not remove the presence of tension zones in the base layer

It must also be noted that the magnitudes of the horizontal compressive stresses predicted by the linear cross-anisotropic and non-linear isotropic models, as a result of subgrade improvement, were still lower than the stresses predicted by the non-linear cross-anisotropic model.

The higher compressive stresses predicted by the nonlinear cross-anisotropic model predicts not only a stiffer base course under load but also the potential for accelerated rutting due to ingress of water and an incremental build-up of pore water pressure with repeated traffic loading. This tendency will be greater in those base courses with higher percent of fines (Lytton, 1998).

CHAPTER VII

FIELD VALIDATION OF RESILIENT RESPONSE

7.1 Background

The cross-anisotropic resilient model developed in this study was verified with field data collected on two pavement sections at the TTI Research Annex. The data used in the field validation was originally collected in a study conducted by Uzan and Scullion (1990) to verify backcalculation procedures. The pavement sections were instrumented with Multi-Depth Deflectometers (MDD). Falling Weight Deflectometer (FWD) loads were applied to the pavement surfaces and pavement response (deflections) were collected. Pavement deflections were determined with the finite element program developed in this study and compared to deflections measured in the field. The effect of using different material models to characterize unbound granular layers on deflections was also studied.

The National Institute for Transport and Road Research (NITRR) in South Africa developed the MDD (Basson, 1981; Scullion et al., 1988). It is used to measure the resilient deflection and permanent deformation in pavement layers. Figure 7.1 is a schematic diagram of the MDD sensor. The MDD consists of modules with LVDTs that are positioned at different depths in the pavement to measure vertical movement in the layers. A maximum of six MDD sensors may be located in a single hole. The field installation and calibration are described elsewhere (Basson, 1981; Scullion et al., 1988).

The two pavement sections have different layer thicknesses. Section 11 has a thin surfacing over a thick crushed limestone base over a sandy gravel subgrade. Section 12 has a thick surface layer over a thick crushed limestone base over a sandy gravel subgrade. The MDD anchors are located at 1.625 and 2.025 meters in the thin and thick sections, respectively. The thin pavement had two MDD sensors and the thick pavement had four. The pavement layer thicknesses and MDD sensor locations are shown in Figure 7.2.

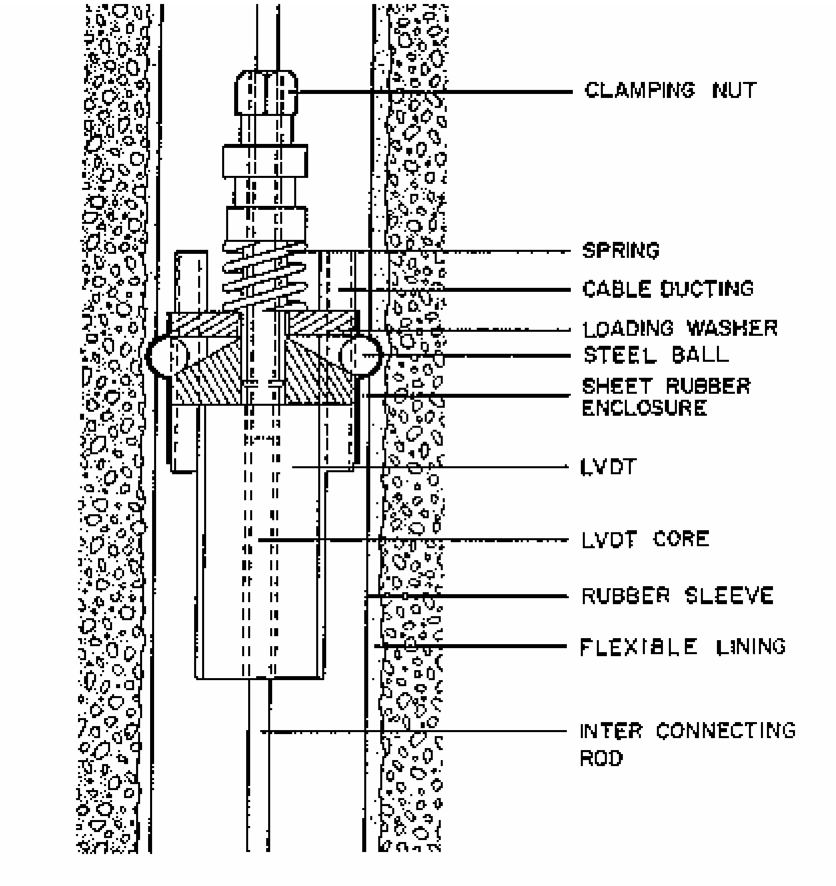

Figure 7.1 The Multi-Depth Deflectometer Sensor (After Basson 1981).

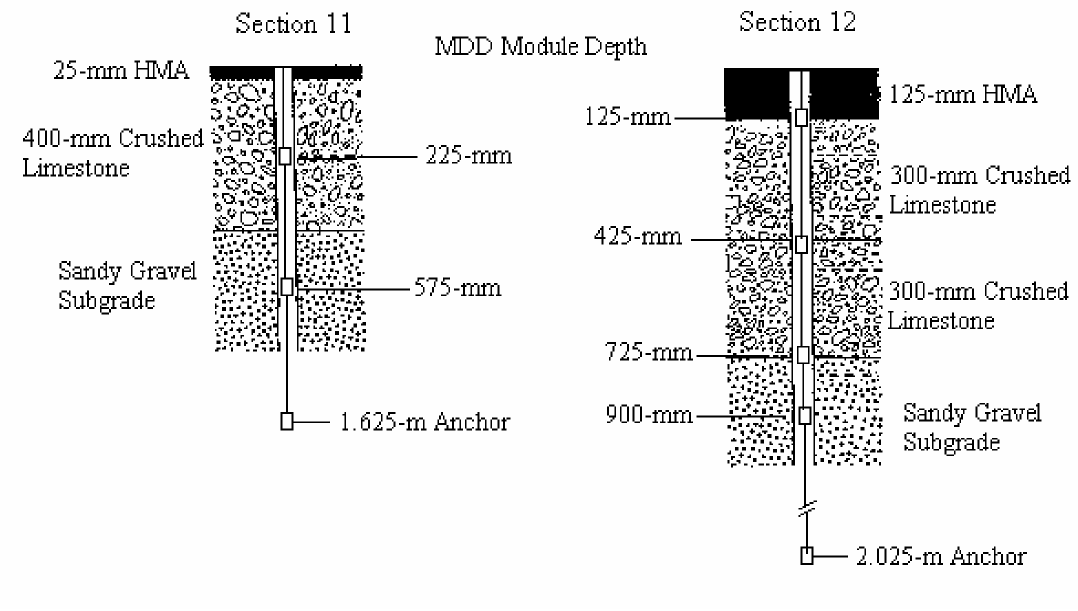

Figure 7.2 Pavement Sections with MDD Sensor Locations.

The FWD load plate was placed close to the MDD hole and four different load levels (approximately 28.9, 40.0, 46.7 and 64.5-kN) were applied. Surface deflections (FWD sensors), depth deflections (MDD sensors) and MDD anchor movement were recorded. The MDD anchor movement was measured with a FWD sensor placed on the MDD setup. Replicate readings were taken at each load level.

The FWD load plate was then repositioned at several distances from the MDD hole and the test repeated. Thus, two-dimensional deflection bowls were recorded using this technique.

The average FWD results for the thick pavement (section 12) are shown in Table 7.1 and the corresponding MMD depth deflections (40.0-kN level only) and anchor movements are shown in Table 7.2. The values in the bracket are normalized deflections, in deflection per unit load. Similar results for the thin pavement (section 11) are shown in Tables 7.3 and 7.4. The FWD and MDD data are plotted in Figures 7.3 and 7.4 for sections 12 and 11, respectively.

Table 7.1 Falling Weight Deflectometer Data on Section 12.

Load (kN)	FWD Surface Deflections, in µm and (µm/kN) Radial Distance (m)					
	0.0	0.3	0.6	0.9	1.2	1.8
28.9	140.7 (4.9)	91.9 (3.2)	52.8 (1.8)	36.6 (1.3)	27.7 (1.0)	16.8 (0.6)
40.0	196.1 (4.9)	131.1 (3.3)	77.7 (1.9)	52.1 (1.3)	40.4 (1.0)	25.9 (0.6)
46.7	234.7 (5.0)	159.5 (3.4)	94.7 (2.0)	64.5 (1.4)	48.3 (1.0)	33.5 (0.7)
64.5	323.6 (5.0)	216.7 (3.4)	131.1 (2.0)	90.4 (1.4)	67.1 (1.0)	47.0 (0.7)

Table 7.2 Multi-Depth Deflectometer Data on Section 12.

Load (kN)	Distance From Load to MDD (m)	Deflection at Depth (µm) MDD Location (m)				Anchor
		0.125	0.425	0.725	0.900	2.025
40.0	0.2	152.1	114.8	92.5	78.0	37.6
40.0	0.4	116.3	98.0	84.3	72.9	37.1
40.0	0.5	95.0	84.1	75.9	67.1	35.3
40.0	0.7	61.7	60.2	60.7	55.9	32.8
40.0	1.1	43.7	45.0	47.8	45.5	30.5

Table 7.3 Falling Weight Deflectometer Data on Section 11.

Load (kN)	FWD Surface Deflection, in μm and (μm/kN) Radial Distance (m)					
	0.0	0.3	0.6	0.9	1.2	1.8
28.9	324.6 (11.2)	125.2 (4.3)	57.4 (2.0)	38.1 (1.3)	30.5 (1.1)	26.2 (0.9)
42.8	449.8 (10.5)	193.8 (4.5)	87.4 (2.0)	59.2 (1.4)	47.8 (1.1)	40.6 (0.9)
64.5	632.2 (9.8)	289.6 (4.4)	132.1 (2.0)	90.4 (1.4)	73.7 (1.1)	62.2 (1.0)

Table 7.4 Multi-Depth Deflectometer Data on Section 11.

Load (kN)	Distance From Load to MDD (m)	Deflection at Depth (μm) MDD Location (m)		Anchor
		0.225	0.575	1.625
42.8	0.23	295.4	185.9	67.6
42.8	0.48	150.1	142.5	68.3
42.8	0.78	76.2	79.0	51.3
64.5	0.23	428.8	299.5	106.9
64.5	0.48	215.9	206.5	99.6
64.5	0.78	117.3	123.7	82.3

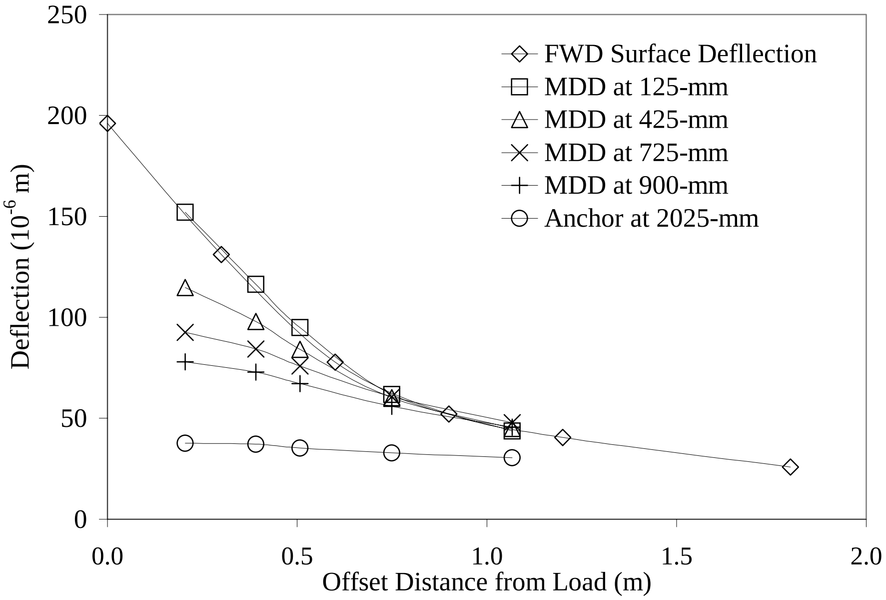

Figure 7.3 Measured Surface and Depth Deflections on Section 12.

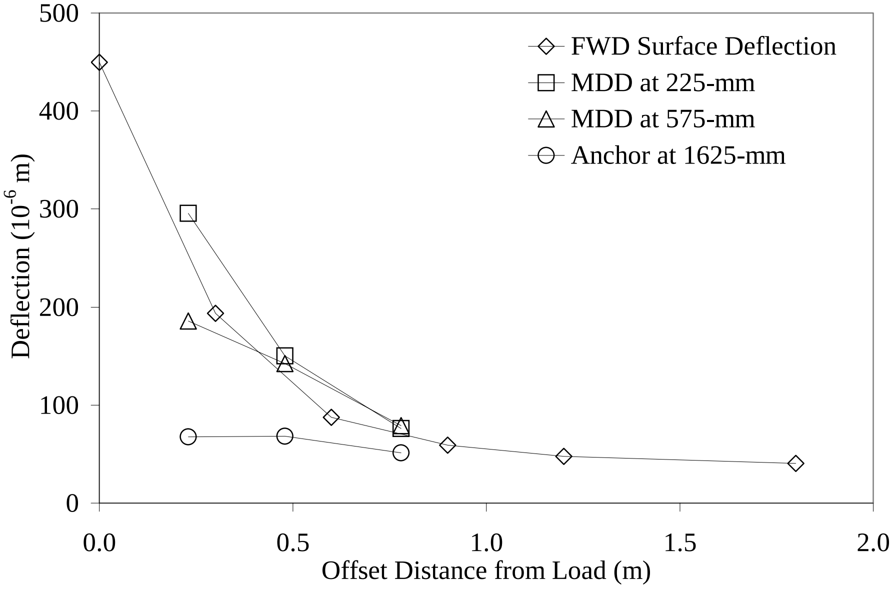

Figure 7.4 Measured Surface and Depth Deflections on Section 11.

7.2 Data Analysis

In figure 7.3 the MDD deflections decrease with depth and are less than the FWD surface deflections in the thick pavement (section 12). In the thin pavement (section 11), the MDD deflections measured within the base layer and subgrade are greater than those measured on the pavement surface (Figure 7.4). This indicates that dilation takes place in the granular layers. The dilated material acts like an internal pressure to uplift the surface and pushes the subbase and subgrade down. Thus, the deflection bowl observed at section 11 can not be explained by standard linear elastic techniques.

Tables 7.1 and 7.3 include absolute surface deflections in μm and normalized surface deflection in μm/kN (deflection per unit load). The deflection per unit load is a good indicator of nonlinear response of the pavement (Uzan and Scullion, 1990). The following observations were made with regard to the absolute and normalized deflections on both pavement sections.

- the absolute deflections (μm) generally increase with increasing load,
- the normalized center deflections (μm/kN) are almost constant in section 12 and decrease with increasing load in section 11, and
- the other normalized deflections (μm/kN) are almost independent of the load.

It is therefore expected that the pavement response is more load-dependent in section 11 than in section 12. The surface and depth deflections were used to backcalculate the material property (moduli) of the pavement layers. Based on the FWD surface deflections and MDD depth deflections, several computer runs were made using the finite element program with different material properties until the average percent error in deflections were less than 10%. In the finite element computer runs, the surface layer and subgrade were assumed to be linearly elastic and the base layer was assumed to be nonlinear cross-anisotropic. The base layer was then analyzed as linear isotropic, nonlinear isotropic and linear cross-anisotropic and the deflections computed were compared to the measured deflection. Tables 7.5 and 7.6 are summaries of the backcalculated material properties used in the finite element program for sections 12 and

11, respectively. The average percent errors of measured deflections are tabulated in Tables 7.7 and 7.8 for the material properties considered in the granular layer.

Table 7.5 Backcalculated Material Properties for Section 12.

Material	Pavement Layer			
Property	HMA	Base	Subbase	Subgrade
k_1	138000	5860	5170	2070
k_2	0.000	0.255	0.255	0.000
k_3	0.000	0.255	0.255	0.000
n	1.00	0.50	0.50	1.00
m	0.35	0.30	0.30	0.35
μ	1.00	1.50	1.50	1.00

Table 7.6 Backcalculated Material Properties for Section 11.

Material	Pavement Layer			
Property	HMA	Base	Subbase	Subgrade
k_1	69000	4480	5170	1930
k_2	0.000	0.255	0.255	0.000
k_3	0.000	0.255	0.255	0.000
n	1.00	0.50	0.50	1.00
m	0.35	0.30	0.30	0.35
μ	1.00	1.50	1.50	1.00

Table 7.7 Average Percent Error of Deflections for Section 12.

Base Layer Material Model	Average % Error in FWD	Average % Error in MDD
Linear Isotropic	39.9	35.7
Linear Anisotropic	34.6	38.6
Nonlinear Isotropic	4.8	10.1
Nonlinear Anisotropic	6.3	4.4

Table 7.8 Average Percent Error of Deflections for Section 11.

Base Layer Material Model	Average % Error in FWD	Average % Error in MDD
Linear Isotropic	48.6	41.9
Linear Anisotropic	47.2	41.0
Nonlinear Isotropic	6.6	7.0
Nonlinear Anisotropic	4.9	7.8

The error values in Tables 7.7 and 7.8 suggest that the behavior of unbound granular materials can not be explained by linear analysis. Nonlinear isotropic and cross-anisotropic material models in the base layer predicted vertical deflections that are close to field deflections in the pavements analyzed.

CHAPTER VIII

CONCLUSIONS AND RECOMMENDATIONS

8.1 Conclusions

An apparent anisotropy is induced in an unbound granular layer during construction, becoming stiffer in the vertical direction than in the horizontal direction even before traffic loads impose further anisotropy.

Existing pavement design and analysis methods rely on empirical procedures which have generally taken a very conservative view of the relative strength properties of granular materials used as base and subbase layers in conventional flexible pavements. The contribution of unbound granular layers to the overall structural integrity of flexible pavements is significant, especially for thinly surfaced low volume roads.

Until particulate mechanics are developed to a level where it can reasonably be applied to characterize unbound granular materials, nonlinear and cross-anisotropic models can be used to characterize the behavior of granular materials in pavements.

There is strong evidence in the literature that nonlinear cross-anisotropic elastic models are superior to isotropic models in characterizing granular materials. However, it has been extremely difficult to determine the cross-anisotropic material properties of unbound granular materials using the conventional triaxial setup.

A laboratory testing protocol has been developed to determine the cross-anisotropic material properties of unbound granular materials in flexible pavements. The testing protocol was developed based on theories of elasticity. The protocol uses three incremental stress regimes in ten stress levels to determine stress sensitivity and cross-anisotropy. A system identification method is used as an analytical technique to compute the five cross-anisotropic material properties. The material properties, once determined from the testing protocol satisfy the requirements elastic work potential.

The testing protocol is an excellent tool for both unbound granular material characterization and comparative analysis of materials. A compaction study on two very different granular materials (rounded river gravel and crushed limestone) was performed in which the aggregates were subjected to impact and gyratory shear compaction. The level of anisotropy in a material is assumed to depend on particle orientation. The differences in the tendency of the compaction method to produce varying levels of particle orientation, which affects anisotropy was evident in the degree of anisotropy measured.

Samples used in this study were compacted for height to diameter ratios of 1:1. This is contrary to the conventional height to diameter ratios of 2:1 used in triaxial testing. The resilient behavior of 1:1 and 2:1 samples were studied. It was observed that difference in sample size did not significantly affect the resilient behavior of the samples tested.

The resilient and permanent deformation behaviors of four granular materials were studied. Material type, gradation, moisture content and stress levels affect the deformation of granular materials. The effect of moisture on resilient moduli depends on material type and gradation. An increase in plasticity and fine content is generally accompanied by a significant variation in moduli due to changes in moisture content.

The moduli ratios, horizontal to vertical modulus, *n*, and shear to vertical modulus ratios, *m*, were fairly constant for a particular material at all stress levels. The Poisson's ratio values varied with the level of stress applied to the sample. Instead of using k_1 through k_9 coefficients to describe a granular material, the moduli and Poisson's ratios, together with k_1, k_2 and can be used. This way, there is no need to write separate subroutines for the convergence of horizontal and shear resilient moduli in the finite element program. Once a subroutine is written for the convergence of vertical resilient modulus, the moduli ratios (*m* and *n*) account for the convergence of horizontal and shear resilient moduli.

Nonlinear regression analysis was used to obtain good fits of the resilient moduli with Uzan and Lytton models. The R-square determined for each material was above

0.90. Regression coefficients, which indicate how well a material can spread traffic loads, were obtained. The regression coefficients are related.

The permanent deformation data was used to fit the Vesys and Three-Parameter models. Model parameters, which indicate the permanent deformation potential of each material, were obtained.

Different granular materials behave differently under repeated loading. At low stress levels, accumulation of permanent deformation may stabilize. At high stress levels however, plastic strains will continuously accumulate. Applied stress levels have significant effect on how permanent strains will accumulate with repeated loading. Although it is easy to study the permanent deformation behavior of granular materials in the laboratory, it is important that stress levels expected in the field be applied to laboratory samples.

Existing analytical techniques use layered elastic procedures, which fall short of accurately predicting horizontal stresses in flexible pavements. A finite element program was modified to incorporate nonlinear cross-anisotropic material behavior and stress dependent Poisson’s ratio. Different pavement sections were analyzed with the finite element program. Nonlinear cross-anisotropic modeling was observed to predict self-confinement within granular layers.

The resilient model was validated with data collected form the field. Finite element runs were performed on pavement sections and it was observed that linear elastic modeling was not adequate to explain the behavior unbound granular layers. The errors in measured pavement deflections predicted using nonlinear cross-anisotropic and isotropic models in the base layers were less than 10%.

8.2 Recommendations

In the development of the testing protocol it was assumed that the material would behave linearly elastic under small stress changes. The stress changes used in the stress regimes were small and do not simulate the stress path under a moving wheel load. It is recommended that larger stress changes be used and compared to the small changes used in this study.

Further testing needs to be done on other granular materials to confirm the general-purpose nature of the system identification method to analyze laboratory data.

More instrumented pavement sections need to be built to obtain a large field database for further validation of the finite element program. Existing modulus backcalculation methods use linear layered elastic techniques. It is extremely difficult to use finite element methods to backcalculate layer material properties. Further research needs to be done to incorporate material non-linearity in backcalculation methods to account for the behavior of unbound granular layers.

Further study needs to be done to establish how the compaction methods considered are related to compaction levels achieved in the field. Undisturbed field cores of unbound granular materials must be obtained and tested in the laboratory to confirm the material properties and the observations made on compaction methods.

REFERENCES

American Association of State and Highway Officials (AASHTO). (1993). “AASHTO Guide for Design of Pavement Structures.” American Association of State and Highway Officials Washington DC.

Adu-Osei, A., Lytton, R. L. and Little D. N. (2000). “System Identification Method for Determining the Anisotropic Resilient Properties of Unbound Aggregates.” Unbound Aggregates in Roads (UNBAR5) Symposium, University of Nottingham, England, June 21-23, 2000.

Alavi, S. H. (1992). “Viscoelastic and Permanent Deformation Characteristics of Asphalt-Aggregate Mixes Tested as Hollow Cylinders and Subjected to Dynamic Axial and Shear Loads.” Ph.D. Thesis, University of California, Berkely, CA.

Allen, J. J. (1973). “The effects of Non-Constant Lateral Pressures on Resilient Response of Granular Materials.” Ph.D. Dissertation. University of Illinois at Urbana-Champaign, Il.

Allen, J. J. and Thompson, M. R. (1974). “Resilient Response of Granular Materials Subjected to Time Dependent Lateral Stresses.” *Transportation Research Record 510*, Transportation Research Board, Washington, DC, 173-182.

Alvin, R. G. and Ulery, H. H. (1962). “Tabulated Values for Determining the Complete Pattern of Stresses, Strains and Deflections Beneath A Uniform Circular Load on a Homogeneous Half Space.” Bulletin 342, *Highway Research Board,* 1-13.

Amadei, B. (1983). “Rock Anisotropy and the Theory of Stress Measurements.” Lecture Notes in Engineering; 2. Springer-Verlag.

Barksdale, R. D. (1971). “Compressive Pulse Times in Flexible Pavements for Use in Dynamic Testing.” *Highway Research Record* No. 345, Highway Research Board, National Research Council, Washington, DC.

Barksdale, R. D. (1972). “Laboratory Evaluation of Rutting in Base Course Materials.” Proceedings, *3rd International Conference on the Structural Design of Asphalt Pavements*, Vol. 1, Ann Arbor, MI, 161-174.

Barksdale, R. D. (1991). "The Aggregate Handbook." National Stone Association, Washington D.C. Mercury Publishing Services, MD.

Barksdale, R. D. and Alba, J. L. (1993). "Laboratory Determination of Resilient Modulus for Flexible Pavement Design." Interim Report No. 2, NCHRP, Transportation Research Board, National Research Council, Washington, DC.

Barksdale, R. D., Brown, S. F. and Chan, F. (1989). "Potential Benefits of Geosynthetics in Flexible Pavements." NCHRP Report 315, Transportation Research Council, Washington, DC.

Bishop, A. W. and Green, G. E. (1965). "The Influence of End Restraint on the Compression Strength of a Cohesionless Soil." *Geotechnique*, Vol. 15, No. 3, 243-265.

Boussinesq, J. (1885). "Application des Potentiels a L'etude de L'equilibre et du Mouvement des Solids Elastiques." Gauthier-Villars, Paris.

Boyce, J. R. (1976). "The Behavior of a Granular Material Under Repeated Load." Ph.D. Thesis, University of Nottingham, Department of Civil Engineering, U.K.

Boyce, J. R., Brown, S. F. and Pell, P. S. (1976). "The resilient Behaviour of a Granular Material Under Repeated Loading." *Proceedings, Australia Road Research Board,* 28, 8-19.

Brown, S. F. (1996). "Soil Mechanics in Pavement Engineering." *Geotechnique* Vol. 46, No. 3, 383-426.

Brown, S. F., O'Reilly, M. P., and Pappin, J. W. (1989). "A Repeated Load Triaxial Apparatus for granular Materials." *Unbound Aggregates in Roads,* London, Butterworth, 143-158.

Burmister, D. M. (1943). "The Theory of Stresses and Displacements in Layered Systems and Applications to the Design of Airport Runways." *Proceedings, Highway Research Board*, Vol. 23, 126-144.

Burmister, D. M. (1945). “The General Theory of Stresses and Displacements in Layered Soil Systems.” *Journal of Applied Physics*, Vol. 16, 84-94, 126-127, 296-302.

Chan, F. W. K. (1990). “Permanent Deformation Resistance of Granular Layers in Pavements.” Ph.D. Thesis, University of Nottingham, UK.

Chan, F. K. and Brown, S. F. (1994). “Significance of Principal Stress Rotation in Pavements.” *Proceedings, 13th International Conference on Soil Mechanics and Foundation Engineering*, Delhi, Vol. 4, 1823-1826.

Chen, W. F. and Mizuno, E. (1990). “Nonlinear Analysis in Soil Mechanics.” Developments in Geotechnical Engineering, Vol. 53, Elsevier, New York, NY.

Clough, R. W. (1960). “The Finite Element Method in Plane Stress Analysis.” *Proceedings, 2nd Conference on Electronic Computation*, ASCE.

Crockford, W. W., Bendana, L. J., Yang, W. S., Rhee, S. K. and Senadheera, S. P. (1990). “Modeling Stress and Strain States in Pavement Structures Incorporation Thick Granular Layers.” Final Report, Texas transportation Institute, College Station, Texas.

De Jong, D. L., Peatz, M. G. F. and Korswagen, A. R. (1973). “Computer Program Bisar, Layered Systems Under Normal and Tangential Loads.” Konin Klijke Shell-Laboratorium, Amsterdam, External Report AMSR.0006.73.

Doddihal, S. R. and Pandey, B. B. (1984). “Stresses in Full Depth Granular Pavements.” *Transportation Research Record* No. 954, Transportation Research Board, National Research Council, Washington, DC, 94-100.

Duncan, J. M. and Dunlop, P. (1968). “The Significance of Cap and Base Restraint.” *Journal of the Soil Mechanics and Foundations Division*, ASCE, Vol. 94, SM1, 271-290.

Duncan, J. M., Monismith C. L. and Wilson, E. L. (1968). “Finite Element Analysis of Pavements.” *Highway Research Record No. 228*, Highway Research Board, Washington, DC, 18-33.

FHWA, Highway Statistics. (1990). Federal Highway Administration, Superintendent of Documents, U.S. Government Printing Office, Washington, D.C.

Foster, C. R. and Alvin, R. G. (1958). “Development of Multiple-Wheel CBR Design Criteria.” *Journal of the Soil Mechanics and Foundation Division*, ASCE, Vol. 84, No. SM2, May, 1647-1 to 1647-12.

Fredlund, D. G. and Xing, A. (1994). “Equations for the Soil-Water Characteristic Curve.” *Canadian Geotechnical Journal*, 31, 521-532.

Garg, N. and Thompson, M.R., (1997), “Triaxial Characterization of Mn/Road Granular Materials.” *Transportation Reserach Record,* 76th Annual Meeting, Washington, D.C.

Han, T. M. (1976). “A Numerical Solution for the Initial Value Problem of Rigid Differential Equation.” *Science Sinaca*.

Hicks, R. G. and Monismith, C. L. (1971). “Factors Influencing the Resilient Properties of Granular Materials.” *Transportation Research Record 345*, Transportation Research Board, National Research Council, Washington, DC, 15-31.

Hicks, R.G. (1970). “Factors Influencing the Resilient Properties of Granular Materials.” Ph.D. Dissertation, University of California, Berkeley, CA.

Hornych, P., Kazai, A. and Piau, J. M. (1998). “Study of the Resilient Behaviour of Unbound Granular Materials.” Proceedings, *5th International Conference on the Bearing Capacity of Roads and Airfields*, R. S. Nordal and G. Rafsdal, Vol. 3, 1277-1287.

Huang, Y. H. (1993). “Pavement Analysis and Design.” 1st Edition, Prentice Hall, Englewood Cliffs, NJ.

Hwang, D. and Witczak, M. W. (1979). “Program DAMA (Chevron) User’s Manual.” Department of Civil Engineering, University of Maryland, MD.

Industrial Process Control (IPC). (1998). “Universal Testing machine Manual. Australia.”

Kopperman, S., Tiller, G. and Tseng, M. (1986). “ELSYM5, Interactive Microcomputer Vertion, User’s Manual.” Report No. FHWA-TS-87-206, Federal Highway Administration, Washington, DC.

Lee, K. L. and Frank J. Vernese. (1978). “End Restraint Effects on Cyclic Triaxial Strength of Sand.” *Journal of the Geotechnical Division, ASCE*, GT6, 705-719.

Lekarp, F., Isaacson, U. and Dawson, A. (2000). “State of the Art. I: Resilient Response of Unbound Aggregates.” *Journal of Transportation Engineering*, ASCE, Vol. 126, No. 1, 66-75.

Lekarp, F., Isaacson, U. and Dawson, A. (2000). “State of the Art. II: Permanent Strain Response of Unbound Aggregates.” *Journal of Transportation Engineering*, ASCE, Vol. 126, No. 1, 76-83.

Lekarp, F., Richardson, I. R., and Dawson, A. (1996). “Influence on Permanent Deformation Behavior of Unbound Granular Materials.” *Transportation Research Record 1547*, TRB, National Research Council, Washington D.C.

Lentz, R. W. and Baladi, G. Y. (1981). “Constitutive Equation for Permanent Strain of Sand Subjected to Cyclic Loading.” *Transportation Research Record, No. 810*, Transportation Research Board, National Research Council, Washington, D.C, 50-53.

Liu, M. (1993). “Numerical Prediction of Pavement Distress with Geotechnical Constitutive Laws.” Ph.D. Dissertation, Texas A&M University, College Station, Texas.

Lytton, R. L. (1998). “Personal Communication.” Department of Civil Engineering, Texas A&M University, College Station, TX.

Lytton, R. L. (1995). “Foundations and Pavements on Unsaturated Soils.” *1st International Conference on Unsaturated Soils*. Paris.

Lytton, R. L., Uzan, J., Fernando, E., Roque, R., Hiltunen, D., & Stoffels, S. M. (1993). “Development and Validation of Performance Prediction Models and Specifications for Asphalt Binders and Paving Mixes.” Strategic Highway Research Program, SHRP A-357, National Research Council, Washington, DC.

Marek, C. R., and Jones, T. R., Jr. (1974). “Compaction-An Essential Ingredient for Good Base Performance.” *Proceedings, Conference on Utililization of Graded Aggregate Base Materials in Flexible Pavements*, Oak Brook, IL.

Milberger, L. J. and Dunlop, W. A. (1966). “A Gyratory Compactor for Molding Large Diameter Triaxial Specimens of Granular Materials.” Texas Transportation Institute Report No. 99-2.

Milton, J. S., and Arnold, J. C. (1995). “Introduction to Probability and Statistics: Principles and Applications for Engineering and Computing Sciences.” McGraw-Hill, Inc. New York, NY.

Moore, W. M. and Milberger, L. J. (1968). “Evaluation of the TTI Gyratory Compactor.” Texas Transportation Institute Report No. 99-3.

National Association of Australian State Road Authorities (1987). “A Guide to the Structural Design of Road Pavements.” Australia.

Nazarian, S., Pezo, R., Melarkode, S. and Picornell, M. (1996). “Testing Methodology for Resilient Modulus of Base Materials.” *Transportation Research Record 1547*, TRB, National Research Council, Washington DC.

Owen, D. R. J. and Hinton, E. (1980). “Finite Elements in Plasticity: Theory and Practice.” Pineridge Press, Swansea, U.K.

Pappin, J. W. (1979). “Charateristics of a Granular Material for Pavement Analysis.” Ph.D. Thesis, University of Nottingham, Department of Civil Engineering, U.K.

Park, S. W. (2000). “Evaluation of Accelerated Rut Development in Unbound Pavement Foundations and Load Limits on Load-Zoned Pavements.” Ph.D. Dissertation, Texas A&M University, College Station, Texas.

Pickering, D. J. (1970). “Anisotropic Elsactic Parameters for Soil.” *Geotechnique* 20, No. 3, 271-276.

Porter, D. W. (1999). “Technical Basis of the 1992 Austroads pavement Design Guide (Flexible Pavements) .” ARRB Transport Research No. RC7095-2, Australia.

Raad, L., Weichert, D. and Haidar, A. (1989). “Shakedown and Fatigue of Pavements with Granular Bases.” *Transportation Research Record 1227*, Transportation Research Board, Washington D.C. 159-172.

Rowe, P. W. and Barden, L. (1964). “Importance of Free Ends in Triaxial Testing.” *Journal of the Soil Mechanics and Foundations Division*, ASCE, SM1, 1-27.

Scullion, T., Uzan, J., Yazdani, J. I. And Chan, P. (1988). “Field Evaluation of the Multi-Depth Deflectometers.” Texas Transportation Institute Research Report 1123-2, College Station, Texas.

Seed, H. B., Chan, C. K. and Monismith, C. L. (1955). “Effects of Repeated Loading on the Strength and Deformation of Compacted Clay.” *Proceedings, Highway Research Board*, 34, Washington, DC, 541-558.

Sharp, R. W. and Booker, J. R. (1984). “Shakedown of Pavements Under Moving Surface Loads.” *Journal of Transportation Engineering*, ASCE, Vol. 110, No.1, 1-14.

Stewart, E. H., Selig, E. T. and Norman-Gregory, G. H. (1985). “Failure Criteria and Lateral Stresses in Track Foundations.” *Transportation Research Record* No. 1022, Transportation Research Board, National Research Council, Washington, DC, 59-64.

Sweere, G. T. H. (1990). “Unbound Granular Bases for Roads.” Ph.D. Dissertation, Delft University of Technology, The Netherlands.

Taylor, D. W. (1941). “7th Progress Report on Shear Strength to U.S. Engineers.” Massachusetts Institute of Technology.

Texas Department of Transportation. (1995). “Molding, Testing, and Evaluation of Bituminous Black Base Materials.” TXDOT Manual of Testing Procedures, Test Method Tex-126-E.

Thompson, M.R. (1998). “State-of-the-Art: Unbound Base Performance.” *Proceedings, 6th Annual Symposium, International Center for Aggregates Research*.

Thompson, M. R., and Nauman D. (1993). “Rutting Rate Analyses of the AASHO Road Test Flexible Pavements.” *Transportation Research Record 1384*, TRB, National Research Council, Washington D.C.

Turner, M. J., Clough, R. W., Martin, H. C. and Topp, L. J. (1956). “Stiffness and Deflection Analysis of Complex Structures.” *Journal of Aeronautical Sciences*, Vol. 23, No. 9, 805-823.

Tutumluer, E. (2000). “Directional Dependency of Aggregate Stiffnesses: An Indicator of Granular Base Performance.” *Proceedings, 8th Annual Symposium of International Center for Aggregate Research*, Denver, CO, April 12-14.

Tutumluer, E. (1995). “Predicting Behavior of Flexible Pavements with Granular Bases.” Ph.D. Thesis, Georgia Institute of Technology, GA.

Tutumluer, E. (1998). “Anisotropic Behavior of Unbound Aggregate Bases.” *Proceedings, 6th Annual Symposium, International Center for Aggregate Research*, St. Louis, MO.

Tutumluer, E., Thompson, M. R. (1997). “Anisotropic modelling of Granular Bases in Flexible Pavements.” *Transportation Research Record*, No. 1577. Transportation Research Board, National Research Council, Washington, DC.

Uzan J. (1992). “Resilient Characterisation of Pavement Materials.” *International Journal for Numerical and Analytical Methods in Geomechanics*, Vol. 16.

Uzan, J. and Scullion, T. (1990). “Verification of Backcalculation Procedures.” *3rd International Conference on Bearing Capacity of Roads and Airfields*. Trondheheim, Norway, 447-458.

Uzan, J. (1985). “Characterization of Granular Material.” *Transportation Research Record* 1022, TRB, National Research Council, Washington DC, 52-59.

Wang, F. & Lytton R. L. (1993). “System Identification Method for Backcalculating Pavement Layer Properties.” *Transportation Research Record* 1384, TRB, National Research Council, Washington, DC, 1-7.

Wardle, L. J. and Rodway, B. (1998). "Recent Developments in Flexible Aircraft Pavement Design Using Layered Elastic Method." *3rd International Conference on Road and Airfield Pavement Technology*. Beijing, China.

Wardle, L. J (1986) "Computer Program CIRCLY, User's Manual." MINCAD Systems Pty Ltd, Richmond, Australia.

Warren, H. and Dieckman, W. L. (1963). "Numerical Computation of Stresses and Strains in a Multiple-Layer Asphalt Pavement System." International Report, Chevron Research Corporation, Richmond, CA.

Witczak, M. W. & Uzan, J. (1988). "The Universal Airport Pavement Design System Report I of V: Granular Material Characterisation." University of Maryland, Department of Civil Engineering, MD.

Zienkiewicz, O. C., Cheung, Y. K. and Stagg, K. G. (1966). "Particular Reference to Problems of Rock Mechanics." *Journal of Strain Analysis*, Vol. 1, No.2. 172-182.

Zienkiewicz, O. C., Valliappan, S. and King, I. P. (1968). "Stress Analysis of Rock as a No Tension Material." *Geotechnique*, Vol. 18, 56-66.

APPENDIX A

TABLES OF AVERAGE RESILIENT STRAIN

Table A1 Average Resilient Strains for Well Graded Texas Limestone at Dry of Optimum Moisture Content.

Stress State		Triaxial Compression		Triaxial Shear		Triaxial Extension	
Stress (kPa)		Strain (με)		Strain (με)		Strain (με)	
Axial	Radial	Axial	Radial	Axial	Radial	Axial	Radial
40.0	25.0	29.6	-10.9	103.7	-84.7	-71.3	46.6
50.0	25.0	50.2	-23.7	79.5	-72.3	-98.8	69.0
70.0	40.0	39.1	-14.8	53.8	-38.3	-93.6	68.8
130.0	60.0	49.0	-21.2	74.1	-65.4	-51.1	43.5
150.0	70.0	43.8	-17.3	63.4	-51.6	-41.7	35.8
170.0	100.0	41.6	-15.2	56.1	-35.4	-87.1	61.7
220.0	120.0	53.3	-18.0	74.1	-49.5	-67.3	48.8
250.0	140.0	49.9	-14.7	64.4	-40.0	-57.5	39.5
250.0	120.0	47.6	-15.8	65.8	-46.9	-59.8	45.4
250.0	105.0	47.2	-16.1	66.9	-54.2	-53.8	42.2

Table A2 Average Resilient Strains for Well Graded Texas Limestone at Wet of Optimum Moisture Content.

Stress State		Triaxial Compression		Triaxial Shear		Triaxial Extension	
Stress (kPa)		Strain (με)		Strain (με)		Strain (με)	
Axial	Radial	Axial	Radial	Axial	Radial	Axial	Radial
40.0	25.0	30.8	-14.4	105.3	-85.7	-81.1	56.3
50.0	25.0	53.7	-26.4	81.4	-72.5	-105.5	76.8
70.0	40.0	41.2	-19.4	58.8	-43.6	-107.7	81.5
130.0	60.0	53.3	-25.3	77.4	-69.7	-54.1	49.1
150.0	70.0	46.7	-20.0	65.4	-54.9	-45.7	39.1
170.0	100.0	43.6	-18.2	62.1	-40.8	-97.3	72.0
220.0	120.0	56.8	-20.3	77.4	-56.6	-74.1	56.7
250.0	140.0	51.4	-17.4	68.5	-46.8	-62.4	47.5
250.0	120.0	51.1	-19.3	72.3	-58.6	-67.4	58.8
250.0	105.0	50.7	-20.0	72.6	-63.5	-58.4	50.6

Table A3 Average Resilient Strains for Fine Graded Texas Limestone at Optimum Moisture Content.

Stress State		Triaxial Compression		Triaxial Shear		Triaxial Extension	
Stress (kPa)		Strain (με)		Strain (με)		Strain (με)	
Axial	Radial	Axial	Radial	Axial	Radial	Axial	Radial
40.0	25.0	36.7	-24.6	137.7	-163.3	-123.2	119.6
50.0	25.0	57.1	-36.9	93.1	-111.4	-133.6	126.0
70.0	40.0	44.1	-24.3	67.6	-65.5	-150.6	143.1
130.0	60.0	54.1	-30.6	88.4	-103.0	-64.1	70.3
150.0	70.0	48.0	-24.2	75.2	-79.7	-53.4	55.8
170.0	100.0	45.6	-21.2	66.5	-54.6	-120.1	104.7
220.0	120.0	57.3	-25.6	85.1	-75.4	-83.8	75.7
250.0	140.0	53.3	-20.6	74.5	-59.7	-70.5	59.7
250.0	120.0	50.6	-22.4	75.6	-74.0	-73.3	73.6
250.0	105.0	48.8	-23.1	74.8	-84.0	-63.2	65.1

Table A4 Average Resilient Strains for Fine Graded Texas Limestone at Dry of Optimum Moisture Content.

Stress State		Triaxial Compression		Triaxial Shear		Triaxial Extension	
Stress (kPa)		Strain (με)		Strain (με)		Strain (με)	
Axial	Radial	Axial	Radial	Axial	Radial	Axial	Radial
40.0	25.0	29.5	-11.9	107.4	-82.9	-68.8	46.7
50.0	25.0	53.1	-24.1	74.0	-62.9	-83.0	56.9
70.0	40.0	39.3	-16.4	56.0	-39.3	-95.2	71.0
130.0	60.0	53.4	-22.9	78.6	-68.0	-52.4	44.0
150.0	70.0	46.3	-19.1	66.4	-54.3	-43.9	37.3
170.0	100.0	44.1	-16.5	58.1	-39.1	-93.3	67.8
220.0	120.0	55.4	-20.5	77.3	-53.3	-70.1	53.1
250.0	140.0	50.4	-16.8	67.1	-43.6	-59.0	43.3
250.0	120.0	50.0	-17.3	70.2	-50.3	-61.6	48.7
250.0	105.0	49.4	-18.3	71.1	-58.3	-57.1	45.1

Table A5 Average Resilient Strains for Fine Graded Texas Limestone at Wet of Optimum Moisture Content.

Stress State		Triaxial Compression		Triaxial Shear		Triaxial Extension	
Stress (kPa)		Strain (με)		Strain (με)		Strain (με)	
Axial	Radial	Axial	Radial	Axial	Radial	Axial	Radial
40.0	25.0	58.1	-53.6	226.4	-343.1	-479.5	545.4
50.0	25.0	69.9	-60.8	121.1	-190.1	-249.9	291.7
70.0	40.0	52.6	-37.3	88.4	-105.6	-279.0	295.6
130.0	60.0	58.0	-37.9	98.8	-137.3	-80.5	98.6
150.0	70.0	49.5	-29.4	81.8	-105.3	-64.1	77.2
170.0	100.0	50.3	-27.1	76.6	-73.3	-165.7	155.7
220.0	120.0	59.9	-30.8	94.8	-97.7	-105.8	103.3
250.0	140.0	55.2	-24.6	80.8	-75.5	-85.4	78.0
250.0	120.0	51.8	-25.2	79.0	-87.4	-82.9	89.8
250.0	105.0	47.5	-25.3	75.5	-94.6	-65.6	73.6

Table A6 Average Resilient Strains for Coarse Graded Texas Limestone at Optimum Moisture Content.

Stress State		Triaxial Compression		Triaxial Shear		Triaxial Extension	
Stress (kPa)		Strain (με)		Strain (με)		Strain (με)	
Axial	Radial	Axial	Radial	Axial	Radial	Axial	Radial
40.0	25.0	34.9	-11.0	113.5	-84.1	-82.9	51.5
50.0	25.0	59.2	-24.1	87.7	-73.7	-109.7	69.2
70.0	40.0	44.1	-16.0	61.6	-42.3	-102.1	72.1
130.0	60.0	55.4	-21.4	78.8	-68.8	-54.0	48.3
150.0	70.0	49.4	-18.1	68.6	-56.6	-47.3	41.3
170.0	100.0	47.3	-15.2	61.2	-40.1	-92.0	67.9
220.0	120.0	60.4	-18.6	76.6	-55.0	-58.2	44.6
250.0	140.0	53.8	-16.7	71.6	-46.5	-63.2	48.4
250.0	120.0	53.5	-16.8	71.2	-53.8	-63.6	54.9
250.0	105.0	52.7	-17.8	71.8	-60.1	-58.4	48.8

Table A7 Average Resilient Strains for Well Graded Texas Gravel at Optimum Moisture Content.

Stress State		Triaxial Compression		Triaxial Shear		Triaxial Extension	
Stress (kPa)		Strain (με)		Strain (με)		Strain (με)	
Axial	Radial	Axial	Radial	Axial	Radial	Axial	Radial
40.0	25.0	28.5	-7.3	86.6	-48.8	-44.5	29.4
50.0	25.0	51.4	-16.3	67.6	-43.8	-67.4	38.5
70.0	40.0	39.2	-14.5	51.7	-32.1	-73.1	57.5
130.0	60.0	53.5	-21.9	76.3	-62.9	-44.9	41.5
150.0	70.0	49.5	-16.8	65.9	-51.4	-37.6	35.6
170.0	100.0	45.3	-17.6	56.5	-39.1	-83.8	73.2
220.0	120.0	59.0	-20.4	79.3	-60.0	-68.2	60.6
250.0	140.0	54.6	-17.7	70.7	-49.8	-59.0	51.3
250.0	120.0	53.5	-17.0	70.3	-55.5	-58.9	55.9
250.0	105.0	51.7	-17.3	68.9	-60.9	-51.3	46.3

Table A8 Average Resilient Strains for Well Graded Texas Gravel at Dry of Optimum Moisture Content.

Stress State		Triaxial Compression		Triaxial Shear		Triaxial Extension	
Stress (kPa)		Strain (με)		Strain (με)		Strain (με)	
Axial	Radial	Axial	Radial	Axial	Radial	Axial	Radial
40.0	25.0	24.6	-3.8	60.7	-21.8	-34.5	13.1
50.0	25.0	39.8	-7.4	47.8	-19.4	-47.3	16.8
70.0	40.0	32.6	-6.0	37.0	-14.3	-47.4	23.6
130.0	60.0	45.7	-9.6	57.5	-28.5	-32.1	19.9
150.0	70.0	40.2	-9.0	52.2	-23.3	-28.6	17.9
170.0	100.0	38.6	-7.7	44.5	-19.4	-55.9	33.1
220.0	120.0	54.2	-9.0	63.8	-28.5	-53.5	29.5
250.0	140.0	48.5	-8.6	56.5	-25.6	-46.0	27.7
250.0	120.0	48.6	-7.6	57.1	-26.8	-44.2	28.7
250.0	105.0	48.3	-7.8	56.3	-28.4	-43.0	22.6

Table A9 Average Resilient Strains for Fine Graded Texas Gravel at Optimum Moisture Content.

Stress State		Triaxial Compression		Triaxial Shear		Triaxial Extension	
Stress (kPa)		Strain (με)		Strain (με)		Strain (με)	
Axial	Radial	Axial	Radial	Axial	Radial	Axial	Radial
40.0	25.0	39.0	-14.9	146.0	-103.9	-97.1	67.8
50.0	25.0	57.5	-20.0	87.2	-68.8	-109.3	73.2
70.0	40.0	41.2	-14.6	62.3	-46.1	-127.1	109.3
130.0	60.0	58.1	-20.6	94.1	-90.9	-59.4	60.1
150.0	70.0	51.2	-16.9	79.3	-69.7	-48.9	50.8
170.0	100.0	51.9	-14.9	73.8	-49.8	-137.3	116.3
220.0	120.0	65.7	-19.9	100.0	-80.5	-96.0	84.5
250.0	140.0	62.7	-17.8	89.2	-63.2	-83.8	67.8
250.0	120.0	60.3	-17.8	84.4	-75.4	-79.9	76.8
250.0	105.0	56.8	-16.8	81.4	-83.0	-63.7	62.7

Table A10 Average Resilient Strains for Fine Graded Texas Gravel at Dry of Optimum Moisture Content.

Stress State		Triaxial Compression		Triaxial Shear		Triaxial Extension	
Stress (kPa)		Strain (με)		Strain (με)		Strain (με)	
Axial	Radial	Axial	Radial	Axial	Radial	Axial	Radial
40.0	25.0	29.8	-6.8	74.5	-26.7	-38.1	16.8
50.0	25.0	49.7	-11.5	59.9	-23.5	-67.6	23.4
70.0	40.0	38.7	-10.1	47.0	-19.0	-63.6	31.7
130.0	60.0	64.6	-18.0	83.4	-43.4	-44.4	27.9
150.0	70.0	58.1	-16.6	74.2	-39.3	-41.0	25.2
170.0	100.0	51.6	-14.5	62.8	-31.6	-82.5	50.3
220.0	120.0	72.9	-21.2	92.3	-50.3	-72.2	45.7
250.0	140.0	67.3	-18.6	83.6	-44.1	-66.9	40.3
250.0	120.0	64.8	-20.0	85.7	-50.5	-67.6	46.0
250.0	105.0	64.9	-19.9	84.1	-55.7	-63.6	40.0

Table A11 Average Resilient Strains for Coarse Graded Texas Gravel at Optimum Moisture Content.

Stress State		Triaxial Compression		Triaxial Shear		Triaxial Extension	
Stress (kPa)		Strain (με)		Strain (με)		Strain (με)	
Axial	Radial	Axial	Radial	Axial	Radial	Axial	Radial
40.0	25.0	31.8	-10.6	93.5	-60.0	-54.1	35.0
50.0	25.0	54.0	-17.2	71.1	-50.1	-77.0	45.8
70.0	40.0	42.6	-14.7	54.0	-36.5	-83.4	66.8
130.0	60.0	59.9	-25.6	86.8	-83.2	-55.9	56.8
150.0	70.0	52.7	-19.9	72.2	-63.7	-46.0	46.4
170.0	100.0	50.0	-20.1	65.6	-50.7	-103.4	93.3
220.0	120.0	64.2	-23.8	87.6	-70.8	-80.6	75.2
250.0	140.0	59.7	-20.8	79.5	-61.1	-70.5	63.9
250.0	120.0	58.7	-21.4	81.5	-68.8	-71.6	72.4
250.0	105.0	56.9	-20.5	79.6	-69.2	-59.7	57.5

Table A12 Average Resilient Strains for Well Graded Minnesota Gravel at Optimum Moisture Content.

Stress State		Triaxial Compression		Triaxial Shear		Triaxial Extension	
Stress (kPa)		Strain (με)		Strain (με)		Strain (με)	
Axial	Radial	Axial	Radial	Axial	Radial	Axial	Radial
40.0	25.0	42.3	-18.2	131.6	-121.9	-98.4	80.7
50.0	25.0	68.5	-37.9	111.7	-121.4	-140.7	121.2
70.0	40.0	49.2	-23.7	75.2	-67.9	-136.0	122.1
130.0	60.0	70.5	-36.5	114.1	-120.5	-76.3	80.3
150.0	70.0	64.6	-29.7	96.8	-95.7	-62.3	66.7
170.0	100.0	61.8	-25.9	84.5	-66.6	-128.7	112.5
220.0	120.0	79.1	-31.6	113.4	-92.3	-103.1	90.9
250.0	140.0	71.3	-27.1	98.0	-75.9	-85.8	75.3
250.0	120.0	68.8	-29.4	99.8	-93.3	-88.8	91.8
250.0	105.0	67.9	-32.0	101.7	-108.9	-81.2	84.1

Table A13 Average Resilient Strains for Well Graded Minnesota Gravel at Dry of Optimum Moisture Content.

Stress State		Triaxial Compression		Triaxial Shear		Triaxial Extension	
Stress (kPa)		Strain (με)		Strain (με)		Strain (με)	
Axial	Radial	Axial	Radial	Axial	Radial	Axial	Radial
40.0	25.0	42.7	-12.4	122.8	-82.4	-84.7	55.0
50.0	25.0	67.2	-23.4	95.3	-74.8	-110.8	69.8
70.0	40.0	48.3	-16.0	65.2	-44.9	-104.8	78.0
130.0	60.0	70.5	-25.7	99.3	-85.7	-60.8	57.4
150.0	70.0	62.3	-21.9	88.5	-68.9	-52.3	49.0
170.0	100.0	58.4	-19.5	76.8	-49.6	-110.4	82.3
220.0	120.0	76.3	-23.6	102.8	-69.6	-88.9	67.9
250.0	140.0	70.2	-20.5	93.1	-57.5	-75.6	58.0
250.0	120.0	68.8	-21.0	93.0	-67.5	-76.2	67.1
250.0	105.0	68.2	-23.9	95.0	-84.5	-77.0	64.7

Table A14 Average Resilient Strains for Well Graded Minnesota Gravel at Wet of Optimum Moisture Content.

Stress State		Triaxial Compression		Triaxial Shear		Triaxial Extension	
Stress (kPa)		Strain (με)		Strain (με)		Strain (με)	
Axial	Radial	Axial	Radial	Axial	Radial	Axial	Radial
40.0	25.0	96.1	-77.4	311.8	-395.6	-483.4	534.8
50.0	25.0	105.5	-83.3	180.7	-262.0	-364.3	413.7
70.0	40.0	88.0	-73.2	151.7	-218.8	-497.1	604.3
130.0	60.0	99.2	-86.2	186.1	-327.6	-171.1	269.8
150.0	70.0	87.5	-69.2	151.8	-259.0	-128.0	216.6
170.0	100.0	87.9	-61.7	151.1	-206.2	-354.0	431.5
220.0	120.0	105.4	-60.9	174.0	-237.6	-203.7	262.5
250.0	140.0	93.5	-52.6	153.2	-196.4	-168.7	215.4
250.0	120.0	90.5	-54.7	149.5	-224.3	-175.1	253.4
250.0	105.0	84.2	-56.2	137.6	-228.5	-129.9	199.4

Table A15 Average Resilient Strains for Fine Graded Minnesota Gravel at Optimum Moisture Content.

Stress State		Triaxial Compression		Triaxial Shear		Triaxial Extension	
Stress (kPa)		Strain (με)		Strain (με)		Strain (με)	
Axial	Radial	Axial	Radial	Axial	Radial	Axial	Radial
40.0	25.0	51.7	-31.8	175.7	-221.0	-189.8	216.1
50.0	25.0	68.4	-42.1	111.5	-156.2	-178.4	195.8
70.0	40.0	52.6	-30.6	82.1	-97.6	-202.6	229.7
130.0	60.0	70.1	-43.6	120.3	-170.2	-91.5	128.5
150.0	70.0	64.4	-37.7	103.9	-135.0	-76.4	99.8
170.0	100.0	63.1	-30.8	92.0	-91.0	-176.1	175.7
220.0	120.0	78.6	-35.7	117.2	-123.6	-123.0	128.0
250.0	140.0	71.0	-30.7	103.2	-98.3	-102.6	102.1
250.0	120.0	68.2	-33.1	106.7	-121.5	-106.5	125.5
250.0	105.0	66.7	-32.5	102.2	-128.1	-89.1	105.2

Table A16 Average Resilient Strains for Fine Graded Minnesota Gravel at Dry of Optimum Moisture Content.

Stress State		Triaxial Compression		Triaxial Shear		Triaxial Extension	
Stress (kPa)		Strain (με)		Strain (με)		Strain (με)	
Axial	Radial	Axial	Radial	Axial	Radial	Axial	Radial
40.0	25.0	40.2	-12.0	116.4	-86.0	-72.2	56.2
50.0	25.0	63.0	-23.5	89.2	-77.0	-104.1	69.8
70.0	40.0	46.4	-17.1	65.7	-49.2	-101.1	87.1
130.0	60.0	70.5	-30.5	101.4	-98.5	-62.3	63.3
150.0	70.0	63.2	-26.6	90.3	-81.2	-53.1	54.4
170.0	100.0	60.1	-20.8	79.7	-57.1	-114.9	95.5
220.0	120.0	79.5	-27.9	109.6	-83.3	-94.6	80.0
250.0	140.0	70.8	-24.6	97.3	-68.7	-82.9	67.2
250.0	120.0	70.2	-24.8	97.0	-80.2	-85.2	76.9
250.0	105.0	67.9	-27.0	98.3	-94.2	-76.1	70.1

Table A17 Average Resilient Strains for Well Graded California Granite at Optimum Moisture Content.

Stress State		Triaxial Compression		Triaxial Shear		Triaxial Extension	
Stress (kPa)		Strain (με)		Strain (με)		Strain (με)	
Axial	Radial	Axial	Radial	Axial	Radial	Axial	Radial
40.0	25.0	47.1	-18.8	148.0	-130.4	-97.4	76.6
50.0	25.0	70.4	-32.9	107.9	-112.2	-141.3	110.1
70.0	40.0	49.7	-19.9	73.7	-62.6	-131.6	111.7
130.0	60.0	76.0	-35.9	113.2	-120.8	-76.3	82.2
150.0	70.0	67.5	-31.3	98.6	-97.3	-65.7	68.4
170.0	100.0	63.0	-23.9	88.0	-68.7	-134.7	111.9
220.0	120.0	79.7	-30.7	113.5	-92.8	-103.6	90.0
250.0	140.0	72.1	-24.8	101.3	-75.7	-90.9	75.6
250.0	120.0	73.0	-26.7	102.7	-88.3	-91.7	88.6
250.0	105.0	69.6	-29.7	103.5	-103.5	-84.1	81.8

Table A18 Average Resilient Strains for Well Graded California Granite at Dry of Optimum Moisture Content.

Stress State		Triaxial Compression		Triaxial Shear		Triaxial Extension	
Stress (kPa)		Strain (με)		Strain (με)		Strain (με)	
Axial	Radial	Axial	Radial	Axial	Radial	Axial	Radial
40.0	25.0	40.4	-11.0	118.8	-84.4	-90.2	61.1
50.0	25.0	62.5	-20.9	90.2	-77.5	-120.5	77.9
70.0	40.0	46.8	-15.0	64.5	-47.0	-116.3	92.5
130.0	60.0	66.7	-24.1	99.8	-96.8	-65.8	66.2
150.0	70.0	62.0	-25.4	88.5	-77.4	-54.8	58.7
170.0	100.0	56.0	-18.2	74.4	-54.7	-112.9	96.5
220.0	120.0	73.5	-23.0	100.5	-77.9	-90.6	78.6
250.0	140.0	67.5	-19.4	89.8	-64.9	-78.2	67.7
250.0	120.0	64.5	-21.4	91.0	-77.8	-79.5	79.5
250.0	105.0	66.3	-25.2	91.6	-87.9	-72.9	70.7

Table A19 Average Resilient Strains for Well Graded California Granite at Wet of Optimum Moisture Content.

Stress State		Triaxial Compression		Triaxial Shear		Triaxial Extension	
Stress (kPa)		Strain (με)		Strain (με)		Strain (με)	
Axial	Radial	Axial	Radial	Axial	Radial	Axial	Radial
40.0	25.0	42.0	-16.2	140.4	-124.8	-108.5	82.8
50.0	25.0	67.8	-33.2	111.3	-117.5	-155.8	124.0
70.0	40.0	52.2	-21.7	76.0	-64.1	-142.5	123.2
130.0	60.0	70.1	-32.9	109.5	-111.9	-74.0	76.5
150.0	70.0	62.1	-25.7	92.7	-91.3	-62.0	64.9
170.0	100.0	60.5	-20.9	82.2	-61.6	-127.9	106.7
220.0	120.0	75.2	-27.3	108.2	-87.2	-98.7	85.9
250.0	140.0	69.4	-23.5	93.7	-71.8	-83.4	72.6
250.0	120.0	68.0	-25.2	100.8	-88.2	-88.7	85.8
250.0	105.0	66.2	-28.3	97.6	-97.6	-77.5	76.2

Table A20 Average Resilient Strains for Fine Graded California Granite at Optimum Moisture Content.

Stress State		Triaxial Compression		Triaxial Shear		Triaxial Extension	
Stress (kPa)		Strain (με)		Strain (με)		Strain (με)	
Axial	Radial	Axial	Radial	Axial	Radial	Axial	Radial
40.0	25.0	47.7	-10.8	134.2	-74.7	-99.1	48.4
50.0	25.0	74.3	-20.9	103.2	-68.2	-131.0	66.1
70.0	40.0	55.7	-15.7	72.6	-42.4	-116.7	73.5
130.0	60.0	74.2	-24.2	107.3	-81.3	-65.6	53.3
150.0	70.0	67.3	-20.0	91.5	-68.0	-53.5	47.6
170.0	100.0	61.8	-17.6	80.5	-49.1	-114.9	83.4
220.0	120.0	79.0	-23.3	107.7	-68.1	-91.8	67.8
250.0	140.0	77.4	-25.2	105.5	-69.1	-91.3	68.5
250.0	120.0	75.7	-25.4	105.0	-80.3	-92.7	79.1
250.0	105.0	71.9	-25.9	100.4	-84.1	-79.4	68.7

Table A21 Average Resilient Strains for Fine Graded California Granite at Dry of Optimum Moisture Content.

Stress State		Triaxial Compression		Triaxial Shear		Triaxial Extension	
Stress (kPa)		Strain (με)		Strain (με)		Strain (με)	
Axial	Radial	Axial	Radial	Axial	Radial	Axial	Radial
40.0	25.0	33.6	-9.2	93.8	-62.1	-61.7	43.0
50.0	25.0	54.7	-15.1	72.4	-55.6	-91.4	53.9
70.0	40.0	42.9	-11.9	55.7	-36.9	-91.4	68.4
130.0	60.0	62.2	-21.7	87.8	-71.7	-52.2	50.7
150.0	70.0	55.1	-18.6	77.7	-59.8	-45.3	42.5
170.0	100.0	53.2	-15.4	66.7	-45.7	-98.8	80.5
220.0	120.0	68.2	-20.5	93.2	-64.4	-78.3	64.3
250.0	140.0	62.2	-17.6	81.8	-54.1	-70.1	54.8
250.0	120.0	63.0	-18.6	84.7	-66.0	-71.6	64.3
250.0	105.0	61.8	-22.0	83.7	-75.2	-65.4	59.7

Table A22 Average Resilient Strains for Fine Graded California Granite at Wet of Optimum Moisture Content.

Stress State		Triaxial Compression		Triaxial Shear		Triaxial Extension	
Stress (kPa)		Strain (με)		Strain (με)		Strain (με)	
Axial	Radial	Axial	Radial	Axial	Radial	Axial	Radial
40.0	25.0	47.4	-23.3	151.1	-136.6	-118.1	91.3
50.0	25.0	67.4	-33.8	113.1	-110.7	-149.7	118.7
70.0	40.0	53.0	-21.0	76.5	-67.7	-145.3	123.8
130.0	60.0	69.8	-31.4	112.3	-116.3	-72.9	81.3
150.0	70.0	63.8	-27.4	99.3	-98.2	-66.1	68.1
170.0	100.0	61.1	-22.2	87.4	-68.0	-139.5	121.7
220.0	120.0	76.1	-29.4	112.6	-95.9	-104.5	95.8
250.0	140.0	72.5	-23.9	99.1	-78.7	-89.4	79.1
250.0	120.0	67.4	-26.5	101.1	-92.0	-90.6	92.5
250.0	105.0	67.9	-28.2	99.9	-105.6	-79.5	81.6

APPENDIX B

TABLES OF MODULI AND POISSON’S RATIO

Table B1 Moduli and Poisson's Ratios for Well Graded Texas Crushed Limestone at Dry of Optimum Moisture Content.

Stress (kPa)		Moduli (MPa)			Poisson's Ratio	
Axial	Radial	Vertical	Horizontal	Shear	Vertical	Horizontal
40.0	25.0	144.0	68.1	40.1	0.173	0.403
50.0	25.0	177.3	72.0	49.7	0.180	0.350
70.0	40.0	237.7	128.0	81.9	0.202	0.373
130.0	60.0	393.3	160.0	107.7	0.180	0.414
150.0	70.0	447.7	200.7	130.3	0.181	0.404
170.0	100.0	460.3	275.7	164.0	0.216	0.405
220.0	120.0	543.3	311.0	182.7	0.196	0.407
250.0	140.0	592.3	377.3	215.3	0.189	0.414
250.0	120.0	604.3	329.7	199.7	0.182	0.392
250.0	105.0	625.3	296.3	185.7	0.166	0.425

Table B2 Moduli and Poisson's Ratios for Well Graded Texas Crushed Limestone at Wet of Optimum Moisture Content.

Stress (kPa)		Moduli (MPa)			Poisson's Ratio	
Axial	Radial	Vertical	Horizontal	Shear	Vertical	Horizontal
40.0	25.0	143.7	63.2	39.4	0.207	0.438
50.0	25.0	169.7	68.7	48.8	0.190	0.359
70.0	40.0	227.3	109.8	73.5	0.225	0.404
130.0	60.0	374.7	145.3	102.1	0.186	0.430
150.0	70.0	426.7	183.3	125.0	0.186	0.430
170.0	100.0	435.0	241.3	145.7	0.228	0.409
220.0	120.0	512.3	266.7	168.0	0.189	0.406
250.0	140.0	575.3	322.0	195.0	0.191	0.407
250.0	120.0	568.3	261.7	172.0	0.176	0.374
250.0	105.0	595.3	250.0	165.3	0.170	0.435

Table B3 Moduli and Poisson’s Ratios for Fine Graded Texas Crushed Limestone at Optimum Moisture Content.

Stress (kPa)		Moduli (MPa)			Poisson’s Ratio	
Axial	Radial	Vertical	Horizontal	Shear	Vertical	Horizontal
40.0	25.0	124.0	33.6	25.3	0.185	0.402
50.0	25.0	156.3	44.5	36.9	0.175	0.325
70.0	40.0	203.3	72.8	56.8	0.202	0.319
130.0	60.0	360.0	102.2	78.7	0.166	0.390
150.0	70.0	404.3	131.3	97.0	0.167	0.384
170.0	100.0	407.7	179.0	124.0	0.203	0.354
220.0	120.0	503.7	204.7	140.7	0.183	0.392
250.0	140.0	549.7	256.3	168.0	0.182	0.394
250.0	120.0	571.7	210.0	151.0	0.166	0.362
250.0	105.0	211.3	232.3	142.3	0.152	0.412

Table B4 Moduli and Poisson's Ratios for Fine Graded Texas Crushed Limestone at Dry of Optimum Moisture Content.

Stress (kPa)		Moduli (MPa)			Poisson's Ratio	
Axial	Radial	Vertical	Horizontal	Shear	Vertical	Horizontal
40.0	25.0	145.7	69.8	39.4	0.191	0.421
50.0	25.0	189.3	75.5	55.6	0.182	0.455
70.0	40.0	237.0	124.3	78.7	0.218	0.390
130.0	60.0	368.7	153.0	102.3	0.182	0.434
150.0	70.0	428.0	189.3	124.3	0.186	0.425
170.0	100.0	437.3	245.7	154.7	0.208	0.411
220.0	120.0	531.0	284.3	172.3	0.202	0.420
250.0	140.0	589.7	345.7	203.3	0.198	0.424
250.0	120.0	581.7	307.7	187.0	0.186	0.395
250.0	105.0	602.3	274.0	174.0	0.174	0.442

Table B5 Moduli and Poisson’s Ratios for Fine Graded Texas Crushed Limestone at Wet of Optimum Moisture Content.

Stress (kPa)		Moduli (MPa)			Poisson’s Ratio	
Axial	Radial	Vertical	Horizontal	Shear	Vertical	Horizontal
40.0	25.0	75.5	11.8	13.2	0.217	0.222
50.0	25.0	116.0	23.3	24.1	0.166	0.216
70.0	40.0	163.0	41.4	38.9	0.208	0.240
130.0	60.0	331.7	74.9	63.7	0.152	0.361
150.0	70.0	389.0	97.7	80.4	0.154	0.354
170.0	100.0	357.0	129.7	100.7	0.198	0.317
220.0	120.0	468.0	156.7	117.3	0.176	0.362
250.0	140.0	522.3	200.3	144.0	0.175	0.375
250.0	120.0	553.7	174.3	135.3	0.157	0.343
250.0	105.0	627.7	168.3	132.3	0.146	0.404

Table B6 Moduli and Poisson's Ratios for Coarse Graded Texas Crushed Limestone at Optimum Moisture Content.

Stress (kPa)		Moduli (MPa)			Poisson's Ratio	
Axial	Radial	Vertical	Horizontal	Shear	Vertical	Horizontal
40.0	25.0	119.3	67.7	38.1	0.171	0.369
50.0	25.0	151.3	70.1	46.6	0.177	0.355
70.0	40.0	208.0	117.7	72.3	0.203	0.380
130.0	60.0	351.0	149.7	101.8	0.167	0.384
150.0	70.0	394.0	180.7	120.0	0.169	0.380
170.0	100.0	407.0	244.7	148.3	0.190	0.381
220.0	120.0	526.0	281.0	171.3	0.173	0.467
250.0	140.0	543.7	327.0	190.7	0.187	0.382
250.0	120.0	547.7	283.7	180.3	0.164	0.355
250.0	105.0	570.0	262.7	171.0	0.160	0.415

Table B7 Moduli and Poisson’s Ratios for Well Graded Texas Gravel at Optimum Moisture Content.

Stress (kPa)		Moduli (MPa)			Poisson’s Ratio	
Axial	Radial	Vertical	Horizontal	Shear	Vertical	Horizontal
40.0	25.0	173.5	120.0	58.6	0.180	0.375
50.0	25.0	205.5	116.5	69.8	0.187	0.427
70.0	40.0	261.0	149.0	90.6	0.216	0.408
130.0	60.0	383.0	164.0	108.0	0.180	0.427
150.0	70.0	416.5	199.0	128.0	0.166	0.393
170.0	100.0	452.5	232.0	157.0	0.199	0.409
220.0	120.0	507.5	252.5	161.5	0.174	0.378
250.0	140.0	557.0	300.5	187.0	0.177	0.387
250.0	120.0	562.0	274.0	178.5	0.158	0.352
250.0	105.0	601.0	259.0	173.5	0.150	0.424

Table B8 Moduli and Poisson's Ratios for Well Graded Texas Gravel at Dry of Optimum Moisture Content.

Stress (kPa)		Moduli (MPa)			Poisson's Ratio	
Axial	Radial	Vertical	Horizontal	Shear	Vertical	Horizontal
40.0	25.0	195.0	250.0	90.9	0.200	0.453
50.0	25.0	250.0	264.0	112.0	0.198	0.429
70.0	40.0	305.0	333.0	146.0	0.199	0.425
130.0	60.0	434.0	368.0	174.0	0.180	0.392
150.0	70.0	489.0	450.0	199.0	0.204	0.382
170.0	100.0	519.0	493.0	235.0	0.188	0.389
220.0	120.0	537.0	533.0	244.0	0.165	0.348
250.0	140.0	612.0	583.0	274.0	0.167	0.351
250.0	120.0	607.0	572.0	268.0	0.148	0.304
250.0	105.0	621.0	555.0	266.0	0.148	0.406

Table B9 Moduli and Poisson's Ratios for Well Graded Texas Gravel at Wet of Optimum Moisture Content.

Stress (kPa)		Moduli (MPa)			Poisson's Ratio	
Axial	Radial	Vertical	Horizontal	Shear	Vertical	Horizontal
40.0	25.0	48.2	25.6	14.3	0.160	0.212
50.0	25.0	88.1	36.1	26.1	0.140	0.250
70.0	40.0	106.0	50.5	36.9	0.145	0.109
130.0	60.0	240.0	82.9	59.7	0.138	0.362
150.0	70.0	261.0	135.0	83.1	0.125	0.250
170.0	100.0	238.0	121.0	85.4	0.155	0.132
220.0	120.0	294.0	198.0	115.0	0.162	0.169
250.0	140.0	318.0	298.0	142.0	0.152	0.053
250.0	120.0	376.0	464.0	188.0	0.152	0.174
250.0	105.0	470.0	546.0	238.0	0.118	0.406

Table B10 Moduli and Poisson’s Ratios for Fine Graded Texas Gravel at Optimum Moisture Content.

Stress (kPa)		Moduli (MPa)			Poisson’s Ratio	
Axial	Radial	Vertical	Horizontal	Shear	Vertical	Horizontal
40.0	25.0	104.0	56.1	30.0	0.193	0.348
50.0	25.0	147.0	76.6	48.1	0.162	0.236
70.0	40.0	192.0	107.0	69.2	0.180	0.168
130.0	60.0	308.0	123.0	81.1	0.137	0.299
150.0	70.0	356.0	157.0	101.0	0.141	0.278
170.0	100.0	310.0	199.0	121.0	0.165	0.147
220.0	120.0	393.0	202.0	125.0	0.147	0.259
250.0	140.0	428.0	251.0	148.0	0.159	0.289
250.0	120.0	455.0	210.0	141.0	0.134	0.280
250.0	105.0	504.0	201.0	137.0	0.119	0.332

Table B11 Moduli and Poisson's Ratios for Fine Graded Texas Gravel at Dry of Optimum Moisture Content.

Stress (kPa)		Moduli (MPa)			Poisson's Ratio	
Axial	Radial	Vertical	Horizontal	Shear	Vertical	Horizontal
40.0	25.0	172.0	192.0	74.1	0.266	0.571
50.0	25.0	196.0	208.0	90.0	0.239	0.502
70.0	40.0	255.0	253.0	114.0	0.251	0.487
130.0	60.0	319.0	238.0	118.0	0.213	0.486
150.0	70.0	356.0	260.0	132.0	0.215	0.501
170.0	100.0	392.0	304.0	159.0	0.219	0.463
220.0	120.0	422.0	300.0	158.0	0.212	0.483
250.0	140.0	457.0	340.0	176.0	0.211	0.485
250.0	120.0	466.0	304.0	165.0	0.205	0.455
250.0	105.0	478.0	281.0	161.0	0.190	0.513

Table B12 Moduli and Poisson's Ratios for Coarse Graded Texas Gravel at Optimum Moisture Content.

Stress (kPa)		Moduli (MPa)			Poisson's Ratio	
Axial	Radial	Vertical	Horizontal	Shear	Vertical	Horizontal
40.0	25.0	152.0	90.9	49.3	0.202	0.469
50.0	25.0	181.5	101.5	62.4	0.173	0.380
70.0	40.0	230.5	128.0	83.3	0.191	0.382
130.0	60.0	337.0	124.0	88.8	0.162	0.388
150.0	70.0	385.0	158.5	111.0	0.160	0.371
170.0	100.0	396.0	186.0	129.0	0.189	0.370
220.0	120.0	465.0	211.0	142.5	0.172	0.362
250.0	140.0	505.5	245.5	161.5	0.173	0.372
250.0	120.0	507.5	224.5	151.5	0.162	0.337
250.0	105.0	541.0	229.5	153.0	0.158	0.401

Table B13 Moduli and Poisson’s Ratios for Well Graded Minnesota Gravel at Optimum Moisture Content.

Stress (kPa)		Moduli (MPa)			Poisson’s Ratio	
Axial	Radial	Vertical	Horizontal	Shear	Vertical	Horizontal
40.0	25.0	110.0	43.2	29.6	0.175	0.403
50.0	25.0	131.0	41.7	32.2	0.168	0.324
70.0	40.0	186.0	72.4	52.4	0.191	0.347
130.0	60.0	276.0	87.0	63.9	0.168	0.389
150.0	70.0	308.0	108.0	77.9	0.164	0.378
170.0	100.0	318.0	146.0	99.3	0.192	0.389
220.0	120.0	371.0	165.0	109.0	0.182	0.389
250.0	140.0	420.0	199.0	129.0	0.182	0.398
250.0	120.0	431.0	164.0	117.0	0.165	0.366
250.0	105.0	449.0	145.0	107.0	0.156	0.423

Table B14 Moduli and Poisson's Ratios for Well Graded Minnesota Gravel at Dry of Optimum Moisture Content.

Stress (kPa)		Moduli (MPa)			Poisson's Ratio	
Axial	Radial	Vertical	Horizontal	Shear	Vertical	Horizontal
40.0	25.0	106.0	65.4	36.6	0.178	0.385
50.0	25.0	137.0	69.1	44.1	0.168	0.336
70.0	40.0	192.0	110.0	68.2	0.188	0.354
130.0	60.0	282.0	122.0	81.1	0.160	0.380
150.0	70.0	318.0	151.0	95.3	0.170	0.371
170.0	100.0	333.0	198.0	119.0	0.198	0.394
220.0	120.0	383.0	221.0	131.0	0.180	0.388
250.0	140.0	422.0	267.0	149.0	0.186	0.386
250.0	120.0	428.0	229.0	140.0	0.165	0.354
250.0	105.0	438.0	189.0	125.0	0.155	0.420

Table B15 Moduli and Poisson’s Ratios for Well Graded Minnesota Gravel at Wet of Optimum Moisture Content.

Stress (kPa)		Moduli (MPa)			Poisson’s Ratio	
Axial	Radial	Vertical	Horizontal	Shear	Vertical	Horizontal
40.0	25.0	47.3	10.6	10.6	0.209	0.281
50.0	25.0	75.3	17.1	16.9	0.166	0.186
70.0	40.0	102.0	19.3	20.2	0.193	0.242
130.0	60.0	195.0	30.2	29.2	0.142	0.314
150.0	70.0	226.0	37.9	36.5	0.136	0.303
170.0	100.0	206.0	45.6	42.0	0.170	0.282
220.0	120.0	268.0	63.4	54.7	0.145	0.299
250.0	140.0	304.0	77.0	64.4	0.149	0.305
250.0	120.0	312.0	66.7	60.2	0.135	0.281
250.0	105.0	361.0	67.3	61.5	0.127	0.358

Table B16 Moduli and Poisson's Ratios for Fine Graded Minnesota Gravel at Optimum Moisture Content.

Stress (kPa)		Moduli (MPa)			Poisson's Ratio	
Axial	Radial	Vertical	Horizontal	Shear	Vertical	Horizontal
40.0	25.0	85.9	21.9	18.9	0.169	0.287
50.0	25.0	122.0	30.6	28.0	0.142	0.208
70.0	40.0	166.0	46.6	41.7	0.174	0.245
130.0	60.0	275.0	60.2	51.6	0.143	0.314
150.0	70.0	304.0	75.5	62.8	0.148	0.344
170.0	100.0	293.0	105.0	82.0	0.176	0.318
220.0	120.0	362.0	123.0	93.4	0.157	0.341
250.0	140.0	407.0	154.0	112.0	0.166	0.355
250.0	120.0	418.0	127.0	98.6	0.150	0.320
250.0	105.0	446.0	123.0	97.7	0.138	0.373

Table B17 Moduli and Poisson's Ratios for Fine Graded Minnesota Gravel at Dry of Optimum Moisture Content.

Stress (kPa)		Moduli (MPa)			Poisson's Ratio	
Axial	Radial	Vertical	Horizontal	Shear	Vertical	Horizontal
40.0	25.0	116.0	63.2	37.1	0.161	0.362
50.0	25.0	148.0	66.5	45.1	0.162	0.344
70.0	40.0	200.0	102.0	65.3	0.185	0.330
130.0	60.0	288.0	105.0	75.0	0.161	0.408
150.0	70.0	323.0	127.0	87.5	0.168	0.404
170.0	100.0	324.0	173.0	110.0	0.183	0.369
220.0	120.0	372.0	184.0	117.0	0.177	0.391
250.0	140.0	419.0	223.0	136.0	0.188	0.400
250.0	120.0	419.0	192.0	127.0	0.164	0.371
250.0	105.0	446.0	170.0	117.0	0.156	0.428

Table B18 Moduli and Poisson’s Ratios for Well Graded California Granite at Optimum Moisture Content.

Stress (kPa)		Moduli (MPa)			Poisson’s Ratio	
Axial	Radial	Vertical	Horizontal	Shear	Vertical	Horizontal
40.0	25.0	99.0	41.8	26.9	0.171	0.419
50.0	25.0	126.0	45.2	34.1	0.158	0.310
70.0	40.0	178.0	79.8	55.1	0.179	0.319
130.0	60.0	261.0	85.2	64.1	0.157	0.383
150.0	70.0	297.0	105.0	76.6	0.166	0.393
170.0	100.0	307.0	146.0	95.7	0.183	0.368
220.0	120.0	365.0	166.0	109.0	0.177	0.388
250.0	140.0	400.0	204.0	127.0	0.177	0.372
250.0	120.0	401.0	174.0	118.0	0.162	0.348
250.0	105.0	430.0	154.0	109.0	0.157	0.411

Table B19 Moduli and Poisson’s Ratios for Well Graded California Granite at Dry of Optimum Moisture Content.

Stress (kPa)		Moduli (MPa)			Poisson’s Ratio	
Axial	Radial	Vertical	Horizontal	Shear	Vertical	Horizontal
40.0	25.0	105.0	64.6	36.9	0.157	0.309
50.0	25.0	136.0	66.9	44.7	0.148	0.255
70.0	40.0	185.0	105.0	67.3	0.173	0.269
130.0	60.0	282.0	110.0	76.3	0.143	0.328
150.0	70.0	324.0	131.0	90.4	0.168	0.359
170.0	100.0	340.0	181.0	116.0	0.171	0.327
220.0	120.0	391.0	198.0	126.0	0.161	0.341
250.0	140.0	429.0	237.0	145.0	0.159	0.330
250.0	120.0	444.0	201.0	133.0	0.150	0.312
250.0	105.0	462.0	178.0	125.0	0.151	0.411

Table B20 Moduli and Poisson's Ratios for Well Graded California Granite at Wet of Optimum Moisture Content.

Stress (kPa)		Moduli (MPa)			Poisson's Ratio	
Axial	Radial	Vertical	Horizontal	Shear	Vertical	Horizontal
40.0	25.0	101.0	44.0	28.3	0.166	0.354
50.0	25.0	122.0	43.7	32.8	0.158	0.261
70.0	40.0	170.0	75.9	53.5	0.185	0.311
130.0	60.0	276.0	93.4	67.8	0.163	0.375
150.0	70.0	311.0	114.0	81.5	0.155	0.349
170.0	100.0	313.0	161.0	104.0	0.178	0.341
220.0	120.0	381.0	178.0	115.0	0.172	0.365
250.0	140.0	424.0	211.0	136.0	0.170	0.370
250.0	120.0	418.0	179.0	119.0	0.159	0.339
250.0	105.0	457.0	163.0	115.0	0.157	0.417

Table B21 Moduli and Poisson's Ratios for Fine Graded California Granite at Optimum Moisture Content.

Stress (kPa)		Moduli (MPa)			Poisson's Ratio	
Axial	Radial	Vertical	Horizontal	Shear	Vertical	Horizontal
40.0	25.0	88.9	74.2	35.9	0.177	0.374
50.0	25.0	116.0	77.2	43.8	0.169	0.300
70.0	40.0	164.0	117.0	65.2	0.196	0.364
130.0	60.0	258.0	132.0	79.5	0.169	0.383
150.0	70.0	293.0	155.0	94.1	0.158	0.356
170.0	100.0	308.0	203.0	116.0	0.186	0.355
220.0	120.0	364.0	229.0	128.0	0.184	0.378
250.0	140.0	378.0	222.0	129.0	0.193	0.403
250.0	120.0	383.0	192.0	121.0	0.170	0.366
250.0	105.0	419.0	188.0	122.0	0.165	0.420

Table B22 Moduli and Poisson’s Ratios for Fine Graded California Granite at Dry of Optimum Moisture Content.

Stress (kPa)		Moduli (MPa)			Poisson’s Ratio	
Axial	Radial	Vertical	Horizontal	Shear	Vertical	Horizontal
40.0	25.0	138.0	86.2	48.1	0.170	0.363
50.0	25.0	164.0	92.1	58.6	0.144	0.280
70.0	40.0	210.0	134.0	80.9	0.170	0.297
130.0	60.0	318.0	145.0	94.0	0.162	0.361
150.0	70.0	359.0	175.0	109.0	0.166	0.364
170.0	100.0	362.0	212.0	133.0	0.167	0.334
220.0	120.0	425.0	242.0	143.0	0.171	0.357
250.0	140.0	471.0	283.0	166.0	0.173	0.363
250.0	120.0	463.0	236.0	149.0	0.152	0.337
250.0	105.0	498.0	209.0	142.0	0.154	0.421

Table B23 Moduli and Poisson's Ratios for Fine Graded California Granite at Dry of Optimum Moisture Content.

Stress (kPa)		Moduli (MPa)			Poisson's Ratio	
Axial	Radial	Vertical	Horizontal	Shear	Vertical	Horizontal
40.0	25.0	99.0	37.9	26.1	0.197	0.443
50.0	25.0	124.0	46.7	33.5	0.171	0.272
70.0	40.0	166.0	72.6	52.0	0.173	0.312
130.0	60.0	272.0	91.6	65.6	0.153	0.338
150.0	70.0	298.0	108.0	75.9	0.157	0.353
170.0	100.0	299.0	147.0	96.6	0.177	0.311
220.0	120.0	372.0	162.0	108.0	0.170	0.354
250.0	140.0	402.0	195.0	127.0	0.163	0.350
250.0	120.0	422.0	170.0	117.0	0.159	0.330
250.0	105.0	442.0	151.0	110.0	0.146	0.398

APPENDIX C

VERTICAL AND HORIZONTAL STRESS DISTRIBUTION

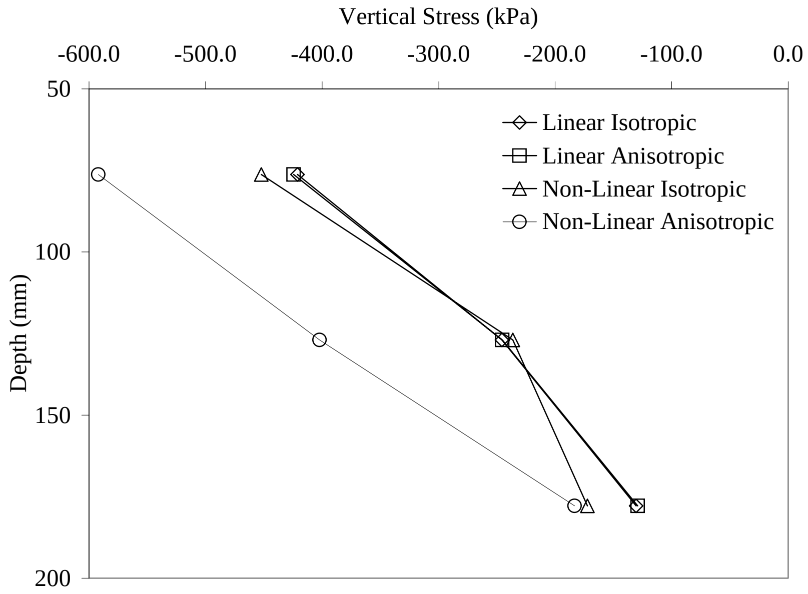

Figure C1 Vertical Stress for 50-mm HMA, 150-mm Base, and 20.7-MPa Subgrade.

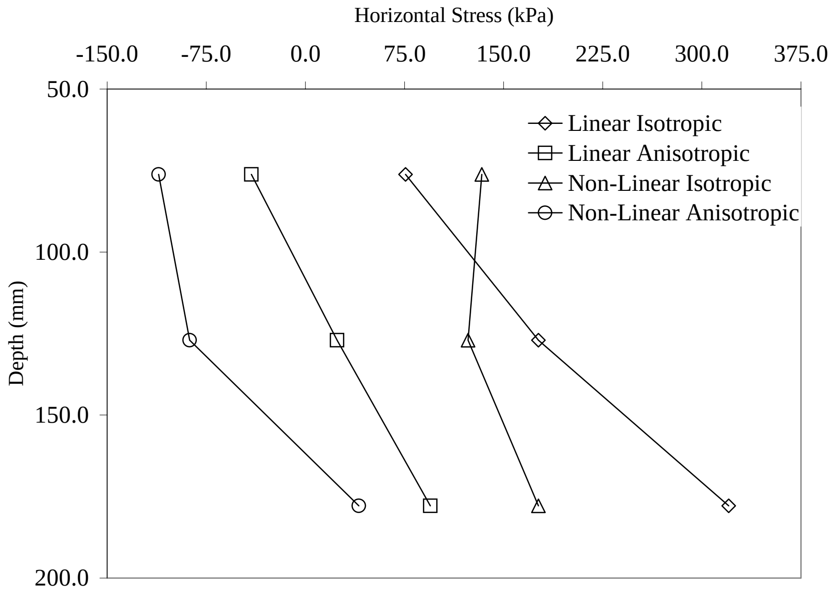

Figure C2 Horizontal Stress for 50-mm HMA, 150-mm Base, and 20.7-MPa Subgrade.

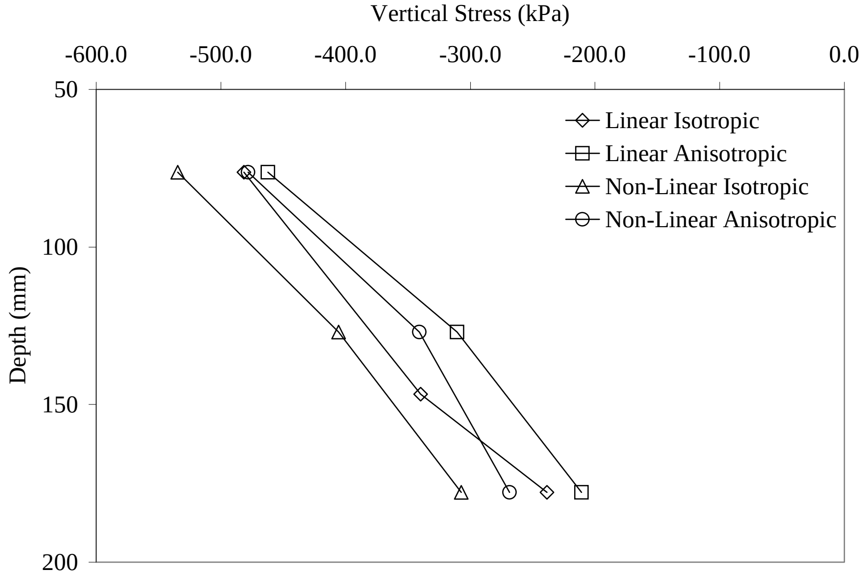

Figure C3 Vertical Stress for 50-mm HMA, 150-mm Base and 103.4-MPa Subgrade.

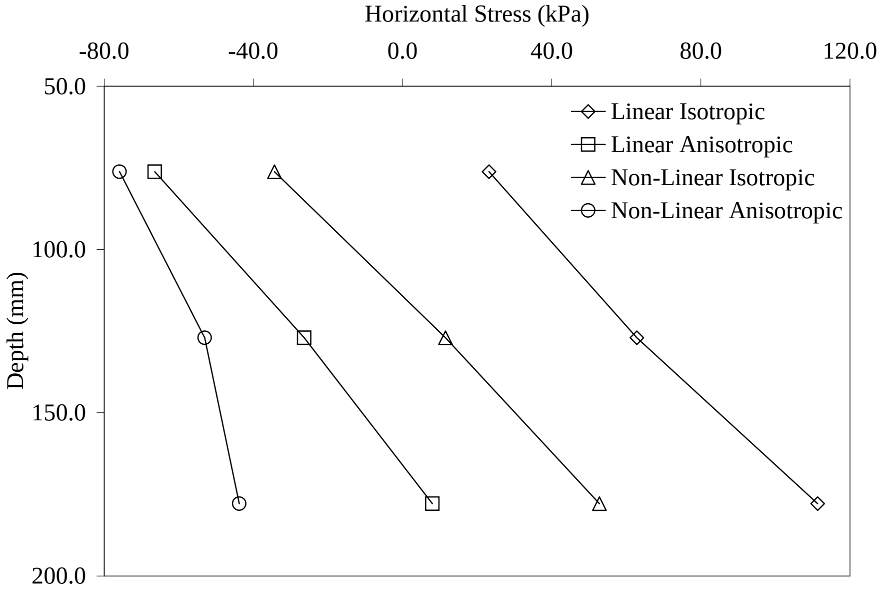

Figure C4 Horizontal Stress for 50-mm HMA, 150-mm Base and 103.4-MPa Subgrade.

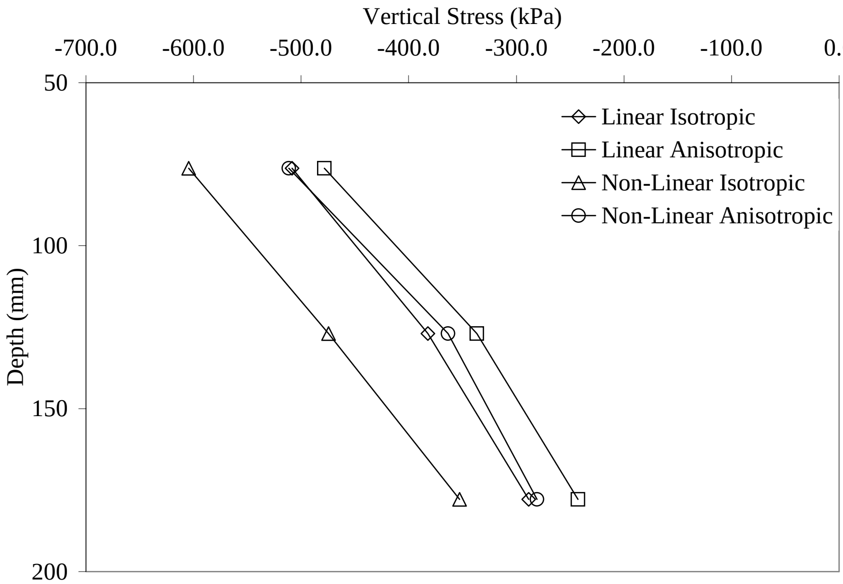

Figure C5 Vertical Stress for 50-mm HMA, 150-mm Base and 206.8-MPa Subgrade.

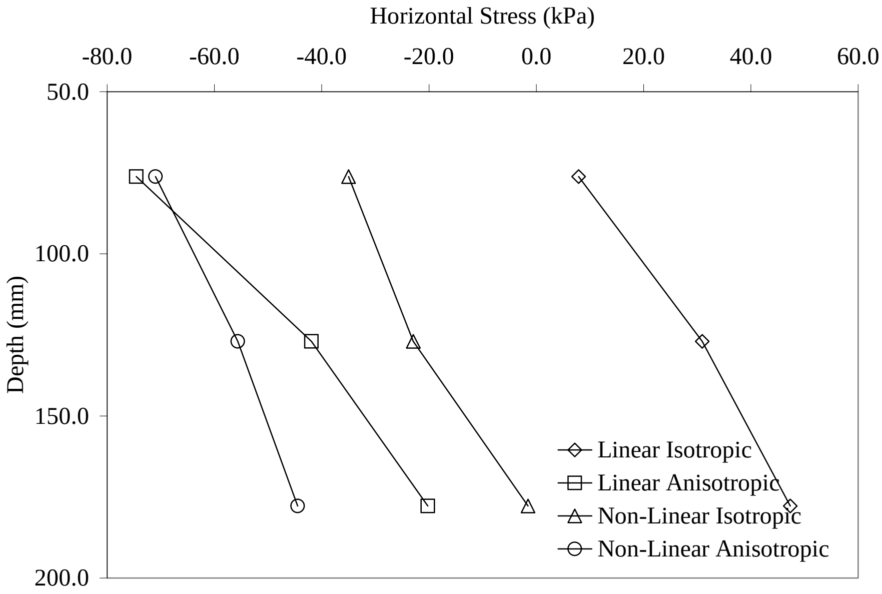

Figure C6 Horizontal Stress for 50-mm HMA, 150-mm Base and 206.8-MPa Subgrade.

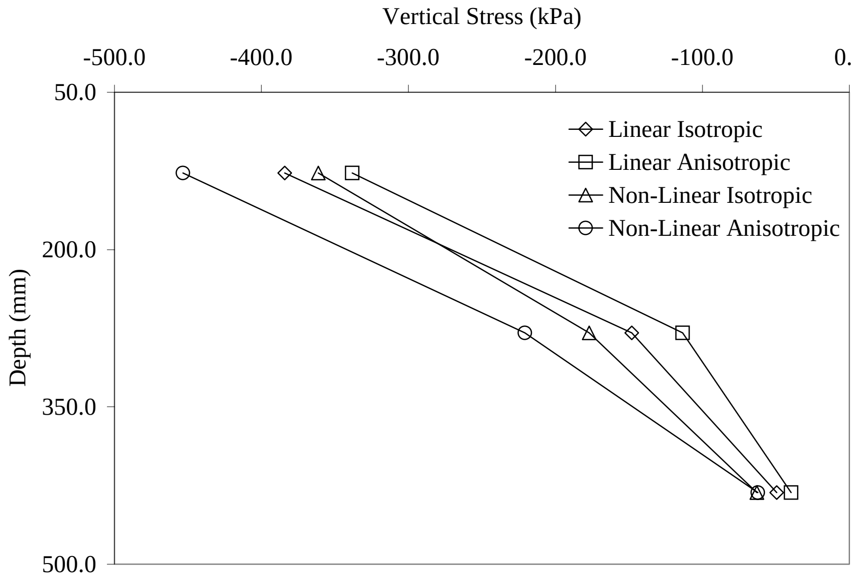

Figure C7 Vertical Stress for 50-mm HMA, 450-mm Base and 20.7-MPa Subgrade.

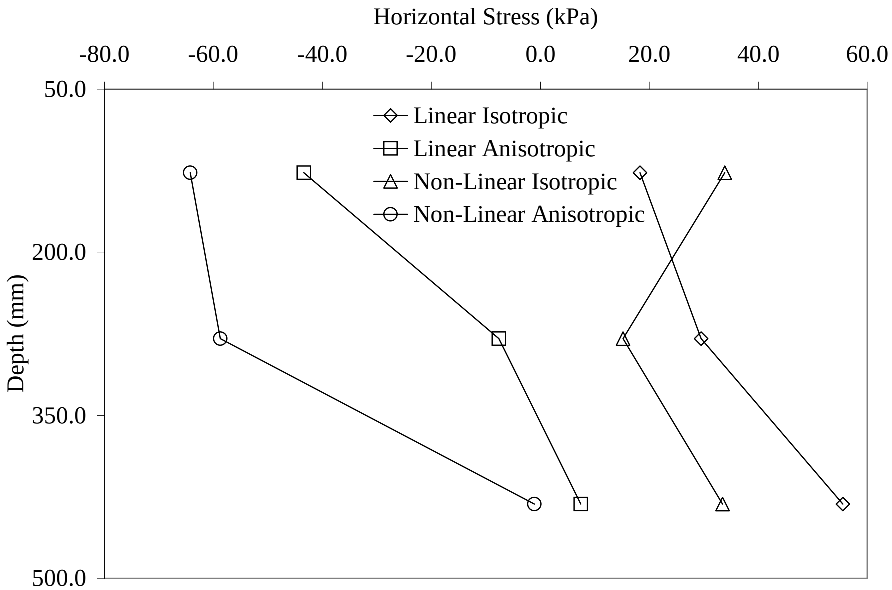

Figure C8 Horizontal Stress for 50-mm HMA, 450-mm Base and 20.7-MPa Subgrade.

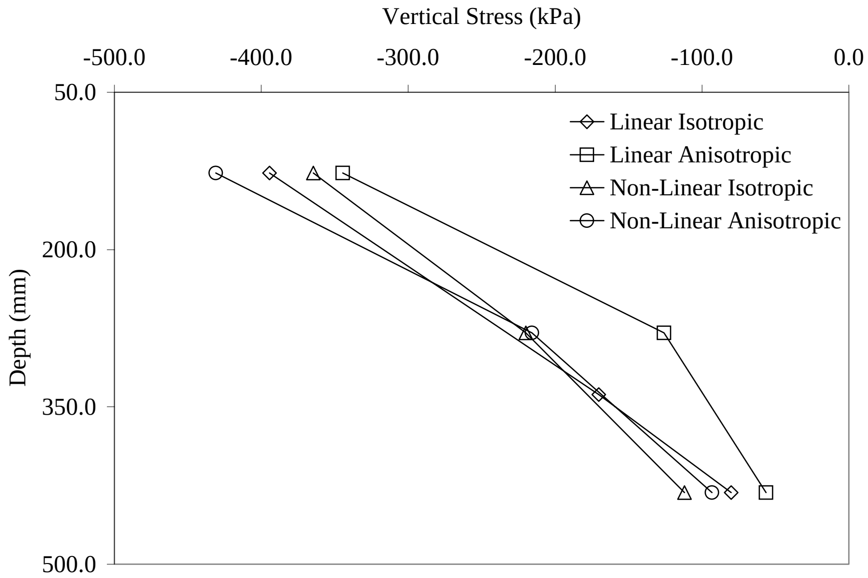

Figure C9 Vertical Stress for 50-mm HMA, 450-mm Base and 103.4-MPa Subgrade.

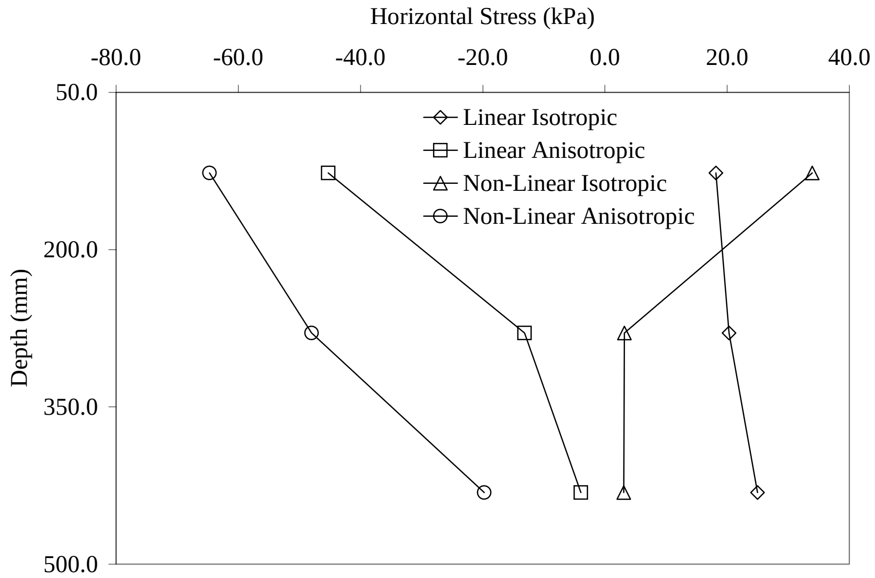

Figure C10 Horizontal Stress for 50-mm HMA, 450-mm Base and 103.4-MPa Subgrade.

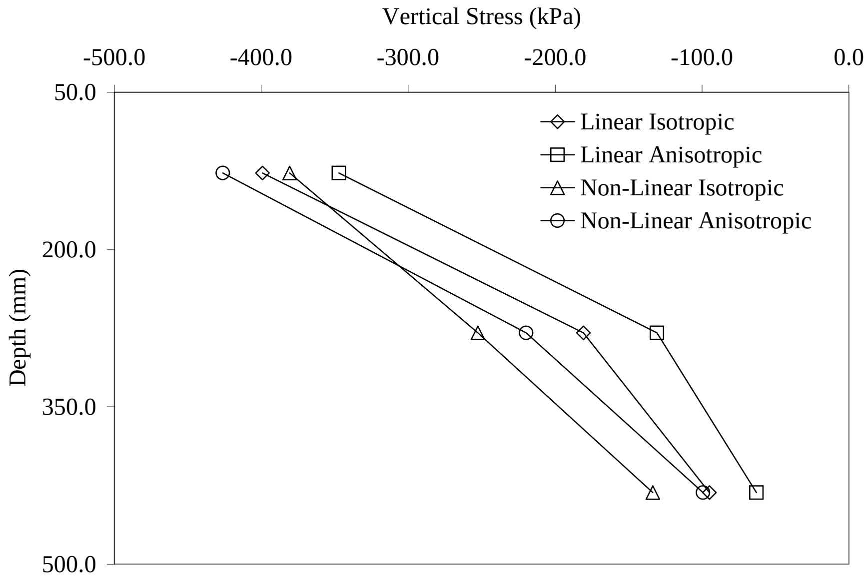

Figure C11 Vertical Stress for 50-mm HMA, 450-mm Base and 206.8-MPa Subgrade.

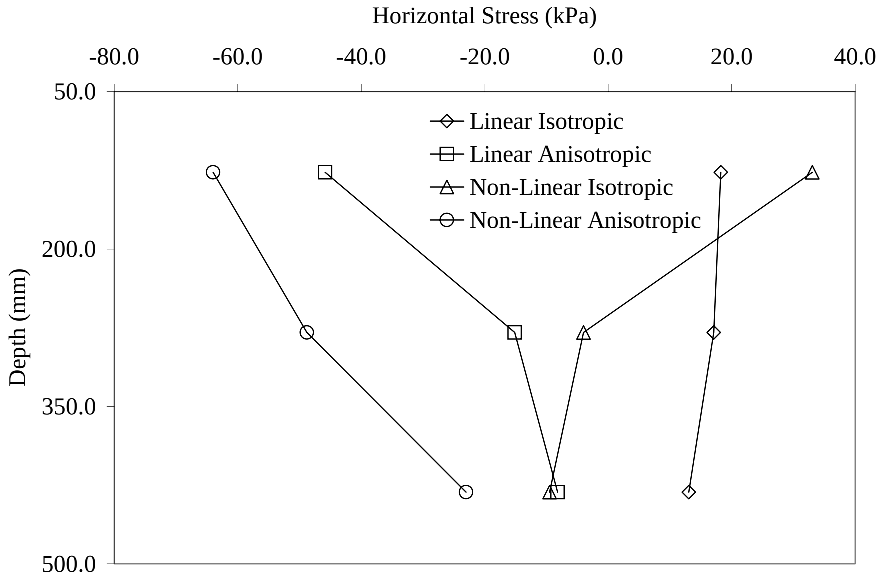

Figure C12 Horizontal Stress for 50-mm HMA, 450-mm Base and 206.8-MPa Subgrade.

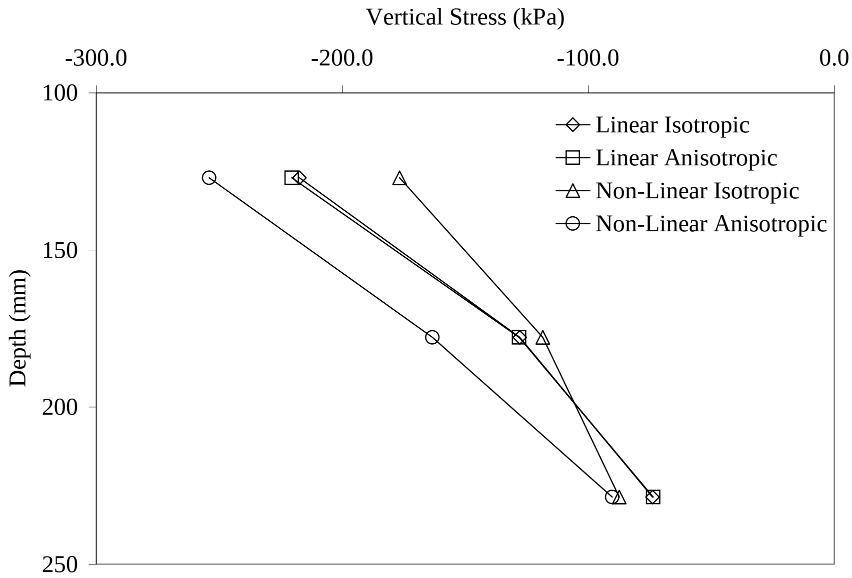

Figure C13 Vertical Stress for 100-mm HMA, 150-mm Base and 20.7-MPa Subgrade.

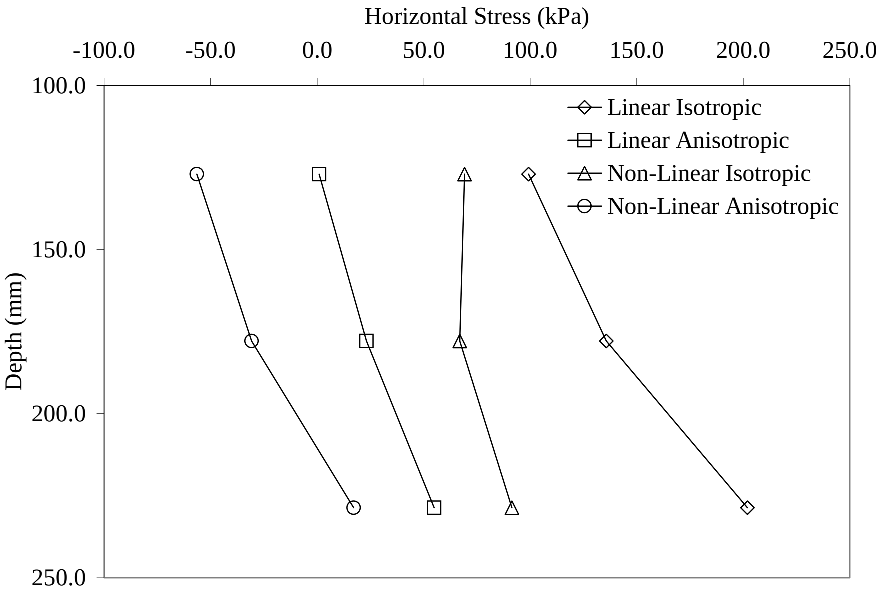

Figure C14 Horizontal Stress for 100-mm HMA, 150-mm Base and 20.7-MPa Subgrade.

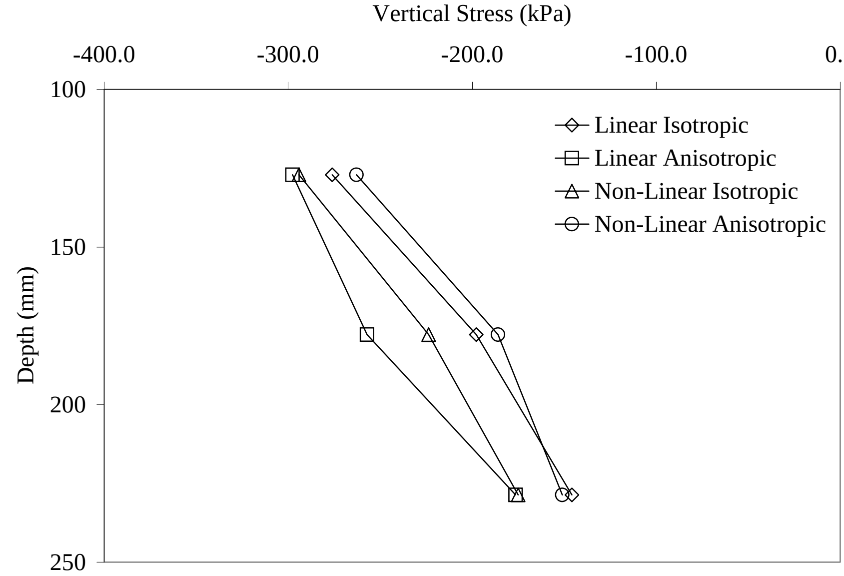

Figure C15 Vertical Stress for 100-mm HMA, 150-mm Base and 103.4-MPa Subgrade.

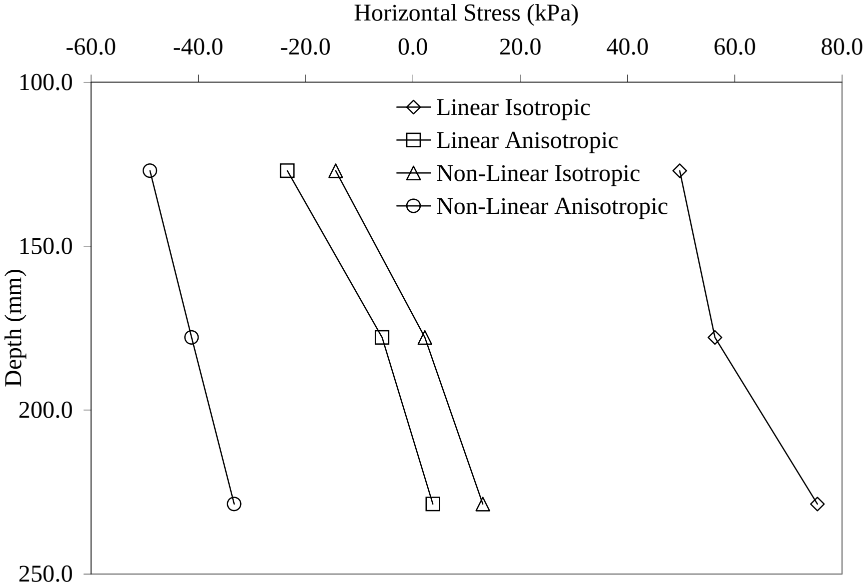

Figure C16 Horizontal Stress for 100-mm HMA, 150-mm Base and 103.4-MPa Subgrade.

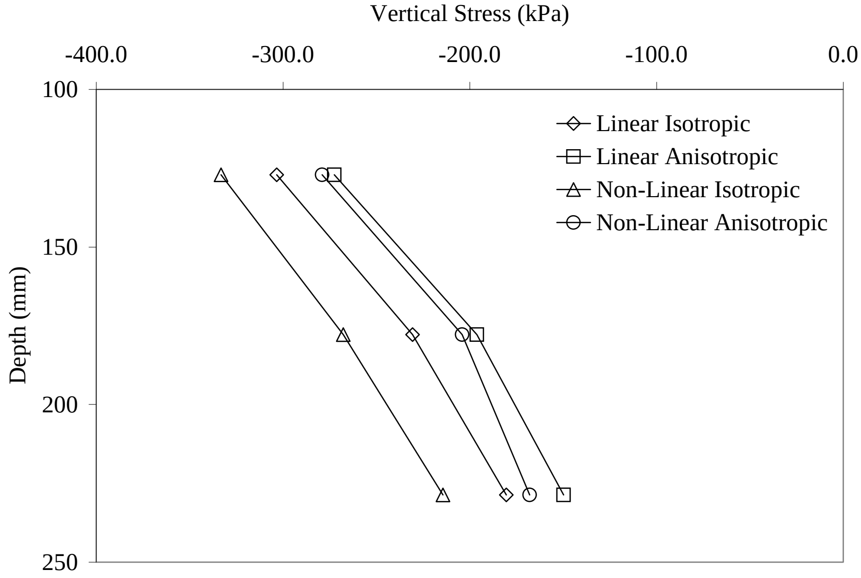

Figure C17 Vertical Stress for 100-mm HMA, 150-mm Base and 206.8-MPa Subgrade.

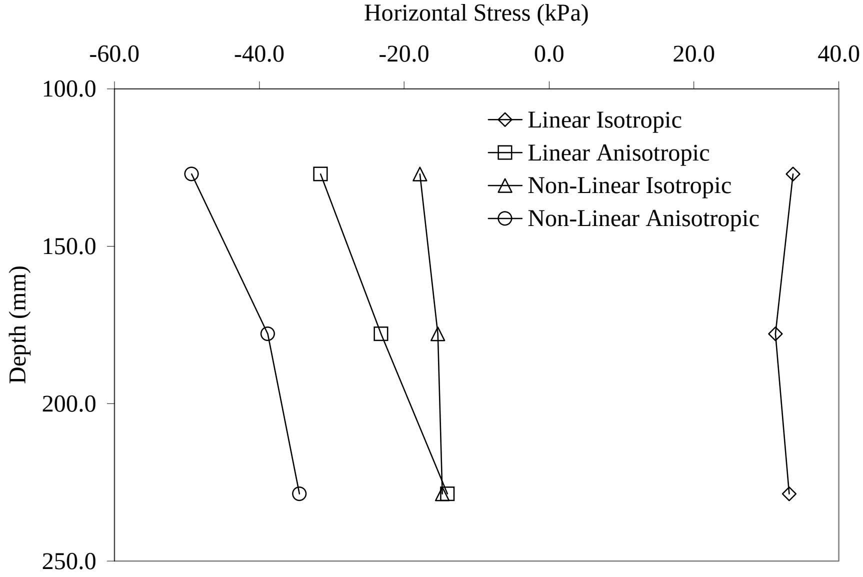

Figure C18 Horizontal Stress for 100-mm HMA, 150-mm Base and 206.8-MPa Subgrade.

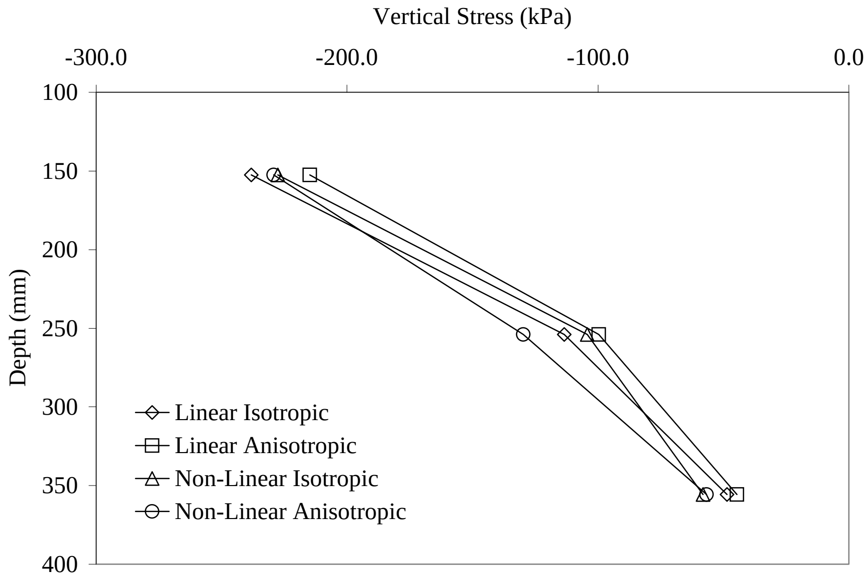

Figure C19 Vertical Stress for 100-mm HMA, 300-mm Base and 20.7-MPa Subgrade.

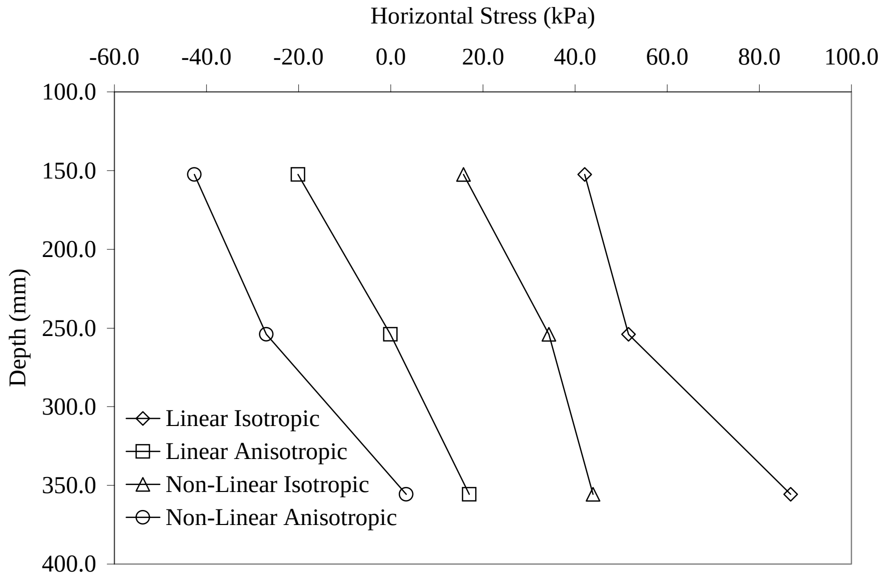

Figure C20 Vertical Stress for 100-mm HMA, 300-mm Base and 20.7-MPa Subgrade.

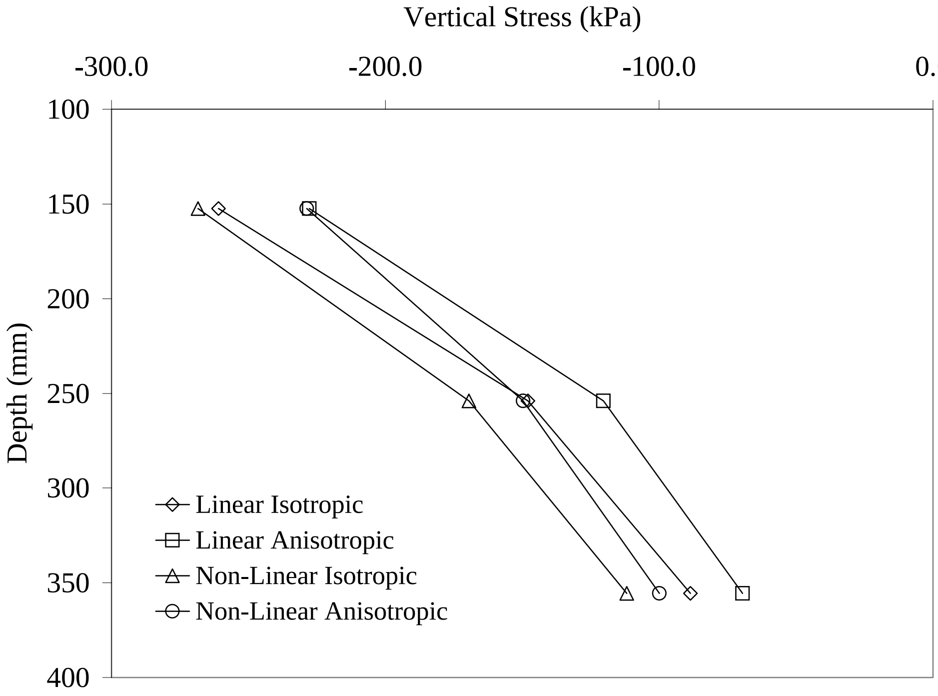

Figure C21 Vertical Stress for 100-mm HMA, 300-mm Base and 103.4-MPa Subgrade.

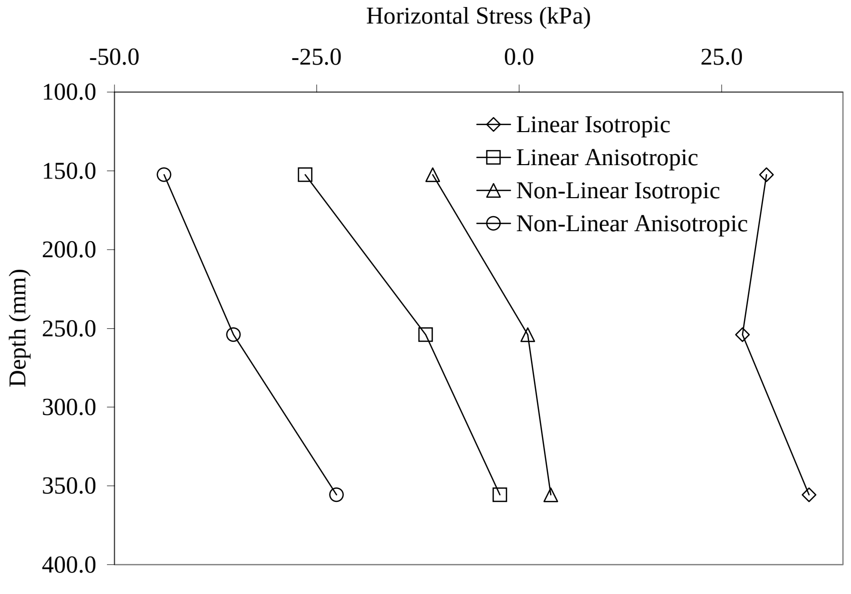

Figure C22 Horizontal Stress for 100-mm HMA, 300-mm Base and 103.4-MPa Subgrade.

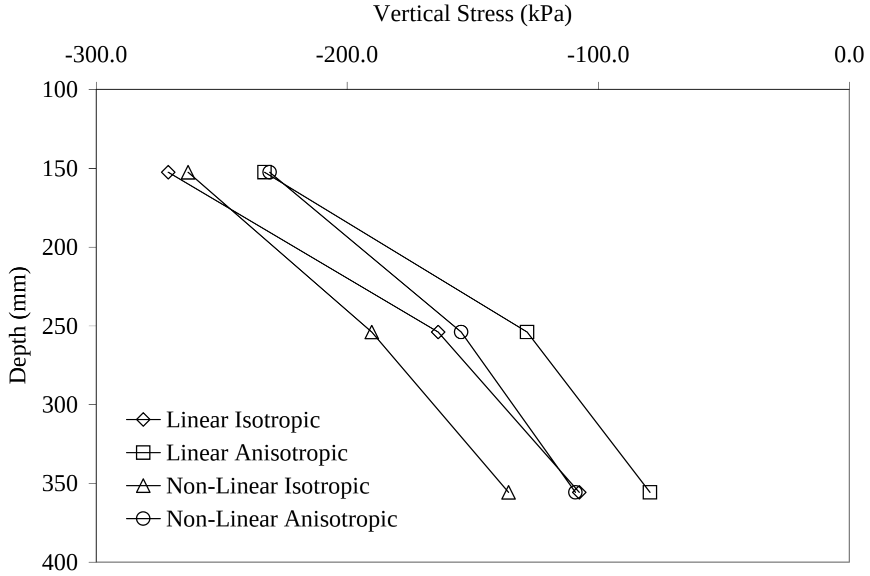

Figure C23 Vertical Stress for 100-mm HMA, 300-mm Base and 206.8-MPa Subgrade.

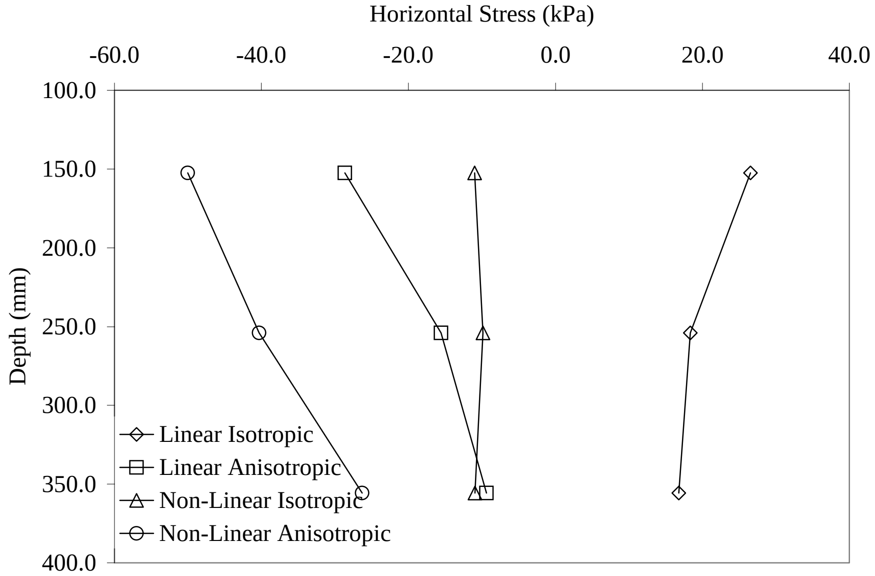

Figure C24 Horizontal Stress for 100-mm HMA, 300-mm Base and 206.8-MPa Subgrade.

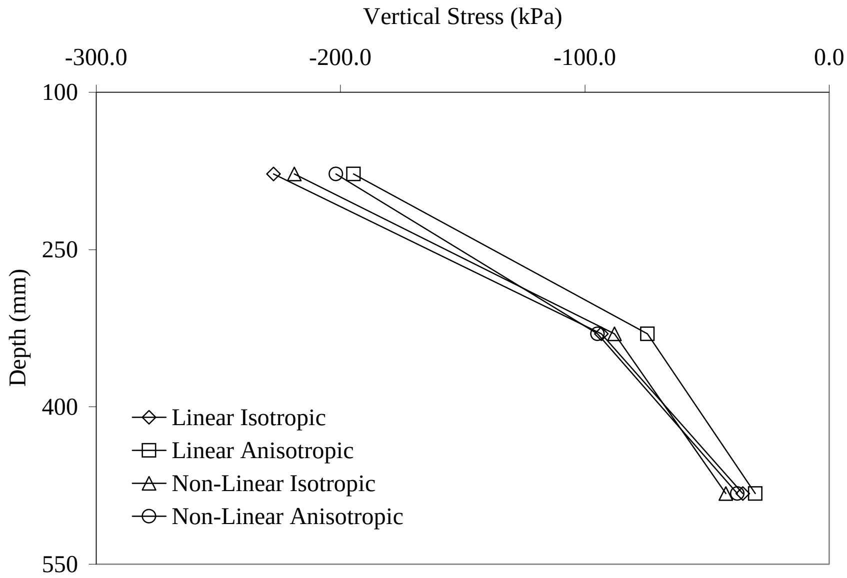

Figure C25 Vertical Stress for 100-mm HMA, 450-mm Base and 20.7-MPa Subgrade.

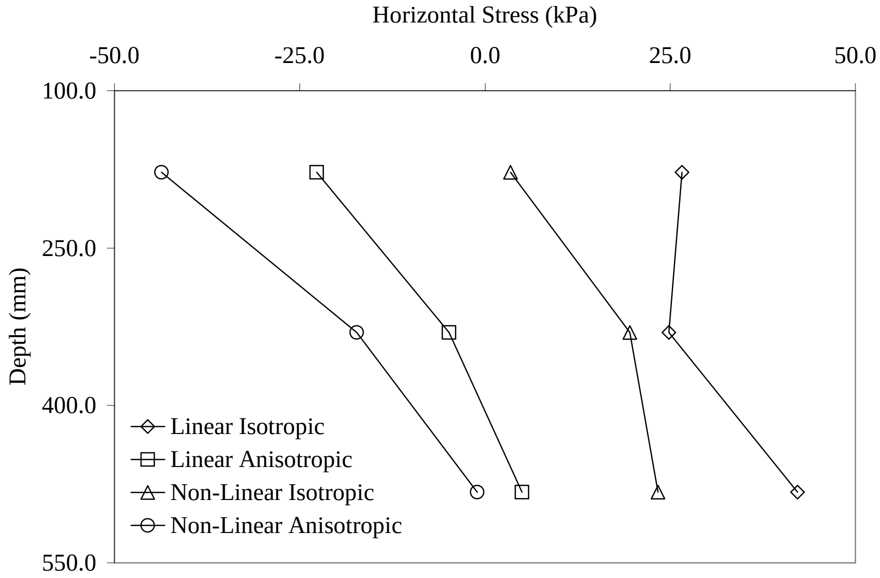

Figure C26 Horizontal Stress for 100-mm HMA, 450-mm Base and 20.7-MPa Subgrade.

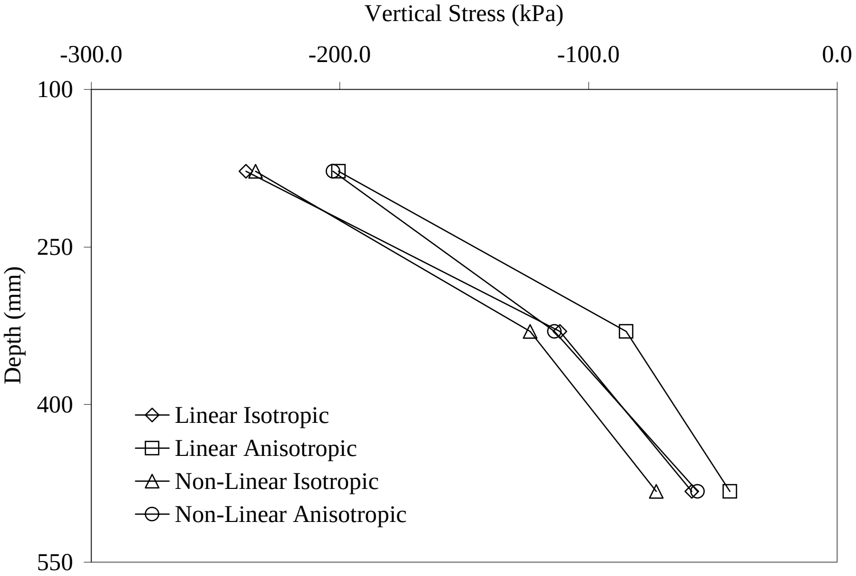

Figure C27 Vertical Stress for 100-mm HMA, 450-mm Base and 103.4-MPa Subgrade.

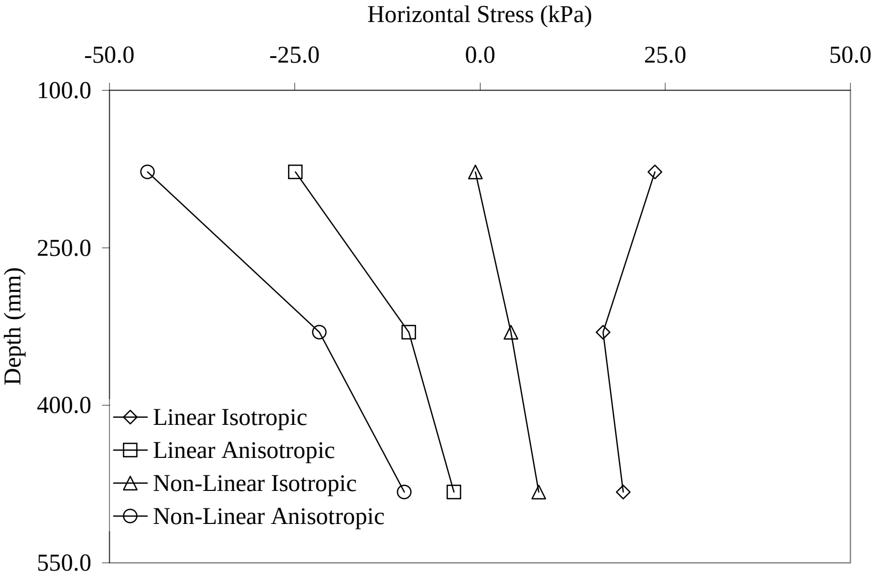

Figure C28 Horizontal Stress for 100-mm HMA, 450-mm Base and 103.4-MPa Subgrade.

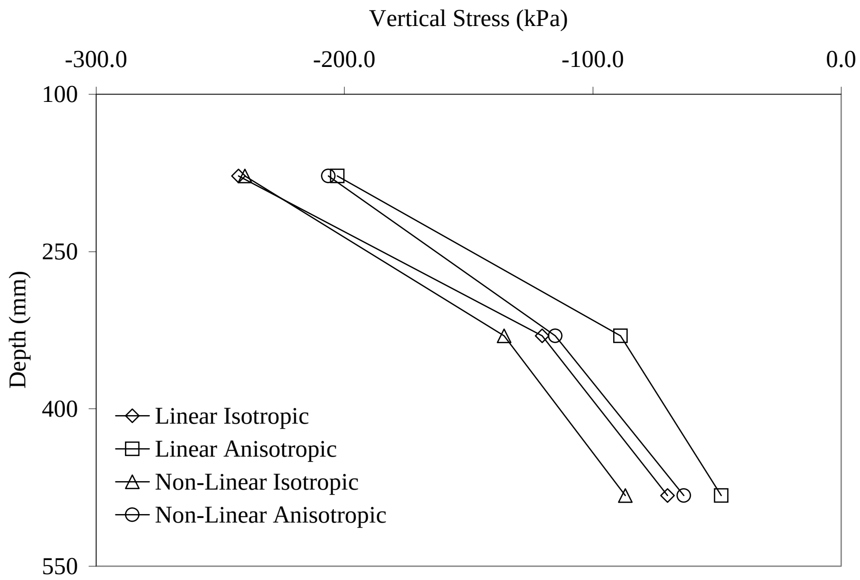

Figure C29 Vertical Stress for 100-mm HMA, 450-mm Base and 206.8-MPa Subgrade.

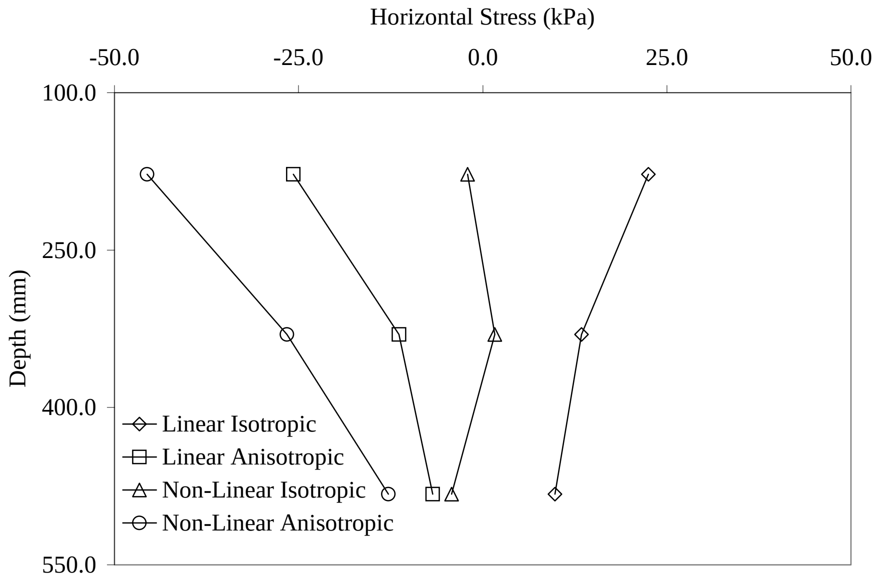

Figure C30 Horizontal Stress for 100-mm HMA, 450-mm Base and 206.8-MPa Subgrade.

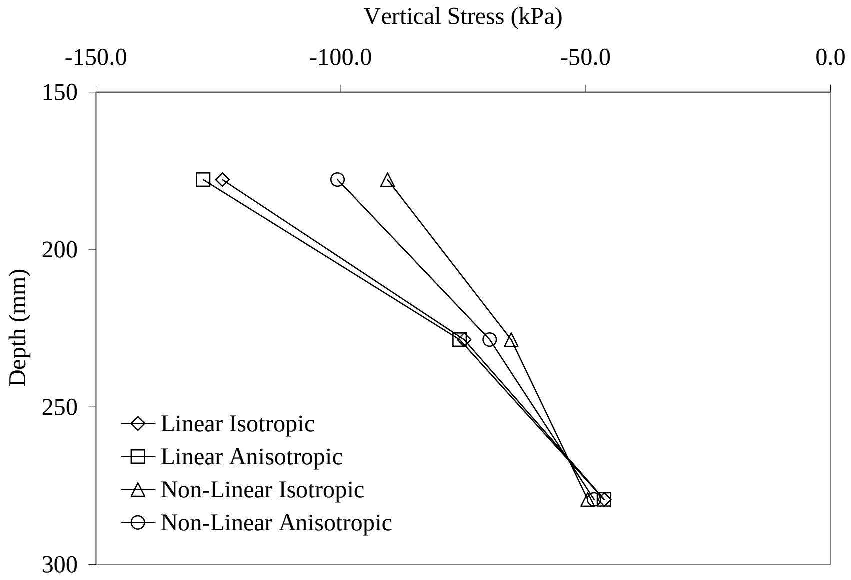

Figure C31 Vertical Stress for 150-mm HMA, 150-mm Base and 20.7-MPa Subgrade.

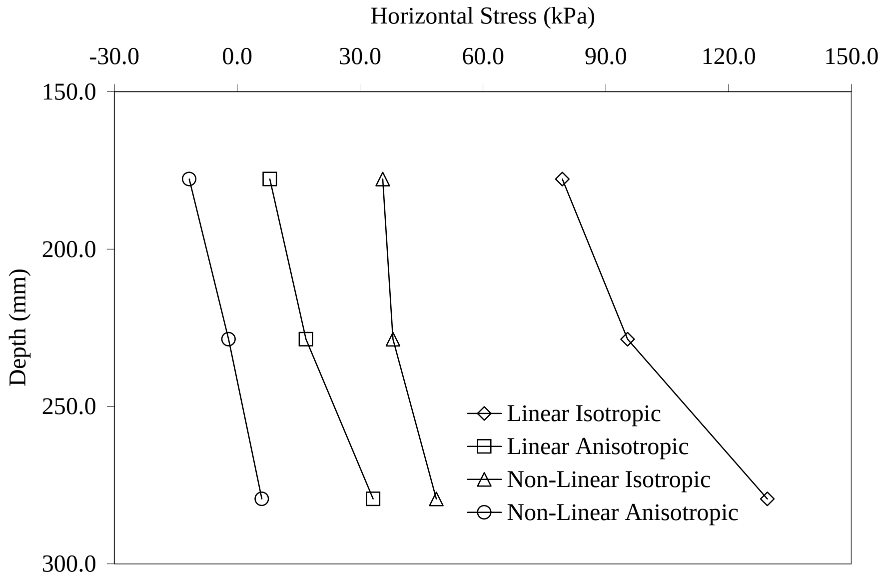

Figure C32 Horizontal Stress for 150-mm HMA, 150-mm Base and 20.7-MPa Subgrade.

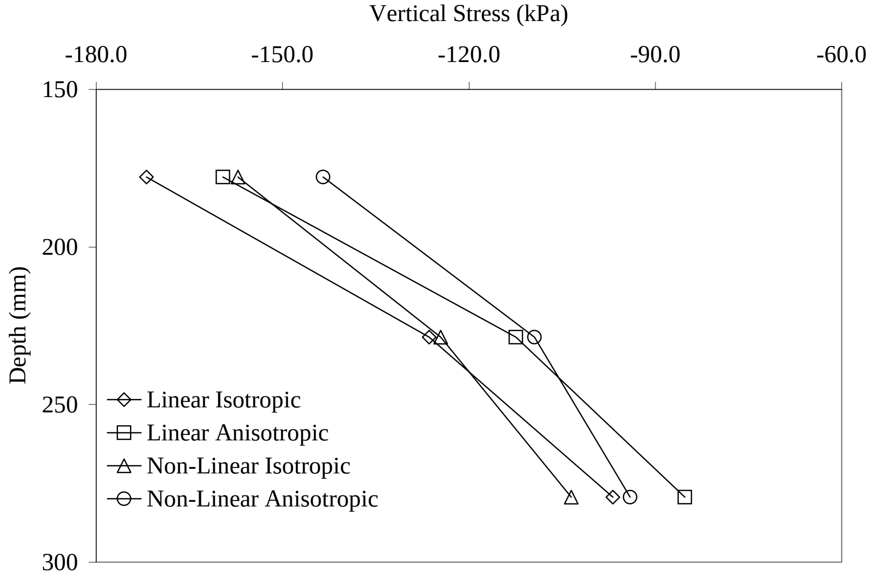

Figure C33 Vertical Stress for 150-mm HMA, 150-mm Base and 103.4-MPa Subgrade.

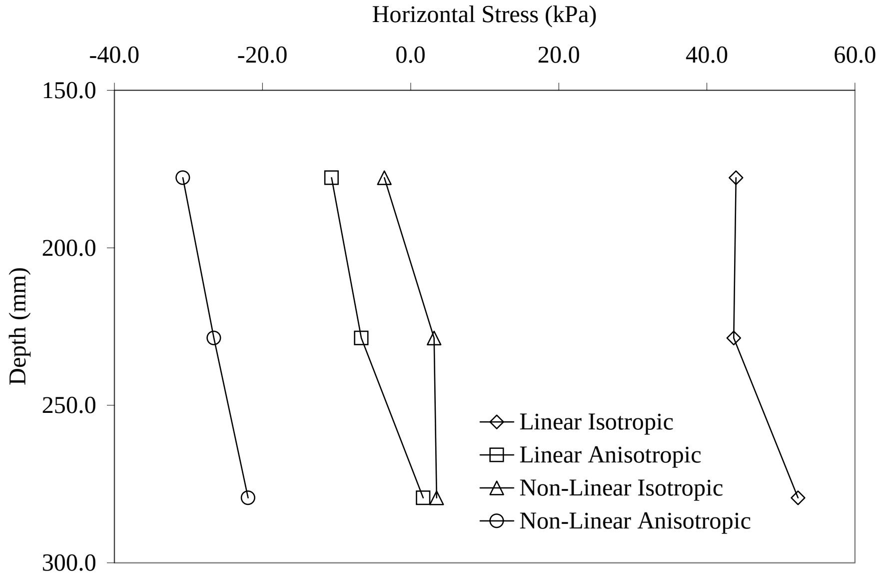

Figure C34 Horizontal Stress for 150-mm HMA, 150-mm Base and 103.4-MPa Subgrade.

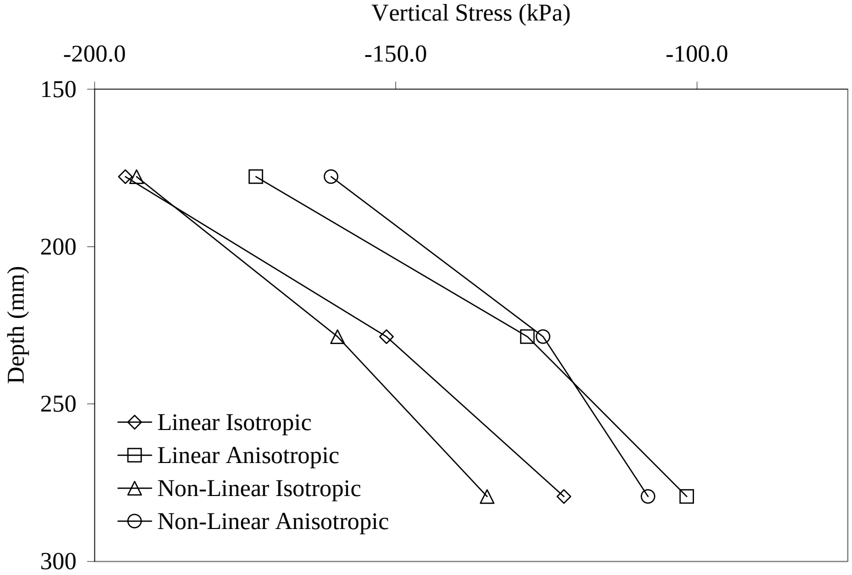

Figure C35 Vertical Stress for 150-mm HMA, 150-mm Base and 206.8-MPa Subgrade.

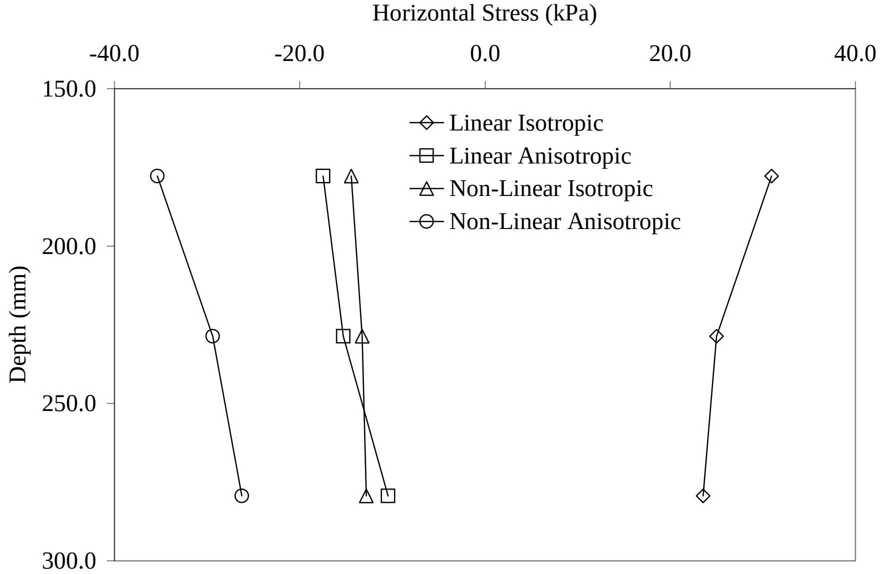

Figure C36 Horizontal Stress for 150-mm HMA, 150-mm Base and 206.8-MPa Subgrade.

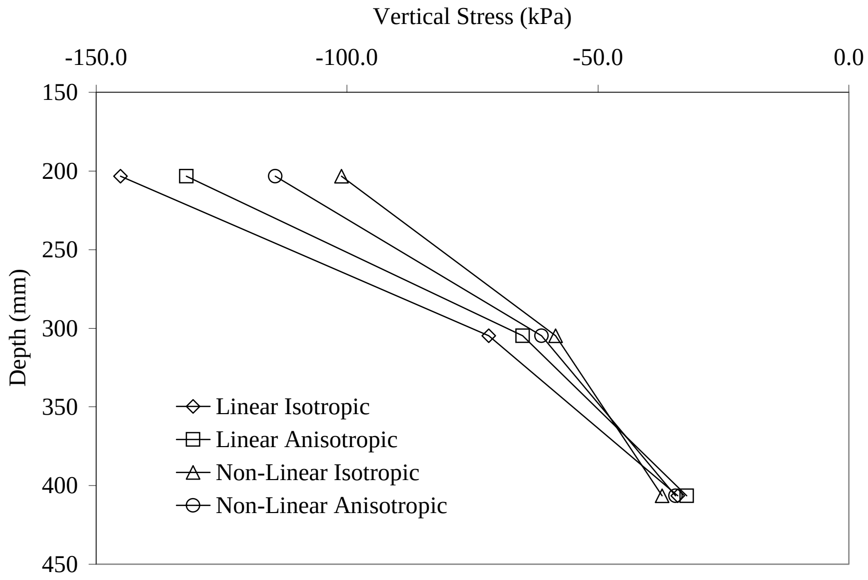

Figure C37 Vertical Stress for 150-mm HMA, 300-mm Base and 20.7-MPa Subgrade.

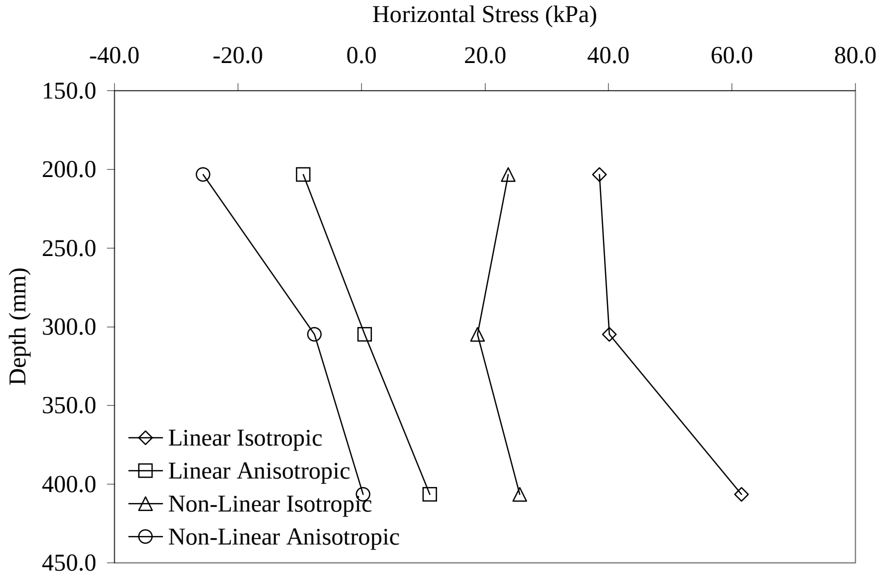

Figure C38 Horizontal Stress for 150-mm HMA, 300-mm Base and 20.7-MPa Subgrade.

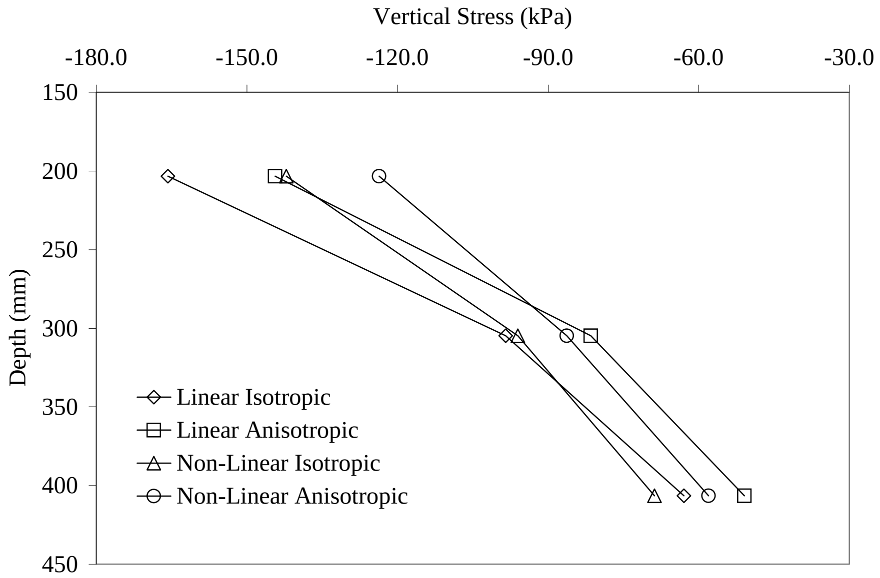

Figure C39 Vertical Stress for 150-mm HMA, 300-mm Base and 103.4-MPa Subgrade.

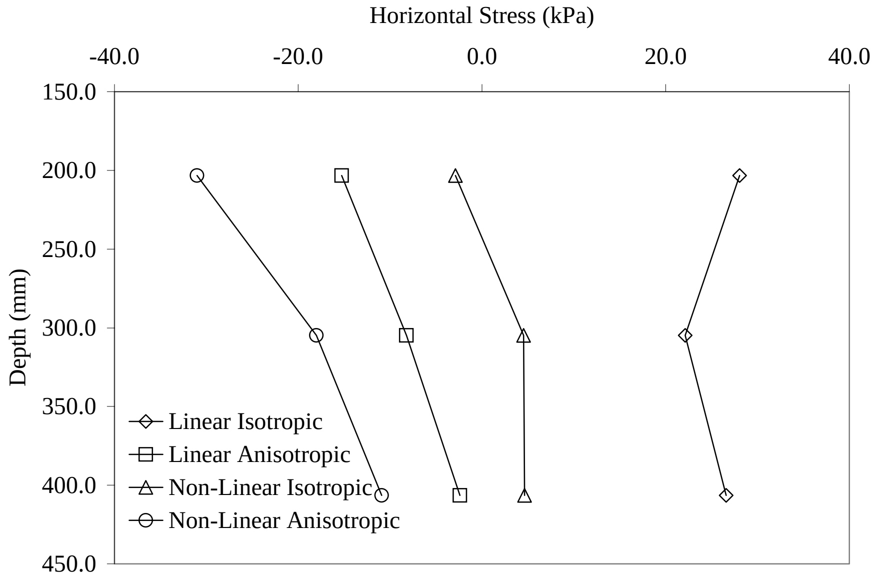

Figure C40 Horizontal Stress for 150-mm HMA, 300-mm Base and 103.4-MPa Subgrade.

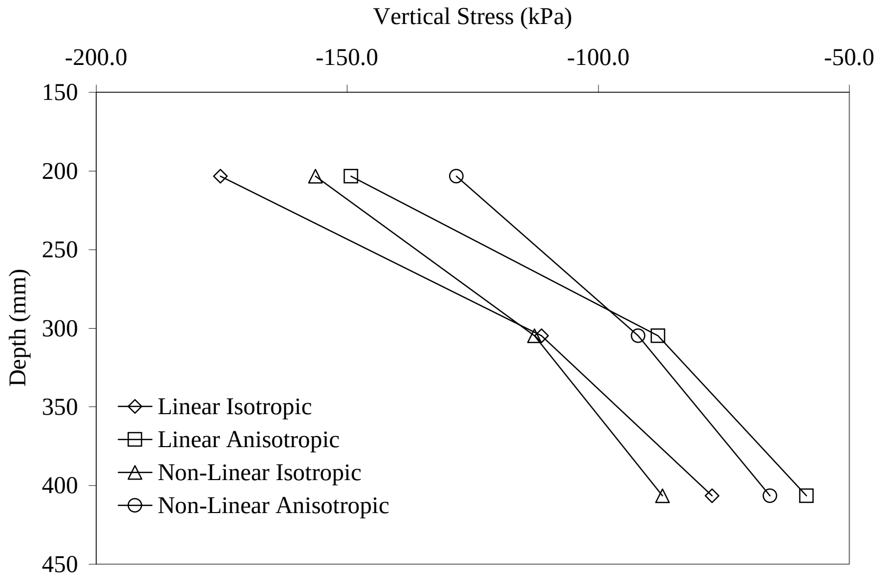

Figure C41 Vertical Stress for 150-mm HMA, 300-mm Base and 206.8-MPa Subgrade.

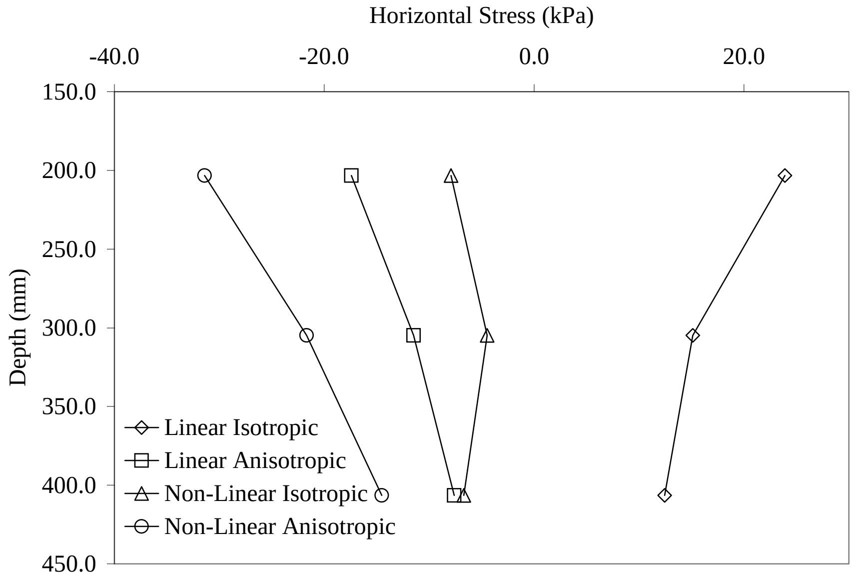

Figure C42 Horizontal Stress for 150-mm HMA, 300-mm Base and 206.8-MPa Subgrade.

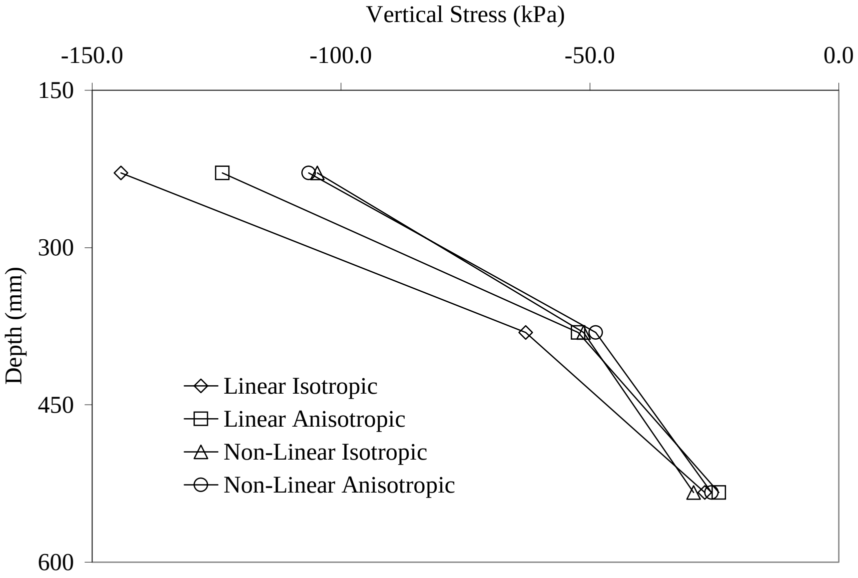

Figure C43 Vertical Stress for 150-mm HMA, 450-mm Base and 20.7-MPa Subgrade.

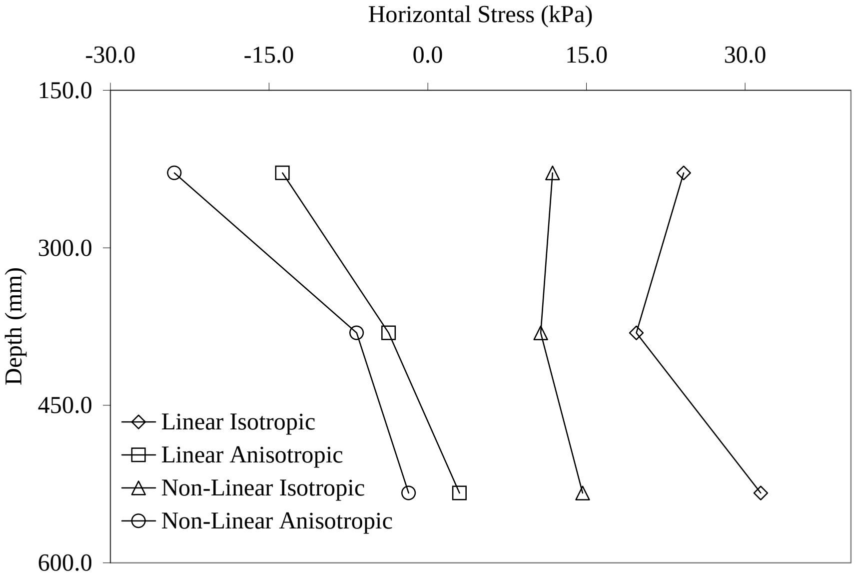

Figure C44 Horizontal Stress for 150-mm HMA, 450-mm Base and 20.7-MPa Subgrade.

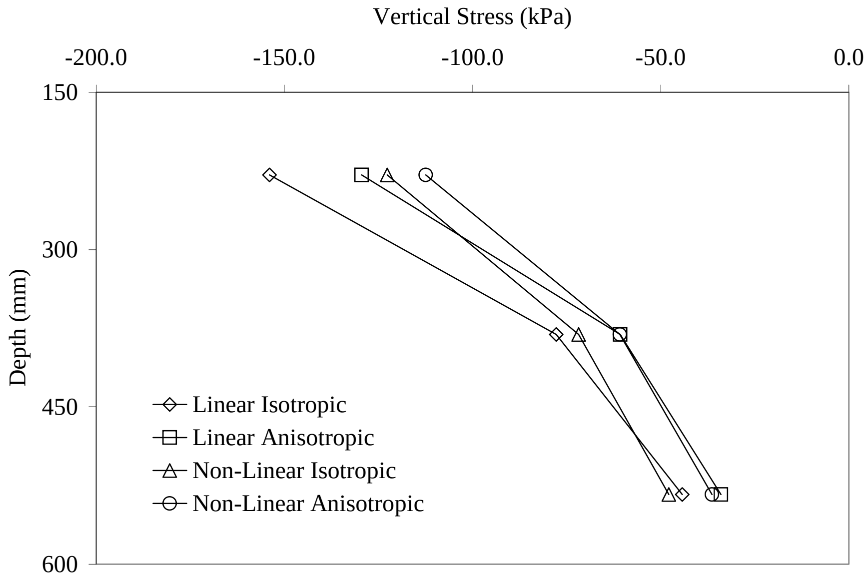

Figure C45 Vertical Stress for 150-mm HMA, 450-mm Base and 103.4-MPa Subgrade.

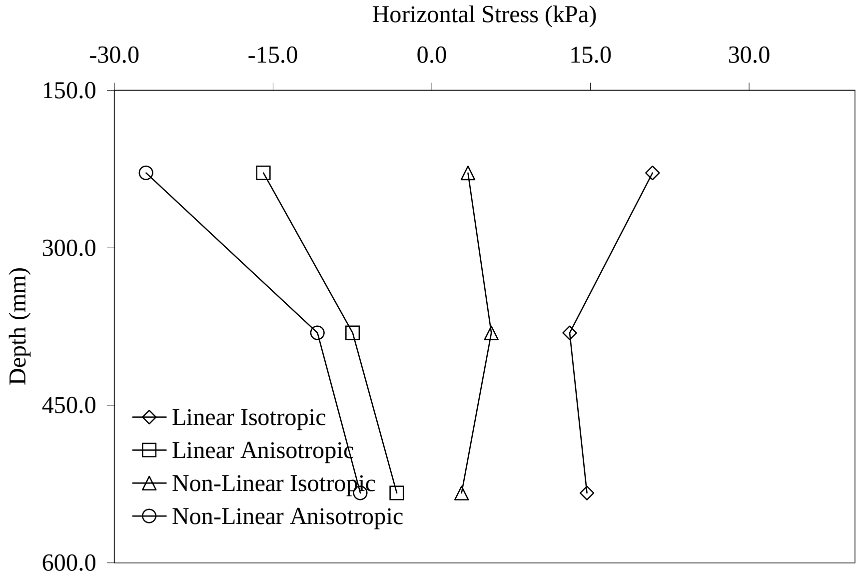

Figure C46 Horizontal Stress for 150-mm HMA, 450-mm Base and 103.4-MPa Subgrade.

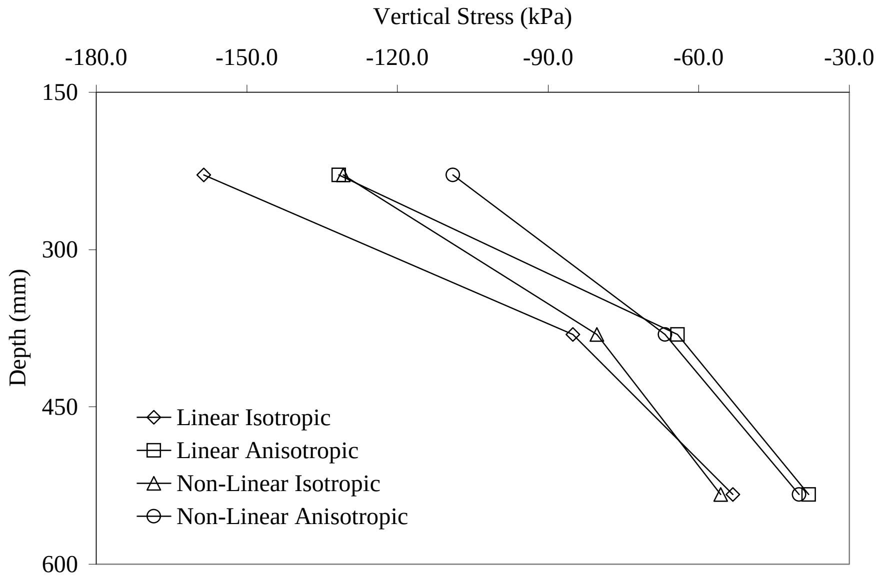

Figure C47 Vertical Stress for 150-mm HMA, 450-mm Base and 206.8-MPa Subgrade.

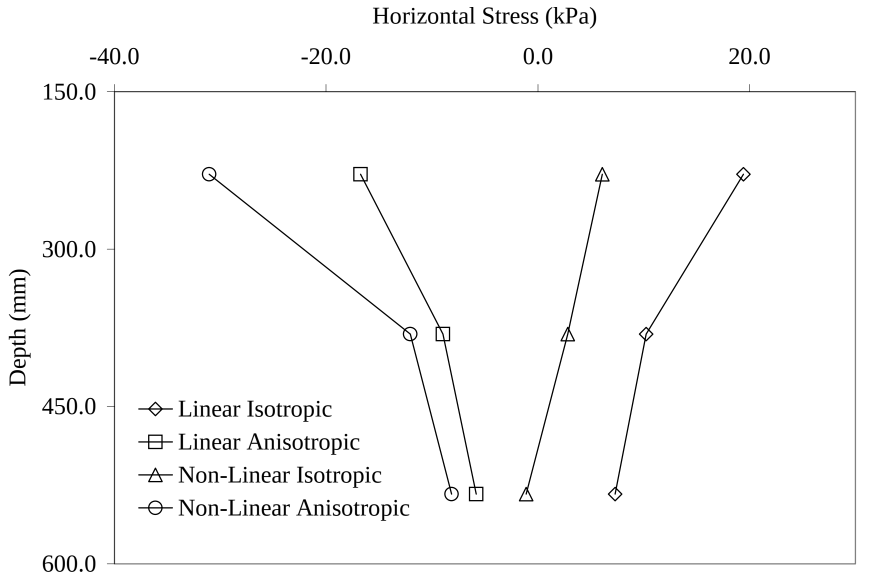

Figure C48 Horizontal Stress for 150-mm HMA, 450-mm Base and 206.8-MPa Subgrade.